MAGNETIC SHELL ENHANCEMENTS DURING MAGNETIC DISTURBANCES*

A. P. WILLMORE AND C. L. HENDERSON†

Langmuir probe observations of electron density on the satellite Ariel I for May–July 1962 show that even on magnetically quiet days longitudinal irregularities appear, particularly near the South Atlantic anomaly. The region of locally depressed density near the shell L=4 shows a diurnal variation of intensity, and in the southern hemisphere it inverts to an increase in density during the late morning. A minimum has been observed at the magnetic equator in the evening hours, about 500 km above the peak of the equatorial anomaly.

For disturbed periods enhancements have been observed with a structure resembling magnetic shells, which tend to merge and to approach lower L values as the disturbance increases. For one disturbed period strong enhancements were noted at night near the South Atlantic anomaly. These phenomena imply the influence of energetic particles on topside irregularities.

INTRODUCTION

Langmuir probe measurements of electron density recorded on the satellite Ariel I during the period May to July 1962 (Willmore et al.) have been used to study the quiet-day distribution, and variations due to magnetic disturbances. No major disturbance occurred in this period, but there were several isolated, moderate storms for which definite enhancements could be identified.

Table 1 lists the magnetic data for these disturbances. Unfortunately there were no probe data for most of the peak disturbance period on May 6 and 31. We have therefore presented results for the three other periods.

METHOD OF ANALYSIS

Since the observations were magnetically recorded on the satellite, data for complete orbits were available.

These were separated into northbound and southbound passes, each covering the full latitude range of 54°N. and S. From 14 successive passes a complete scan of latitude and longitude could be mapped. Because of the slow motion of perigee in the orbit, and the slow rotation of the orbital plane, a line of constant latitude on such a

TABLE 1.

Date	3-hourly Kp values	Kp sum
May 4	1−0o 1+0o	0o 0o 0+1o	3+
5	0o 0o 1−0+	0+1−1+3o	6+
6	2−2o 1+3+	4+5o 5−4+	27−
7	3+2+1+1+	2−1−1+2o	14o
8	2+2o 1o 0+	1o 1o 1−3−	11o
May 25	0o 0o 0o 0+	0+0+0+1o	2+
26	0+1−1−1−	1o 1−1+2+	8−
27*	2o 3o 3−2+	3o 4−2o 3−	21−
28	1−1o 1−2−	2o 2o 3−2+	13o
29	1+2o 2+2−	1+1o 1+1o	12o
30	0+1o 1o 0+	1o 0o 1−1o	5+
31	0+2o 3+5−	5o 4−3−4o	26−
June 1	3−2o 3o 3−	2o 1o 2o 2o	17+
2	1+1+1−2−	1−1−2−2−	10−
3	1−0o 0+1−	2−2−1+3−	9o
June 8	0o 1−1+1−	1−1−1o 1o	6o
9	3−4o 3+4−	4−3−4o 5−	29−
10	5−4−3+4o	3o 2−2o 1o	23+
11	1o 2o 2o 1+	2−1−1+2o	12o
12	2+1−2+2+	3−2o 2o 1o	15+
13	1+1+2+2−	1−1−1o 1−	10−
June 19	1−1o 1o 1−	2o 2−1+1o	9+
20	1+1o 1+1o	1−1−1o 1o	8o
21	1o 1o 0+3o	3o 4−4o 2+	18+
22	3− 4−3−2−	1+1+3−2o	18o

*s.c. at 0414 hrs.

*This paper was contributed to *Goddard Space Flight Center* under the joint United Kingdom-United States program which developed and launched the satellite Ariel I.

†Both authors are affiliated with the Department of Physics, University College, London, England.

map is also a line of constant height to within ± 10 km, and of constant local time to ± 10 minutes. This form of presentation was used to show the longitude and magnetic latitude variations of electron density on quiet days. (figs. 1–4).

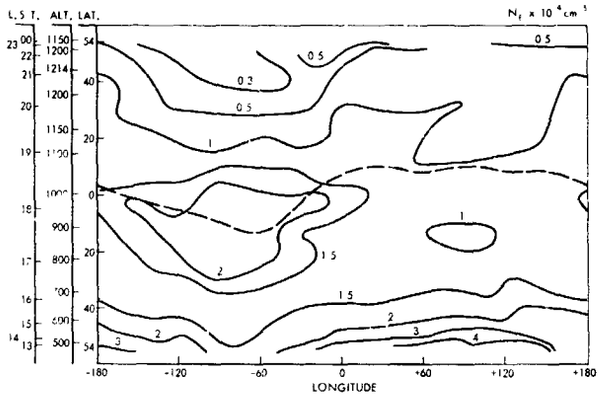

FIGURE 1.—Contours of electron density for northbound passes on May 24, 1962. The dashed line is the magnetic equator.

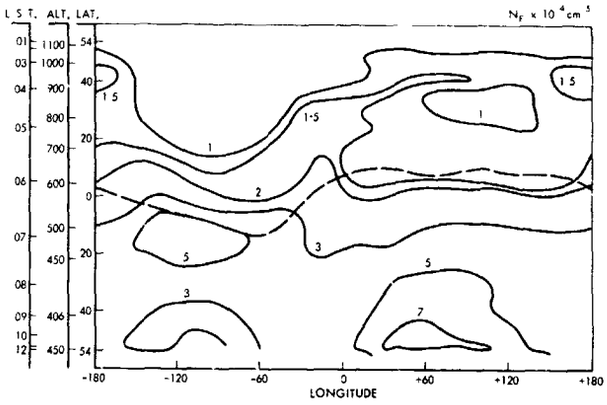

FIGURE 2.—Contours of electron density for southbound passes on May 24, 1962.

For determining disturbance effects, plots of electron density versus latitude for "corresponding" passes on successive days were superimposed. The days included, but were not confined to, those listed in Table 1. The passes were at intervals of 14 orbits, and for corresponding latitudes there was a daily shift of 2° longitude eastwards, a change of less than 20 km in height, and a decrease of 20 minutes in local time. Variations of electron density at a given latitude due to these orbital shifts are in general linear, and can therefore be distinguished from variations which correlate with Kp. A region was classed as showing a disturbance effect only when the electron density for a given latitude differed significantly on the disturbance day from that on the neighboring quieter days.

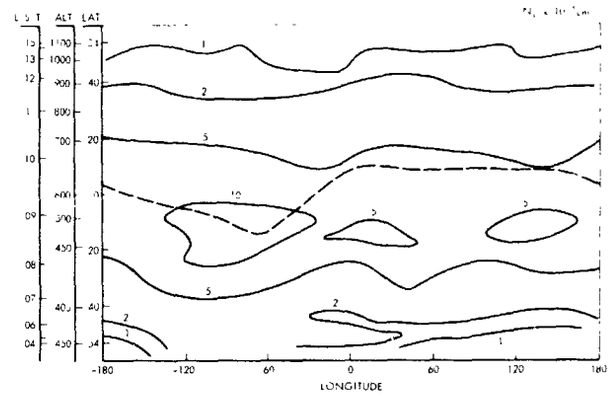

FIGURE 3.—Contours of electron density for northbound passes on June 20, 1962.

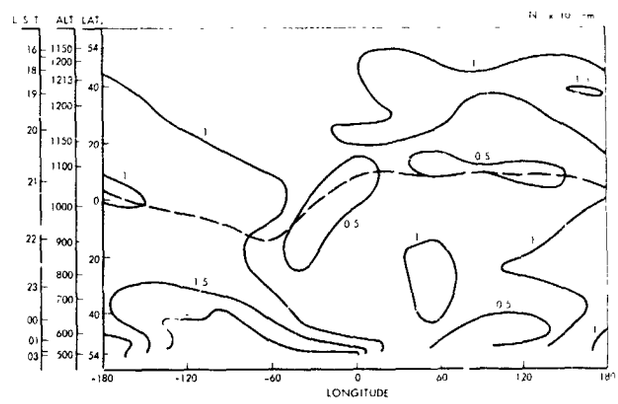

FIGURE 4.—Contours of electron density for southbound passes on June 20, 1962.

No decrease in electron density was unambiguously associated with magnetic activity. Nelms and Warren (this conference) observed a decrease over a wide range of latitudes when Kp reached very high values, up to 9–. However, this referred to altitudes near the maximum of the F layer and so was lower than our observations.

Several regions of increased electron density were observed, and are depicted in figs. 5–8. Bold lines indicated enhancements, fine lines no significant disturbance effect, and blank spaces an absence of data. In some places where there

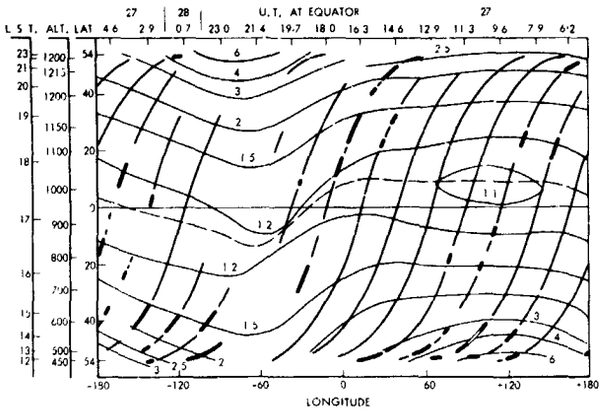

FIGURE 5.—Enhancements for May 27–28, northbound passes. The contours are intersections of L shells with the satellite orbit.

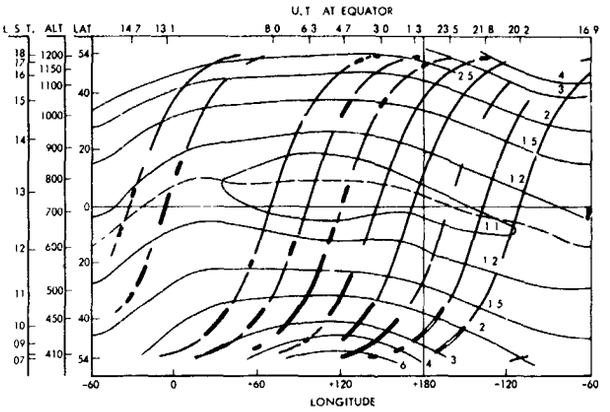

FIGURE 7.—Enhancements for June 9–10, northbound passes.

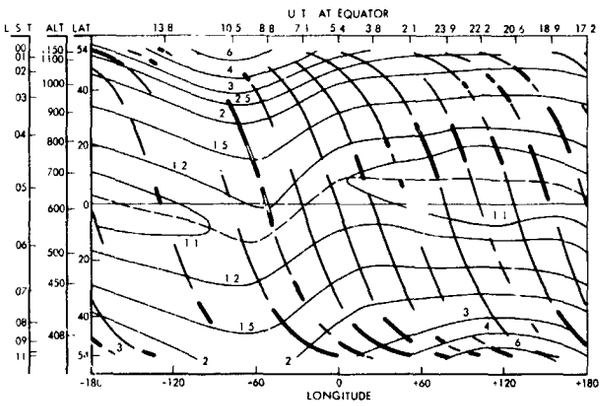

FIGURE 6.—Enhancements for May 27, southbound passes.

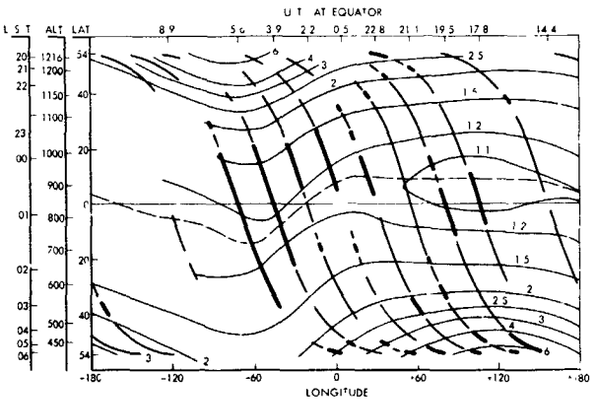

FIGURE 8.—Enhancements for June 9–10, southbound passes.

was a small gap but the sourrounding data suggested a high probability of enhancement, the gap has been bridged by double fine lines. The magnetic equator has been shown as a dashed line, and contours of L values have been drawn. Each pass has been identified by the universal time when the geographic equator was crossed.

QUIET DAY VARIATIONS

Figures 1 and 2 show the contours of electron density for northbound and southbound passes on May 24th, a very quiet day (K sum = 3+). Figures 3 and 4 give the contours for June 20th, when K sum = 8o.

Several interesting regions can be seen:

1. There is a strong maximum on the magnetic equator, centered at longitude —90° This is well-defined on figures 1, 2 and 3, but is absent on figure 4. It is near the South Atlantic anomaly, but displaced about 45° westward. This maximum persists for se eral days at a time, and on other occasions disappears completely. The presence of the maximum is not inconsistent with the model of the diurnal variation of the equatorial anomaly described by King et al (1963a), since the anomaly would not have formed at the local times of figs. 2 and 3, and for fig. 1 the peak would be below the altitude of Ariel. The absence of a maximum in fig. 4 is more puzzling.
2. The regions of high magnetic latitude centered in the northern hemisphere at longitude −90°, and in the southern at

+90°. Muldrew (1963) and others have noted a minimum in electron density extending for about 3° in latitude in the vicinity of the magnetic shell $L=3$ to 4. Figures 1, 2, and 4 show this minimum in the northern hemisphere. It is not present on figure 3. The southern hemisphere region shows a minimum only on figure 4. There is no evidence of it on 1 and 3, and there is a strong maximum on 2. From these and other contour maps it is evident that there is a diurnal variation of this feature. For the southern (winter) hemisphere the electron density (relative to that of neighbouring latitudes) is a minimum during the local night hours, and a maximum in the late morning. For the northern (summer) hemisphere, the local time variations are similar, except that the minimum is deeper and more persistent, and just disappears near noon. It is interesting to note in the high southern latitudes near longitued −100° that the diurnal variation of relative electron density is opposite to that at longitude +90°.

3. On figure 4 a pronounced minimum is evident along the magnetic equator. In the original data this minimum could be for every pass over the equator. It appears to be a feature of the evening ionosphere. It also deviates south of the magnetic equator into the region of the South Atlantic anomaly. The altitude and local time for the minimum as seen in figure 4 are such as to place it some 500 km above the peak of the equatorial anomaly. It is therefore a new and apparently independent phenomenon.

DISTURBANCE EFFECTS

For details of the magnetic conditions for the different disturbance periods, refer back to Table 1. The general impression from the curves of figs. 5–8, and other similar plots, is a tendency for enhancements to occur along magnetic shells, which merge as the disturbance increases. The patterns do not show complete shell formation except in the region of $L>3$. This may be linked with the comparative weakness of the disturbances, and the fluctuations of magnetic activity. Favoured L values would appear to be 1.2 ± 0.1, 1.5 ± 0.1, 2.0 ± 0.2, 2.5, and generally for $L>3$. Other disturbance features seem to vary from storm to storm.

Figures 5 and 6 show enhancements for the minor disturbance of May 27th. From the scale of universal time it will be seen that the passes have been folded to accommodate them all on one scan of longitude. For example on fig. 5 the pass for 0.7 hours on May 28th is next to that for 2.9 hours on May 27th, and the upper portions of passes for 6.2 and 7.9 hours appear on the left of the diagram. A comparison of the enhancements in the high southern latitudes reveals differences in distribution which are due partly to differences in storm time, in that a clear progression to lower L values occurs, particularly in fig. 6. This is probably masked by local time effects to some extent in fig. 5, in that the higher level of undisturbed electron density reduces the relative size of an increase. In fig. 6 it is notable that the enhancements near the magnetic equator are confined almost entirely to the northern hemisphere.

The effects due to a more significant disturbance on June 9th-10th are shown in figs. 7 and 9. Rothwell et al (1963) have reported on the enhancements in the high southern latitudes for this disturbance. Note the shift in the origin of the longitude scale in fig. 7 in order to include the more marked enhancements on the one graph. The major feature of this plot is the broad region of enhancement in the southern hemisphere, which moves toward the equator as the storm intensifies. This storm-time effect receives further support from the coincidence that the disturbance lasted 36 hours, and so a direct comparison of enhancements for the same latitude, longitude, height and local time could be made for successive days. Passes at 1.8, 3.5 and 5.1 hours on June 9th (not shown in the figure) show enhancements in high southern L regions for $L>3$. This compares with L down to 2, 1.5 and 1.3 for the corresponding passes on June 10th. The equatorial enhancements for this figure are similar to those noted by King et al (1963b) in the equatorial anomaly region for the major disturbance of September 22nd, 1963. Figure 8 is

remarkable for the strong night-time enhancement near the magnetic equator, which was most pronounced in the vicinity of the South Atlantic anomaly. Passes for 2.7 and 4.3 hours on June 9th also show this strong equatorial enhancement. The northern hemisphere part of the Sayers shell for $L=1.27$ was very prominent in the longitude region $-70°$ to $+40°$ for the whole of the period June 8th-13th.

The disturbance on June 21st-22nd, the graphs for which are not reproduced, showed enhancements confined almost entirely to the high latitude regions.

CONCLUSIONS

1. Longitudinal irregularities exist even in magnetically very quiet periods. However, the pattern changes to some extent between successive quiet periods.
2. The enhancements show a structure resembling magnetic shell forms, which suggests a particle origin. The tendency of L values to decrease as magnetic activity increases also resembles precipitation zones of the outer Van Allen belt; also the occurrence of a maximum over the South Atlantic anomaly.
3. Therefore it appears that particle effects are at least partly responsible for the ionization irregularities. In this case, the changes in the pattern cannot reflect variations in flux associated with local geomagnetic field changes in the vicinity of the measurements. They must therefore be mapping in some way the geomagnetic field at high L values, where the particles must either be produced or accelerated.

REFERENCES

KING, J. W., SMITH, P. A., ECCLES, D. and HELM, H. 1963a. "The structure of the upper ionosphere as observed by the topside sounder satellite, Alouette." Radio Research Station document No. RRS/I. M.94.

KING, J. W. *et al.* 1963b. "Further studies of the topside ionosphere based on the topside sounder satellite data." Radio Research Station document No. RRS/I.M.112.

MULDREW, D. B. 1963. Canad. J. Phys. **41**, 199.

NELMS, G. L., and WARREN, E. S. "Some irregular variations of the electron density in the topside of the ionosphere." Presented at COSPAR 1964.

ROTHWELL, P., SAYERS, J. and WAGNER, J. H. 1963. "Distribution at high latitudes and during magnetic disturbances." Proc. Roy. Soc. Ariel Discussion Meeting.

WILLMORE, A. P., HENDERSON, C. L., Boyd, R. L. F., and BOWEN, P. J. 1963. "Electron temperature in the upper F-region." Proc. Roy. Soc. Ariel Discussion Meeting.

V. FIELDS AND PARTICLES

MEASUREMENT OF PRIMARY COSMIC RAY CHARGE AND ENERGY SPECTRA DURING 1963*

V. K. BALASUBRAHMANYAN† AND F. B. McDONALD

The differential energy spectra of *H* and *He* nuclei in the interval 100–800 Mev/nuc, the integral *H* and *He* flux >800 Mev/nuc and the cosmic ray charge spectra in the range $Z=1-8$ have been measured using a three element telescope consisting of two thin scintillation counters and a Cerenkov Counter. The measurements were made from Fort Churchill, Canada on a Skyhook balloon flight during June, 1963. The ratio of $Li+Be+B/C+N+O$ appears to be constant in the two regions 400–800 Mev/nuc and >800 Mev/nuc. This ratio extrapolated to the top of the atmosphere is $0.28\pm.08$. A marked difference is observed in the form of the low rigidity differential spectra of *H* and *He*. These measurements are compared with the results available from the last solar cycle.

INTRODUCTION

The objectives of the experiment reported here are two fold:

(a) To develop an improved detector system with adequate charge and energy resolution so that individual charges, their absolute intensities, energy spectra and time variation could be studied with the long range aim of using the detector in a satellite borne experiment.

EXPERIMENTAL SET-UP

A schematic drawing of the detector system is shown in Fig. 1. The system is similar in principle to that reported by McDonald and Webber[1] except for some technical improvements to achieve better charge and energy resolution. For each particle traversing the telescope, the pulse height from all three detectors are recorded. For each detector there is a 512 channel pulse height analyzer and the data is recorded on a balloon borne tape recorder. The total weight of the complete system including batteries and pressure can is 65 lbs.

The results of a balloon flight on 24 June 1963 are reported here. During this flight the balloon remained for 12 hours at a ceiling altitude of 5 gms/cm². The equipment performed reliably throughout the flight and the pre-flight and post-flight calibrations were in agreement with each other. The period during the flights was characterized by a quiet sun, with no abnormal activity.

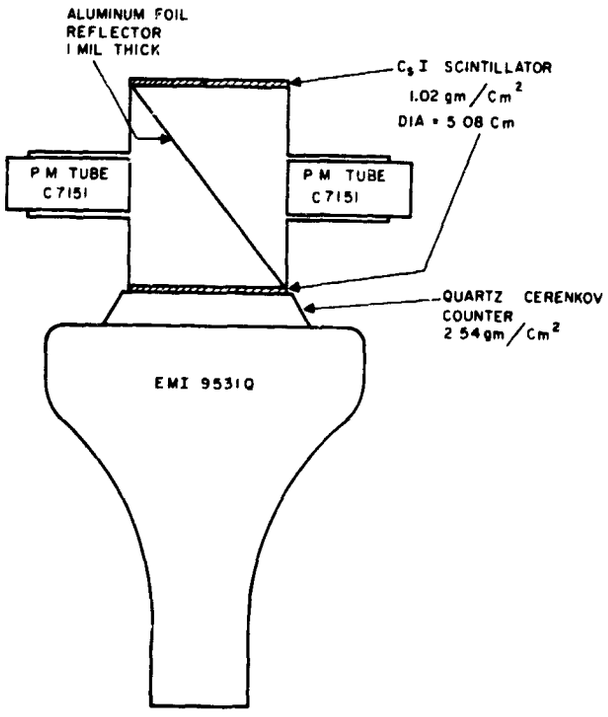

FIGURE 1.—Geometry

*Published as *Goddard Space Flight Center Document X-611-64-63*, 1963.

†National Academy of Science fellow on leave from Tata Institute of Fundamental Research, Bombay, India.

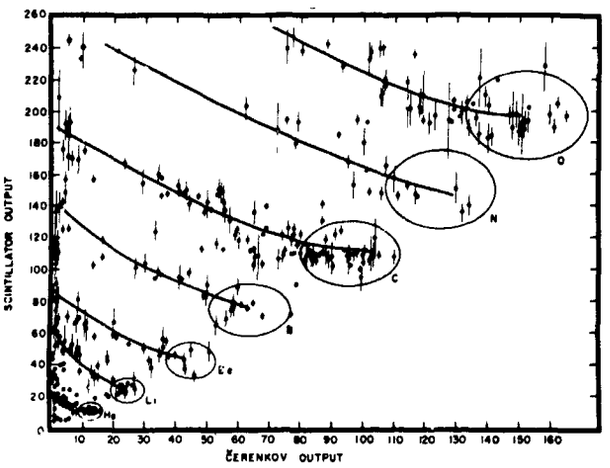

FIGURE 2.—Plot of Cerenkov output vs. ionization loss in telescope.

RESULTS

Fig. 2 shows the charge resolution obtained in the region $Z=2-8$. In the region 350 Mev/nuc (>5 Cerenkov Pulse height) there is excellent resolution between all components. The L/M ratio at the observation level of 5 gm/cm^2 for the energy range 400–800 Mev/nucleon, $=.36\pm.07$ where as for the energy >800 Mev/nucleon the ratio is $.36\pm.09$. The ratio extrapolated to the top of the atmosphere using fragmentation parameters of Friedlander et al.[2] is $0.28\pm.08$ in agreement with the results at Texas 41°N.[3]

A summary of the results on the charge distribution obtained in this experiment is shown in Table 1. Also shown there, are results from previous measurements from other experiments.

MODULATION

Fig. 3 shows the integral intensity of *He* nuclei, the medium and heavy nuclei as a function of neutron count. For rigidity >1.5 BV the agreement between the curve obtained by Webber and McDonald during the last solar minimum, shows that at medium rigidities the sea level neutron count correlates well with the direct measurements. This gives a measure of confidence regarding the accuracy of the measurements.

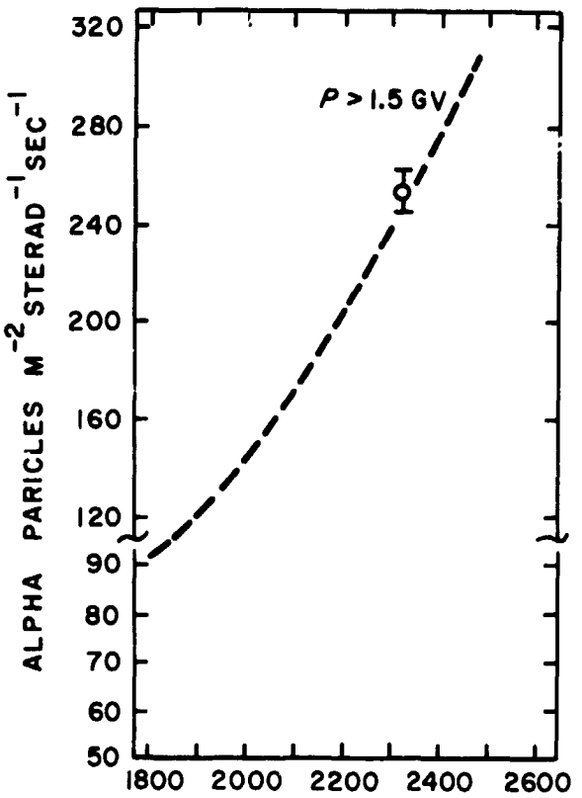

FIGURE 3.—Mt. Washington neutron rate.

Fig. 4 shows the differential rigidity spectra of protons and *He* nuclei. There are some interesting

TABLE 1.—*Comparison of Charge Distributions Obtained at the Top of the Atmosphere Charge Distribution (Percent)*

Charge	Balasubrahmanyan & McDonald	Waddington[3]	Aizu[4] et al	Tamai[5]	Fichtel[6]	O'Dell[7] et al
Li	8.8	3.9	8.8	10.0	7.4	5.3
Be	6.4	1.7	6.0	14.0	5.7	2.3
B	8.1	11.6	10.9	15.7	9.0	7.4
C	31.4	26.0	29.2	18.8	27.1	30.1
N	9.2	12.4	14.8	7.8	15.3	9.7
O	16.6	17.9	14.4	7.3	14.4	19.4
Z 10	19.5	23.9	21.7	20.5	21.7	23.5

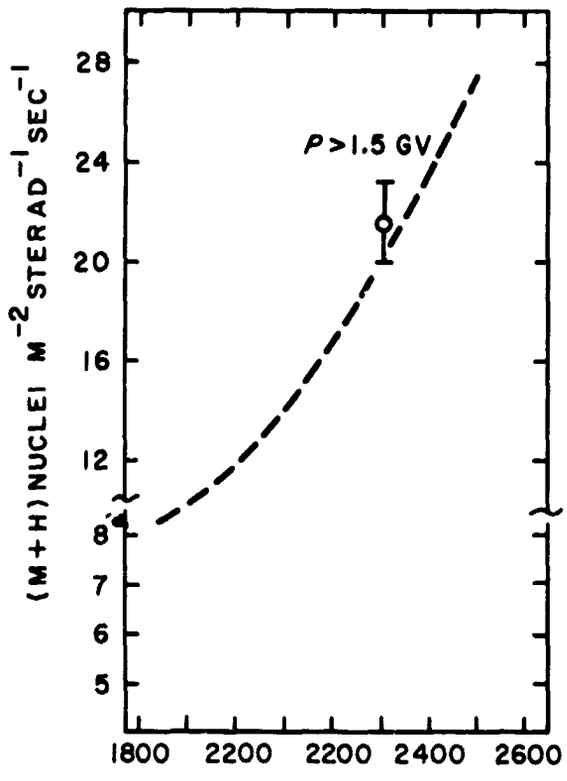

FIGURE 4.—Mt. Washington neutron rate.

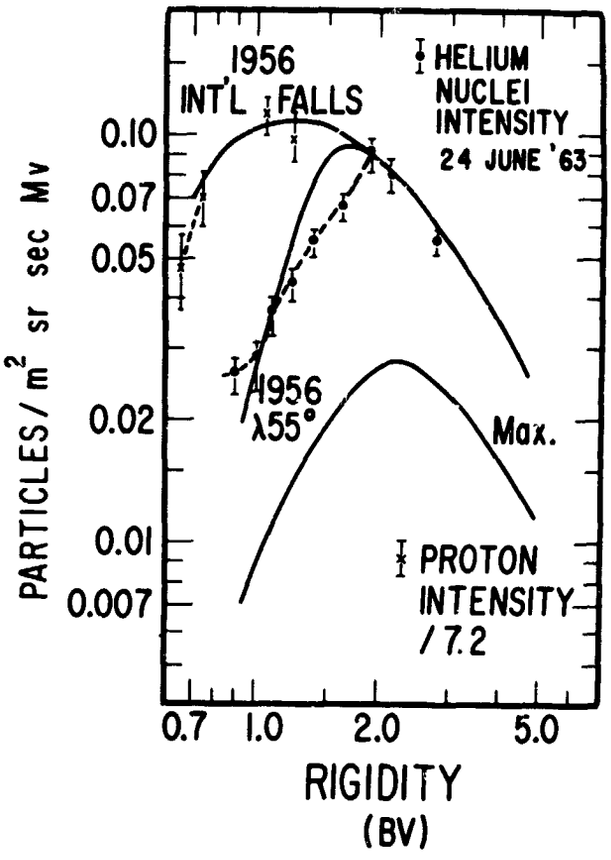

FIGURE 5.—Alpha and Proton Rigidity Spectra

features which this figure reveals. First the differential intensity of Helium nuclei of rigidity >2BV appears to have recovered to the previous solar minimum period. On the low energy side, the previous measurement at International Falls, Minnesota is higher than both the proton and *He* curves of the present experiment. So, on the low rigidity side the recovery is still not complete.

Another interesting feature is the difference in rigidity spectra between the proton and *He* nuclei curves. The recovery for protons has been faster than for *He* nuclei for the same rigidity. In Fig. 5 the results of the counter measurements and that of Nuclear Emulsion measurements by Fichtel et al.[8] are shown. The good agreement between the results of these two entirely different experiments, particularly in the field of intensity measurements of low energy protons, where the secondary corrections etc. are applied on an entirely different and independent basis, gives one a measure of confidence in the interpretation of these results and their bearing on the modulation process.

Parker[9,10] has proposed a diffusion model, wherein the solar wind is responsible for the modulation. In this model, the modulation at a given rigidity is different for particles with different charge to mass ratios because of the velocity dependence of the diffusion mechanism. This model predicts that the differential spectra of the helium nuclei and protons should be different, with the *He* nuclei being suppressed more than

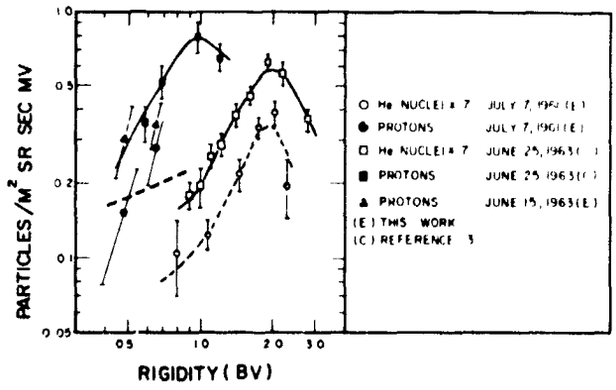

protons. The observations reported here are at least in qualitative agreement with Parker's theory.

REFERENCES

1. F. B. McDonald and W. R. Webber[1], Proceedings of Kyoto Conference II, pp. 429, 1962.
2. M. W. Friedlander, K. A. Neelakantan, S. Tokunaga, G. R. Stevenson and C. J. Waddington, Report of the Cosmic Ray Group, Washington University, St. Louis.
3. C. J. Waddington, Proc. Kyoto Conference, 1961
4. H. Aizu, H. Y. Fujimoto, S. Hasegawa, M. Koshiba, I. Mito, J. Nishimura, K. Yokoi, and M. Schein, Phys. Rev. 121, 1206, 1961.
5. E. Tamai, Phys. Rev. 117(5), 1345, 1960.
6. C. E. Fichtel, Nuovo Cimento, 19(6), 1100, 1961.
7. F. W. O'Dell, M. M. Shapiro, and B. Shiller, Proc. of Kyoto Conference III, pp. 23, 1619.
8. C. E. Fichtel, D. Guss, D. A. Kniffen and K. A. Neelakantan, Proc. Jaipur Conference, 1963.
9. E. N. Parker, Phys. Rev. 109, 1874, (1958).
10. E. N. Parker, Phys. Rev. 110, 1445, (1958).

MAGNETOHYDRODYNAMIC SHOCK STRUCTURE IN A MOVING MAGNETIC FIELD*

DAVID B. BEARD†

The shock structure around a cylinder immersed in a cold collisionless plasma stream containing a weak magnetic field has been investigated in two dimensions. The stream pressure on the boundary of the sheath is proportional to $\cos^2\psi$ where ψ is the angle between the stream velocity and the normal to the sheath. The thickness of the sheath and particle density in the sheath on the upstream side of the cylinder have been found to be nearly constant. A tear drop shaped vacuum is formed downstream from the cylinder. The plasma electrons have essentially all the ion stream kinetic energy in the transition sheath upstream of the cylinder but the ion stream energy is regained downstream from the cylinder. The importance of this shock structure when applied to the earth's magnetosphere and the generation of Type I comet tails is discussed briefly.

1. INTRODUCTION

The solar wind, consisting of a cold plasma flowing constantly at high velocity away from the sun, is now known to contain a weak magnetic field [1,2] oriented somewhat perpendicular to the stream velocity vector. Though the magnetic field carried along in and moving with the stream velocity is so weak that the magnetic field pressure is only one percent of the stream pressure, the field prevents the particles from moving independently of one another. The result is that any object larger than a few ion gyroradii will create a magnetohydrodynamic shock when immersed in the solar wind.[3-9]

The distinctive features of shocks generated in the solar wind are caused by the shape of the object creating the shock and the effect of arresting the velocity of the magnetic field lines which initially must move with the wind velocity since the stream pressure is overwhelmingly greater than the magnetic pressure. The plasma and its field are compressed on the upstream surface of the obstacle and much of the stream kinetic energy is diverted to gyromotion perpendicular to the compressed magnetic field. A simple extension of ordinary M theory of the magnetic pinch effect shows that on entering the compressed field region through the charge separation electric field on the surface, the plasma electrons will acquire essentially all of the kinetic energy of the ion stream in the solar wind. This energy is returned to the ion stream after the plasma in the compressed field region moves around to the downstream side of the obstacle.

In the work presented here a simple model is discussed in which a cylinder of intense magnetic field parallel to its axis presents an obstacle to a cold plasma stream containing a weak magnetic field parallel to the cylinder axis. Besides the inherent interest of the model in understanding magnetohydrodynamic shock structure under such unusual conditions, the model illuminates some gross aspects to be expected in astrophysical problems which occur, for example, in the boundary of the earth's magnetic field and in the tail rays of comets.

2. PHYSICAL CHARACTERISTICS OF THE TRANSITION SHEATH SURROUNDING A CYLINDER IN A MAGNETIZED PLASMA STREAM

The simple idealized model considered here is illustrated in Fig. 1. A proton-electron plasma, collisionless and with no thermal motion, is streaming parallel to the polar axis with velocity v_0, and encounters a cylinder of radius R containing an arbitrarily intense magnetic field sufficient

*Published as *Goddard Space Flight Center Document X-640-64 164*, June 1964.

†Goddard Space Flight Center, University of California, Davis, California, and University of Kansas, Lawrence, Kansas.

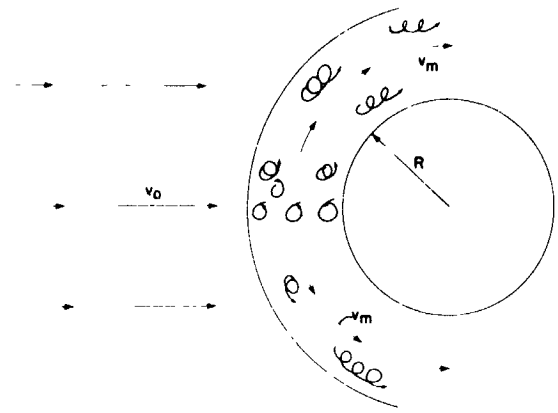

FIGURE 1.—Illustration of solar wind containing a weak magnetic field perpendicular to the plane of the figure incident on a cylinder of radius R. The arrows represent the velocity of the field lines (particle guiding centers) in the free stream v_0, and in the transition sheath, v_m. The circles and loops represent partial trajectories of the particles while in the sheath.

to exclude the incident plasma stream. (In general the obstacle need furnish only a spatially varying magnetic field pressure, $H_g^2/8\pi$, but a cylindrical shape has been introduced at the start to simplify the discussion of the paramount physical features resulting from the analysis.) Finally, the incident plasma stream is assumed to contain a weak magnetic field, parallel to the cylinder axis, which is carried along with the plasma. The stream magnetic field exerts a pressure of only one percent of the stream pressure and the field traveling with the stream velocity v_0 is maintained by the small gyromotion of the plasma in the moving velocity frame of the plasma stream. In this connection it might be noted that the preliminary analysis by Dr. M. Neugebauer of the Mariner R plasma data yielded an effective plasma thermal energy of the order of 10–30 electron volts in a stream energy of the order of a kilovolt. Dr. Neugebauer's analysis was made by examining the energy spread parallel to the stream motion, but the presence of a magnetic field and the gyromotion it causes guarantees that the result is valid for the particle energy component perpendicular to the stream motion as well.

The particle pressure on the outer boundary of the transition sheath is given by

$$p_p = (n_0 v_0 \cos\psi)(m_p v_0 \cos\psi) = n_0 m_p v_0^2 \cos^2\psi \qquad (1)$$

where n_0 is the proton density in the stream m_p is the proton mass and ψ is the angle between the normal to the outer boundary surface of the transition sheath and the stream velocity vector. The second paranthetical factor represents the momentum change of the incident particles at the boundary as they enter the sheath. The external pressure confining the particle and enhanced magnetic field pressure in the sheath acts perpendicularly to the surface. Hence there is no change in particle center of motion momentum component parallel to the boundary which would result in a momentum change factor not linearly dependent on $\cos\psi$.

There is, of course, a very important change in the particle motion on crossing the boundary of the sheath and that is that near the stagnation point, in particular, much of the stream motion is diverted to gyromotion perpendicular to the magnetic field. Although the magnetic field is too weak to contribute effectively to the pressure near the stagnation point, it does cause the charges to rotate about the lines of force. Particle pressure, however, dominates every other consideration and the guiding center of the particles are caused to move towards decreasing pressure gradients "dragging" the magnetic field lines along with them. The particle pressure within the transition sheath is given by

$$p_p = \tfrac{1}{2} n_s m_p v_p^2 = \tfrac{1}{2} n_s m_p (v_0^2 - v_m^2) \qquad (2)$$

where n_s is the ion density within the sheath, v_p is the particle velocity component perpendicular to the field, and v_m is the velocity of the guiding center, that is, the velocity of the magnetic lines of force. The factor 1/2 arises because of the two dimensional motion of the particles within the sheath as opposed to the monodirectional motion of the stream pressure. In three dimensions, where the particle motion is also along the lines of force, the factor might be 1/3.

We thus obtain an expression for the pressure equality on the boundaries of the sheath.

$$n_0 m_p v_0^2 \cos^2\psi + H_0^2/8\pi = \tfrac{1}{2} n_s m_p (v_0^2 - v_m^2) + (n_s^2/n_0^2) H_0^2/8\pi = H_c^2/8\pi \qquad (3)$$

where H_c is the magnetic field intensity in the cylinder at the inner boundary. Since the plasma is collisionless, the magnetic field intensity is directly proportional to the particle density, and

thus the magnetic field intensity anywhere in the sheath is $(n_s/n_0)H_0$. Particle thermal pressure would be easy to include for similar reasons. Since n is proportional to H and the square of the thermal velocity, v_{pt}^2, is proportional to H if the motion is adiabatic, the particle thermal pressure is a constant multiple of the magnetic pressure and may be included by multiplying H_0^2 by an appropriate factor.

The change in the external pressure, P, as a function of the distance along the boundary of the sheath, l, results in a pressure gradient which accelerates the plasma within the sheath.

$$n_s m_p \frac{dv_m}{dt} = n_s m_p v_m \frac{dv_m}{dl} = -\frac{dP}{dl} + \frac{d}{dl}\left(\frac{n_s^2}{n_0^2}\frac{H_0^2}{8\pi}\right) + \frac{m_p}{2}(v_0^2 - v_m^2)\frac{dn_s}{dl} \quad (4)$$

which may also be obtained by differentiating Eq. 3 with respect to l. Throughout most of the upstream side of the cylinder H^2_0 is negligible compared with the particle pressure and Eq. 3 may be approximated by

$$n_s = 2P/m_p(v_0^2 - v_m^2)$$

which satisfies Eq. 4 since the last two terms in Eq. 4 are negligible in these circumstances. Thus, $v_m \sim v_0 \sin\psi$ throughout the transition sheath on the upstream side and n_s is nearly constant and equal to $2n_0$. As ψ approaches $\pi/2$, however, the magnetic pressure becomes significant and n_s decreases with l depending on ψ as

$$n_s \sim n_0[1 + \tfrac{1}{4}(8\pi n_0 m_p v_0^2/H_0^2)\cos^2\psi - (3/32)(8\pi n_0 m_p v_0^2/H_0^2)^2\cos^4\psi] \quad (5)$$

Using the approximations valid on the upstream side of the cylinder the position of the outer boundary to the transition sheath is easily obtained by requiring particle conservation. The number of particles arriving per second per unit cylinder length within a distance, y_2, from the polar axis is $n_0 y_2 v_0$; the number leaving the transition region per second per unit cylinder length is $n_s(r_2 - r_1)v_0 \sin\psi$ (see Fig. 2).

$$r_2 - r_1 \sim r_2 \sin\theta_2/2 \sin\psi \quad (6)$$

For a cylindrical obstacle for which r_1 is constant, $\theta_2 = \psi$, and

$$r_2 = 2r_1 \quad (7)$$

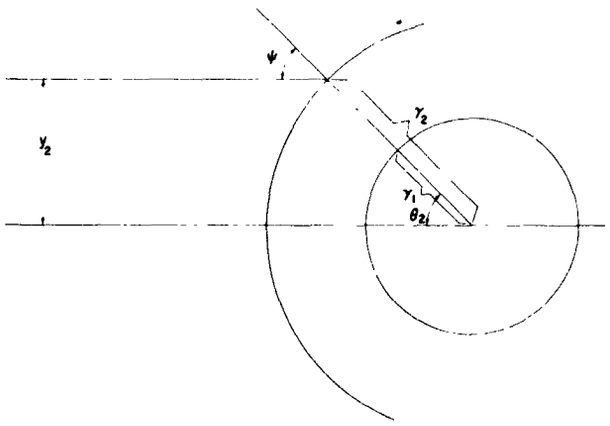

FIGURE 2.—Diagram of use of constant flux condition in determining the sheath thickness, $r_2 - r_1$, by which particles leave a volume of unit height after entering the volume within the length y_2.

If the obstacle were not cylindrical a differential form of the constant flux condition, Eq. 6, would be required

$$n_0 v_0 d\,l \cos\psi = n_s(r_2 - r_1)v_0 d(\sin\psi)$$

$$\frac{d\psi}{dl} = \frac{n_0}{n_s}\frac{1}{r_2 - r_1} = \frac{1}{r_2}\frac{d\psi}{d\theta} \quad (8)$$

which yields Eq. 7 in the region where $n_s = 2n_0$ if r_1 and r_2 are now regarded as functions of ∂. If n_s is a decreasing function of θ, as it is near $\theta \sim \psi \sim \pi/2$, $r_2 - r_1$ increases faster than r_2 and $\frac{d\psi}{d\theta}$ is less than unity. In this region, the parametric equations 5 (or rather 3) and 8 must be solved numerically.

The magnetic pressure cannot be neglected in the region

$$\theta \sim \psi \gtrsim \cos^{-1}[H_0/(8\pi n_0 m_p v_0)^{1/2}] \sim 84° \quad (9)$$

where the stream velocity is

$$v_m \sim v_0 \sin\psi \sim 0.99 v_0 \quad (10)$$

and

$$(v_0^2 - v_m^2)^{1/2} \sim 0.10\, v_0$$

Therefore, on the downstream side of the cylinder, the guiding center of stream velocity in the transition sheath is again approximately v_0, and the velocity perpendicular to the field lines and v_0 is less than $0.10\, v_0$. The stream expands freely into the vacuum behind the cylinder so as to form a diffuse triangle shaped tail, based on

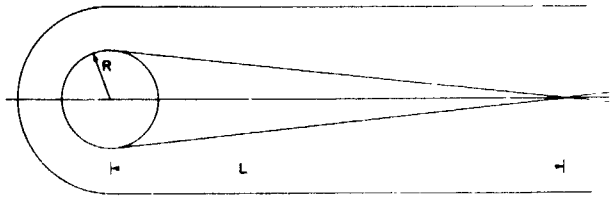

FIGURE 3.—The shock structure behind a cylinder of radius R. The length of the vacuum downstream from the cylinder $L \sim RV_0/(v_0^2 - v_m^2)^{\frac{1}{2}}$.

simple kinematics, which closes more than ten cylinder radii downstream and leaves a turbulent wake as illustrated in Fig. 3.

3. THE SHOCK PRODUCED ENERGETIC ELECTRONS IN THE TRANSITION SHEATH

The preceding section has given us a general description of our simple two dimensional model problem as illustrated in Figs. 1–3. A weakly magnetized plasma moving with velocity v_0 enters a transition sheath where the velocity of the particle's guiding centers, that is, the velocity of the magnetic lines of force, changes abruptly at the outer boundary of the transition sheath to a lower velocity, v_m. Ferraro[10] and especially Dungey[11] and Rosenbluth[12] have shown how a charge separation layer will be created at any boundary where the magnetic field is suddenly increased on the side away from the plasma. Beard,[13] Grad,[14] and Sestero[15] have further developed the theory of the electric field on the boundary which serves to energize the electrons at the expense of the positive ions. The electric field arises due to the difference in momentum between the electrons and the positive ions, and thus there is no field in any region where the momenta of the opposite charges are equal.

In the simple two-dimensional problem discussed in this paper, it might be anticipated that when the plasma enters and passes through the transition sheath the charges will have gained or lost potential energy (depending on the sign of their charge) as though they had passed through permeable condenser plates at the boundary. Hence, if there is no reverse electric field, the electrons will have acquired essentially all of the initial stream kinetic energy of the positive ions.

Following Rosenbluth's [12,13] analysis in which the plasma did not enter the region of increased field intensity, we write, for the changed conditions of this problem, the equations of motion of a charge initially moving parallel to the x axis

$$\ddot{x} = \frac{q}{m}E(x) + \frac{q}{mc}H\dot{y} \tag{11}$$

$$\ddot{y} = -\frac{q}{mc}H(\dot{x} - v_m) \tag{12}$$

where the coordinate system is illustrated in Fig. 4, q and m are the charge and mass of the charged

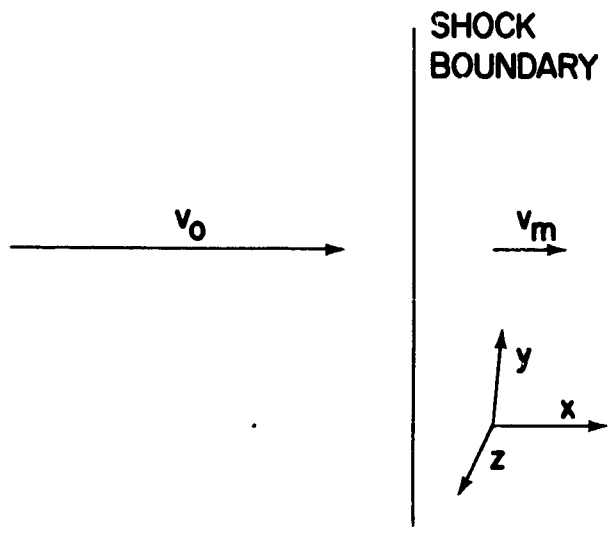

FIGURE 4.—The coordinate system used in analyzing particle motion in a magnetic field parallel to the z axis whose field lines travel with a velocity v_0 to the left of the shock boundary and with velocity v_m to the right of the shock boundary.

particle, E is the electric field perpendicular to the boundary which is tangent to the y, z plane, H is the magnetic field and is parallel to the Z axis, and v_m is the velocity of the guiding centers (i.e. the magnetic lines of force) which are assumed to be moving entirely parallel to the x axis for this part of the analysis. Eq. 12 is easily integrated and yields the y component of the particle velocities.

$$\dot{y} = \frac{-q}{mc}x / \int_{-\infty}^{t} H\,(x' - v_m)dt' \tag{13}$$

Hence the y component of the particle momenta is the same for both electrons and protons.

The particle densities are inversely proportional to the x component of the average velocity of the particles. To avoid the impossibly large electric

fields resulting from excessive charge separation the x component of the average velocities of the particles must be kept equal everywhere. This requires that in being slowed from an initial velocity v_0 to the final guiding center velocity of V_m, the x-component of the deceleration of the electrons must be equal to the deceleration of the ions. Thus Eq. 11 and 13 yield the equality

$$\frac{e}{m_e}E(x)-\left(\frac{e}{m_e c}\right)^2 H\int_{-\infty}^{t} H\,(x'-v_m)dt'=-\frac{e}{m_i}E\,(x)$$

$$-\left(\frac{e}{m_i c}\right)^2\int_{-\infty}^{t} H\,(x'-v_m)dt'$$

where the subscripts e and i refer to electron and positive ion and $q_e=-e$, $q_i=e$. Neglecting the right hand side of this equation as being of order m_e/m_i smaller than the left hand side we obtain the familiar M theory result

$$E(x)=\frac{e}{m_e c^2}H\int_{-\infty}^{t} H\,(x'-v_m)dt' \qquad (14)$$

If Eq. 13 and 14 are inserted into Eq. 11, then the integral of Eq. 11 after multiplication by x is to zero order in m_e/m_i

$$x_i^2=v_0^2-\frac{2e}{m_i}\int_{-\infty}^{x} E\,(x')dx'$$

Let X_M represent the position at which the incident proton first reaches the final guiding center velocity, V_m, (i.e. the position beyond which the compressed field is constant.) then,

$$\tfrac{1}{2}m_i(v_0^2-V_m^2)=e\int_{-\infty}^{X_M} E\,(x')dx' \qquad (15)$$

Eq. 15 has the very obvious physical interpretation that the total potential drop for $-\infty<x<x_M$ is equal to the change in the ion stream kinetic energy divided by the ion charge. For $x>x_M$ charge neutrality does not require $\dot{x}_e/x'_i$; only their averages, V_m, must be equal.

Since the momenta of the electrons and protons are equal, no further charge separation takes place; the gyroradii of the particles are equal. The momentum of an ion in the stream $m_i v_0$ has been reduced to $(m_e/m_i)^{1/2}m_i v_0$ in exerting the pressure on the boundary needed to confine the enhanced magnetic field interior to the boundary. The kinetic energy of the ions has been reduced, however, from $\frac{1}{2}m_i v_0^2$ to $\frac{1}{2}m_e v_0^2+\frac{1}{2}m_i v_M^2$. The considerations of the previous section are still valid since the total particle pressure in the transition layer is not affected by the electrical potential at the boundary since the electron energy in the transition layer is $\frac{1}{2}m_i v_0^2-\frac{1}{2}m_i v_M^2$.

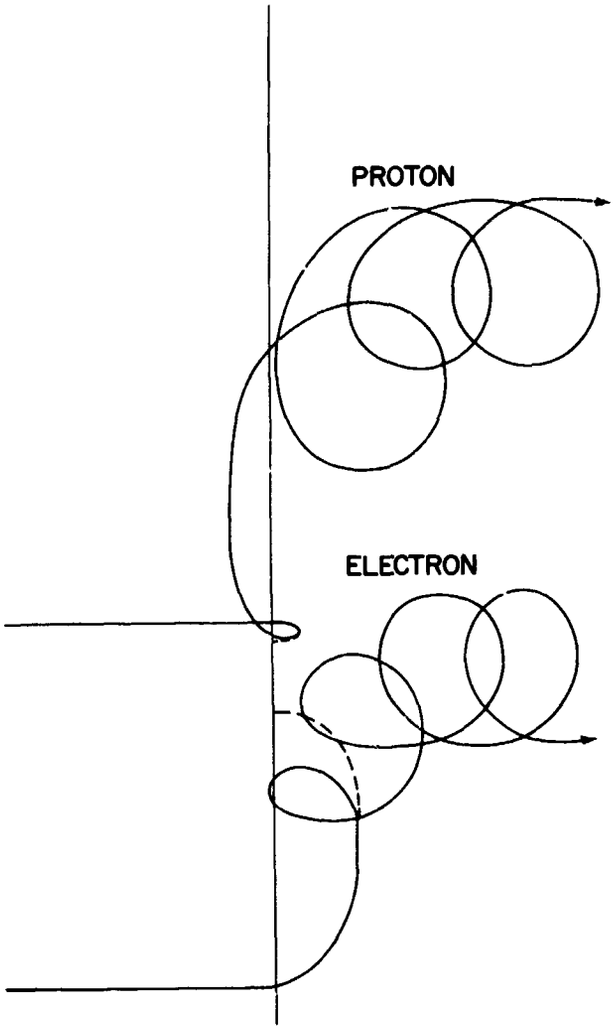

FIGURE 5.—Electron and proton trajectories initially traveling with a moving magnetic field which is slowed down and compressed, downstream from the shock boundary.

A free hand drawing of the particle motion as it crosses the boundary is shown in Fig. 5 for conditions near the stagnation point. The conclusions are essentially unchanged at other points on the boundary as illustrated in Fig. 6 if one considers only the component of the guiding center

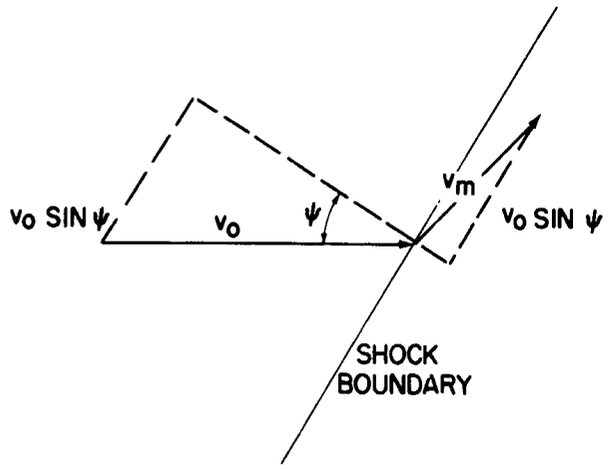

FIGURE 6.—The geometry of the guiding center or field line motion on both sides of the shock boundary for oblique incidence.

motion perpendicular to the boundary. The component of the stream velocity parallel to the boundary is the same on both sides of the boundary and therefore the problem reduces to the stagnation point case in a coordinate frame which moves with the velocity $v_0 \sin\psi$ parallel to the boundary and $v_0 \cos\psi$ supplants v_0 in the stagnation point considerations. In accelerating to nearly the free stream velocity again in its motion away from the stagnation point, the motion of the plasma in the transition sheath causes the initial ion kinetic energy to be recovered at the expense of the electron energy.

CONCLUSIONS

A cold plasma stream containing a weak magnetic field (field pressure much less than particle stream pressure) will be compressed on the upstream surface of a cylindrical obstacle whose axis is parallel to the magnetic field. The particle density and magnetic field intensity within the transition sheath on the upstream side are double their free stream value. The thickness of the sheath is equal to the cylinder radius over almost all of the upstream surface and thickens slightly near the joining of the upstream and downstream surfaces due to the additional magnetic pressure, however small, in the transition sheath. The enhanced magnetic pressure in the transition sheath, however slight, prevents the ions from returning completely to their initial free stream motion on the downstream side of the cylinder. As a result, a plasma stream, even though the particles initially have a unique velocity, will expand into the vacuum behind the cylinder. In the case of a plasma with some thermal velocity $(kT/2\pi m)^{1/2}$ the vacuum downstream would be a diffuse isoceles triangle whose height would be $v_0 (2\pi m/kT)^{1/2} R$ where v_0 is the initial stream velocity and R is the cylinder radius (1/2 the triangle base.)

The enhanced magnetic field in the transition sheath creates a charge separation layer at the boundary of the undisturbed plasma stream. The total change in electrical potential across this layer is equal to half the stream pressure on the transition sheath. The plasma stream moves through the charge separation layer, and, on entering the transition sheath, the electrons acquire all the kinetic energy the ions would have had perpendicular to the magnetic field in the absence of the charge separation layer. At the stagnation point the electron kinetic energy in the transition sheath equals the initial ion kinetic energy in the free stream, but elsewhere in the transition sheath the electron kinetic energy equals the difference between the ion free stream kinetic energy and the ion stream energy in the transition layer.

ASTROPHYSICAL APPLICATIONS

The application of this work to Type I comet tails is straightforward and will be reported elsewhere. The slight ionization of massive cometary molecules through charge transfer with protons in the solar wind cause the interplanetary magnetic field lines to slow down drastically in overcoming the inertia of the massive cometary ions initially at rest. The energetic electrons in the transition sheath which forms on the surface of the "slowed" field lines then rapidly and efficiently ionizes hundreds of cometary molecules per cc. The energetic electrons will further rapidly diffuse out along the field lines (as suggested by Axford in private conversion) and pull the ions out along the field lines so as to form the striking ray structure known as Type I comet tail rays.

The simple model examined in this paper also yields a good qualitative understanding of the phenomena observed at the edge of the earth's magnetic field and enables predictions about the

energy of the charges in the magneto-sheath to be made. The sphericity of the earth's magnetosphere introduces a new physical dimension. In the plane containing the stagnation point and the magnetic field lines the particle pressure both inside and outside the outer boundary of the transition sheath (A. J. Dessler has suggested the name magneto-sheath) is still proportional to $\cos^2\psi$. The particles are decoupled, however, from the magnetic field in the direction of the field, and conservation of magnetic flux requires that the magnetic field intensity be approximately independent of distance from the stagnation point or $\cos\psi$ in the case of a cylinder and to *increase* away from the stagnation point in the case of a sphere. Therefore, in this plane the shock boundary around a circular surface would expand faster than in the plane at right angles to the interplanetary magnetic field. The particle density in this plane away from the stagnation point is less than in the plane perpendicular to the magnetic field.

The particle pressure in this plane is *not* communicated along the field lines and this introduces a complication in the analysis depending on the isotropy of the particle velocity discussed below. Free hand drawings of the field lines are illustrated in Figs. 7 and 8.

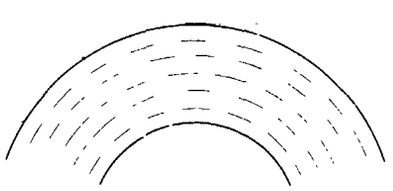

FIGURE 7.—Magnetic field lines indicated by dashed lines in free interplanetary space and in the transition sheath in the plane containing the field direction.

Another aspect of the magnetosphere problem is that turbulence on the surface or the sharp kinks produced in magnetic field lines where the interplanetary field lines are joined to the lines in the magnetosheath will invalidate the simple two dimensional analysis presented in this work. The particle motion in the magnetosheath will be more nearly isotropic in three dimensions

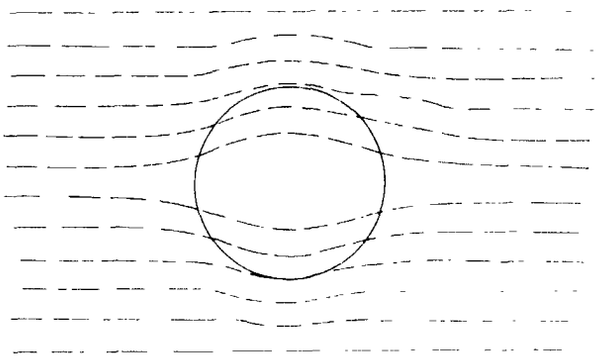

FIGURE 8.—Magnetic field lines, indicated by dashed lines, viewed in projection from the upstream side as they diverge and slide around a spherical obstruction bowing out most pronouncedly in the equatorial plane.

instead of being isotropic in twod imensions. This causes the particle density and field intensity to be three times the interplanetary values and the thickness of the sheath near the stagnation point to be more nearly one-half of the radius of curvature of the magnetosphere.

Independent of these considerations the sudden increase of the magnetic field intensity from the interplanetary field value to the magnetosheath value will cause the magnetosheath electrons to have the same momentum perpendicular to the field lines as the protons do. Thus the particle energy and pressure perpendicular to the field lines will be monopolized by the electrons. The particle energy and pressure parallel to the field lines will be monopolized by the protons, however, since charge separation effects will cause the electron and proton velocities to equalize.

ACKNOWLEDGEMENT

I would like to thank Dr. John Banister of Sandia Corporation for a helpful discussion of this problem. I would also like to thank both the Sandia Corporation and the Goddard Space Flight Center for their hospitality and support of this work.

REFERENCES

1. P J. COLEMAN JR., L. DAVIS JR., E. J. SMITH, and C. P. Sonett Science, **138**, 1099, (1962)
2. N. F. NESS, C. S. SCEARCE, and J. B. SEEK, J. Geophys. Res., in press, (1964).
3. F. DE HOFFMAN and E. TELLER, Phys. Rev. **80**, 692, (1950).
4. P. L. AUER, H. HURWITZ JR., and R. W. KILB, Phys. of Fluids, **5**, 298 (1962).

5. P. J. KELLOGG, J. Geophys. Res., **67**, 3805, (1962).
6. J. R. SPREITER, and W. P. JONES, J. Geophys. Res., **68**, 3555, (1963).
7. W. I. OXFORD, J. Geophys. Res., **67**, 3791, (1962).
8. D. B. BEARD, J. Geophys. Res., **69**, 1159, (1964).
9. L. LEES, Proc. AIAA New York meeting, Jan. 1964 and Cal. Inst. of Tech. preprint.
10. V. C. A. FERRARO, J. Geophys. Res., **57**, 15, (1952).
11. J. W. DUNGEY, Cosmic Electrondynamics, Cambr. Univ. Press, Cambridge, England, 132–152, (1958).
12. M. N. ROSENBLUTH, Dynamics of a Pinched Gas contribution to Magnetohydronamics edited by R. Landshoff, Sanford Univ. Press, Palo Alto, 57–66, (1957).
13. D. B. BEARD, J. Geophys Res., **65**, 3559, (1960).
14. H. Grad, Phys. Fluids, **4**, 1366, (1961).
15. A. SESTERO, Phys. Fluids, **7**, **45**, (1964).

SOLAR CYCLE CHANGES IN INNER ZONE PROTONS

ROBERT C. BLANCHARD† AND WILMOT N. HESS

Time dependent calculations of the inner Van Allen belt proton population show that large changes of the population up to a factor of 50 will take place during the solar cycle. The effect is most pronounced for the region of B–L space corresponding to minimum altitudes of 300–700 km. Because different energy protons respond to the changing solar cycle at different rates the proton energy spectra will change with time also.

The purpose of this paper is to calculate the expected changes in inner zone proton populations with time in the solar cycle.

Freden and White [1959] identified the penetrating component of the inner zone of the Van Allen belt as due to energetic protons and measured the energy spectrum of the protons of $E>75$ Mev. This and subsequent experimental work on Atlas rockets [Freden and White, 1960; Freden and White, 1962; Armstrong, Harrison, Heckman and Rosen, 1961] has confirmed and extended this finding and we now have a well-established proton energy spectrum at $L\sim1.4$, $B\sim.20$, which is about apogee for these flights, for near solar maximum (see Fig. 1). The analysis of this spectrum [Freden and White, 1960] has shown conclusively that the protons are produced by neutron decay.

One of the features of this component of the radiation belt is the time constancy. Measurements after a solar flare [Freden and White, 1962] gave essentially the same fluxes of protons as before the flare. For $L>1.6$ changes in proton spectra are seen [Naugle and Kniffen, 1961] associated with solar proton events [Pizzella, 1961]. These may be explainable in terms of neutrons produced in the polar regions by solar protons [Lenchek, 1962; Lingenfelter, to be published]. For $L<1.6$ only gradual changes in the proton populations have been observed on Explorer VII [Pizzella, 1961]. It was originally suggested [Pizzella, 1961] that such changes implied that neutrons could not produce all inner zone protons but this does not seem to be the case. Hess [1962] showed that slow changes in proton population were expected due to changes in the galactic cosmic ray flux during the solar cycle and more

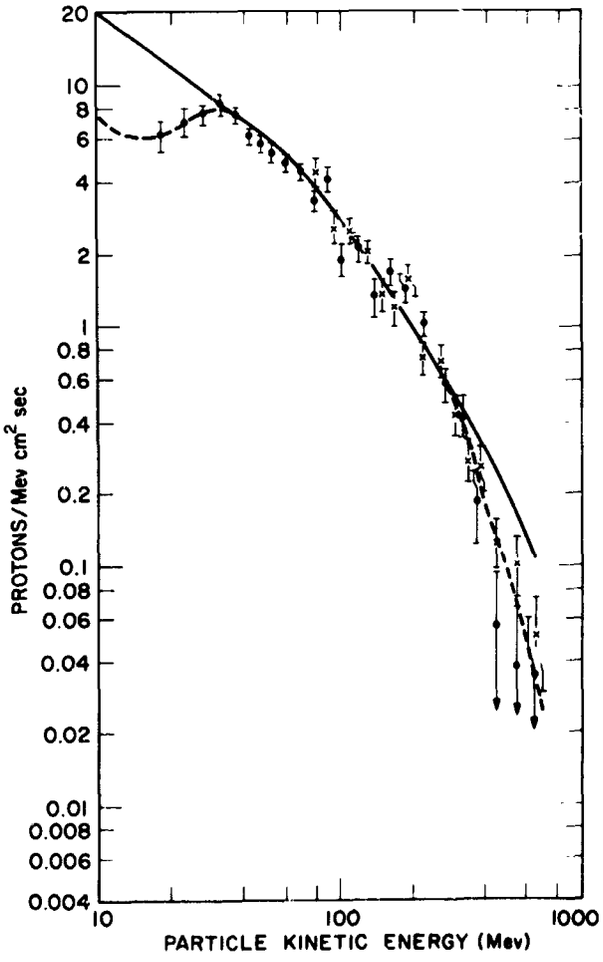

FIGURE 1.—The experimentally measured inner zone proton energy spectrum (Freden and White 1962) for $L\sim1.4B\sim.20$.

†This work was done as part of the requirements for a Master's Degree from the College of William and Mary.

importantly due to changes in the upper atmospheric density during the solar cycle. We will now make a quantitative discussion of the expected changes in proton populations for $L<1.6$.

The continuity equations for protons is usually written [Singer, 1958; Hess, 1959; Freden and White, 1960]

$$\frac{dN(E)}{dt}=+S(E)-L(E)+\frac{d}{dE}\left[N(E)\frac{dE}{dx}v\right]=0 \quad (1)$$

and the steady state population of protons $N(E)$ solved for. We are now interested in time variations so we will write the time dependent form of this equation

$$\frac{dN(E,t)}{dt}=+S(E,t)-L(E,t)+\frac{d}{dE}\left[N(E,t)\frac{dE}{dx}(t)v\right] \quad (2)$$

The source term $S(E, t)$ will use the neutron decay source strength of Hess for solar maximum $S(E)$ multiplied by a function of time $f(t)$ to consider the solar cycle variation in galactic cosmic ray flux as determined by McDonald and Webber [1961]

$$S(Et)=S(E)f(t)=\frac{0.8E^{-2\cdot0}}{\nu\gamma T_n}\frac{re^3}{r}F(t) \quad (3)$$

where $f(t)$ varies from 1.0 at solar max to 1.25 at solar min in a similar way to Fig. 2.

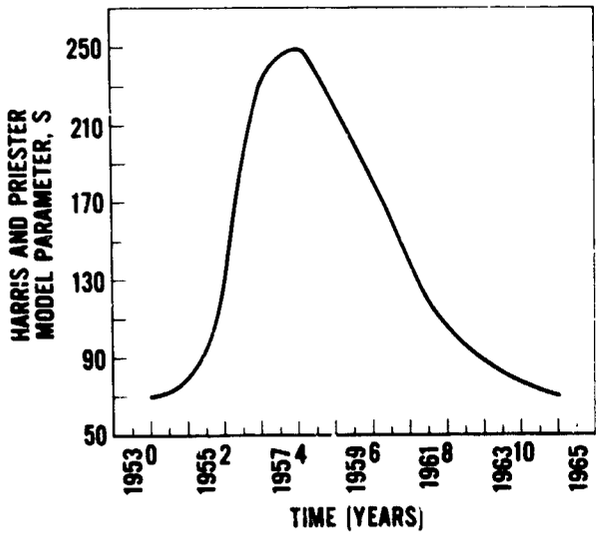

FIGURE 2.—Solar cycle used in these calculations S is the Harris and Priester (1962) model parameter which is related to but not the same as the 10 cm flux intensity.

For the loss term $L(E, t)$ following Freden and White [1960] we consider nuclear collisions

$$L(E,t)=N(E,t)v\Sigma_i\sigma_i\bar{\rho}_i(t) \quad (4)$$

where $\bar{\rho}_i(t')$ is the average atmospheric density of atmospheric component i (O_2, O, N_2 or He) and σ_i is the inelastic cross section for collisions (assumed geometric).

The last term in equation 2, the change in proton population due to slowing down, varies with the solar cycle due to the atmospheric density change

$$\frac{dE}{dx}=\left[\frac{\rho(t)}{2.69\times10^{19}}\right]\times\frac{dE}{dx}\Big|_{NTP} \quad (5)$$

where $\bar{\rho}$ (t) is the average atmospheric density of equivalent oxygen atoms. The variation of $\bar{\rho}_i(t)$ and $\bar{\rho}(t)$ with time in the solar cycle is the major reason for the change in proton population.

AVERAGE ATMOSPHERIC DENSITIES

A major part of this problem was to determine the average atmospheric densities used in calculating the loss rate of trapped protons by coulomb scattering. To do this the theoretical model of the upper atmosphere developed by Harris and Priester [1962] was used. This model gives the time dependences of the atmosphere for both solar cycle and diurnal variations. It agrees well with several measurements of density by satellite drag (King-Hele, 1963; Bryant, to be published) and recently has been checked by preliminary data of densities from the Explorer XVII satellite. Spencer et al [1963] This model atmosphere is the most complete description of the time dependence of atmospheric densities available and agrees well with the current experimental data. We must perform several operations on the H and P model data to get it in form to use for this problem. Harris and Priester give the atom densities n_i of the several atmospheric constituents i in the form of.

$$n_i(h, t, S)$$

where h is altitude above the earth, t is local time, and S is a model parameter related to, but not the same as, the intensity of the average 10 cm solar flux, F, in watts/m^2-cps$\times10^{-22}$. Recent studies of atmospheric densities [Harris and

Priester, 1963] show that the model number S is the same as $\bar{F}$ near solar max but near solar min $S<\bar{F}$. For example, $\bar{F}=70$ corresponds to the model $S=100$. Fig. 2 shows the solar cycle variation of S we have used based on the last solar cycle.

The first operation on the H and P atmosphere is to average over local time. The protons we will consider live long enough so that they will encounter the midday density bulge and the nighttime minimum many times and will average them out.

Secondly, we perform a longitude average. As the particles drift around the earth their mirror points do not stay at constant altitude but rather follow a certain path in B–L space. Several such constant B–L rings are shown in altitude-longitude coordinates in Fig. 3. The particles dip

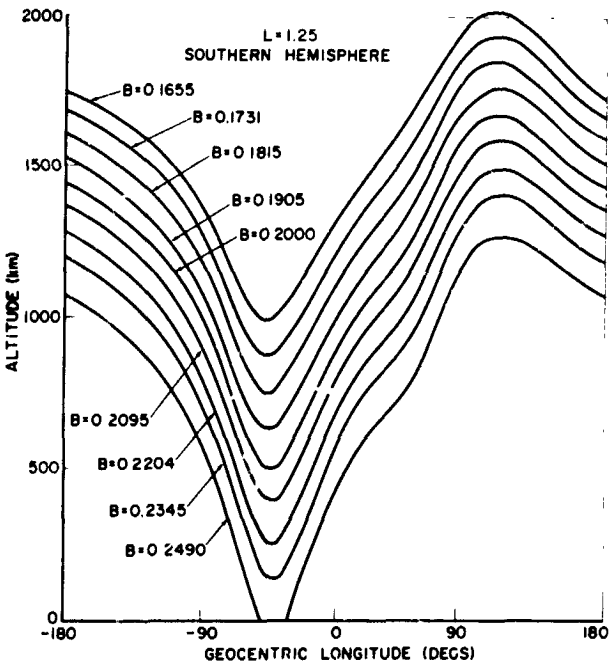

FIGURE 3.—Variation of the altitude of B-L rings with longitude.

lowest in the South Atlantic due to the nature of the earth's magnetic field. A B–L map of minimum altitudes is shown in Fig. 4. Due to the variation in altitude of the protons' mirror point, longitude averages were made using the B–L rings every ten degrees in both northern and southern hemispheres. This step gives the average mirror point density for a proton's motion. Walt has recently shown that the protons do not

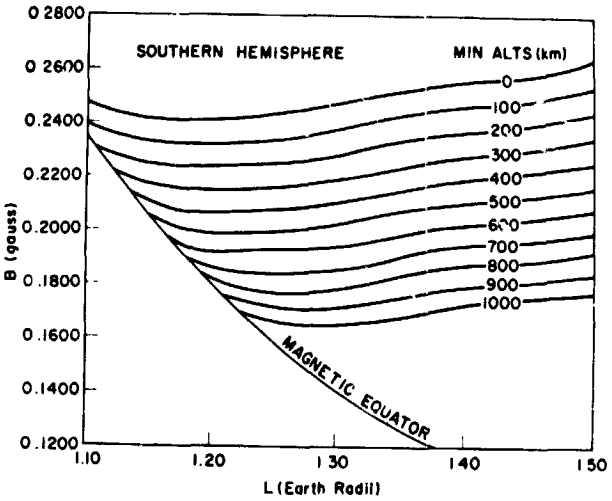

FIGURE 4.—B–L map of minimum altitudes.

drift in longitude at a constant rate because of the variation of the magnetic field gradient and field line curvature. This effect is ignored here. It probably amounts to about a 20 percent correction on average densities. Values of atmospheric densities are not known that well now anyway.

The third operation on the H and P atmosphere is to average over a bounce from one mirror point to the conjugate mirror point. Since the protons live much longer than a bounce period, and since no change in direction of the proton is considered during slowing, it is permissible to average the density in this fashion. A dipole field is assumed in carrying out this step.

Ray [1960] gave the bounce averaging process as

$$\rho=\frac{\int\rho(\lambda)ds}{\int ds} \tag{6}$$

where the element of length along the particle's orbit is

$$ds=\frac{vdt}{\cos\alpha}=\frac{d\ell}{\cos\alpha} \tag{7}$$

where $d\ell$ is the element of length along the field line. Using

$$d\ell^2=dr^2+r^2d\lambda^2 \tag{8}$$

and

$$r=L\cos^2\lambda \tag{9}$$

with the mirror equation and the expression for the magnetic field variation along a field line

combining and substituting in equation 6 gives

$$\bar{\rho}_i = \frac{\int \rho_i(\lambda) A(\lambda) d\lambda}{\int A(\lambda) d\lambda} \tag{10}$$

where

$$A(\lambda) = \frac{\cos^4 \lambda 1 + 3 \sin^2 \lambda}{[\cos^6 \lambda (1+3 \sin^2 \lambda_m)^{\frac{1}{2}} - \cos^6 \lambda_m (1+3 \sin^2 \lambda)^{\frac{1}{2}}]^{\frac{1}{2}}} \tag{11}$$

The subscript m here corresponds to the particles' mirror point. This bounce averaged density has been integrated on a computer.

The last step is to combine the five i constituents N_2, O_2, O, He and H to give the averaged number of equivalent oxygen atoms

$$8\bar{\rho} = 14\bar{\rho}(N_2) + \bar{\rho}(O) + 16\bar{\rho}(O_2) + 2\bar{\rho}(He) + \bar{\rho}(H) \tag{12}$$

Values of $\bar{\rho}$ at different times in the solar cycle for $L = 1.25$ are shown in Figure 5.

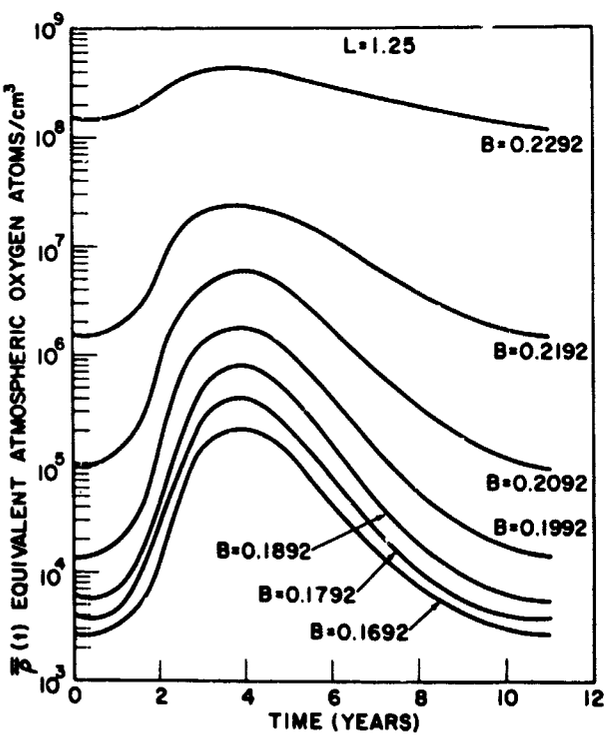

FIGURE 5.—Average atmospheric densities at different times of the solar cycle at different B–L points.

We can use the data on the rate of energy loss dE/dx for oxygen at NTP [Aaron, Hoffman and Williams, 1949] in equation 5 with this averaged density $\bar{\rho}$ to calculate the loss rate.

RESULTS

Equation (2) is integrated stepwise starting with $N(E) = O$ at $t = O$ to build up to an oscillating proton population which is the same from one

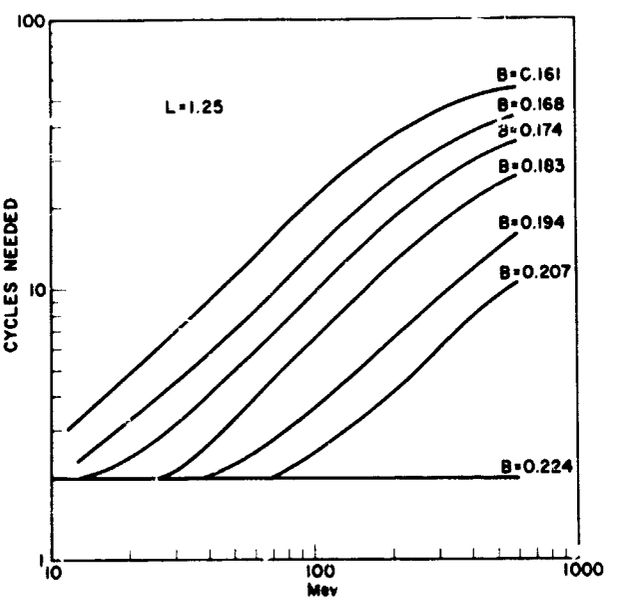

FIGURE 6.—The number of solar cycles needed for a group of protons to come within 1% of its final oscillating population for $L = 1.25$ starting with $N(E) = O$ at $t = O$.

solar cycle to the next. In Figure 6 is shown the number of solar cycles after which the population change per cycle is less than 1 percent for $L = 1.25$. After achieving this final condition the proton energy spectrum varies during one solar cycle as shown in Figures 7–11. The dotted curves top and bottom in these figures are what the proton spectrum would be if steady state conditions were achieved at solar max and solar min. Steady state clearly is not achieved for high energy protons or for high altitudes.

It is also interesting that this calculation predicts a spectral peak above 100 Mev for certain conditions (Figure 7, year 3) due to the time lag

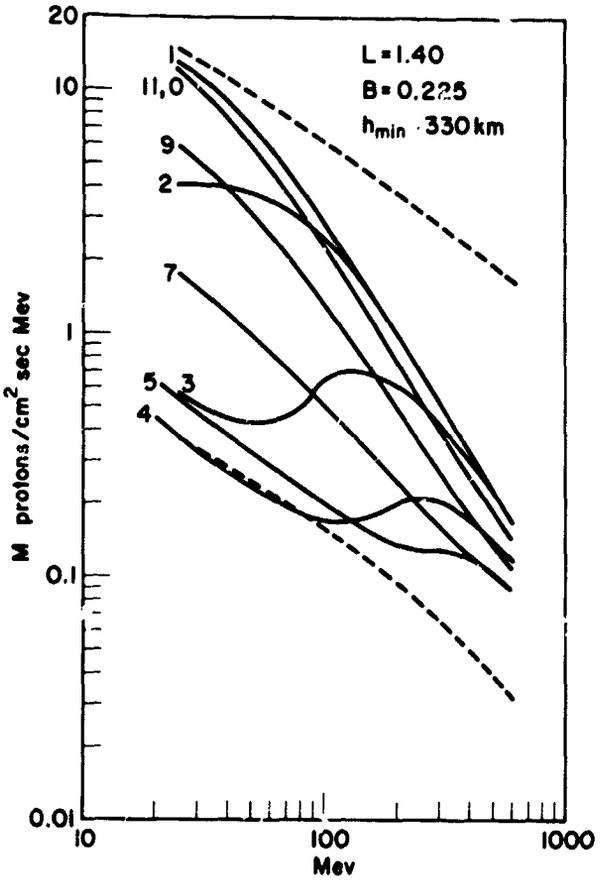

FIGURE 7.—Proton energy spectra at different times in the solar cycle for $L=1.40$, $B=.225$. The curves are labeled by the time in years from solar min.

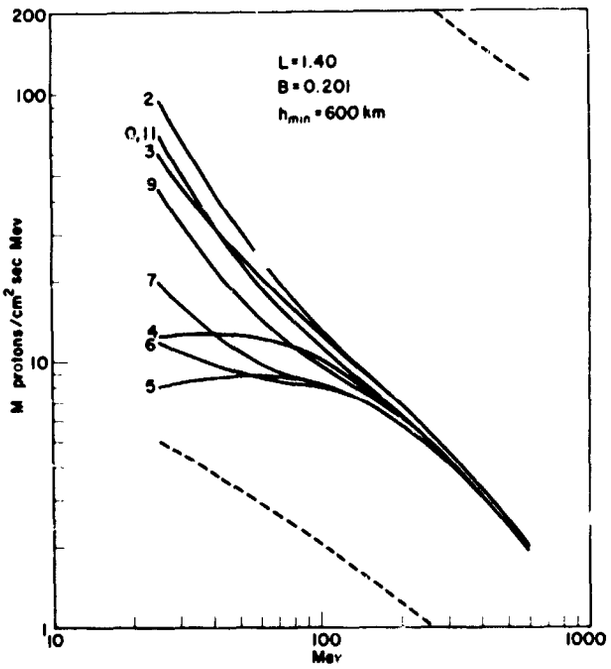

FIGURE 8.—Proton energy spectra at different times in the solar cycle for $L=1.40$, $B=.201$. The curves are labeled by the time in years from solar min.

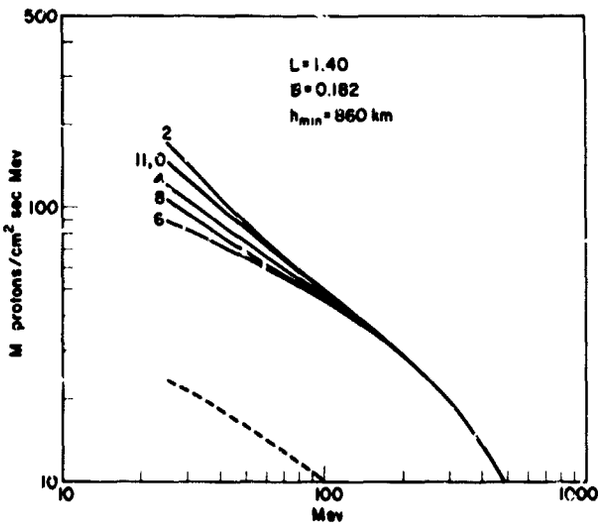

FIGURE 9.—Proton energy spectra at different times in the solar cycle for $L=1.40$ $B=.181$. The curves are labeled by the time in years from solar min.

in different energy protons adjusting to solar cycle changes.

Figures 12 and 13 show time histories for various conditions. Large variations from solar max to solar min populations are seen in these figures. The amplitude of these changes for $L=1.25$ and 1.40 are shown in Figures 14 and 15.

A comparison of past experimental results and the calculations of this paper is shown in Table I. In discussing these experiments we can consider three types of information.

In comparing time changes of the proton fluxes two situations occur:

1. Some individual experiments run long enough (a year or more) so that they should see proton flux changes directly. From Table I, experiments (*c*) and (*d*) are of this time. Although in experiment (*d*) it is not one experiment on one satellite, it is many identical experiments on essentially identical satellites, and therefore this experiment falls in this category.

2. Different experiments on different satellites can be compared to provide data on proton flux changes. Data of this type is given in experiments (*a*), (*e*) and (*f*) in Table I.

The third type of data is given by:

3. Direct measurement of the proton energy

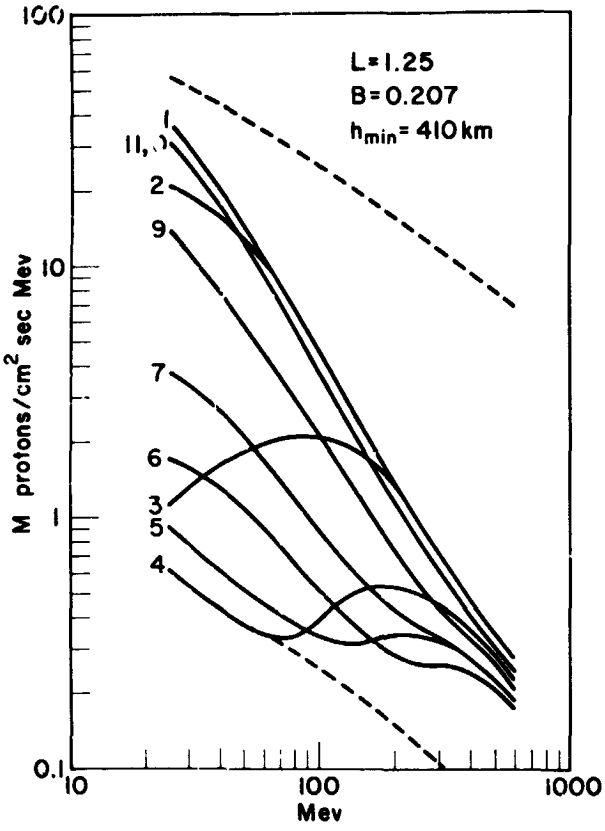

FIGURE 10.—Proton energy spectra at different times in the solar cycle for $L=1.25$, $B=.207$. The curves are labeled by the time in years from solar min.

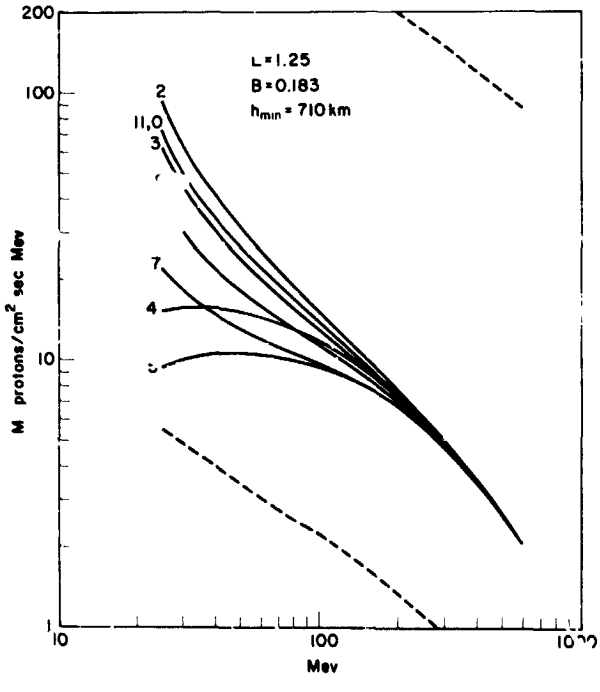

FIGURE 11.—Proton energy spectra at different times in the solar cycle for $L=1.25$, $B=.183$. The curves are labeled by the time in years from solar min.

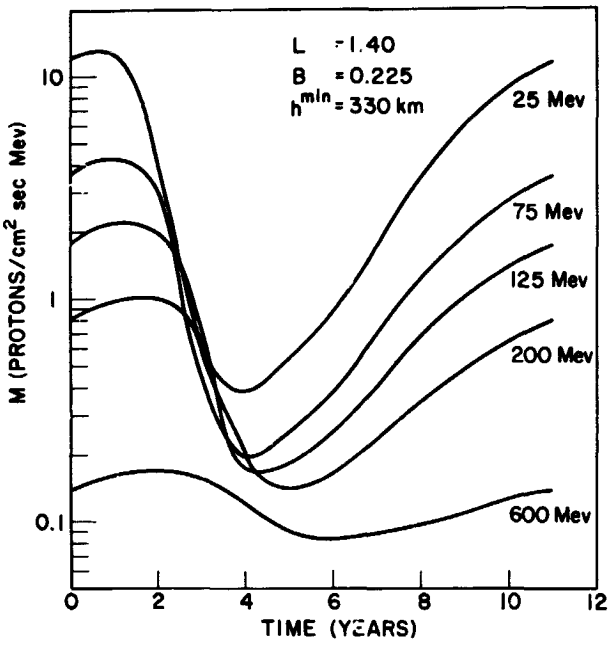

FIGURE 12.—Proton time histories for $L=1.40$, $B=.225$.

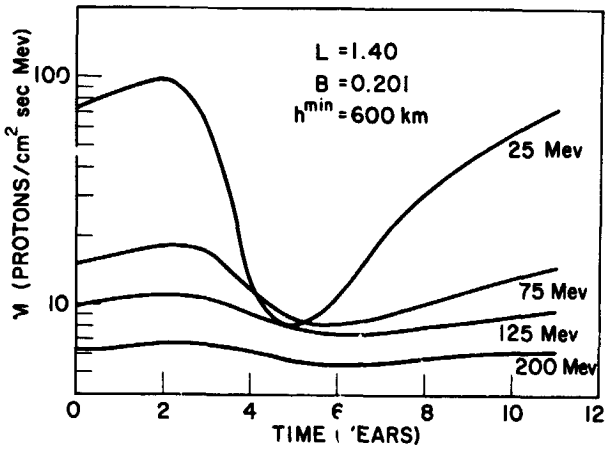

FIGURE 13.—Proton time histories for $L=1.40$, $B=.201$.

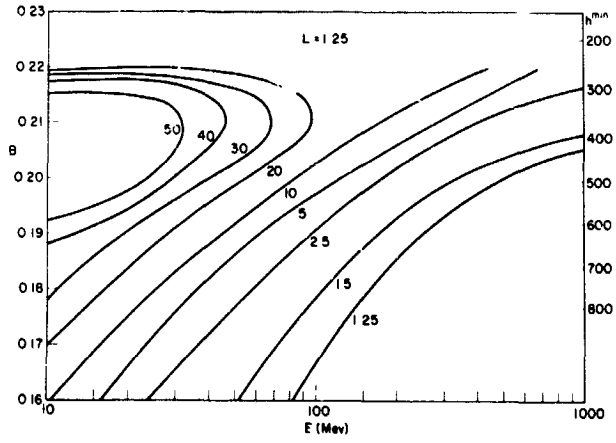

FIGURE 14.—The amplitude of the proton population change during the solar cycle for $L=1.25$.

TABLE 1.

Experiment	Date of Experiment	Time in Solar Angle	L	B	H Min.	Results of Experiment	Predictions from Present Paper
(a) Naugle and Kniffen (1963)—Emulsions on NERV	Sept., 1960	6.7	(a) 1.54	.209	610 km	Spectrum~flat from 20 to 60 MeV $\frac{Jo\ (31)\text{ at }6.7}{Jo\ (31)\text{ at }4.1\text{ (Exp. IV)}} \sim k$	Spectrum should fall about a factor of 3 in this energy range (Fig. 8. curve 7) $\frac{Jo\ (31)\text{ at }6.7}{Jo\ (31)\text{ at }4} = 1.3$ (Fig. 8)
			(b) 1.47	.223	400 km	Spectrum~flat from 10 to 100 MeV $\frac{Jo\ (31)\text{ at }6.7}{Jo\ (31)\text{ at }4.1\text{ (Exp. IV)}} \sim 2.5$	Spectrum should fall about a factor of 4 in this energy range (Fig. 7, curve 7) $\frac{Jo\ (31)\text{ at }6.7}{Jo\ (31)\text{ at }4} = 3.5$ (Fig. 7)
(b) Freden and White (1962)—Emulsions on Atlas	1960	6.5	~1.40	~.202	600 km	Spectrum peaks at ~ 40 MeV $\frac{Jo\ (20)}{Jo\ (40)} \sim .75$	No spectral peak at t=6.5 (Fig. 8) $\frac{Jo\ (20)}{Jo\ (40)} \sim 2.0$ but at t=5 do have spectral peak $\frac{Jo\ (20)}{Jo\ (40)} = 0.9$
(c) Pizzella, McIlwain and Van Allen—GM counter on Exp. VII	Oct. 1959 to Dec. 1960	5.8 to 7.0	1.40	.22	390 km	$\frac{Jo\ (E>18)\text{ at }7.0}{Jo\ (E>18)\text{ at }6.0} \sim 2.3$	$\frac{Jo\ (E=25)\text{ at }7.0}{Jo\ (E=25)\text{ at }6.0} = 2.0$ (Fig. 12)
(d) Filz and Yagoda—Emulsions on Discoverer	Dec. 1960 to June 1962	7.0 to 8.5	vary-ing	vary-ing	400 km	$\frac{Jo\ (E>55)\text{ at }8.5}{Jo\ (E>55)\text{ at }7.0} \sim 2.0$	$\frac{Jo\ (E=75)\text{ at }8.5}{Jo\ (E=75)\text{ at }7.0} \sim 2.3$ (Fig. 12)
(e) Heckman and Nakano—Emulsions on Low altitude polar satellites	Sept. 1962 to Sept. 1963	8.7 to 9.7	vary-ing	vary-ing	400 km	$\frac{Jo\ (65)\text{ at }9.5}{Jo\ (65)\text{ at }9.0} = 1.0 \pm .10$ $\frac{Jo\ (65)\text{ at }9.5}{Jo\ (65)\text{ at }4.1\text{ (Exp. IV)}} \sim 3$	$\frac{Jo\ (65)\text{ at }9.5}{Jo\ (65)\text{ at }9.0} = 1.2$ $\frac{Jo\ (65)\text{ at }9.5}{Jo\ (65)\text{ at }4.1} = 12$
(f) Freden and Paulikos—Solid state counters on Polar satellites	Sept. and Oct., 1962	8.8	1.30	.200	530 km	$\frac{Jo\ (7)}{Jo\ (85)} \sim 13$	
			1.47	.223	400 km	$\frac{Jo\ (7)}{Jo\ (85)} \sim 23$	$\frac{Jo\ (10)}{Jo\ (85)} \sim 11$ (Fig. 7)
			1.54	.209	610 km	$\frac{Jo\ (7)}{Jo\ (85)} \sim 43$	$\frac{Jo\ (10)}{Jo\ (85)} \sim 24$ (Fig. 8)
			low	high		$\frac{J\ (E>31)\text{ at }8.8}{J\ (E>31)\text{ at }4.1\text{ (Exp. IV)}} \sim 3$	$\frac{J\ (E=50)\text{ at }8.8}{J\ (E=50)\text{ at }4.1} = 13$
(g) Rowland Bakke, Imhof, Smith (1963) scintillators on Atlas pods	March, 1963	9.2	1.27	.216	340 km	no maximum at 40 MeV $\frac{Jo\ (20)}{Jo\ (40)} \sim 2.0$	$\frac{Jo\ (20)}{Jo\ (40)} = 2.2$ (Fig. 10)
						$\frac{Jo\ (10)}{Jo\ (60)} \sim 8.0$	$\frac{Jo\ (10)}{Jo\ (60)} = 9.0$

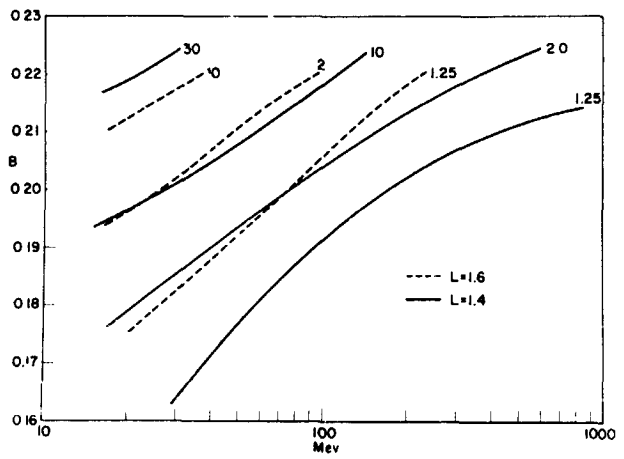

FIGURE 15.—The amplitude of the proton population change during the solar cycle for $L=1.4$ and 1.6.

spectrum in one experiment. Experiments (*a*), (*b*), (*e*), (*f*) and (*g*) are of this type.

In comparing flux time change experiments of type (1) with the calculations, the agreement is good. Two experiments covering the period 1959 to 1962 give results consistent with the calculations.

Comparing with type (2) data does not work as well. The observed changes of flux with time agree qualitatively with those predicted but not quantitatively. The experimental flux ratios are smaller than the calculated ones. Two remarks are in order here. First, type (2) data usually has larger errors attached to it than type (1) because it involves the systematic errors of two experiments while type (1) data involves no systematic errors—only statistical errors are involved in the time variations in the flux. Because of this the experimental flux ratios using type (2) data are probably not as accurate as those using type (1) data. Secondly all the comparisons of type (2) data involve Explorer IV data so there is no independent check of experimental consistency.

We may have over-estimated the amplitude of the change of proton populations in this present calculation by as much as a factor of two because our solar cycle model uses $S=70$ at solar minimum while recent data of Harris and Priester (1963) shows that $S=100$ is probably more appropriate. Changing the shape of the model solar cycle (Figure 2) will also affect the results of the calculation. The solar cycle must rise more rapidly towards solar max. than it falls to solar min. in order to produce the changes in spectrum calculated here. Solar cycle 16 was quite symmetrical and should not give the calculated results.

Of the five experiments of type (3) that help understand the proton energy spectrum the first two (*a*) and (*b*) in 1960 showed a modest sized peak at about $E=40$ Mev. The more recent experiment (*g*) of Rowland et al in 1962 shown in Figure 16 does not show such a peak. The solid curve on Figure 16 compared with the data of Rowland is the results of the present calculations normalized. The agreement is fairly good. Recent experiments (*f*) (*g*) show a large low energy proton population but cannot be compared with early experiments because the early ones did not go down to such low energies. Figures 7–11 show that the calculated spectral shape should not change much during the period of these measurements—from 6 to 9 years solar cycle time The proton fluxes should increase but the shape of the spectrum stays nearly the same. Striking changes in spectral shape should occur on the upswing of the solar cycle. The agreement with spectral shape in Figure 16 is not bad but the peaks in experiments (*a*) and (*b*) should not occur at $t=6$. It may be that a neutron absorption as suggested

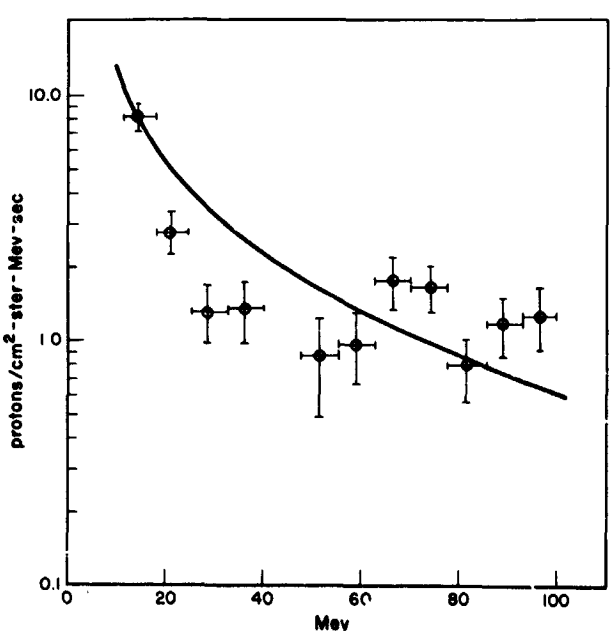

FIGURE 16.—The energy spectrum of inner zone protons measured by Rowland et al, 1963, on an Atlas pod at $L=1.27$, $B=.216$ shown for comparison is the spectrum calculated in this paper for $L=1.27$, $B=.207$, $t=9$.

by Freden and White (1962) is required to explain the peak.

All of the information presented so far on Figures 6 through 15 are mirror point fluxes M, that is, the flux of protons mirroring per unit volume at one particular B and L. For low altitudes where the atmosphere changes rapidly with altitude it is nearly correct to compare this flux with measured omnidirectional flux values. For these low altitudes the omnidirectional flux is very nearly the same as the mirror point flux. To show a more complete picture of the solar cycle proton changes we have converted to omnidirectional fluxes using equations (24) of Hess and

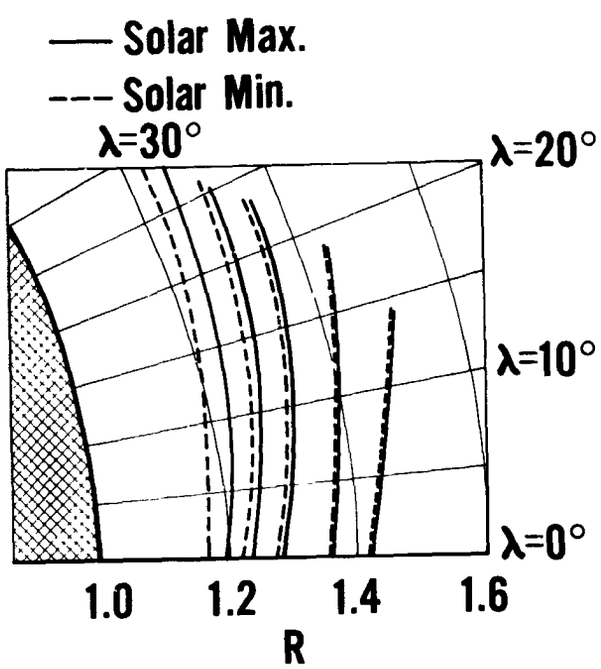

FIGURE 17.—An $R-\lambda$ map of the omnidirectional flux of $E=25$ Mev protons at solar max and solar min.

Killeen (1961). Figure 17 shows a calculated R–λ map of the 25 Mev proton omnidirectional fluxes J at solar max and solar min. An isoflux contour is clearly at lower R for solar minimum.

In conclusion we have shown that large changes in proton fluxes will take place during the solar cycle for those regions of B–L space corresponding roughly to minimum altitudes of about 300–700 km. Changes in proton spectra will occur also. Comparison of the calculations with available experimental information are not conclusive. Some kinds of experimental data agree quantitatively with the calculations. Other data agrees qualitatively but not quantitatively. The crucial tests of the calculations will involve measuring changes in the proton flux and spectrum as we approach solar maximum during 1966–68. We know experimentally (King-Hele 1963) that the atmospheric density changes used in the calculation are reasonable These calculated effects must take place with about the magnitudes shown here unless there are features of the inner belt protons which we do not now understand.

REFERENCES

1. ARMSTRONG, A. H., F. B. HARRISON, H. H. HECKMAN, and L. ROSEN, Charged particles in the inner Van Allen radiation belt, *J. Geophys. Research*, 66 351–8 (1961).
2. ARON, W. A., B. S. HOFFMAN, F. C. WILLIAMS, "Range-Energy Curves" (2nd Rev. 1949) U. S. A.E.C., Univ of Calif. Rad. Lab.
3. BRYANT, R., Densities Obtained from Drag on the Explorer XVII Satellite, to be published.
4. FILZ, R., and H. YAGODA "Observations on Trapped Protons in Emulsions Recovered from Satellite Orbits" to be published in Space Research IV and private communication.
5. FREDEN, S. C., R. S. WHITE, Protons in the Earth's Magnetic Field Phys. Rev. Letters **3** 9–11 (1959).
6. FREDEN, S. C., R. S. White, "Particle Fluxes i the Inner Radiation Belt" *J. of Geophys. Res.*, vol. 65, no. 5, May 1960.
7. FREDEN, S. C., R. S. WHITE, "Trapped Proton and Cosmic-Ray Albedo Neutron Fluxes", J. of Geophys. Res., vol. 67, no. 1, January 1962, p. 25.
8. FREDEN, S. C., and G. A. PAULIKAS, "Trapped Protons at Low Altitudes in the South Atlantic Magnetic Anomoly" Tech. Doc. SSD-TDR-63-342, Aerospace Corporation, Inglewood, Calif.
9. HARRIS, I., and W. PRIESTER, "Theoretical Models for the Solar-Cycle Variation of the Upper Atmosphere" X-640-62-70, June 1962, and J. A. S. **19** 286 (1962), Time-Dependent Structure of the Upper Atmosphere.
10. HARRIS, I., and W. PRIESTER, Relation between Theoretical and Observational Models of the Upper Atmosphere, J. of Geophysical Res. **68** 5891, 1963.
11. HECKMAN, H. and G. H. NAKANO "East-West Assymmetry in the Flux of Mirroring Geomagnetically Trapped Protons" J.G.R. **68** 2117, 1963 and private communications.
12. HESS, W. N., "Discussion of paper by Pizzella, McIlwain and Van Allen" J. of Geophys. Res., **67** 4886 (1962) and "Lifetime and Time Histories of Trapped Radiation Belt Particles" Space Research Vol. III, to be published.
13. HESS, W. N. and J. KILLEEN "Special Distribution of Electrons from Neutron Decay in the Outer Radiation Belt" J. G. R. **66** 3671 (1961).

14. Hess, W. N., "Van Allen Belt Protons from Cosmic-Ray Neutron Leakage" Phys. Rev. Letter **3** 11 (1959).
15. King-Hele, D. G., "Decrease in Upper-Atmosphere Density since the Sunspot Maximum of 1957–58" Nature **198** 832 (1963).
16. Rowland, J. H., J. C. Bakke, W. L. Imhof, and R. V. Smith, "Radiation Environment Experiment" Tech. Report SSD-TDR-63-194, Lockheed Missiles and Space Co., Palo Alto, California.
17. Lencheck, A. M., J. of Geophys. Res., **67** 2145 (1962).
18. Lingenfelter, R. E., to be published.
19. McDonald, F. B., and W. R. Webber, "A study of the rigidity and charge dependence of primary cosmic ray temporal variations" Journal of the Physical Society of Japan, vol. 17, Supplement A-II, Proceedings of the International Conference on Cosmic Rays and the Earth Storm, September 4–15, 1961.
20. Naugle, J. E., and D. A. Kniffen, Flux and Energy Spectra of the Protons in the Inner Van Allen Belt, Phys. Rev. Letter **7** 3 (1961) and "Variations of the Proton Energy Spectrum with Position in the Inner Van Allen Belt" J.G.R. **68** 4065 (1963).
21. Pizzella, G., C. E. McIlwain and J. A. Van Allen, Time Variations of Intensity of the Earth's Inner Radiation Zone, October 1959 through December J.G.R. **67** 1235, 1962.
22. Ray, Ernest C., "On the Theory of Protons Trapped in the Earth's Magnetic Field" J. of Geophys. Res., vol. **67**, no. 4, April 1960, pp. 1125–1133.
23. Singer, S. F., "Trapped Albedo Theory of the Radiation Belt" Phys. Rev. Letter **1** 181 (1958).
24. Spencer, N. W., L. H. Brace, C. R. Corignan, D. R. Taeusch and H. Niemann, "The Concentration and Temperature of Molecular Nitrogen and Electrons in the 120 to 350 km Region," L. H. Brace and N. W. Spencer, "Geophysical Implications of Explorer XVII Electrostatic Probe Measurements," Horowitz, R., and G. P. Newton, "First Direct In-Site Measurements of Atmospheric Density from Explorer XVII," Reber, C. C., "Preliminary Results Regarding Neutral Atmosphere Composition from the Explorer XVII Satellite," abstracts at the Boulder AGU Meeting, Dec. 1963, Transactions of AGU **44** 884 (1963).

N64-27353

A NEUTRAL-POINT EXPANSION OF THE IDEAL MAGNETOSPHERE*

RONALD BLUM†

The idealized model of the geomagnetic field–solar wind interaction yields a singular (neutral) point on the magnetopause at which the magnetic field vanishes. If we expand the fields in a power series around this point, including quadratic terms, we can derive an approximate equation of the magnetopause in a small neighborhood of the neutral point which is consistent with the idealized boundary conditions to fourth order. We then consider the additional pressure due to multiple reflections of particles in this neighborhood and show that less than a 4 per cent correction to the single-reflection pressure condition is necessary.

INTRODUCTION

In the idealized model of the geomagnetic field–solar wind interaction [*Beard*, 1960] we assume the field to be excluded from the plasma and contained in a cavity called the magnetosphere. The boundary of the cavity, or magnetopause, is unknown, but we stipulate the dynamic condition that the magnetic pressure just inside the magnetopause be exactly balanced by the kinetic pressure of solar wind particles elastically reflected from the surface (thermal effects are neglected). Figure 1 is a schematic drawing of the magnetosphere with the dipole located at the origin of coordinates and perpendicular to the direction of the plasma stream.

Mathematically, this situation is described by the field

$$\mathbf{H} = -\text{grad}\ \Omega \qquad \nabla^2\Omega = 0 \qquad (1)$$

inside the magnetosphere, and the boundary conditions

$$\mathbf{H}\cdot\text{grad}\ F = 0 \quad \text{(confinement)} \qquad (2)$$

$$\mathbf{H}\cdot\mathbf{H} = \beta^2 \cos^2\chi \quad \text{(pressure)}$$

which hold on the surface, $F(x', y', z') = 0$, where χ is the angle of incidence of the incoming plasma (Figure 1), and $\beta^2 = 8\pi(2nm_iV^2)$. V, n, and m are the plasma drift velocity, ion number density, and ion mass, respectively.

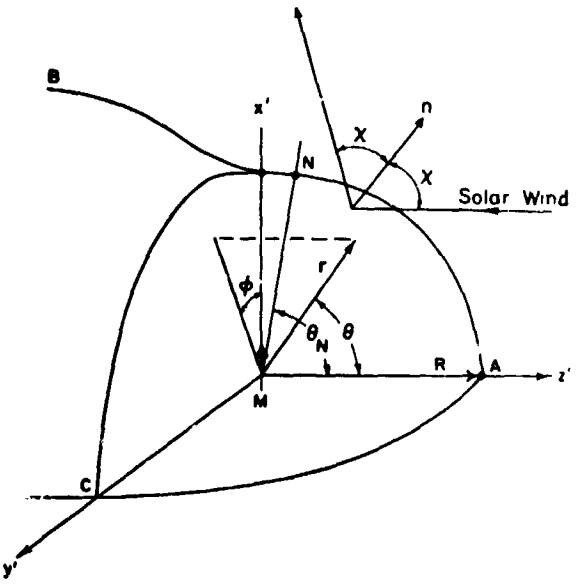

FIGURE 1.—Schematic drawing of the magnetosphere.

A singular point on this unknown surface is N, the neutral point, where the magnetic field lines 'split,' the field vanishes, $\chi = \pi/2$, and the gradient is in the x' direction. Although the problem is unsolved as yet, there are some good approximations to the general shape [*Mead and Beard*, 1963; *Spreiter and Briggs*, 1962; *Midgley and Davis*, 1963]. However, these approximations generally fail in the region of the neutral point, a region of interest since, if it does exist, it is likely to be

*Published in *Journal of Geophysical Research*, 69(9): 1765–1768, May 1, 1964.

†National Academy of Sciences—National Research Council Postdoctoral Research Associate with NASA.

unstable, and a possible point of entry for high-energy particles into the magnetosphere.

The neutral point considered here is an X-type neutral point [*Dungey*, 1958, pp. 39–41, 51–52, 98–102]; however, it lies *on* a bounding surface, which must run parallel to one of the limiting

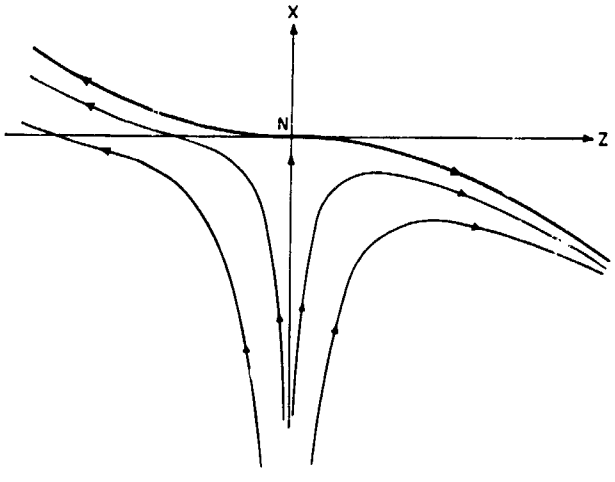

FIGURE 2.—Fields near the neutral point in the noon meridian plane.

field lines (Figure 2). We must assume that surface currents can be made to account for the disappearance of the field outside the surface (magnetopause).

SERIES REPRESENTATION

We can represent the field $\mathbf{H}=\beta\mathbf{h}$ by means of its scalar potential Ω. We first transform to the (x, y, z) coordinate system with origin at N such that

$$R(dx, dy, dz)=(dx', dy', dz') \tag{3}$$

In a region small compared to the apex radius R, we have $x^2+y^2+z^2\ll 1$. The scalar potential is expanded in the form

$$-\Omega/\beta=ax^2+by^2+cz^2+dx^3+ey^3+fz^3 +mxy^2+nxz^2+rzx^2+szy^2 \tag{4}$$

We must include cubic terms in the potential, since we expect the limiting field lines to be curvilinear in the xz plane. There are no linear terms, because the field must vanish at N; terms in y to the first power are deleted, because symmetry requires $H_y=0$ in the xz plane. The dependence on xz has also been omitted, since for $y=0=z$ there should only be an x component of H on the x axis (Figure 2).

The gradient of (4) yields the normalized field:

$$\begin{aligned} h_x&=2ax+3dx^2+my^2+nz^2+2rxz \\ h_y&=2by+3ey^2+2mxy+2szy \\ h_z&=2cz+3fz^2+2nxz+rx^2+sy^2 \end{aligned} \tag{5}$$

and the requirement $\nabla\cdot\mathbf{H}=0$ yields

$$\begin{aligned} &a+b+c=0 \quad 3d+m+n=0 \\ &3f+r+\cdots\ e=0 \end{aligned} \tag{6}$$

Furthermore, as Figure 2 shows, we expect $a<0$, $c>0$.

NOON MERIDIAN CONTOUR

In the xz plane the boundary conditions (equation 2) on the noon meridian contour become $(dx/dz=x')$:

$$h_x/h=-F_z/F_x=x' \tag{7}$$

$$h_x^2+h_z^2=x'^2/(1+x'^2) \tag{8}$$

If we substitute for x' in (7) and (8), then

$$h_x^4+h_x^2(2h_z^2-1)+h_z^4=0 \tag{9}$$

and, since both components must vanish at N,

$$h_x^2=(1-2h_z^2-(1-4h_z^2)^{1/2})/2\to h_z^4\to N \tag{10}$$

From Figure 2 we see that h_x is opposed in sign to the coordinate z on the noon meridian countour. Thus, sufficiently close to N,

$$h_x=\pm h_z^2 \text{ for } z\lesssim 0 \tag{11}$$

If we substitute into (7) and differentiate,

$$x''=\pm dh_z/dz \quad z\lesssim 0 \tag{12}$$

which leaves two alternatives: either x'' is discontinuous at N or $x''=0$ at N. The latter implies $c=0$, which is inconsistent with the geometry of the limiting field line in the xz plane. Thus the curve, $\{x=x(z),\ y=0\}$, must be represented as two separate power series for $z\lesssim 0$. Since (11) must be satisfied on the noon meridian contour, it gives an implicit representation of that contour near N. This must agree with $x=\int dz h_z/h_z$ of

(7) and with Figure 2. The leading term of (11) is

$$2ax+nz^2=\pm 4c^2z^2 \qquad (13)$$

If $n=0$, equation 13 implies that a is of positive sign, which contradicts Figure 2. Therefore we must assume that n has two different values, according to the sign of z. This is permissible as long as $\mathbf{h}$ remains continuous at $z=0$, and $\nabla\cdot\mathbf{h}=0$ everywhere. If we compare (13) with the leading term of (7), we find

$$x'=\pm h_z\lesssim 0 \qquad x=\pm cz^2 \qquad (14)$$

near N. Thus, (13) becomes

$$n=\pm 2c(2c-a) \text{ for } z\lesssim 0 \qquad (15)$$

SURFACE REPRESENTATION

Since the gradient is in the x direction at N, we can represent the surface by two second-order expansions in (y, z):

$$F(x,y,z)=x-A^{\pm}z^2-B^{\pm}y^2-C^{\pm}yz=0 \qquad (16)$$

for $z\lesssim 0$. By symmetry, $B^+=B^-=B$; (14) requires $A^+=-A^-=c$. If we form the dot product $H\cdot\nabla F=0$ and substitute for x form (16) we find the confinement condition satisfied to second order in z^2, y^2, and yz when

$$m=2B(2b-a) \qquad (17)$$

$$C^{\pm}(1-b/a-c/a)=0 \qquad (18)$$

The divergence conditions (equations 6) require that d also be discontinuous, since $3d+m+n=0$, although m is continuous. Therefore, from (17) and (15),

$$3d=\pm 2c(a-2c)+2B(a-2b)z\lesssim 0 \qquad (19)$$

Equation 18 is incompatible with $a+b+c=0$ unless $C^{\pm}=0$. Although (19) forces h_z to be discontinuous at $z=0$ ($a\neq 2c$), the 3 dx^2 term is negligibly small compared to the ax term in (5).

Third-order terms in $\mathbf{H}\cdot\nabla F=0$ are eliminated by simply setting $f=0=s$. Then, by the divergence condition, $r=0$ also. Thus in the power series representation, the confinement condition of (2) is satisfied up to fourth-order errors, on the postulated surface of (16). If we substitute the expansions for $\mathbf{h}$ and $F(x, y, z)$ into the pressure condition of (2), we find

$$h_x^2+h_y^2+h_z^2=\cos^2\chi$$
$$\doteq(\partial F/\partial z)^2(1-\text{2nd-order terms}) \qquad (20)$$

and expanding $\mathbf{b}$ yields

$$4c^2z^2+4b^2y^2+\text{4th-order terms}$$
$$=4c^2z^2(1-\text{2nd-order terms}) \qquad (21)$$

By setting $b=0$ we can reduce the error in the second boundary condition to fourth order. Our final expansion for the field in the neighborhood of N is given by:

$$-\Omega/\beta=cz^2-cx^2-(m\pm 6c^2)x^3/3$$
$$+mxy^2\pm 6c^2xz^2 \qquad (22)$$

and the surface of the magnetosphere near N is given by

$$F(x,y,z)=x-(\pm)cz^2-my^2/2c \qquad (23)$$

for $z\gtrsim 0$.

MULTIPLE REFLECTIONS AT N

Midgley and Davis [1963] have observed that the effect of multiple reflections of particles near N might seriously alter the pressure condition (equation 2) near the neutral point. In the second-order approximation, we can show that the shape of the surface is consistent with the pressure condition to within 4 per cent. This effect would be most pronounced in the xz plane; we shall calculate the added pressure δp at a point (x, z) on the noon meridian contour due to multiple reflections.

Figure 3 represents a particle incident on the point (x_0, z_0) on the contour $x=cz^2$, $z\lesssim 0$, $y=0$, with an angle of incidence χ_0. This particle, on first reflection, strikes the magnetopause again at (x, z) where

$$(x-x_0)/(z-z_0)=c(z+z_0)=\tan 2\chi_0 \qquad (24)$$

and

$$\cot\chi_0=-x'(z_0)=-2cz_0 \qquad (25)$$

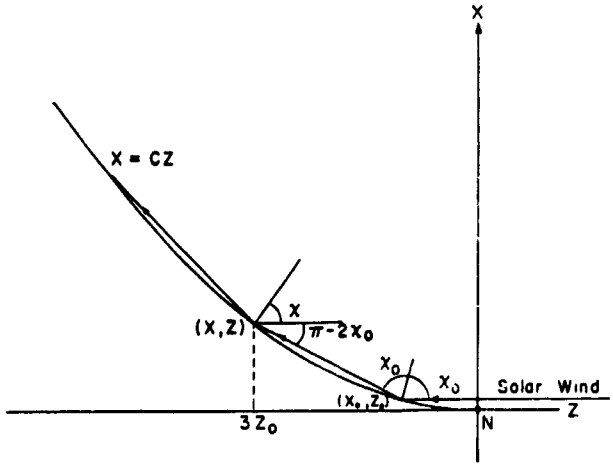

FIGURE 3.—Multiple reflections near the neutral point.

therefore,

$$z = 4cz_0/(1-4c^2z_0^2) - z_0 \doteq 3z_0 \qquad (26)$$

as indicated in Figure 3. We note that the angle of incidence is $\pi - 2\chi_0 + \chi$ at (x, z), and the change in the normal component of momentum will be correspondingly smaller. If we pursue the particle to the third point of reflection we find

$$c(z+3z_0) = \tan 2(\chi - \chi_0) \quad z \doteq 5z_0 \qquad (27)$$

However, the effect of the particle, by this time, is negligible.

We now consider the additional pressure δp at (x, z) due to particles reflected from (x_0, z) and compare it with the pressure $p = 2nmV^2 \cos^2 \chi$ of the incident plasma stream (ignoring the y coordinate). If $nV\, dx_0$ particles/sec are incident on an area of $ds_0 = (dx_0^3 + dz_0^2)^{1/2}$ at (x_0, z_0), they are reflected onto an area $ds = (dx^2 + dz^2)^{1/2}$ at (x, z), where their momentum changes by $2mV \cos(\pi - 2\chi_0 + \chi)$ per particle. Therefore, since $dx = 9dx_0$,

$$\delta p = -2mnV^2 \cos(\chi - 2\chi_0)(dx/ds)/9 \qquad (28)$$

If we substitute for χ, χ_0 from (25) and note that $dx/ds = \cos\chi$, then we find

$$\delta p/p = 1/27 \ll 1 \qquad (29)$$

We can conclude that the effect of multiple reflections near the neutral point is negligible and that the pressure condition is valid over the entire magnetosphere in this idealized representation.

REFERENCES

BEARD, D. B., The interaction of the terrestrial magnetic field with the solar corpuscular radiation, *J. Geophys. Res.*, *65*, 3559–3568, 1960.

DUNGEY, J. W., *Cosmic Electrodynamics*, 184 pp., Cambridge University Press, Cambridge, 1958.

MEAD, G. D., and D. B. BEARD, The shape of the geomagnetic-field solar-wind boundary, Goddard Space Flight Center rept., November 1963.

MIDGLEY, J. E., and L. DAVIS, JR., Calculation by a moment technique of the perturbation of the geomagnetic field by the solar wind, *J. Geophys. Res.*, *68*, 5111–5123, 1963.

SPREITER, J. R., and B. R. BRIGGS, Theoretical determination of the form of the boundary of the solar corpuscular stream produced by interaction with the magnetic dipole of the earth, *J. Geophys. Res.*, *67*, 37, 1962.

POSSIBLE SOURCE MECHANISM FOR LOW-ENERGY GALACTIC ELECTRONS

KARL A. BRUNSTEIN*

A calculation is made of the expected secondary electron flux resulting from the knock-on collisions of the primary nuclear beam with the interstellar gas. The model includes ionization losses and a statistical Fermi-mechanism energy gain. Comparison is made with recent satellite experimental data.

INTRODUCTION

Recent interest in cosmic-ray electrons has been confined largely to higher energies. Specifically, experimental results [1–3] in the energy region of the order of 100 MeV to several BeV have been of interest because of their bearing on the problem of galactic radio emission. The study of lower energy electrons, although probably not of direct importance to the radio emission question, is of importance because of its relationship to the higher energy electron spectrum, and because of its bearing upon the questions of solar modulation and energetic electron production.

Several workers in the field have arrived at the conclusion that the primary cosmic-ray beam must traverse several g/cm^2 of interstellar material prior to being sampled at or near the earth.[4–6] This necessarily implies a flux of low-energy electrons in equilibrium with the primary beam due to the knock-on process in the interstellar gas. This problem has been extensively studied for knock-on electrons due to muons in various substances.[7–9] The equilibrium problem in the interstellar gas is somewhat different from the laboratory experiments described in Refs. 7 and 8 because of the absence of the cascading process in the interstellar gas and the enhanced ionization loss rate in the partially ionized hydrogen.[10] In addition, there is the possibility of further acceleration of the secondary electrons in the inter-stellar material.[11]

It is not clear that these galactic electrons of low rigidity could penetrate into the solar cavity; however, recent work by Palmeira and Balasubrahmanyan [12] suggests that, at least during solar minimum, they can. This question is not considered here. The question of solar modulation is a separate one. By considering the knock-on flux as expected in the absence of solar influence and comparing with experimental data obtained outside the magnetosphere, new information concerning solar influence may be inferred.

PROCEDURE

A model is adopted in which the knock-on electrons, once produced, lose energy due to the ionization effect and gain energy due to a statistical Fermi mechanism. It is further assumed that the electrons tend to remain in the somewhat localized regions in which they are produced and that the losses due to diffusion out of the galaxy are negligible at these low rigidities. In addition, synchrotron losses are neglected at the energies in question here. Then, assuming a source of knock-on electrons and the predominance of the ionization loss and statistical gain mechanisms, a calculation of the low-energy electron spectrum is made.

Assuming a primary proton beam not varying appreciably with time, one can write the equation for the density of knock-on electrons as

$$\partial N(E,t)/\partial t+\alpha N(E,t)-(k-\alpha E)[\partial N(E,t)/\partial E] = Q(E)$$

*National Aeronautics and Space Agency—National Academy of Sciences—National Research Council Regular Post-Doctoral Resident Research Associate.

with $N(E,0)\equiv 0$, where

$N(E,t)$ = electron density at energy E and time t in electrons/m³-MeV,

$(dE/dt)_{\text{Fermi}}=\alpha(E+M_e c^2)$ defines α,

$k=|dE/ds|\rho c-\alpha M_e c^2$, dE/ds being the ionization loss rate, and

$Q(E)$ = production rate in electrons/m³-MeV-sec.

It is possible to solve the differential equation for arbitrary production rate $Q(E)$. The solution is found to be

$$N(E,t)=\sum_{n=0}^{\infty}\frac{(k-\alpha E)^n(1-e^{-\alpha t})^{n+1}}{(n+1)!\alpha^{n+1}}\frac{d^n}{dE^n}Q(E).$$

Adopting the Bhabha[9] cross section for knock-on production and the rigidity spectrum of McDonald and Webber [13] for the galactic proton beam, we may write for the production rate

$$Q(E)=\varphi(E)/E^2-\gamma(E)/E,$$

where

$$\varphi(E)=8\pi CM_e c^2 a\left(\frac{Mc^2}{Ze}\right)^{-1.25}\times\int_{(1-2M_e c^2/E)^{1/2}}^{\beta_{\max}}\beta^{-4.25}(1-\beta^2)^{-0.375}d\beta$$

$$\gamma(E)=4\pi Ca\left(\frac{Mc^2}{Ze}\right)^{-1.25}\times\int_{(1-2M_e c^2/E)^{1/2}}^{\beta_{\max}}\beta^{4.25}(1-\beta^2)^{0.625}d\beta,$$

$C=0.150$ cm²/g,

and

$a(Mc^2/Ze)^{-1.25}=5420$ (m²-sr-sec)$^{-1}$.

The dependence of φ and γ upon E makes this rigorous approach impractical. Instead, by use of the mean value theorem, one finds that $Q(E)$ may be approximated by

$$Q(E)\cong AE^{\delta},$$

where A and δ are readily evaluated. Substitution of $Q(E)=AE^{\delta}$ into the differential equation for $N(E,t)$ enables one to use the method of characteristics to solve the equation to yield

$$N(E,t)=\frac{1}{k-\alpha E}\left(\frac{A}{\delta+1}\right)\left[\frac{1}{\alpha^{\delta+1}}\left(k-\frac{k-\alpha E}{e^{\alpha t}}\right)^{\delta+1}-E^{\delta-1}\right].$$

Taking $\rho=2\times10^{-26}$ g/cm² [14] and letting $t\to\infty$, we get, setting $dJ/dE=(C/4\pi)N(E)$

$$\frac{dJ}{dE}=\frac{2.48\times10^{-13}}{1.625\alpha}\,\frac{E^{-1.625}-(k/\alpha)^{-1.625}}{(k/\alpha)-E}.$$

In addition to this flux calculated for the primary proton on hydrogen interaction, there will be a significant contribution from the heavier nuclei in the cosmic-ray beam. The knock-on production rate at a given primary velocity is very nearly a function of Z^2.[15] We then write the relation for the contribution of nuclei of change Z_i as

$$\left(\frac{dJ}{dE}\right)_i=Z_i{}^2\frac{J_i(>\beta)}{J_p(>\beta)}\left(\frac{dJ}{dE}\right)_p.$$

Using relative fluxes as given in the review by Ginzburg and Syrovatsky,[14] we arrive at the conclusion that the knock-on contribution from primaries of charge $Z\geq 2$ will be approximately 0.75 times the proton contribution. The total expected knock-on flux is then approximately 1.75 times the proton contribution.

The ionization loss rate for electrons of 3 to 15 MeV is nearly independent of energy for materials of low Z. In the interstellar hydrogen gas, however, it is fairly strongly a function of the degree of ionization. A degree of ionization of 10 per cent with a corresponding dE/ds value of 5 MeV/g/cm² has been taken.[10]

The calculated electron fluxes for different values of α are plotted in Figs. 1 and 2.[16] It is seen that the resultant intensity is a strong function of α, the parameter in the statistical acceleration mechanism. Typical electron fluxes as measured with IMP-A are also shown in the figures. It is seen that the range of α values selected, $1/\alpha=3\times10^{14}$ sec to $1/\alpha=3\times10^{15}$ sec, allows a fairly good matching of the theoretical and experimental fluxes. The value $\alpha\sim10^{-15}$ sec^{-1} does not appear unreasonable.[17,18]

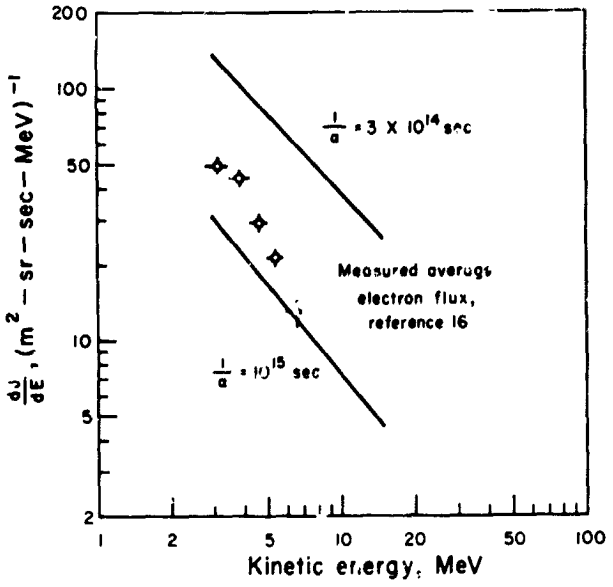

FIGURE 1.—Calculated spectra for values of α indicated. Circles: average electron flux from Ref. 16.

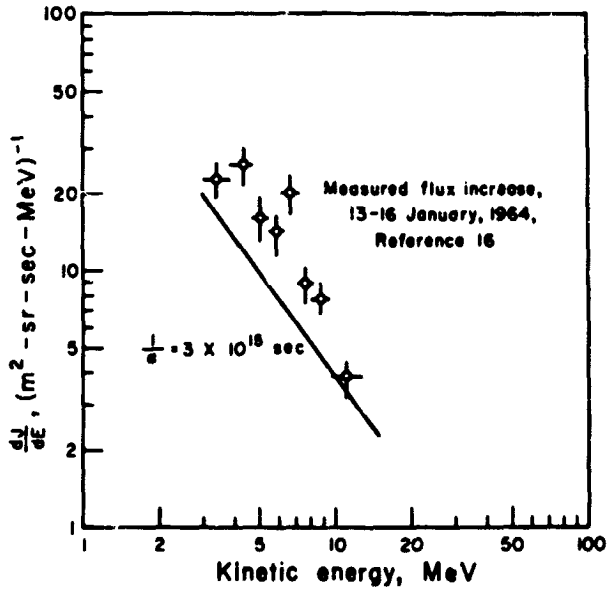

FIGURE 2.—Calculated spectrum for $1/\alpha = 3 \times 10^{15}$ sec. Circles: a typical flux increase, taken from Ref. 16.

It is not clear at this time whether the measured flux increase or the entire measured flux can be attributed to the knock-on process. Both possibilities are suggested by the reasonableness of the α values required.

CONCLUSION

The electron-positron flux resulting from the proton-proton interactions in the interstellar material has been discussed by several authors.[19,20] DeShong, Hildebrand, and Meyer[3] conclude, based on electron-positron ratios, that a substantial portion of the electron flux above 50 MeV must have an origin other than proton-proton collisions. It is speculated that a substantial portion of the lower energy electron flux seen in space may be attributed to knock-on electrons acted upon primarily by ionization losses in the interstellar gas and a Fermi type acceleration process. This, of course, requires that the low-energy electron flux should be composed largely of negative electrons. In addition, any long term solar modulation should be of an inverse activity dependence, similar to the primary nuclear beam. Both of these expectations will be subjected to experimental test by proposed experiments during the next solar half-cycle.

The knock-on process should produce secondary electrons in the BeV energy range also. The theoretical cross section in this case contains spin-dependent terms, and one does not feel as trusting of it as in the low-energy case where the interaction is one of Coulomb force only. In addition, these higher energy electrons may diffuse out of the galactic disk more readily and will also be subject to synchrotron losses. It is nevertheless interesting to plot the low-energy electron

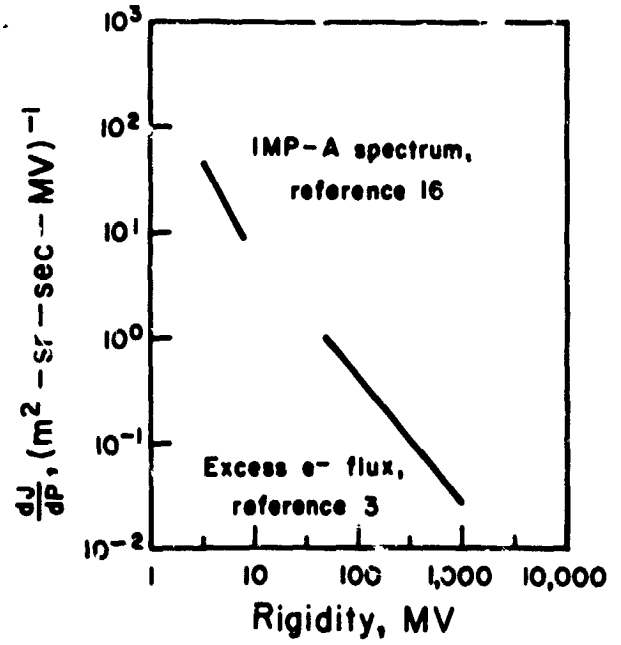

FIGURE 3.—The average electron flux from Ref. 16 shown along with the excess electron flux arrived at in Ref. 3.

flux along with the higher energy flux as has been done in Fig. 3. It is suggested by Fig. 3 that the knock-on process at higher energies may also be of significance.

Adopting for the moment the conclusion that the low-energy electrons as seen by IMP-A are due to the knock-on process, leads to the conclusion that the Fermi mechanism must be moderately effective for these low-energy electrons and that the parameter α has the value $\alpha \sim 10^{-15}$ sec^{-1}.

ACKNOWLEDGEMENT

I would like to express my appreciation for help given by Dr. Phillip Abraham in overcoming mathematical complexities. Dr. Thomas L. Cline kindly made his data available prior to publication.

REFERENCES

[1] J. A. Earl, Phys. Rev. Letters **6**, 125 (1961).

[2] P. Meyer and R. Vogt, Phys. Rev. Letters **6**, 193 (1961).

[3] J. A. DeShong, R. H. Hildebrand, and P. Meyer, Phys. Rev. Letters **12**, 3 (1964).

[4] F. W. O'Dell, M. M. Shapiro, and B. Stiller, International Conference on Cosmic Rays and the Earth Storm, Kyoto, 1961 (unpublished).

[5] S. Hayakawa, K. Ito, and Y. Terashima, Progr. Theoret. Phys. (Osaka) Suppl. **6**, (1958).

[6] H. Aizu, Y. Fujimoto, S. Hasegawa, M. Koshiba, I. Ito, J. Nishimura, and K. Yokoi, Progr. Theoret. Phys. Suppl. (Kyoto) **16**, 54 (1960).

[7] W. W. Brown, A. S. McKay, and E. D. Palmatier, Phys. Rev. **76**, 506 (1949).

[8] W. E. Hazen, Phys. Rev. **64**, 7 (1943).

[9] H. J. Bhabha, Proc. Roy. Soc. **A164**, 257 (1938).

[10] S. Hayakawa and K. Kitao, Progr. Theoret. Phys. (Kyoto) **16**, 139 (1956).

[11] E. Fermi, Phys. Rev. **75**, 1169 (1949).

[12] R. Palmeira and V. K. Balasubrahmanyan, J. Geophys. Res. (to be published).

[13] F. B. McDonald and W. R. Webber, Goddard Space Flight Center Contributions to 1961 Kyoto Conference on Cosmic Rays and the Earth Storm, Greenbelt, Maryland, 1961 (unpublished)

[14] V. L. Ginzburg and S. I. Syrovatsky, Progr. Theoret. Phys. (Kyoto) Suppl. **20**, 1 (1961).

[15] N. F. Mott, Proc. Roy. Soc. (London) **A124**, 425 (1929).

[16] T. L. Cline, F. B. McDonald, G. H. Ludwig, Phys. Rev. Letters (to be published).

[17] V. L. Ginzburg, *Progress in Elementary Particles and Cosmic Ray Physics* (North-Holland Publishing Company, Amsterdam, 1958), Vol. IV, Chap. V, p. 335.

[18] P. Morrison, S. Olbert, and B. Rossi, Phys. Rev. **94**, 440 (1954).

[19] S. Hayakawa and H. Okuda, Progr. Theoret. Phys. (Kyoto) **28**, 517 (1962).

[20] F. C. Jones, Journal Geophys. Res. **68**, 4399 (1963).

STUDIES OF SOLAR PROTONS WITH EXPLORERS XII AND XIV*

D. A. BRYANT†, T. L. CLINE, U. D. DESAI‡ AND F. B. McDONALD

Four solar proton events observed by Explorers XII and XIV in 1961 and 1962 are discussed. These events are directly associated with solar activity, and in three cases, are followed either by secondary events delayed about 2 days or by recurrent events on succeeding solar rotations. It is shown that the rate of propagation of solar protons in some of these primary events is linearly dependent on particle velocity and that this dependence makes it possible to separate the source characteristics from the propagation effects. In each event which shows this velocity dependence the propagation curves of all observed energies agree and reach maximum intensity at a time much greater than the rectilinear travel time. These results lead immediately to the conclusions that propagation involves an important degree of scattering and that the degree of scattering is independent of energy over the observed range of 1.4 to 500 mev. The energy spectrum at the time of escape from the sun, the "source spectrum," is determined in each event which shows this velocity dependence and is described by a power law in kinetic energy from a few mev to several hundreds of mev. A striking feature of all events is the existence of periodic fluctuations in intensity, which are simultaneous at all energies, having a period from 1. to 1.5 hours depending on the event. This result indicates a local origin, and it is suggested that the fluctuations reflect processes occurring in the region between the magnetosphere and the earth's shock front.

I. INTRODUCTION

During the last solar cycle it has become apparent that large solar flares are often accompanied by the acceleration of protons and other nuclei to energies sometimes exceeding tens of bev. Over a five-year period centered around the last solar maximum about sixty of these events were observed. Solar-proton events have been studied by many techniques. Ionization chambers, mu-meson telescopes, and neutron monitors at sea level provide indirect information at energies above a few bev. With high-altitude balloons, measurements down to about 80 mev are possible. Rocket measurements have no inherent low-energy threshold but are limited to brief samples of an event. Studies by radio techniques of the ionization produced in the D layer are sensitive to energies down to about 10 mev but have little energy resolution. Satellite studies can combine the advantages of the other techniques: they can provide almost continuous coverage with good energy and time resolution and with no inherent energy threshold, yielding a higher probability of detection of solar-proton events than can be provided by the other methods. Finally, a satellite with a sufficiently eccentric orbit can provide measurements of solar protons free of interaction with the earth's magnetic field and free of disturbances by the earth's trapped radiation.

The satellites Explorer XII and Explorer XIV carried cosmic-ray instruments with response for solar protons of energy as low as 1.4 mev. They were active from 16 August to 5 December 1961 and from 2 October 1962 to 1 August 1963, respectively. We discuss here several findings resulting from the study of the major solar proton events observed with these satellites during 1961 and 1962. Anomalous features of certain other events will be treated in later papers.

II. THE APPARATUS

Explorers XII and XIV were essentially identical satellites with similar orbits. The apogee of

*Published as *Goddard Space Flight Center Document X-611-64-217*, July 1964.

†Goddard Space Flight Center and D.S.I.R. Radio Research Station, Slough, Bucks, England.

‡Goddard Space Flight Center and Physical Research Laboratory, Navrangpura, Ahmedabad, India.

Explorer XII was about 13 earth radii and that of Explorer XIV about 16 earth radii; thus, for more than half the time in each orbit they were beyond the outer edge of the magnetosphere which varied from about 7 to over 12 earth radii. Gaps about 8 hours wide appear in the data as a result of discarding the observations made during the passes of the satellite through the magnetosphere. Various characteristics of the satellites are listed in Table I.

The detectors used for solar proton measurements in Explorers XII and XIV provided differential energy measurements from 1.4 mev to 500 mev and an integral measurement at about 600 mev. There were three detectors: a scintillation-counter telescope, a geiger-counter telescope and a single scintillation counter. The scintillation-counter telescope with a 32-channel pulse-height analyzer provided the differential-energy measurements for energies above 50 mev and the integral measurement at 600 mev. The geiger-counter telescope used in the single mode and in the coincidence mode gave integral measurements at 30 mev and 100 mev. Low-energy measurements were made with the single scintillation counter and an 8-channel integral pulse-height analyzer. The axis of the geiger-counter telescope was oriented parallel to the satellite's spin axis and the other detectors were normal to it. A summary of the dynamic range and resolution of each of the detectors is given in Table II. Corrections were applied to all the data for particles penetrating the detector shielding and for particles clipping the edges of the scintillators; only when these corrections were small were the data used for analysis. The detectors are described more fully in a previous publication (Bryant *et al.*, 1962).

III. THE EVENTS

In this paper we confine our attention to the solar proton events following the flares of 10 September, 28 September, and 10 November 1961 and the flare of 23 October 1962. Some details of these flares and the plage regions producing them are given in Table III. The table also contains comments on the flares (H. Prince and R. Hedeman, private communication, 1963) and on the accompanying type IV radio emission (A. Maxwell, J. Warwick, private communications, 1963). Some of the flares were followed by delayed effects and these are also listed. Effects delayed by the prompt 2-day sun-to-earth transit of enhanced plasma and effects delayed by the rotation of the sun (27-day recurrent events) are listed separately.

A calendar of all the solar particle events observed during the intervals discussed here is shown in Figure 1, in which the occurrence of

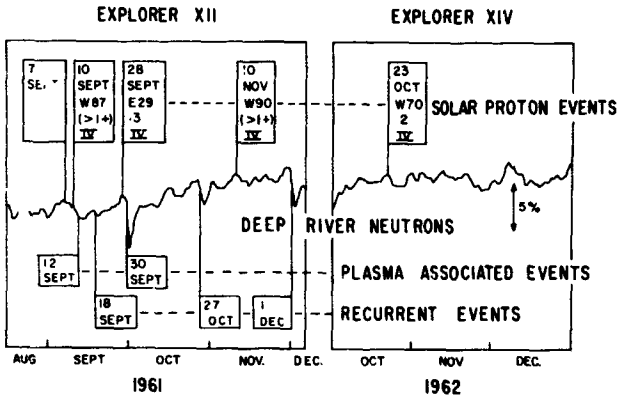

FIGURE 1.—Solar particle events observed with Explorers XII and XIV during 1961 and 1962. The occurrence of each primary solar proton event is indicated above the cosmic-ray neutron intensity plots with a flag which displays the solar longitude and classification of the parent flare and the existence of associated type IV radio bursts. Occurrences of both varieties of delayed proton events are also indicated; a plasma-associated event occurs with a delay of two days and a recurrent event takes place when a long-lived solar streamer passes central meridian on a succeeding solar rotation.

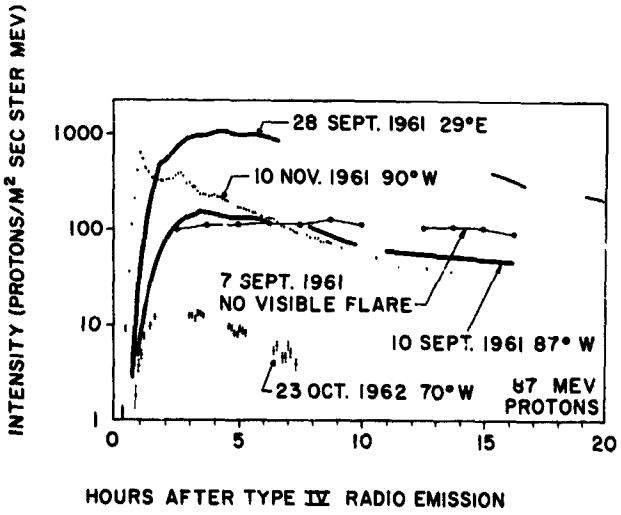

FIGURE 2.—The intensities of 87-mev protons vs time after the type IV emissions during the five primary solar proton events. The shapes of only two events, those of 28 September 1961 and 23 October 1962, are seen to be quantitatively similar, as monitored in this manner.

TABLE I.—*Satellite Characteristics*

Parameter	Explorer XI	Explorer XIV
Dates of Operation	16 Aug. to 5 Dec. 1961	2 Oct. 1962 to 1 Aug. 1963
Orbital Period	26.5 hours	36.5 hours
Apogee, Geocentric	83,600 km.	104,800 km.
Initial G. Perigee	6,700 km.	6,700 km.
Sun-apogee angle from earth	≈0° min. to ≈110° max.	≈70° to 180° and back to ≈0°
Initial Spin Period	2.2 seconds	5. seconds
Direction of Spin Axis	+47° right ascension −27° declination	(Uncertain due to precession)

TABLE II.—*Detector Characteristics*

Detector	Plastic Scintillator Telescope	Geiger Counter Telescope	CsI Crystal
Proton Energy Range	>55 mev	>30 mev	1.4 to 22 mev
Information Recorded	32 differential channels	Coincidence mode: / Single mode:	8 integral levels
Energy Intervals Processed	Energy Interval; Mean Energies 55 to 118 — 87 mev 118 to 150 — 135 mev 150 to 200 — 175 mev 200 to 255 — 228 mev 255 to 335 — 295 mev 335 to 500 — 418 mev (above 600 mev)	Energy Lower Limits ≈30 mev / ≈100 mev (sensitivity is a function of energy)	Mean Energies 2.2 mev 3.8 mev 5.7 mev 7.9 mev 14.5 mev
Geometric Factor (cm^2 ster)	13.4	150. / 12.7 (at 100 mev)	2.85
	(Corrections take into account variation of geometric factor with energy)		
Time Resolution	5 minutes of storage each 7 minutes	1.6 seconds of storage each mode during 5 out of 7 minutes	1.6 seconds of storage each level for 5 out of 7 minutes
Direction of Detector Axis	Normal to spin axis	Parallel to spin axis	Normal to spin axis

TABLE III.—*Details of the Flares*

Event	10 Sept. 1961	28 Sept. 1961	10 Nov. 1961	23 Oct. 1962
Plage				
Number	6212	6235	6264	6581
Rotation Order	2	3	4	2
Earlier, later	6197, 6235	6212, ----	----------	6563, ----
Flares Produced	69	15	9 after 5 Nov.	----------
Flare				
Class	>1+	3	>1+	2
Position	W87, N12	E29, N13	W90, N19	W70, N03
H α (UT):				
Start, Max., Stop	1950, 2020, 2054	2202, 2223, 2530	1434, 1444, 1450	1642, 1708, 1745
Type IV Onset (UT)	1937	2212	1445	1656
Comments	A very large, bright flare.	A very large, bright flare.	Accompanied by unusual loop activity.	Occurs where there are no spots.
Optical and Radio Observations (UT)	Loops at 2017, throughout 2025–2055	Type III bursts earlier on 27 Sept.	Limb prominence at 1430. Loops for many hours with max. at 1555	Type III G at 1649 and later.
	Considerable Type II	Type III G and Type II	Type III G and Type II	Type II
2-Day Delayed Effects				
Cosmic Ray Decreases	11 to 14 Sept.	30 Sept. to 5 Oct.	None	None
Low Energy Particles	12 Sept. max.	30 Sept. max.	None	None
Geomagnetic Activity	11 Sept., 1606 U.T.	30 Sept., 2108 U.T.	None	None
Recurrent Effects				
Cosmic Ray Decreases	None (central meridian passage on 28–30 Sept.)	28 Oct. to 1 Nov.	1 Dec. to 4 Dec.	None
Low Energy Particles	----------	27 Oct. max.	1 Dec. max.	None
Geomagnetic Activity	----------	26 Oct., 1940 U.T. 28 Oct., 0820 U.T.	1 Dec. to 4 Dec.	None

primary events and delayed effects are plotted against the cosmic-ray intensity measured by a sea-level neutron monitor (courtesy of H. Carmichael, private communication, 1962). Examination of the data showed no evidence either for any other smaller discrete events or for any separate, continuous increases over the general background level. The intensity of one energy interval of protons, centered at 87 mev, is plotted for all five primary events in Figure 2, indicating the widely varying behavior of the events. The event of 7 September 1961, which does not lend itself to obvious correlation to any known flare, will be discussed in a later paper.

IV. THE EVENT OF 28 SEPTEMBER 1961

The solar proton event of 28 September 1961 was initiated by a class 3 flare 29° east of central

meridian. Table III shows the pertinent solar and geophysical data. Some aspects of the event were considered in an earlier paper (Bryant *et al.*, 1962).

Intensity vs. time profiles of various energy components of the event are shown in Figure 3. Time is measured in hours from 2208 UT, the time of emission at the sun of a brief x-ray burst observed by Anderson and Winckler (1962) from 2216 to 2217 UT. For the first few hours points are plotted at intervals of about 7 minutes, and later points are hourly averages. The energy parameter is the mean energy of each interval as outlined in Table II. It is clear that the time taken to reach maximum intensity increases with decreasing energy. The data are less complete at the lower energies because at first the correction due to high-energy particles which penetrate the shielding of the low-energy particle detector is large, and because the satellite entered the trapped-radiation zone soon after the first effect became small.

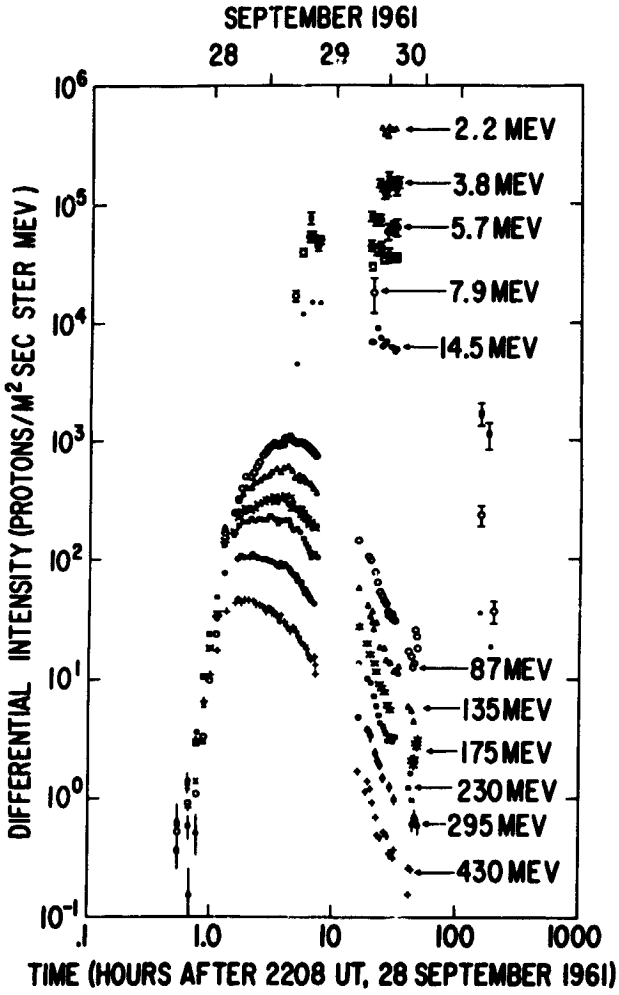

FIGURE 3.—The differential intensities of solar protons during the 28 September 1961 event plotted against time after the x-ray burst at the sun. The data are interrupted when the satellite passed through the magnetosphere and when the delayed increase occurred on 30 September 1961.

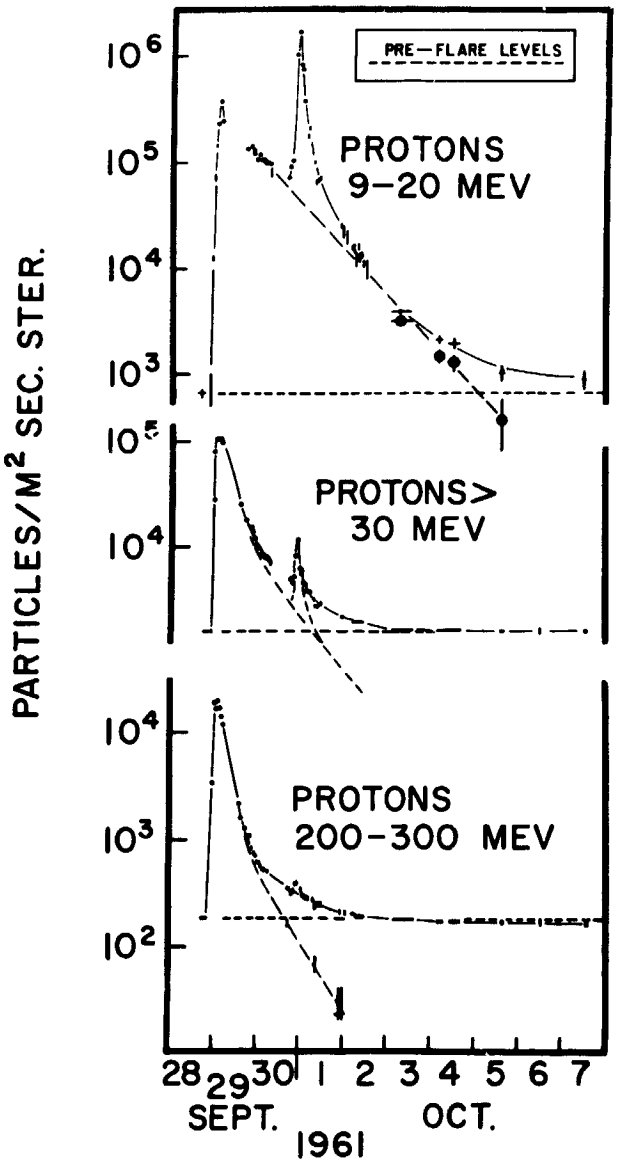

FIGURE 4.—Representative proton intensities between 28 September and 7 October, showing the delayed intensity increase of predominately lower-energy protons on 30 September 1961. The energy spectra of these particles are relatively constant with time, unlike those of the velocity-ordered primary solar proton event, and their arrival times are essentially constant with energy, occurring at the time of arrival of the enhanced solar plasma, two days after the flare.

There is a departure from a smooth decay at about 48 hours. At that time an increase took place in the intensity of low-energy particles which was associated with the arrival of a solar plasma stream that produced a sudden-commencement geomagnetic storm and a Forbush decrease. This occurrence is described in detail in the earlier paper, but for the sake of completeness it is briefly described here. The details of this increase, omitted in Figure 3, are shown for some energy intervals in Figure 4 on a linear time scale. Late on 30 September there is a sudden increase in intensity which is more marked at lower energies. The increase starts at about 1930 UT just before the sudden commencement of a magnetic storm at 2108 UT. The maximum intensity of particles of energy above 3 mev during the increase is more than ten times that attained during the main solar-proton event. Axford and Reid (1962) reported riometer observations of this burst of low-energy protons and had previously observed a similar event on 10 February 1958 (Reid and Axford, 1962). Other events of this kind have been reported by Charakhchyan *et al.* (1963).

After a full rotation of the sun, when the plage region responsible for the flare of 28 September was again close to central meridian, there was another burst of low-energy protons. This time the increase was much smaller. Figure 5, which is a plot of the total intensity above 3 mev on a further-compressed linear time scale, shows the full sequence of events. This recurrent event was also associated with enhanced solar plasma responsible for a recurrent geomagnetic storm and a recurrent Forbush decrease. We have put forward this event and a similar one following the 10 November 1961 flare as new evidence for the existence of long-lived solar streams (Bryant *et al.*, 1963).

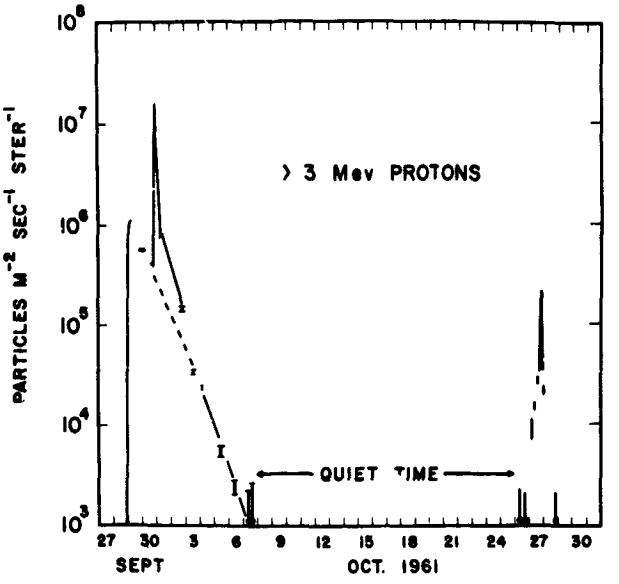

FIGURE 5.—The intensity of protons of energy above 3 mev between 30 September and 28 October 1961. The delayed increase on 30 September is superposed on the primary solar-proton intensity decay and the recurrent event on 27 October follows the completely event-free intervening period.

a) Velocity Dependence

The energy dependence of the rate of rise of intensity suggests that the propagation of the particles is a velocity-dependent process. A striking linear dependence on velocity is revealed by the following analysis.

We assume that all particles were accelerated at the same time or, more strictly, that they were all accelerated within a time interval short compared with the interval between acceleration and observation. We may then determine the distance a particle has traveled between acceleration and observation by taking the product of particle velocity and time from the beginning of the event. The time used here for the beginning of the event is 2208 UT, the time of the x-ray burst at the sun. We then convert the intensity vs. time profile to an intensity vs. distance profile. The intensity vs. distance profile is effectively a distribution in distance traveled. This distribution is a property of the medium through which the particles have traveled. Figure 6 shows the result of this treatment in which the distance traveled is measured in astronomical units. In constructing this figure the intensities of each component have been scaled to give the best fit to a common curve. The physical meaning of this normalization will be examined further below.

We note from Figure 6 that all components lie very closely on a common curve, apart from small-scale deviations to be discussed later as a separate topic. The fact that we have essentially a common curve shows that particles of all energies have traveled a given path length with equal probability; this is true for all path lengths to the extent that the various components of Figure 6 do

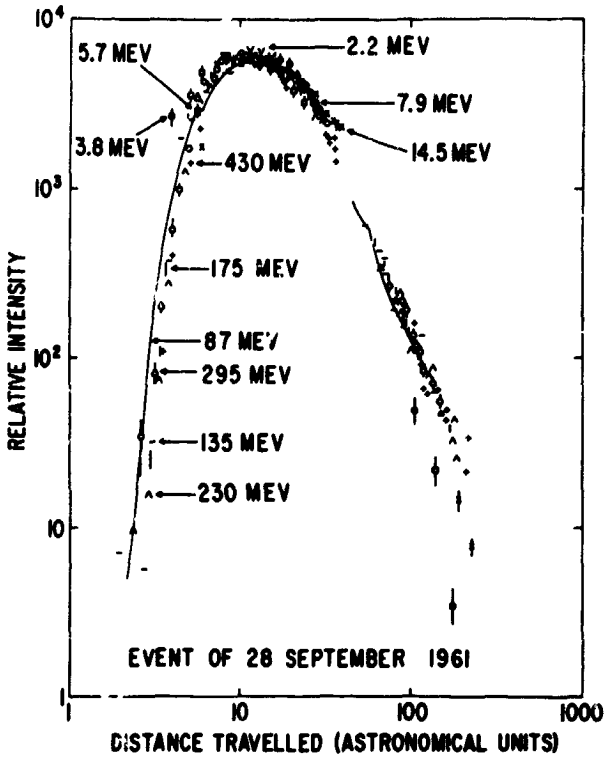

FIGURE 6.—The intensity vs time plots of Figure 3 converted to relative intensity vs distance plots. The distance is computed for each energy component by taking the product of the corresponding particle velocity and time from the event; the intensities are scaled to give the best fit to a common propagation curve. This fit occurs over a dynamic range in energy of a few hundred and a velocity range of 14, and over a time duration of several days.

lie on a common curve. We note that the distance traveled by most particles is many astronomical units, which indicates that propagation involved an important degree of scattering. Further, the degree of scattering is not a function of energy over the observed range. This suggests that the mode of propagation is a diffusion-like process and that energy-dependent processes, such as drift across magnetic field lines, play a minor role. In fact, it has been shown that the equation for simple diffusion describes the propagation curve of this particular event through its maximum (Bryant *et al.*, 1962). It fails to do so, though, during both the early anisotropic phase and the later stages where boundary conditions are important.

b) Source Spectrum

We now discuss the physical meaning of the scaling factors used to construct Figure 6. Consider the relative intensity of any two components of the event. We have recorded the intensities not as a function of time but as a function of distance traveled, and found that the relative intensity is essentially constant over a range from 2 to more than 100 astronomical units. There is nothing to suggest that an extrapolation back to zero distance in invalid. The relative intensity of two components at zero distance is, by definition, a measure of the shape of the source spectrum.

The scaling factors used to produce Figure 6 provide these relative intensities and Figure 7 shows the source spectrum obtained directly from them. The source spectra of two other events analyzed in a similar way are also shown. The ordinate of Figure 7 is arbitrarily chosen to show the maximum intensity reached at the earth. The differential intensities shown are proportional to the absolute differential intensities of protons produced at the sun and retain, therefore, the same spectral form, but the constant of proportionality which depends on the geometry of propagation is unknown. The spectrum is well represented by a power law in kinetic energy with a slope of about -1.7.

We note that, apart from small-scale fluctuations, this event is completely described by two graphs: the source spectrum of Figure 7 and the distribution of path length during propagation of Figure 6.

V. THE EVENT OF 23 OCTOBER 1962

The event of 23 October 1962 is the smallest discussed here and probably the lowest-intensity primary solar-proton event studied to date. It was initiated by a class 2 flare occurring 70° west of central meridian; further details of the flare and associated phenomena are listed in Table III. The event was also observed by the cosmic-ray equipment on Mariner II (H. Anderson and V. Neher, J. Van Allen, private communications, 1963).

Figure 8 shows the intensity vs. time profiles of various components of the event. We see that again the higher-energy components reach a maximum earlier than the lower-energy components. The intensity vs. time profiles, corrected for particle velocity and superimposed in the same way as for the event of 28 September 1961, are shown

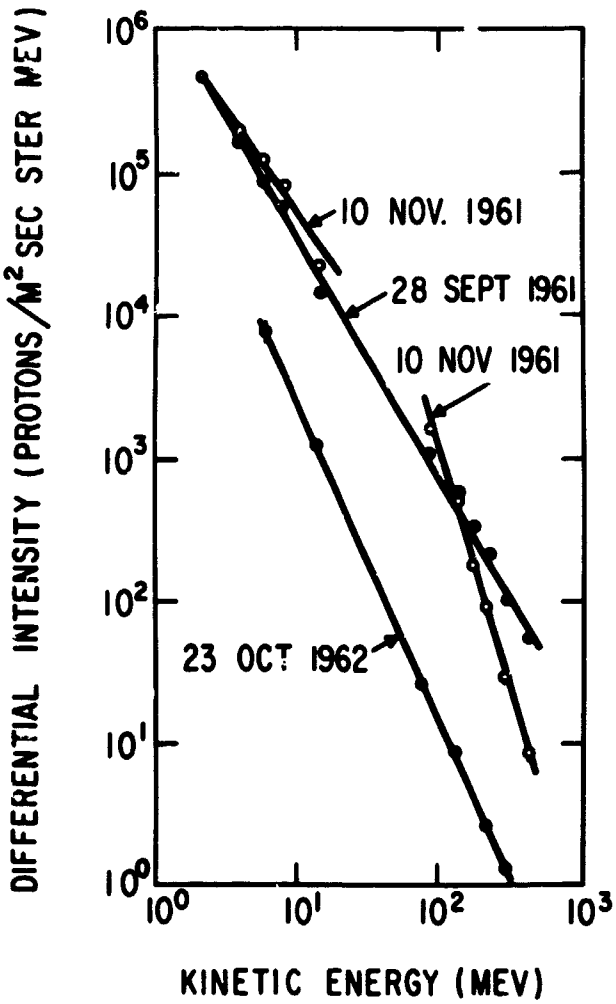

FIGURE 7.—The source spectra of three solar proton events. The intensities plotted are arbitrarily chosen to show the maximum intensities reached at the earth; as explained in the text the relative scaling of the two sections of the spectrum of 10 November is not necessarily meaningful. In the case of the solar proton events which totally conform to a velocity-dependent behavior, such as those of 28 September 1961 and 23 October 1962, the source spectrum is the unique differential energy spectrum of the protons at the time of their escape from the sun; in each event the source spectrum is proportional to that shown here with a constant which depends in an unknown way on the geometry of propagation.

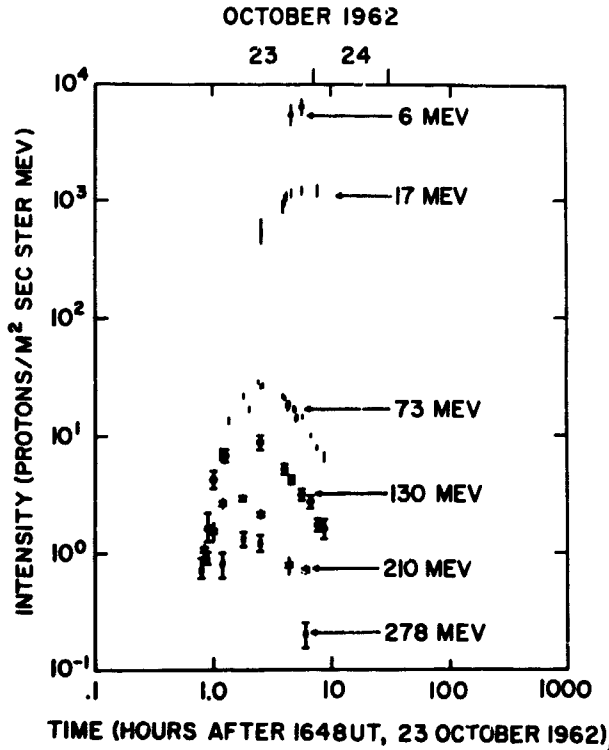

FIGURE 8.—The differential intensities of solar protons during the 23 October 1962 event plotted against time after the onset at the sun of type IV radiation. The behavior of this event is qualitatively similar to that of the early portion of the 28 September 1961 event. Due to the relatively low intensity of the event, the differential intensities of protons of energy above 300 mev could not be measured, the protons of energy below 5 mev did not arrive until after the satellite entered the magnetosphere.

in Figure 9. We find a good fit to a common curve so again the observation that higher-energy particles arrive earlier is explained quantitatively as a dispersion effect. The source spectrum obtained from the relative normalization used to construct Figure 9 is shown in Figure 7. We note that again it is well represented by a power law in kinetic energy. The slope of the spectrum in this case is about -2.3.

VI. THE EVENT OF 10 NOVEMBER 1961

The solar proton event of 10 November 1961 was one of two events observed by Explorer XII resulting from flares on the West limb of the sun (Table III). A long-lived solar stream emanating from the flare region produced a recurrent event 21 days later on 1 December (Bryant *et al.*, 1963).

Intensity vs. time profiles for this event are shown in Figure 10. A feature of these curves is a sudden drop in intensity at 1.3 hours (1546 UT). It occurs in all components that show a measurable intensity at this time. A second drop occurs at 3 hours (1730 UT). As we shall mention again in Section VII, these fluctuations are very likely unusually large cases of a feature common to all

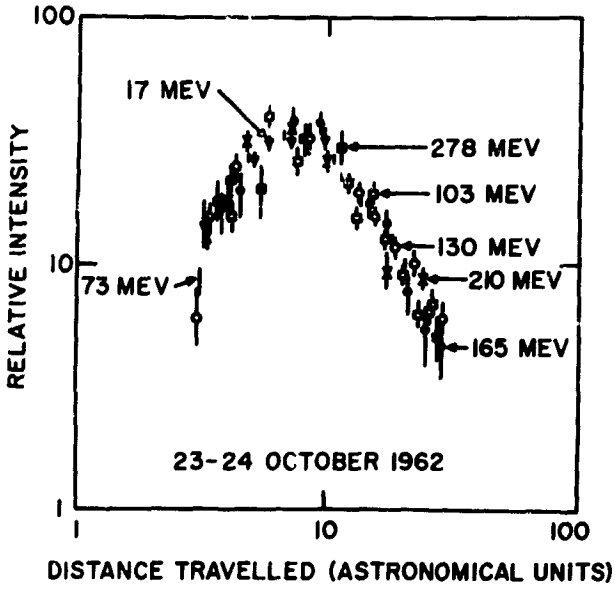

FIGURE 9.—The intensity vs time plots of Figure 8 converted to a relative intensity vs distance plots, scaled to give the best fit to a common propagation curve.

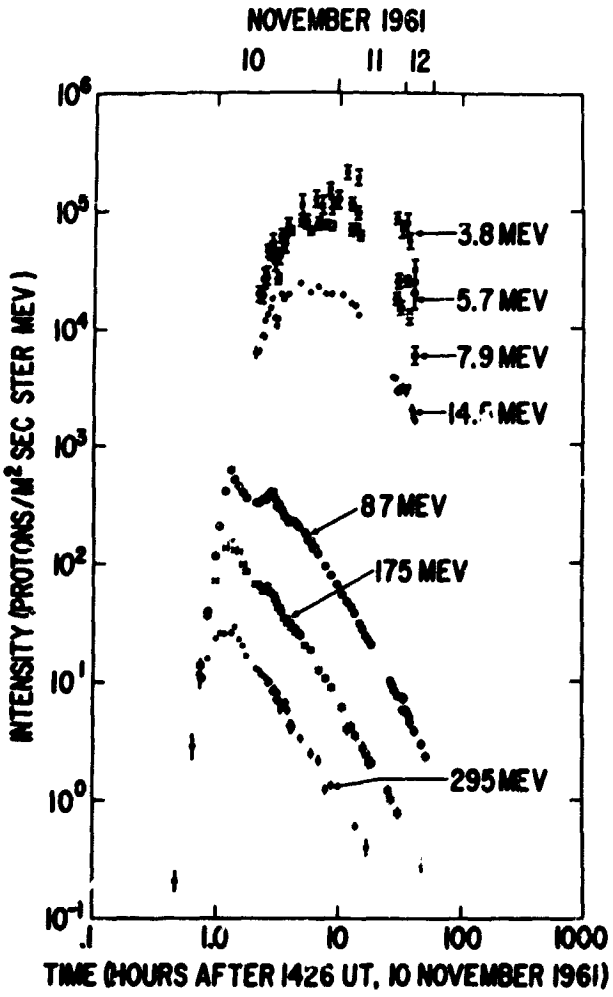

FIGURE 10.—The differential intensities of solar protons during the 10 November 1961 event plotted against time after the flare. A sudden drop in the intensities of the higher-energy protons occurs at 1.3 hours; this discontinuity in the slopes of the propagation curves occurs before the arrival of most of the lower-energy protons.

four primary events discussed here, namely a periodic intensity fluctuation with a period of about one hour. However, since these particular changes are so unusually large and sharp they may be due to some other cause. The flare producing this event was accompanied by unusual loop activity, so it may not be by chance that the solar-proton intensity exhibits unusual behavior. We are unable to link any specific happening at the sun with the changes taking place near the earth but we are able to deduce when it should occur. Figure 11 shows the integral intensities above 60 mev and above 200 mev plotted in a linear scale to show how drastically the behavior changed. The data are consistent with the breakdown having occurred simultaneously at all energies, but the time resolution of the measurements would permit a 15 minute dispersion and so is consistent with the dispersion to be expected from the velocity difference acting over a distance of 1 astronomical unit. The breakdown occurs in the 87 mev component somewhere between 1546 and 1556 hours. Since 87 mev particles take 20 minutes to travel 1 a.u., the first ones to bring information of a change would have left the sun between 1526 and 1536 if they traveled in a straight line, but (more likely) between 1521 and 1531 if they traveled along a curved path defined by the interplanetary magnetic field. Optical or radio information would reach the earth 8 minutes later, somewhere between 1529 and 1539. Though the flare showed great activity (see Table III for comments) we have found no evidence for any drastic change of conditions in this period.

a) Velocity Dependence and Source Spectra

The complicated structure of this event defies a description in terms of velocity dependence alone. As will be shown below, there are occasions on which a velocity dependence is revealed. Figures 12a and 12b show velocity-compensated intensity-distance profiles for the higher and lower energies taken separately. The higher-energy

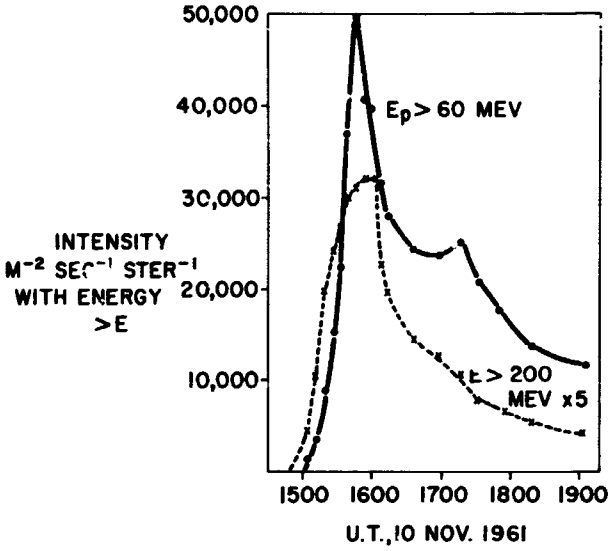

FIGURE 11.—The integral intensities of protons above 60 mev and above 200 mev during the first few hours of the 10 November 1961 event, plotted on a linear scale. These components are chosen so as to display the maximum dispersion of the times of peak intensity; since measurements were made every 7 minutes, the data are consistent with the peak intensities having occurred simultaneously.

components are velocity dependent before the sudden drop in intensity at 1.3 hours, and the lower-energy components are velocity dependent throughout the event. The fact that the lower-energy components do not show a measurable intensity until after the breakdown of velocity dependence at higher energy introduces a further uncertainty in interpretation.

Two source spectra are shown for this event in Figure 7, one for the higher and one for the lower energies. Since the velocity-compensated intensity vs. time profiles are different, the relative normalization of the two sections of the spectrum is not meaningful. The normalization for each section of the spectrum is arbitrarily chosen to be the maximum intensity reached at the earth. It may be that the common fit of the low-energy intensity curves is not significant, since the deviation from a common propagation envelope increases as energy decreases among the high-energy groups.

b) Time Dependence

Although this event shows a velocity dependence that holds very well at certain times, it cannot be completely described by a single source

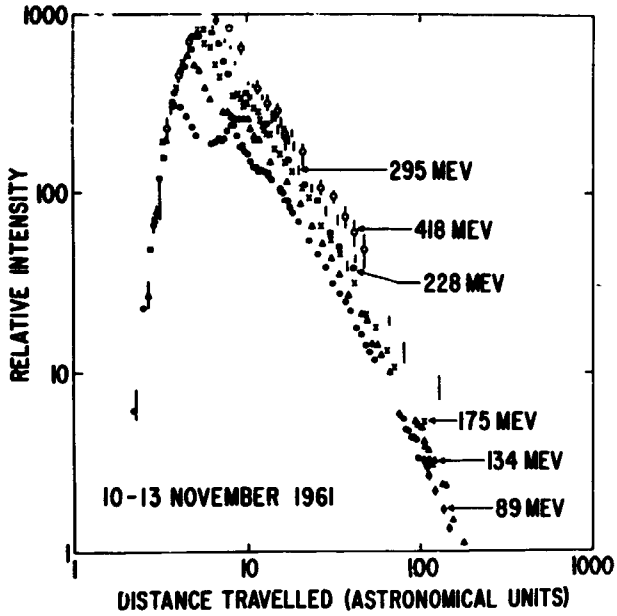

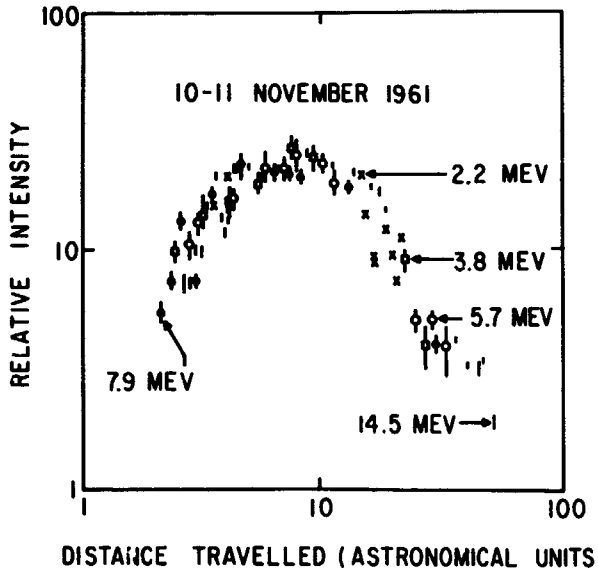

FIGURES 12a and 12b.—The intensity vs time plots of Figure 10 converted to relative intensity vs distance plots. Two groups are separately scaled to give the best fit to a common high-energy curve before the 1.3-hour peak, and to a common low-energy curve after it. A unique high-energy propagation curve does not exist throughout the event, but appears to be approached asymptotically with increasing energy. A common low-energy curve is apparent, but it may relate more directly to a local modulation than to interplanetary propagation.

spectrum and single propagation curve. Further, there are two sudden intensity drops that occur over a wide energy range with no dispersion. They almost certainly result from sudden changes

in the propagation medium which probably take place near the earth but, from the above discussion, which may also take place at the sun. Other effects of this kind are described in the next section and discussed more fully in section VIII.

VII. THE EVENT OF 10 SEPTEMBER 1961

The event of 10 September 1961 was initiated by a flare on the west limb of the sun. The intensity vs. time profiles of Figure 13 show that the event was dominated by intensity changes occurring simultaneously at all energies. Only gross features, such as the fact that the lower-energy components reach maximum intensity later than the higher-energy components, can be attributed to dispersion. There are no systematic changes of behavior with energy and consequently no quantitative fit to velocity dependence. A linear plot of three sample components (Figure 14) typifies the irregular behavior of the event. The high intensity reached by this and lower-energy components early on 12 September, about 1 day after the flare, is probably due to the arrival of enhanced solar plasma that produced a small cosmic-ray decrease at about that time following geomagnetic activity at 1106 UT on 11 September. This increase is like the delayed arrival of low-energy particles seen about 48 hours after the 28 September 1961 event, but in this case there is a much slower onset no doubt having to do with the west limb location of the flare.

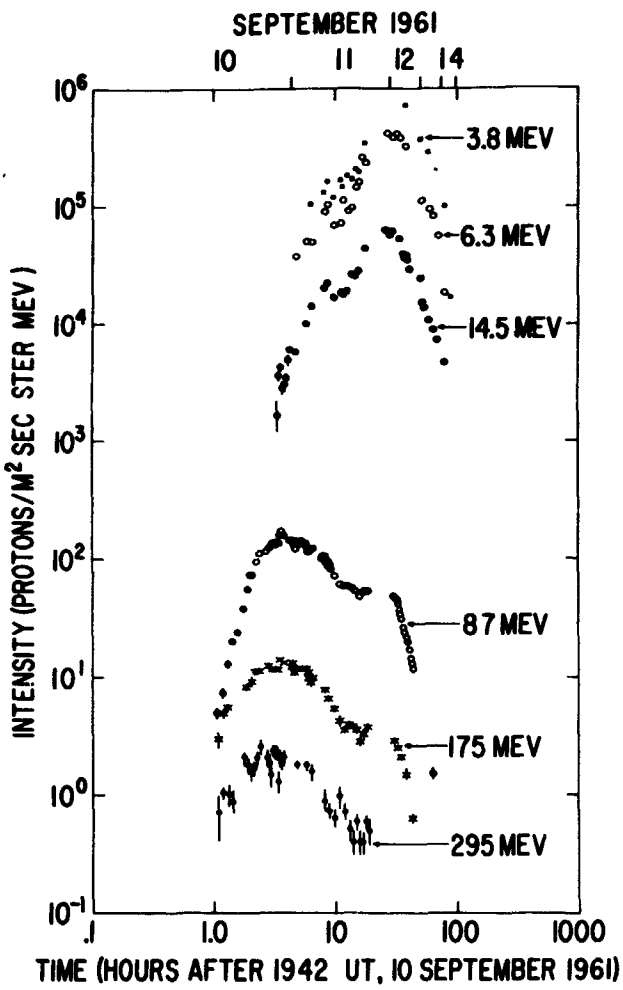

FIGURE 13.—The differential intensities of solar protons during the 10 September 1961 event plotted against time after the flare. There is a qualitative velocity ordering for the first 10 hours; during this time the higher-energy protons tend to increase in intensity before the lower-energy protons do, but there is no quantitative fit to a velocity dependence. Later in this event the intensities of protons of all energies increase together in a manner qualitatively similar to that of 30 September; this occurrence is also accompanied by cosmic-ray and geomagnetic fluctuations associated with the arrival of enhanced solar plasma.

a) Fluctuations

Superimposed on the large-scale features of the intensity vs. time profiles are a series of fluctuations which are nearly periodic, with the same frequency and phase at all energies. They take place in all these events, but are most clearly marked in the event of 10 September 1961. Figure 15, which shows the integral intensity vs. time profiles on a linear scale for the 5.7-mev and the 30-mev components of this event, illustrates these

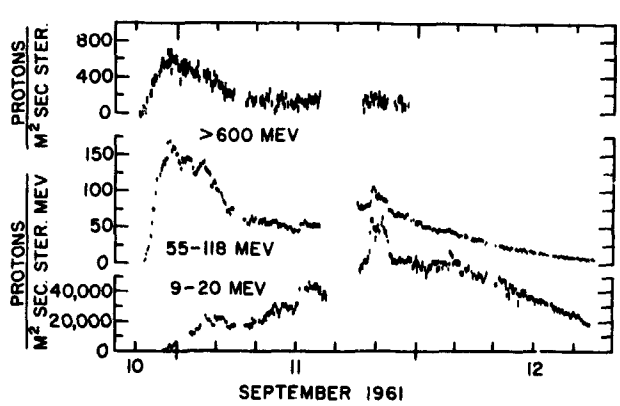

FIGURE 14.—A linear plot of the intensity of minimum-ionizing protons and of two lower-energy groups during the 10 September event, displaying both the irregular behavior of the intensity early in the event and the delayed increased on 11 September. These intensity variations dominate the pattern of this event.

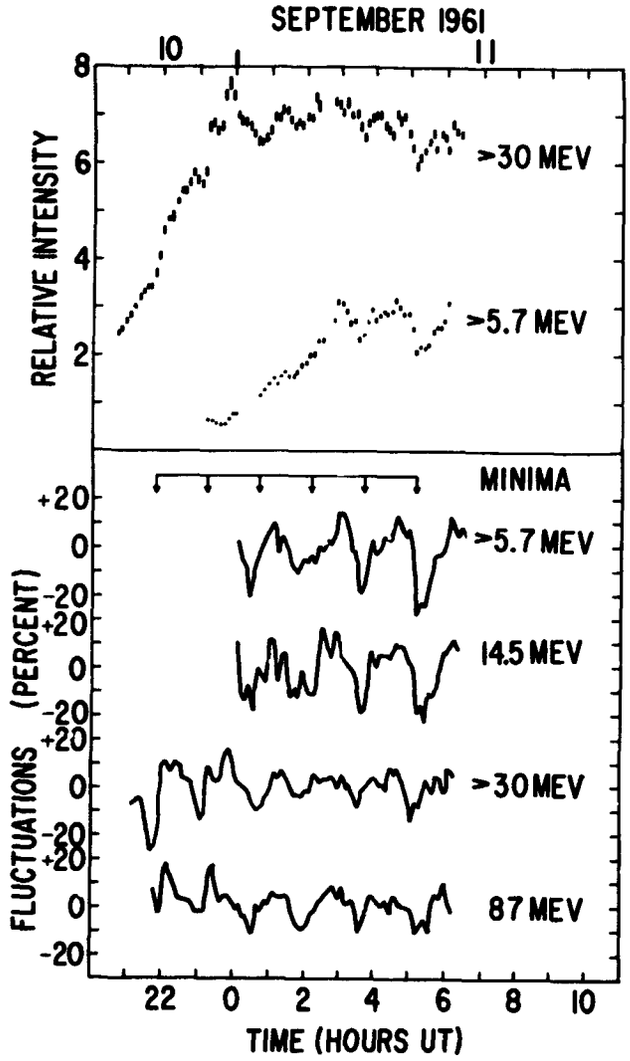

FIGURE 15.—Linear plots vs time of two integral proton intensities during the 10 September event; the deviations from the running means of intensity of these and two differential intensities are also shown in order to illustrate the relative fluctuations. A regular modulation appears having period and phase that are constant with energy; the times of minimum relative intensity are indicated to illustrate the approximate periodicity. Since there is no discernible velocity dispersion of this modulation within an event, these fluctuations are believed to have a local origin.

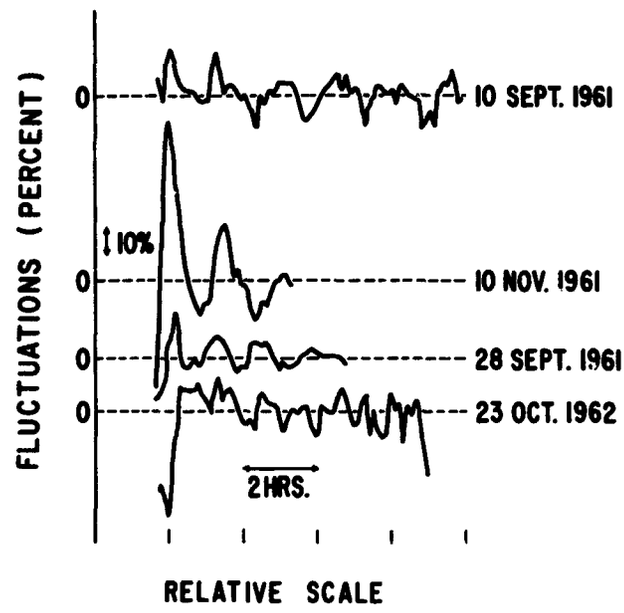

FIGURE 16.—The fluctuations of the 87-mev component of the solar proton intensities of four solar proton events. The period of the fluctuation is constant within an event but varies from 1. to 1.5 hours with the event.

fluctuations. To show the periodic fluctuations more clearly, the lower-frequency components have been removed by subtracting the running mean of one period length; the result for several energy components is shown in the lower half of the figures. Fluctuations of this kind occur to some extent in all events: Figure 16, in which the relative time scale is in units of hours, shows the fluctuation of the 87-mev component for all events. The sudden drops in intensity near the beginning of the 10 November 1961 event have the same frequency and phase as the other fluctuations, so it appears that they may not be isolated happenings caused directly by activity at the sun but the first two members of a series of fluctuations, although they were unusually large and very sharp. The amplitude of the fluctuations depends little on energy in any of the events. Table IV summarizes the periods and amplitudes of the fluctuations.

VIII. DISCUSSION

The following general statements can be made summarizing the results presented above.

(1) Solar proton events observed in the 2- to 600-mev energy region fall into at least three categories: the primary events have maximum intensity soon after the parent flare; these are sometimes followed about two days later by secondary events that occur with the arrival of the solar plasma; they also are occasionally followed by recurrent events that do not immediately follow solar activity but occur when the parent plage region passes central meridian on successive 27-day intervals.

TABLE IV.—*Solar-Proton Event Characteristics*

Event	10 Sept. 1961	28 Sept. 1961	10 Nov. 1961 Low Energy	10 Nov. 1961 High Energy	23 Oct. 1962
Energy Range of Velocity Dependence (mev)	(none detected)	1.4 to 500	1.4 to 22	55 to 500	4 to 330
Exponent of Source Spectrum		−1.7	−1.5	−3.5	−2.3
Scale of Source Spectrum at Max. Intens. $(cm^2\ sec\ ster\ mev)^{-1}$		1.6×10^6	1.4×10^6	$7.\times10^9$	$4.\times10^5$
Most Probable Distance (a.u.)		12	8	9	8
M.F.P. (a.u.) from Diffsuion Theory		0.04	0.06	0.055	0.06
Fluctuation Period (hours)	1.4	1.3	(none detected)	1.5	1.0

(2) The intensity vs. time profiles often show a linear velocity dependence. In two of the events under discussion (28 September 1961 and 23 October 1962) this velocity dependence lasts throughout the events. Exceptions occur in the event of 10 November 1961, which shows some early departure from this behavior and in the event of 10 September 1961, which shows no quantitative agreement with velocity dependence.

(3) All events show a series of periodic intensity fluctuations with a period of from 1. to 1.5 hours. These occur without dispersion.

If we convert those intensity vs. time profiles which show a quantitative, linear velocity dependence to probability vs. distance profiles, we are led directly to the following conclusions:

(4) Properties of the propagation medium and properties of the source can be studied separately and, in particular, the shape of the energy spectrum at the source can be obtained.

(5) Propagation involves an important degree of scattering (since the most likely distance traveled is about 10 astronomical units).

(6) The degree of scattering is independent of particle rigidity in the region below 1.5 bv (since all the propagation curves are the same).

a) Velocity Dependence

The analysis described in section IV, showing the velocity dependence of these events, has constituted a necessary but insufficient test. For example, we might have found an even closer fit had we compensated the intensity vs. time profiles by velocity raised to the power n, where n is close to but not equal to 1. We now show that the best value of n is indeed 1. To find the best value of n, the various intensity vs. time profiles were shifted horizontally and vertically to give the best fit to a chosen reference curve. No account was taken of particle velocity at this stage. The factors by which the curves were horizontally shifted were then plotted against particle velocity. The result is shown in Figure 17a in which, for comparison, lines of slope unity have been drawn through the points. The normalizations are arbitrary and depend on the curves chosen for reference. We find that the slopes of all lines are close to unity, the mean value being 1.0 ± 0.1. The energy intervals over which this test could be performed are implied by the figure and are indicated in Table IV. The various parts of Figure 17a have been superimposed in Figure 17b, where, as in 17a, a line of slope unity has been drawn through the points for comparison. (The energy range studied here does not extend sufficiently far into the relativistic region to permit a test of rigidity dependence as opposed to simple velocity dependence.)

Further evidence of velocity-dependent propagation in solar-proton events was provided by a comparison of alpha-particle and proton intensities during the events of 12 November 1960 and

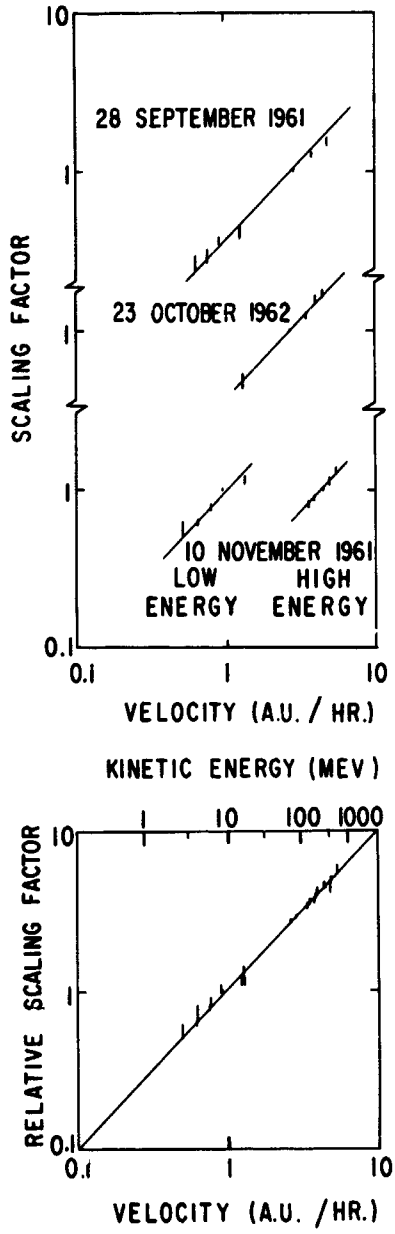

FIGURE 17a and 17b.—The scaling factors by which the differential intensity vs time plots of each event were shifted horizontally to give the optimum fit to a common curve. This effort was made to determine the nature of the dependency on velocity; comparison lines of slope 1 are used to indicate the closeness of fit to a linear velocity dependence.

15 November 1960 by Biswas *et al.* (1962, 1963). Several rockets carrying nuclear emulsions were fired into these events, and the relative intensity of alpha particles and protons having the same velocity was found to be the same at certain times even though the energy spectra of protons and alpha particles were changing with time.

b) The Source Spectrum

We note from Figure 7 that a given source spectrum is well represented by a power law in kinetic energy, although the event of 10 November 1961 is an exception in that two power-law spectra are required. The 28 September 1961 spectrum is remarkable in that it fits a power law over a dynamic range of nearly three decades in energy. The fact that there is no deviation from this smooth, simple spectral representation, even at the low-energy portion of this source spectrum, prompts us to put forward the argument, based purely on aesthetic grounds, that the amount of matter traversed by the solar protons after acceleration was less than the range of 1 mev proton, that is, about 1 milligram cm^{-2}. If we consider a beam of particles penetrating an absorber, we find the emerging spectrum very much depleted in particles with energies near that required to just penetrate the absorber. There is consequently a rapid change of slope at low energies. It seems unlikely, therefore, that an excess production of lower-energy protons would occur in such a manner as to exactly compensate their absorption in an amount of material greater than their range resulting in so simple a form of source spectrum.

We can draw no conclusions here about the solar-proton acceleration process from the shape of the source spectra, since there probably are a number of processes that would produce the observed spectra. Table IV gives the slopes of the spectra observed in the events under discussion.

c) The Propagation Medium

For the purpose of this discussion we define the propagation medium to be the medium through which solar protons travel after acceleration and escape from the acceleration mechanism. Let us now consider where the scattering takes place.

Meyer, Parker and Simpson (1956) suggested that during the 23 February 1956 event scattering took place in interplanetary space beyond the earth's orbit. Parker (1963) has discussed a mechanism of simple diffusion throughout interplanetary space; E. Roelof (private communication, 1963) has found that scattering by magnetic fields in interplanetary space that are irregular in space and/or time would produce a degree of scattering that is a function of particle rigidity.

McCracken (1962) introduced the idea of small-angle scattering caused by irregularities in an otherwise quasi-radial interplanetary field to account for the onset of isotropy in several solar-proton events. Anderson *et al.* (1959) and Gold (1962) have suggested that the processes of scattering and drift in the strong magnetic fields near the sun must play an important part in solar-proton propagation. Bryant *et al.* (1962) and Hoffman and Winckler (1963) found that the intensity vs. time profiles of several solar-proton events are well represented by those to be expected from a process of simple diffusion in interplanetary space.

The propagation curves of the three velocity-dependent events are compared in Figure 18.

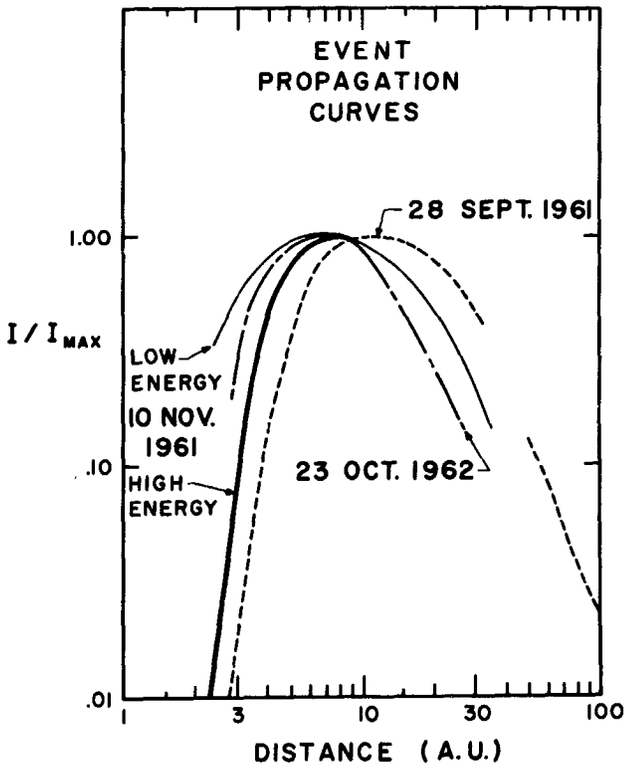

FIGURE 18.—The propagation curves of the three velocity-dependent events. These curves represent distributions in the distance travelled by solar protons from release into the propagation medium to the point of observation.

Apart from that of the low-energy component of 10 November 1961, the curves are geometrically similar to a remarkable degree. It is meaningful, therefore, to associate with each of the curves a parameter describing the rate of propagation of the event. A convenient parameter, though somewhat poorly defined, is the most probable distance traveled—that is, the distance traveled by the particles arriving at maximum intensity. These distances are listed in Table IV. We notice that the ordering of the propagation geometry in the three events correlates either with the phase of the solar cycle or with the displacement in longitude of the flare from about 70 degrees west, the origin of the earth-intercepting garden-hose line. For example, the slowest event is that from a flare at 29 degrees east; it is also the first in time. No significance is claimed for either correlation on the basis of such a small number of events.

We have mentioned that the intensity curves which fit a common propagation curve in a given event also fit the equation for simple diffusion. The resulting effective mean free paths and other parameters are listed in Table IV. In spite of this fit, it is difficult to see how solar protons could undergo a process of simple diffusion in interplanetary space especially since the garden-hose magnetic field has been observed to play an important part in guiding solar protons away from the sun. Another difficulty is that the observed velocity independence of the scattering implies that the scattering takes place at discrete scattering centers, rather than as a continuous process, as would otherwise seem more reasonable. The finding that the degree of scattering is independent of rigidity, combined with Roelof's result for continuous scattering in irregular magnetic fields, rules out such a mechanism at least for the events under discussion.

In order to reconcile a diffusive propagation with the previously observed guiding by the garden-hose interplanetary field, we consider a model in which scattering occurs near the sun and the particles escape to the earth after diffusing from the flare to the foot of a line of force providing direct access to the earth (Gold, 1959). We meet at once with two difficulties. Firstly, particle drift produced by gradients and curvatures in any general field near the sun would lead to a rigidity-dependent propagation. Secondly, there must be a certain amount of scattering in interplanetary space to account for the onset of isotropy (McCracken, 1962). Since any pitch-angle scattering would in general be accompanied by a change of guiding center there would be some

motion across the lines of force. The question then arises of the relative importance of motion along the lines of force and motion across them. We have then reached a process of anisotropic diffusion in interplanetary space instead of one of simple isotropic diffusion. Anisotropic diffusion conceivably could account for the observations, but there is no present theoretical treatment against which to test the data.

d) The Stability of the Propagation Medium

One important consequence of a velocity-dependent propagation is that low-energy protons travel through the propagation medium later than the high-energy protons and yet suffer the same degree of scattering. The average properties of the propagation medium can, therefore, remain constant for at least two days. It is important to remember, though, that changes must have been occurring in the magnetic field structure during the period of propagation. During the event of 28 September 1961, for example, there was an enhanced solar plasma moving out from the sun. Where the solar protons are isotropic in interplanetary space, even gross changes in magnetic field structure can produce only small effects if they take place many mean free paths from the point of observation. Only changes in magnetic field structure occurring near the satellite could strongly influence the measured intensity. We suggest that the character of the 10 September 1961 event was largely determined by such effects, dominating the intensity vs. time character more than the dispersion that otherwise should have been present. One can only speculate at this stage on the details of the mechanism producing time-dependent effects.

e) Local Disturbances of the Propagation Medium

As was mentioned above, the periodic intensity fluctuations are almost certainly a result of magnetic field structure in the region of interplanetary space near the earth. The fluctuations could result from, for example, adjacent regions of strong field and weak field constituting a trapping region or "magnetic bottle." Such regions would exclude some incident particles, thereby lowering the particle density in the region of the weaker field. Such regions might eventually become filled as a result of scattering from magnetic irregularities and, in fact, the magnitude of the fluctuation does decrease with time. This mechanism does not account for the regularity of the fluctuation unless there is postulated a characteristic wave motion of interplanetary plasma. The wave motion is not a property of all interplanetary plasma but is confined to the region between the magnetosphere and the quasi-stationary bow wave postulated by Axford (1963) and others. They pointed out that interaction between the solar wind and the magnetosphere should create a bow wave standing several radii from the magnetosphere on the sunlit side of the earth; this phenomenon was recently observed with a plasma detector (Bridge *et al.*, 1964) and a magnetometer (Ness *et al.*, 1964) on Explorer XVIII. All solar-proton measurements reported here were made outside the magnetosphere but behind this bow wave. It is possible, therefore, that the modulation of solar-proton intensity was confined to this region alone: regular structure in this region may be due directly to regular structure in the solar wind or it may be a natural frequency of the region.

Fluctuations with a period of approximately one hour were noted in the Explorer X magnetic field and plasma data (Heppner *et al.*, 1963; Bonetti *et al.*, 1963) where they were interpreted as a result of the passage of the space probe in and out of the pulsating boundary of the magnetosphere. Mathews *et al.* (1961) noted fluctuations with a period of 1.25 hours in neutron monitor records of the event of 12 November 1960. They suggested that these fluctuations were a direct result of pulsating decreases in the horizontal component of the earth's field measured at the equator. Winckler *et al.* (1961) also observed similar fluctuations in balloon measurements of solar-proton intensity. All of these forms of fluctuation may have been due to the same cause, namely, either a regular structure in the interplanetary plasma density or a natural frequency of the region between the bow wave and the magnetosphere.

REFERENCES

ANDERSON, K. A., ARNOLDY, R., HOFFMAN, R., PETERSON, L., and WINCKLER, J. R. 1959, *J. Geophys. Res.*, **64**, 1133.

ANDERSON, K. A., and WINCKLER, J. R. 1962, *J. Geophys. Res.*, **67**, 4103.

AXFORD, W. I., and REID, G. C. 1962, *J. Geophys. Res.*, **67**, 1962.

A*xford*, W. I. 1962, *J. Geophys. Res.*, **67**, 3791.

BISWAS, S., FICHTEL, C. E., and GUSS, D. E. 1962, *Phys. Rev.*, 128, 2756.

BISWAS, S., FICHTEL, C. E. GUSS, D. E., and WADDINGTON, C. J. 1963, *J. Geophys. Res.*, **68**, 3109.

BONETTI, A., BRIDGE, H. S., LAZARUS, A. J., ROSSI, B., and SCHERB, F. 1963, *J. Geophys. Res.*, **68**, 4017.

BRIDGE, H., EGIDI, A., LAZARUS, A., and LYON, E. *Explorer XVIII Symposium*, Gaddard, 1964.

BRYANT, D. A., CLINE, T. L., DESAI, U. D., and MCDONALD, F. B. 1962, *J. Geophys. Res.*, **67**, 4983.

———. 1963, *Phys. Rev. Letters*, **11**, 144.

CHARAKHCHYAN, A. N., TULINOV, V. E., and CHARKHCHYAN, T. N. 1961, *Proc. Intern. Conf. Cosmic Rays and the Earth Storm*, Kyoto, 2, 365.

GOLD, T. 1959, *J. Geophys. Res.*, **64**, 1665.

———. 1962, *J. Phys. Soc. Japan*, **17** (A–2), 600.

HEPPER, J. P., NESS, N. F., SCEARCE, C. S., and SKILLMAN, T. L. 1963, *J. Geophys. Res.*, 68, 1.

HOFFMAN, D. J., and WINCKLER, J. R. 1963, *J. Geophys. Res.*, 68, 2067.

MATHEWS, T., TAMBYAHPILLAI, T., and WEBBER, W. R. 1961, *Monthly Notices of the Royal Astron. Soc.*, **123**, 97.

MCCRACKEN, K. G. 1962, *J. Geophys. Res.*, **67**, 423, 435 and 447.

MEYER, P., PARKER, E. N., and SIMPSON, J. A. 1956, *Phys. Rev.*, **104**, 768.

NESS, N., SCEARCE, C., and SKILLMAN, T. *Explorer XVIII Symposium*, Goddard, 1964.

PARKER, E. N. 1963, *Interplanetary Dynamical Processes*, (New York: Interscience Publishers).

REID, G. C., and AXFORD, W. I. 1962, *J. Geophys. Res.*, **67**, 3590.

WINCKLER, J. R., BHAVSAR, P. D., and PETERSON, L. 1961, *J. Geophys. Res.*, **66**, 995.

cont'd on enclosure

N65-10683

VELOCITY DEPENDENCE AND SOURCE SPECTRA OF SOLAR PROTON EVENTS*

D. A. BRYANT†, T. L. CLINE, U. D. DESAI‡ AND F. B. McDONALD

It has become clear from recent satellite measurements[1,2] that solar protons can be transported from the sun to the earth in three distinct ways in addition to the direct way sometimes observed with cosmic-ray monitors at sea level.[3] We wish to describe these four modes of propagation and then show how the velocity dependence of one of these modes makes it possible to determine the energy spectrum of the particles at the time of release from the sun.

We classify solar particle events consisting of radiation with energy above 1 Mev into four distinct classes. The distinction between the classes depends upon the way in which the particles are transported from the sun to the region of the earth. The first two classes consist of particles that arrive at the earth in a manner determined by particle velocity; the first class consists of predominantly higher-energy anisotropic particles that arrive after nearly a direct transit and the second class consists of those that arrive after a diffusive propagation; the third class consists of those that arrive in a manner determined by the motion of enhanced solar plasma; the fourth class consists of those that depend upon the rotation of the sun. Typical delays between the occurrence of a solar flare and the arrival at the earth of particles in these four classes are different. The delay of the first class event is close to the rectilinear transit time for highly relativistic particles and is therefore only a few minutes. The arrival-time delay of the second class depends upon the rate at which particles propagate through interplanetary space and so varies with energy up to a number of hours. The typical delay for particles in the third class is not a function of energy since particles of all energies arrive with the enhanced solar plasma responsible for Forbush decreases and geomagnetic storms; it is the transit time of solar plasma across one astronomical unit, that is, about two days. The fourth class event takes place near the time of central-meridian passage of a plage region responsible for a flare and solar particle events of the other classes during the previous solar rotation. This fourth class is closely associated with long-lived solar streams. The delay between the parent flare and the arrival of these particles is not a function of energy since particles of all energy arrive with the plasma stream. The delay depends upon the solar longitude of the parent flare and may therefore be as long as one solar rotation, or 27 days. Figure 1 shows the times of occurrence of events of the latter three classes seen by Explorers XII and XIV during parts of 1961 and 1962. Four sequences of events are evident.

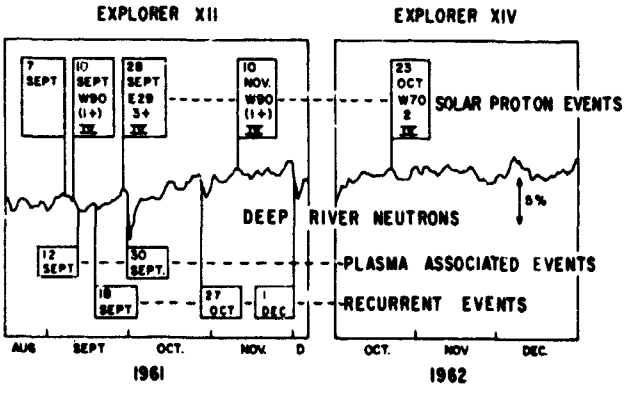

FIGURE 1.

*Published as *Goddard Space Flight Center Document X-611-64-63*, and also published in the *Proceedings* of the International Conference on Cosmic Rays, Jaipur, India, 1:70–82, April 1964.

†Goddard Space Flight Center and D.S.I.R. Radio Research Station, Slough, Bucks, England.

‡Goddard Space Flight Center and Physical Research Laboratory, Narrangpura, Ahmedabad, India.

No events of the first class were seen with sea-level monitors during these time intervals. Figure 2 shows the variation in intensity of interplanetary protons of energy greater than 3 Mev during a sequence involving all the three classes of events seen. Superimposed on the intensity decay of the velocity-ordered event of 28 September is the plasma-associated event of 30 September, followed in turn after 27 event-free days by a recurrent event on 27 October.

We now confine our attention to several velocity-ordered events observed on Explorers XII and XIV. We show how it has been possible in these events to determine separately the influence of the propagation medium and the form of the energy spectrum of particles released from the sun, that is, the source spectrum. These deductions were made possible by the fact that differential energy measurements could be made outside the magnetosphere with the equipment carried by these satellites.

A striking velocity dependence was shown by the solar proton event of 28 September 1961. This is shown by Figures 3 and 4. Figure 3 shows intensity vs. time profiles for various differential energy components. The abscissa is in units of hours from the time of the flare. Figure 4 shows the behavior of the intensities of the same differential components of the event but this time plotted not as a function of time but as a function of distance traveled. The distance traveled is simply the product of particle velocity and time from the flare. The intensity curves of the various components have been vertically scaled to give the best fit to a common curve. The physical meaning of this normalization will be examined further below. We note from Figure 4 that all components lie very closely on a common curve. We may interpret Figure 4 as a measure of the probability that a particle should travel a given distance before reaching the earth from the sun. The fact that we have essentially a common curve shows that particles of all energies traveled a given path length with equal probability. This is true for all path lengths to the extent that the various components of Figure 4 lie on a common curve. The statistical distribution of path length traveled is clearly a property of the propagation medium of interplanetary space. We note that the distance traveled by most particles is an order of

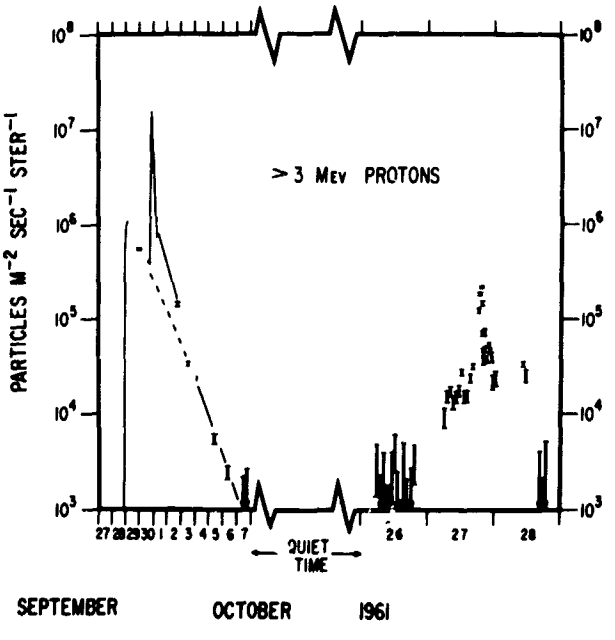

FIGURE 2.

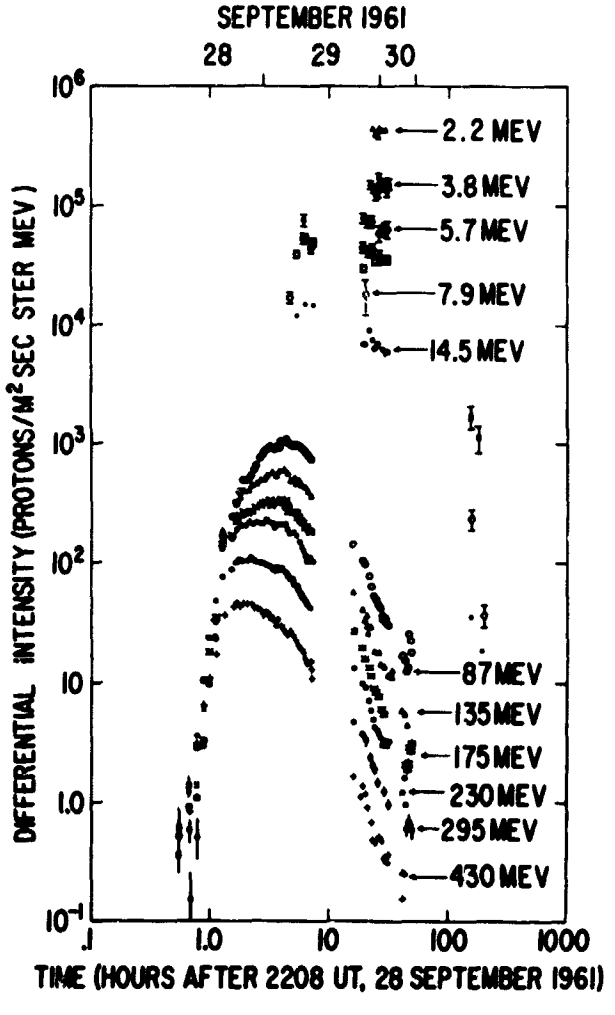

FIGURE 3.

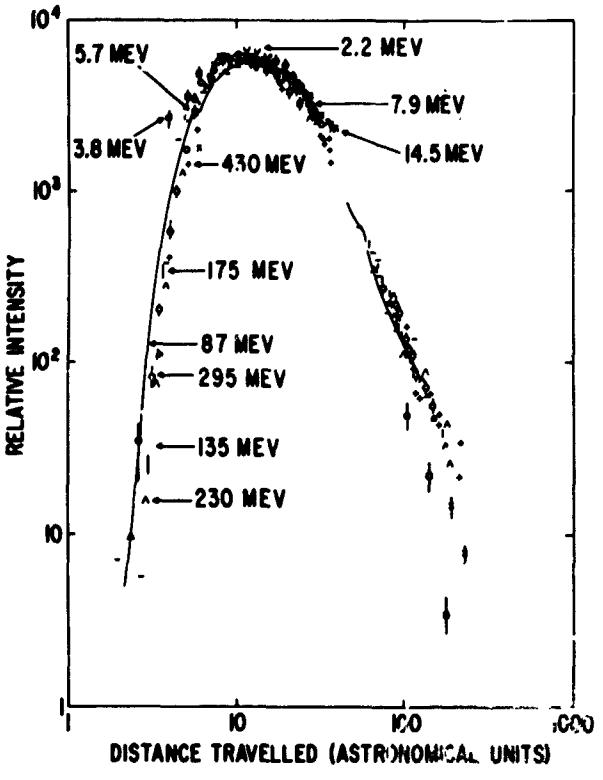

FIGURE 4.

magnitude larger than one astronomical unit. This indicates that propagation involved an important degree of scattering. Further, the degree of scattering is not a function of energy over the range examined. This suggests that the mode of propagation is a diffusion-like process and that energy-dependent processes, such as drift across magnetic field lines, do not play a dominant role. In fact, the equation for simple diffusion fits the propagation curve of this particular event through its maximum. It does not fit, though, at the beginning where anisotropy is dominant and at the end where boundary conditions must be taken into account.

Some of the other solar proton events we have observed with Explorers XII and XIV show the same degree of good fit to common, velocity-compensated, intensity vs. distance curves, but a few contrast by not fitting at all. We believe that these exceptions do not weaken our argument for velocity dependence but strengthen it by illustrating that there are times when the properties of the propagation medium cannot, by this technique, be sorted from the source characteristics because, for example, the medium could be changing as the particles are propagating through it. In fact, some solar events may thereby be combinations of events of our first three categories. Although our observations indicate that solar proton intensities in some cases depend very closely upon the first power of velocity, a choice between velocity and rigidity dependence cannot be made from these data alone. There are indications from earlier emulsion measurements of solar proton and alpha intensities,[4] however, that velocity dependence is preferable.

We discuss now the physical meaning of the scaling factors used to construct Figure 4. Let us consider the relative intensity of two components of the event. We have recorded the intensities not as a function of time but as a function of distance traveled and found that the ratio of intensities is essentially constant over a range from 2 astronomical units to more than 100 astronomical units. There is nothing to suggest that an extrapolation back to zero distance is invalid.

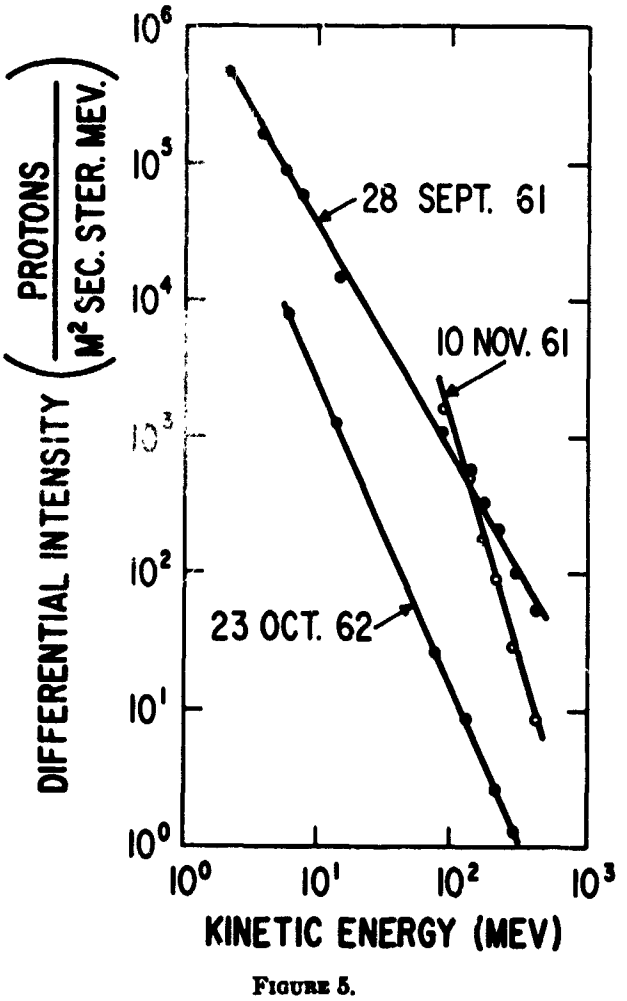

FIGURE 5.

The ratio of the intensities of two components at zero distance is, by definition, a measure of the shape of the source spectrum. Figure 5 shows the source spectrum obtained directly from the scaling factors used to produce Figure 4. The source spectra of two other events analyzed in a similar way are also shown. The ordinate of Figure 5 is arbitrarily chosen to be the maximum intensity reached at the earth. The differential intensities shown are proportional to the absolute differential intensities of protons produced at the sun and retain, therefore, the same spectral form, but the constant of proportionality depends on the geometry of propagation, which is unknown. (For example, since simple diffusion theory fits this propagation curve through maximum intensity, the numerical solution it gives for the source intensity is of the same spectral form, but that solution is for diffusion in an infinite, isotropic sphere, and is probably not a meaningful one.)

We note from Figure 5 that the source spectra are commonly very well represented by power laws in kinetic energy. This fact prompts us to put forward the argument, based purely on aesthetic grounds, that the amount of matter traversed by the solar protons after acceleration was less than the range of 1 Mev proton, that is, about 1 milligram cm^{-2}. It seems highly unlikely that an excess production of lower-energy protons would so exactly compensate their absorption in an amount of material greater than their range such as to produce so simple a form of source spectrum.

An interesting feature of these events is the existence of small-scale deviations from a common curve. Superimposed on the generally velocity-dependent intensity-time profiles are fluctuations which are nearly periodic with the same frequency and phase over the entire energy range studied. These fluctuations are evident in the velocity-ordered events discussed above, but are more striking in the 10 September 1961 event which showed no velocity dependence and was no doubt influenced by greater interplanetary disorder. Figure 6 shows plots of some sample intensities and indicates the periodic fluctuations. In this event the period is about 1.5 hours; in other events the period is slightly different. Since the transit-time dispersion over the energy range studied is significant, the fact that, in any given

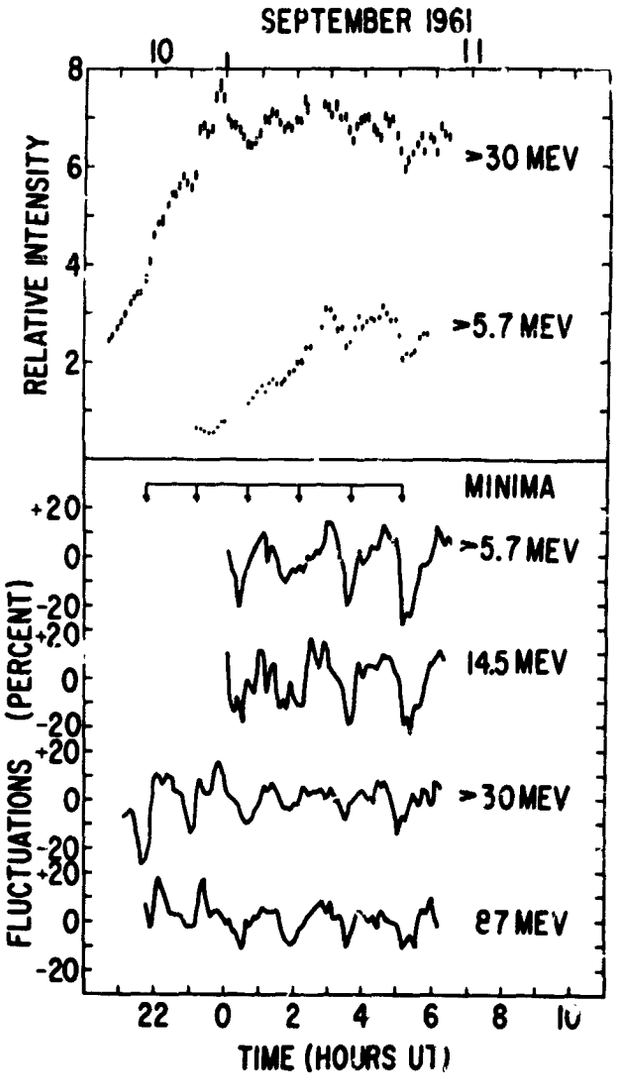

FIGURE 6.

event, the fluctuations have the same period and are in phase at all energies shows that their origin is local. We suggest, therefore, that they reflect the magnetic field structure in local interplanetary space, but we as yet have no explanation for their periodicity.

REFERENCES

1. New Evidence for Long-Lived Solar Streams in Interplanetary Space, D. A. Bryant, T. L. Cline, U. D. Desai and F. B. McDonald, *Phys. Rev. Letters*, 11, No. 144 (15 August 1963)
2. Explorer 12 Observations of Solar Cosmic Rays and Energetic Storm Particles after the Solar Flare of September 28, 1961, D. A. Bryant, T. L. Cline, U. D. Desai and F. B. McDonald, *J. Geophys. Res.*, 67, No. 13, 4983, (December 1962)

3. Observation of a Short-Lived Cosmic-Ray Solar Flare Increase with a High-Counting-Rate Meson Detector, R. A. R. Palmeira and K. G. McCracken, *Phys. Rev. Letters*, 5, No. 1, 15, (July 1, 1960).

4. Hydrogen, Helium and Heavy Nuclei from the Solar Event on November 15, 1960, S. Biswas, C. E. Fichtel, D. E. Guss and C. J. Waddington, *J. Geophys. Res.*, 68, No. 10, 3190, (May 15, 1963).

See A65-15-23

COMMENTS ON THE VANGUARD 3 MAGNETIC FIELD DATA AND ANALYSIS*

JOSEPH C. CAIN AND SHIRLEY HENDRICKS

The principal results of the Vanguard 3 magnetic field experiment are summarized in a report and a paper [*Cain et al.*, 1962 *a*, *b*]. Since some of the material presented in these documents has been used by several authors, it is worth while to clarify a few points and to report a modification indicated by a later analysis.

The Vanguard 3 report gives a series of 63 spherical harmonic coefficients fitted to the data themselves by the iterative procedure of *Jensen and Cain* [1960] (reviewed by *Heppner* [1964]). This field, designated Vanga, used g_n^m and h_n^m to $n=m=7$ and gave an rms deviation from the data of 21 γ. The data selected for this fit were the 2797 observations given by *Cain et al.* [1962*a*] as $L=0$(=best data), excluding four such observations with residuals (measured F−computed F) over 100 γ. These observations were those recorded at Blossom Point, Maryland, on October 4, 1959, at 0h 47m 23s, 0h 47m 37s, 19h 50m 11s and 19h 50m 29s. In the Vanguard 3 report we said 'The Vanga field should be construed only as a smooth curve through these data and not necessarily as a physically meaningful description of the geomagnetic field in regions remote from the Vanguard measurements.' We should note here that there is also no claim that the Vanga coefficients provide a description of other than the *total scalar field* $|\bar{F}|$ within the spacetime volume over which the data are taken. The validity of these statements is amply illustrated by *Leonard* [1963] in connection with the Johnson Island tests. In his paper he shows that the observed auroral emission seen at a point conjugate to the bomb explosions could best be predicted by the set of 48 coefficients derived by *Jensen and Cain* [1962] and that the worst agreement resulted from using the Vanga coefficients. This disagreement is not surprising, since the field line tracing requires a knowledge of the vector field and since the nearest Vanguard 3 observation was made more than 3000 miles away!

One feature of the Vanguard 3 data relative to the Vanga fit was the systematic variation of the residuals with altitude. This fact was illustrated in Figure 2 of *Cain et al.* [1962*b*] and led to the conclusion that 'A smaller systematic variation of the field was noted that appeared to require external sources. . . .' Subsequent analysis of the data using a slightly modified technique has changed this conjecture. This improvement was to solve the whole set of equations simultaneously in the linear expansion of potential rather than using the previously adopted technique of solving for small sets (up to 16) of coefficients at once, holding the rest constant, and iterating so as to correct all coefficients for a given n at a time. These methods were used, since difficulties were originally found in finding stable solutions to the Vanguard 3 data, and it was thought that the problem was one of losing accuracy in the solution involving large determinants.

The results of using the improved techniques are shown in Table 1, where we give the smallest

TABLE 1.—*rms Residuals between Vanguard 3 Data and Sets of Spherical Harmonics using Different Numbers of Coefficients*

Maximum $n=m$	No. of Coefficients	rms Residuals, γ
3	15	83.2
4	24	25.6
5	35	17.6
6	48	16.9 Vangb
7	63	16.7

*Published in *Journal of Geophysical Research*, 69(19):4187–4188, October 1, 11964.

rms residual to the Vanguard 3 data that could be determined with the specified number of coefficients. As can be seen in this table, it was possible to obtain a fit to a rms of 17.6 γ with only 35 coefficients, whereas the previous best fit of 21 γ required 63 coefficients. Only spatial terms are used here owing to the short period of 84 days over which the data are taken. However, an inspection of the isoporic charts in F over the regions of measurement show changes in the earth's surface up to 15 γ in a quarter year. It is thus likely that a somewhat better fit to the Vanguard 3 data will be made possible by the inclusion of secular change terms even over this short an interval.

The 48-term set designated 'Vangb' in Table 1 was used to re-evaluate the conclusions drawn in the Vanguard 3 paper. The only change is illustrated in Figure 1, which gives the average deviation with altitude of the observations from this new field. The systematic shift with altitude illustrated in Figure 2 of the original paper [*Cain et al.*, 1962*b*] vanishes. Thus there are no longer any detectable local sources in the volume of the Vanguard 3 measurements that contribute systematically to the field at the level $\sim 6\gamma$. The major conclusion of the Vanguard 3 paper that the sources of the D_{st} field must lie above altitudes of the order of 2500 km remains unaltered. The positive correlations previously obtained between D_{st} at the earth's surface and the residuals to the new fit are not lessened. Instead, the correlations shown in Figure 9 of the Vanguard 3 paper are slightly more positive.

Although the Vangb field gives comparable results in serving as a tool for analysis of the Vanguard 3 magnetic field data, its validity outside the regions of the data is even less than for Vanga. This fact was well illustrated when we attempted to find the Vangb conjugate point for Johnson Island to compare with those computed and observed by *Leonard* [1963]. The result is that for Vangb the magnetic equator passes nearly *through* Johnson Island and thus the conjugate point starting with an altitude of zero falls within 100 km!

Further analyses of the main geomagnetic field have been done which include the use of the Vanguard 3 data as a valuable addition to the total data set. The results of this work were reported recently [*Daniels and Cain*, 1964] and will form the basis of a publication in which a realistic field will be presented. It is hoped that workers in the field of geomagnetism will meanwhile confine the use of the Vanga set of coefficients to interpolations of the scalar field $|\bar{F}|$ in the spacetime volumes enclosed by the Vanguard 3 data and not attempt extrapolations to other regions where the result is likely to be fictitious.

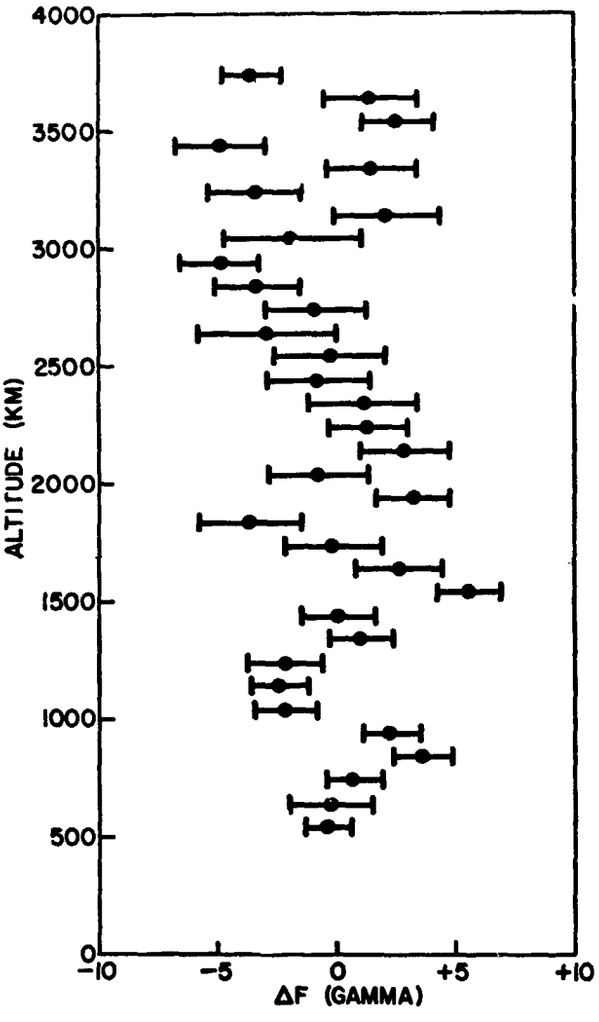

FIGURE 1.—Average deviation of the Vanguard 3 magnetic data from the 48 coefficient Vangb field plotted as a function of altitude. These average residuals are given with error bars signifying the standard error of each mean.

REFERENCES

CAIN, JOSEPH C., IVAN R. SHAPIRO, JOHN D. STOLARIK, and JAMES P. HEPPNER, Measurements of the geomagnetic field by Vanguard 3 satellite, *NASA Tech. Note D-1418*, 1962*a*.

CAIN, JOSEPH C., I. R. SHAPIRO, J. D. STOLARIK, and J. P. HEPPNER, Vanguard 3 magnetic-field observations, *J. Geophys. Res.*, **67**, 5055–5069, 1962*b*.

DANIELS, W. E., and J. C. CAIN, An evaluation of the confidence levels of the spherical harmonic coefficients for the geomagnetic field (abstract), *Trans. Am. Geophys. Union*, **45**, 39, 1964.

FINCH, H. F., and B. R. LEATON, The earth's main magnetic field—epoch 1955.0, *Monthly Notices Roy. Astron. Soc., Geophys. Suppl.*, **7**(6), 314–317, 1957.

HEPPNER, J. P., The world magnetic survey, *Space Sci. Rev.*, **2**, 315–354, 1963.

JENSEN, D. C., and J. C. CAIN, An interim geomagnetic field (abstract), *J. Geophys. Res.*, **65**, 2500, 1960.

LEONARD, Robert S., Selection of a model of the earth's magnetic field, *J. Geophys. Res.*, **68**, 6437–6440, 1963.

PARTICLE ACCELERATION IN CISLUNAR SPACE*

A. G. W. CAMERON

The recent discovery[1] of a characteristic red luminescence when enstatite achondrites are bombarded by 40-keV protons led Kopal and Rackham[2, 3] to observe the Moon in order to determine whether a similar luminescence might be excited in lunar materials by solar wind bombardment. On the night of November 1–2, 1963, Kopal and Rackham observed an enhanced red emission from the vicinity of the crater Kepler. The duration of the red glow was of the order of 10 min or longer, and it appeared twice within a 2-h period. No repetition of this phenomenon was observed on the following night or at the next lunation.

Among the circumstances which may be relevant to an explanation of this phenomenon are the following: the enhanced emission occurred within one day of Full Moon. There had been a class 3 solar flare on October 28 and two class 1 flares on November 1, and the Earth was in a magnetically disturbed region of space. Cosmic-ray neutron counts indicated that recovery from a Forbush decrease was occurring at the time of the luminescence.

Kopal and Rackham [2] noted that the red glow from the Kepler region approximately doubled the brightness of the lunar surface there, so that the amount of energy emitted in the red was approximately 10^4 ergs/cm^2 sec. They further concluded [2] that since the highest luminescent efficiency (in the Bustee meteorite) had been found to be 20 percent,[1] it was likely that the incoming energy responsible for the luminescence was at least 5×10^4 ergs/cm^2 sec. The other two enstatite achondrites examined by Derham and Geake [1] had a luminous efficiency lower by a factor of three, so it is not unlikely that the incident energy exceeded 10^5 ergs/cm^2 sec. Because approximately the same luminous efficiency is found during bombardment of the meteorite powder by photons of several MeV as by protons of 40 keV[4], it appears likely that the above conclusions ear not sensitive to the energy of the particles bombarding the lunar surface.

Kopal and Rackham [2] have discussed a possible interpretation that the above events resulted from bombardment of the lunar surface by an enhanced flow of solar plasma initiated by the preceding solar activity. They noted that the energy flux required was five orders of magnitude greater than that normally available in the solar wind, which must be considered a difficulty. Kopal [4] has suggested that an alternative mechanism might be required in which the lunar bombardment would involve particles, of energy greater than those of the solar wind, which had been accelerated in the preceding class 3 flare and trapped by the chaotic magnetic field configuration then existing in interplanetary space. It is the purpose of this communication to suggest a further alternative.

The region of interaction between the solar wind and the Earth's magnetosphere is very complex; but the following general picture has emerged (see, for example, Hines [5]). In the solar direction the pressure of the solar wind compresses the magnetosphere, but the solar wind must then flow around the magnetosphere, so that in the antisolar direction a long cavity is formed into which the terrestrial magnetic field can expand. Quite large energetic particle fluxes are observed near the magnetosphere boundary in the antisolar direction, and it has been suggested that the region of trapped radiation may extend to a distance comparable with that of the Moon.[6] A recent analysis of terrestrial magnetic activity has shown that the general level of activity is slightly changed for several days on either side of Full Moon, suggesting that the antisolar magnetic cavity may extend to the lunar distance.[7] Since the solar wind

*Published in *Nature* 202(4934):785, May 23, 1964.

exhibits supersonic flow with respect to the Earth, it is necessary that a standing shock wave must be formed beyond the magnetopause. The highly turbulent magnetic fields between the shock front and the magnetopause have been observed.[8]

It seems to be the case that wherever turbulent fluid motions and chaotic magnetic fields exist in Nature, the acceleration of charged particles to energies much exceeding thermal energies takes place. This is inferred to be the case in strong extragalactic radio sources, in supernova remnants, in solar flares, and in the magnetosphere itself. One acceleration mechanism which can be very efficient in certain circumstances is the second-order acceleration of charged particles traversing time-varying fluctuations in a magnetic field system.[9] This is probably responsible for the acceleration of particles in the outer part of the magnetosphere which are then dumped directly into the atmosphere to produce aurorae. The process will be enhanced at times of greater magnetic activity when the solar wind is exerting varying pressure on the magnetopause.

It is a logical extension of these considerations to expect that extensive particle acceleration will take place in the shock zone beyond the magnetopause. The particles thus accelerated will be discharged down the magnetic field lines in the antisolar direction. By analogy with the auroral discharges, it is possible that the particle beams in the antisolar direction may carry an energy flux large compared to that in the solar wind. However, since the energy going into the charged particle beams must be derived from that of the solar wind, it is evident that such particle streams will be isolated in local regions of space, and that the integrated energy flux of plasma and particles together cannot exceed the initial energy flux of the plasma flow.

The luminescence near the crater Kepler observed by Kopal and Rackham may have been produced by these energetic particle streams. It may also have been produced by trapped radiation in the distant tail of the magnetosphere. Many more observations will be needed to evaluate the plausibility of these two possibilities. In either case, such luminescence can be expected to occur principally at times near Full Moon and during unusually large magnetic activity on the Earth. Because of the localized nature of the incident particle streams, lunar luminescence excited in this way is likely to be observed only in small regions of the Moon at any one time and to exhibit variations with periods of a few minutes.

Because of the complex character of the phenomena suggested here, it is not possible to suggest the range of energies to which particles are likely to be accelerated in the shock zone, and hence it is not clear whether such particle streams will constitute a radiation hazard to a manned lunar landing or to manned spaceflight in the antisolar direction.

I wish to thank Prof. Z. Kopal for a stimulating discussion of his observations.

REFERENCES

[1] Derham, C. J., and Geake, J. R., *Nature*, **201**, 62 (1964).

[2] Kopal, Z., and Rackham, T. W., *Nature*, **201**, 239 (1964).

[3] Kopal, Z. and Rackham, T. W., *Sky and Telescope*, **27**, 140 (1964).

[4] Kopal, Z. (private communication).

[5] Hines, C. O., *Science*, **141**, 130 (1963).

[6] Frank, L. A., Van Allen, J. A., and Macagno, E., *J. Geophys. Res*, **68**, 3543 (1963).

[7] Stolov, H., and Cameron, A. G. W. (to be published).

[8] Ness, N. F., *IMP Satellite Symposium at Goddard Space Flight Center* (March 1964).

[9] Shen, C. S. (to be published).

N65-19722

DETECTION OF INTERPLANETARY 3- TO 12-MEV ELECTRONS*

T. L. CLINE, G. H. LUDWIG, AND F. B. McDONALD

In this Letter we report the direct observation of interplanetary electrons of energy above 3 MeV with the IMP-1 satellite (Explorer 18).

Electrons observed in the primary interplanetary radiation in the BeV energy region by Earl[1] and in the 200-MeV energy region by Meyer and Vogt[2] are believed to be of galactic origin because their energies are as high as those assumed to be necessary for their penetration into the inner solar system and because their measured intensity agrees with that which was anticipated to account for galactic radio emission. Support was lent to this hypothesis when the modulation characteristics of these particles were observed[3] to be similar to those of cosmic-ray protons and their positron-to-electron ratio was found[4] to be compatible with an origin of at least half of them in meson-producing cosmic-ray interactions in the interstellar medium. We feel that the existence of an interplanetary flux of electrons lower in energy by orders of magnitude is interesting because of the possibility that these too may have a cosmic origin. If so, their study should yield entirely new information about the galactic electron sources and modulation characteristics. If they are of solar origin, there are analogous implications. We wish to demonstrate here that the flux of lower-energy electrons we observe is indeed a primary component of the interplanetary radiation, and to discuss its properties in terms of its possible origin, either galactic or solar.

The observations reported here were made with a scintillator telescope on Explorer 18, a satellite placed in an elliptic orbit with an apogee height of 193,000 kilometers. Data were taken from the launch, on 27 November 1963, until 6 May 1964 when the satellite passed into a long period in the earth's shadow, causing failure of the detector. During this time interval the apogee moved from the sunlit side of the earth beyond the magnetosphere (terminating at about 70,000 km) and beyond the earth's shock front (observed with a magnetometer[5] and plasma sensor[6] at about 100,000 km) to the region behind the earth and inside the shock front. Electron data taken only when the satellite was beyond 125,000 kilometers are reported here; throughout the life of the instrument these data continued to be free from effects due to the trapped radiation.

The detector was developed[7] to study low-energy cosmic-ray protons, electrons and light nuclei. It is composed of three scintillators: two in coincidence, measuring energy loss and total energy, and a guard counter in anti-coincidence. When a table of intensity vs. measured energy loss vs. measured total energy is constructed from data taken at apogee, there is seen a distinct counting rate component of minimum-ionizing energy loss and of low apparent energy. An analysis of the topology of distributions in energy loss and in total energy through this minimum-ionizing component indicates that indeed it is composed of three distinct particle groups: On group with total energies corresponding to electrons that stop within the detector, a much smaller group with a high apparent total energy equal to or exceeding the energy loss of a minimum-ionizing cosmic ray traversing the detector, and a third group with very low total energies. We believe that the latter two components are surely secondary radiations composed of, respectively, cosmic rays that avoid detection by the guard counter (for example, by turning into neutrals through reactions within the detector) and gamma rays made locally in the spacecraft, producing random and coherent coincidences between the energy loss and total energy detectors.

*Published as *Goddard Space Flight Center Document X-611-64-368*, November 1964

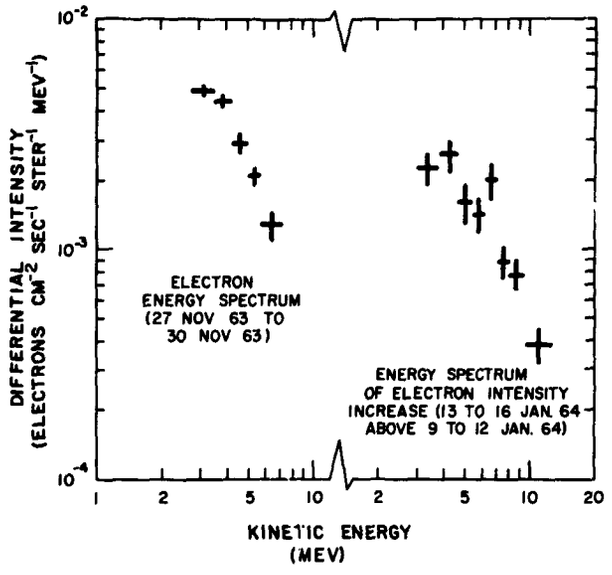

FIGURE 1.—Differential energy spectra of electrons observed beyond 125,000 kilometers from the earth. The first spectrum is from the apogee of the first orbit; the second is the difference between measurements from the 13th and 12th orbits and indicates the first significant increase in intensity.

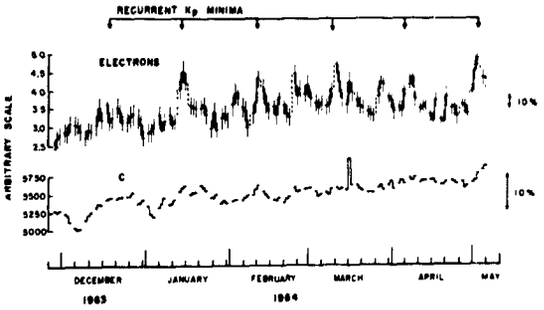

FIGURE 2.—Integral counting rate of electrons throughout the active life of the instrument plotted in quarter-orbit averages. The counting rate "C" of cosmic rays into a thinly shielded scintillator and the times of one recurrent minimum of the interplanetary index K_p are also shown. Recurrent Forbush decreases are seen in the cosmic rays in early December and January and a small solar proton event occurs in March; other increases can be largely attributed to the electron mixture in the cosmic rays.

These secondary effects were eliminated to produce Figure 1a, which shows the energy spectrum of electrons obtained during the first orbit (27 to 30 November 1963) at a time when the observed electron intensity was at a typical minimum and when there were no measurable time variations. Figure 1b shows, for comparison, a spectrum of the difference between the first statistically significant intensity increase (13 to 16 January 1964) and the immediately preceding intensity (9 to 12 January). No background corrections were necessary to produce the latter distribution since the electron intensity increase was unaccompanied by an increase of either secondary gamma rays or spurious cosmic rays; it was therefore possible to determine the intensity to higher energies. The nearly identical shapes of the two corrected spectra suggest that the electrons seen daily may have the same origin as the extra ones seen on days of increased electron flux. The integral intensity of electrons of energy between 2.7 and 7.5 MeV is $210. \pm 10.$ electrons/m²sec.ster., and that of the increase between 3. and 12.5 MeV an additional $100. \pm 10.$ electrons/m²sec.ster.

To demonstrate that most of the observed electrons are not of local or secondary origin at the satellite (e.g., such as knock-on or cascade-shower electrons produced in or near the detector) we consider their time variations. Figure 2 shows the counting rate of these electrons, partially corrected for slow gain drifts in the detector, plotted in the form of one-quarter-orbit averages throughout the active life of the instrument. (The gaps in the data occur at times when the satellite is within 125,000 kilometers; the other three points per orbit are plotted so that each center one represents data taken from beyond 185,000 kilometers.) Also shown are a comparison plot "C" of the integrated cosmic-ray flux into a scintillator with about 0.3 gram cm^{-2} shielding, and the times of a recurrent minimum in the interplanetary magnetic activity index K_p with a period of one solar rotation.

A dominant feature of the electron rate is the appearance of many statistically meaningful intensity increases, including one series apparently coincident with the recurrent K_p minimum. These electron intensity increases were not accompanied by comparable increases in the integral cosmic-ray intensity above 15 MeV: the magnitude of the electron modulation is 50 per cent on occasions, while the cosmic rays undergo modulations of less than 5 per cent. Further, following the flare of 16 March 1964 there was a solar-proton event, accompanied by Type IV solar radio emission,[8] during which the flux of protons of energy between 15 and 75 MeV briefly increased by

several orders of magnitude, while the 3- to 8-MeV electron flux rose less than 50 ± 25 per cent. (Figure 2 shows the quarter-orbit average of the total integrated cosmic ray flux increasing at that time by about 10 per cent.) These comparisons demonstrate that, at most, an insignificant fraction of the electron modulation results from modulations of cosmic rays of energy above 15 MeV.

Modulations of protons with energies below 15 MeV, such as 27-day recurrent solar proton events similar to those observed[9] with Explorer 12, were not monitored with our apparatus; but these would be expected at the times of recurrent Forbush decreases and geomagnetic activity, rather than at the time of our repeating electron increases. Several such 1- to 10-MeV proton intensity increases were observed early in the life of the satellite by Fan, Gloeckler and Simpson[10] but these were about two weeks out of phase with our electron enhancements and appear to be accompanied by, if anything, decreases in the electron intensity and in the galactic cosmic rays.

Finally, a study of 3-hour averages of the observed intensity of these electrons indicates no variations with distance from the earth, either during orbits of minimum intensity or during times of increased intensity; the electron rate is constant through the shock front to a distance of up to 50 per cent beyond it. Further, the satellite's passage through the wake of the moon[5] was unaccompanied by an electron intensity variation. Thus, these electrons are not secondary to cosmic rays or solar protons or due to geophysical processes.

We feel that the question of whether these primary electrons originate at the sun or in the galaxy cannot be difinitely answered on the basis of the available data; however, the following properties of these electrons are consistent with their being galactic. First, the differential energy spectrum of this 3- to 12-MeV component fits smoothly onto a spectral plot of the cosmic-ray electron intensities [1, 2, 4] at much higher energies. Second, the time variations of the electrons can be compared to those of cosmic rays in that there is a strong correlation between the electronint ensity increases and quiet interplanetary conditions, evidenced by K_p minima and very small sea-level cosmic-ray intensity increases. Third, there appears to be a long-term increase of electron intensity after a correction of the same order is applied for a slow, monitored drift in detector gain; if this increase is real, it is similar to the 11-year modulation of cosmic rays as solar minimum is approached. However, the fact that the differential cosmic-ray proton intensity is peaked at about 1 BV/c rigidity and negligible below 150 MV/c markedly contrasts with the fact that electrons of rigidity $\gtrsim 3.5$ MV/c are more abundant than those of greater rigidity. Parker has recently pointed out[11] that particles with gyroradius close to the idealized irregularity scale of the modulating medium should be deflected more than those of either extreme; thus these electrons of low rigidity might originate in the galaxy and penetrate the solar system as easily as those of great rigidity.

In spite of the foregoing arguments for galactic origin, it is not impossible that the electrons came instead from the sun. Several possibilities present themselves. For example, relativistic electrons might be generated over most of the upper surface of the solar atmosphere, in which case regions of enhanced and expanded plasma (which contain recurrent proton fluxes) would tend to contain fewer electrons while regions of quiet-time streaming would contain more, as we have observed. Further, the deceleration of the electrons in the enhanced plasma might be much greater than that in the quiet-time streaming. Alternatively, the electrons might be associated with the development of new sunspot regions, which is a characteristic of this phase of the solar cycle and appears to correlate weakly with the observed pattern of intensity increases.[12] We have not, however, found a correlation with any solar radio or optical activity.

The results we quote here are preliminary: an evaluation of the detector response, providing a more exact spectrum, and a detailed investigation of the time variations will be given elsewhere. We are happy to acknowledge the efforts of the many people who made the IMP-1 a success.

REFERENCES

1. J. A. Earl, Phys. Rev. Letters 6, 125 (1961).
2. P. Meyer and R. Vogt, Phys. Rev. Letters 6, 193 (1961).

3. P. MEYER and R. VOGT, J. Geophys. Res. **66**, 3950 (1961).
4. J. A. DESHONG, JR., R. H. HILDEBRAND and P. MEYER, Phys. Rev. Letters **12**, 3 (1964).
5. N. F. NESS, C. S. SCEARCE and J. C. SEEK, Space Research **5**, N. Holland Publ. (COSPAR Proceedings, Florence, 1964).
6. H. S. BRIDGE, A. EGIDI, A. LAZARUS, E. F. LYON and L. JACOBSON, Space Research **5**, N. Holland Publ. COSPAR Proceedings, Florence, 1964).
7. D. A. BRYANT, G. H. LUDWIG and F. B. MCDONALD, I.R.E. Transactions on Nuclear Science *NS*-**9**, 376 (1962).
8. A. MAXWELL, private communication.
9. D. A. BRYANT, T. L. CLINE, U. D. DESAI and F. B. MCDONALD, Phys. Rev. Letters **11**, 144 (1963).
10. C. Y. FAN, G GLOECKLER and J. A. SIMPSON, Goddard IMP Symposium, March 1964.
11. E. N. PARKER, J. Geophys. Res. **69**, 1755 (1964).
12. H. DODSON PRINCE and R. HEDEMAN, private communication.

7164-2601/1

TELEVISION CINEMAPHOTOGRAPHY OF AURORAS AND PRELIMINARY MEASUREMENTS OF AURORAL VELOCITIES

T. N. DAVIS† AND G. T. HICKS‡

During October 1963 a series of tests were performed at Fort Churchill, Manitoba on the usefulness of an image orthicon closed-circuit television system for indirect auroral photography. The system used was similar to one described in a paper by Hicks (1963). It was equipped with an f/0.75 lens providing an effective field of view of 16°. Recording was accomplished by photographing the television monitor with a 16 mm cinema camera.

Operated at maximum sensitivity, the system enabled direct viewing of 8th and 9th magnitude stars on the television monitor. At this sensitivity level, the system was somewhat better than the unaided, dark-adapted human eye in the detection of weak auroral structures. No difficulty was found in obtaining: auroral photographs of even the weakest structures, with exposures of 1/60 sec at the normal sound cinema rate of 24 frames per second. For brighter forms it was necessary to electronically reduce the system sensitivity. Examples of some of the photographs are presented in Figure 1.

Most of the photographs were recorded on Eastman Plus-X black and white film. In addition, color photographs on Eastman High-Speed Ektachrome film were obtained by sequential insertion of broad-band color filters into the optical system. A color cycle consisting of the placement of red, green and blue filters into the system, was completed in 1/8 sec. The result was a cinema film strip showing a frame with a red image, then a frame with green image, and finally a frame of blue image; the cycle was then repeated. Projected at normal sound speed, the color film shows

FIGURE 1.—From top to bottom, four consecutive photographs of a rayed arc with evenly-spaced and relatively stable ray structures. The exposure of each photograph is 1/60 second; the interval between adjacent photographs is 1/24 sec. The spacing between the ray structures is near 1.8 Km. Note the subtle temporal changes in the aurora that are evident by comparing adjacent photographs.

†Goddard Space Flight Center. NASA-National Academy of Sciences—National Research Council Post-Doctoral Resident Associate on leave of absence from Geophysical Institute, University of Alaska, College, Alaska.

‡E. O. Hulburt Center for Space Research, U.S. Naval Research Laboratory, Washington, D.C.

much flicker but the eye integrates sufficiently so that the colors are additive. Since the spectral response of the system is broader in wavelength than the eye, the color films show more red (due to OIλ6300–6364 and N_2 First Positive bands) and blue (due mainly to N_2^+ First Negative bands near λ4278 and λ4652) than one normally sees by direct visual observation. The filters used in the preliminary tests are very wide, near 800Å at half peak transmission. In the future much narrower filters will be employed in order to isolate specific auroral emissions.

Both the color and black and white television cinema-photography techniques provide data for the study of a variety of morphological aspects of auroral structures. These aspects include auroral motions, auroral pulsations, and the growth, decay and configurations of individual structures. The technique may allow the examination of the relative spatial distributions of the principal auroral emissions in more detail than has been possible previously.

Preliminary analysis of the data has been aimed at the measurement of apparent horizontal velocities with emphasis on the faster motions. These fast motions are of folds within auroral structures, of ray bundles or of well defined regions of enhanced luminosity (streaming). In some cases it is not clear which type of motion is being observed. A summary of 49 velocity measurements is presented in Figure 2. The values presented there are obtained by assuming an auroral lower border height of 100 Km. This assumption and the limited precision of angular calibration of the television system as used in October 1963 lead to uncertainties in the velocity magnitudes which are estimated at 10 percent. The measurements were performed on moving structures visible on consecutive film frames ranging in number from 6 to 125 (time duration 0.2 to 5 secs.).

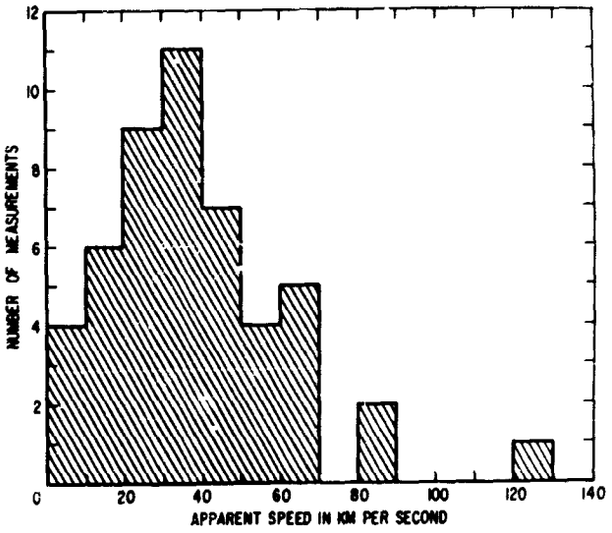

FIGURE 2.—Range of 49 measurements of horizontal speeds of auroral rays and regions of enhanced luminosity. The speed spectrum between 0 and 130 Km per/sec is divided into 13 equal blocks and the number of measurements falling within each block is shown.

REFERENCES

HICKS, G. T., Image orthicon techniques and satellite cinemaphotography; ANNA 1-B, *Photographic Science and Engineering*, 7, 328-330, 1963.

N65-19714

AN EXPERIMENTAL EXAMINATION OF LOW-ENERGY COSMIC RAY HEAVY NUCLEI*

C. E. FICHTEL, D. E. GUSS, AND K. A. NEELAKANTAN†

In a sounding rocket experiment flown from Fort Churchill on September 4, 1963, a finite flux of cosmic ray nuclei with charges greater than that of helium was detected at energies below the experimental energy cutoff of balloon-borne experiments. The particles were examined by extending large sheets of nuclear emulsions from the sides of the rocket during its period outside the atmosphere. The flux of medium nuclei ($6 \leq Z \leq 9$; Z = nuclear charge) in the energy range from 30 to 150 MeV/nucleon was measured as $0.67 \pm .13$ particles/($m^2 sr$ sec), and the flux of ($10 \leq Z \leq 19$) nuclei in the energy range from 40 to 190 MeV/nucleon was $0.31 \pm .09$ particles/($m^2 sr$ sec). A finite flux of light nuclei ($3 \leq Z \leq 5$) was also seen in the 30 to 110 MeV/nucleon region. The abundances of medium and ($10 \leq Z \leq 19$) nuclei relative to helium nuclei in the same energy intervals were found to be significantly less than the relative abundances previously determined at high energies. However, within the statistical uncertainty, the relative differential flux values observed in the vicintiy of the earth are consistent with the helium, medium, and ($10 \leq Z \leq 19$) nuclei having the same source spectrum at least above about 0.2 BeV/nucleon for a wide range of source spectral shapes and an interstellar path length of the order of those normally assumed (i.e., 2.5 g/cm^2 or slightly larger). Other possible interpretations also are considered.

INTRODUCTION

Over the last decade the study of cosmic radiation has progressed considerably and has reached the point where the fundamental properties are becoming reasonably well established.[1–3] The proton energy spectrum now is being measured from 0.01 BeV/nucleon to approximately 10^{10} BeV/nucleon, and the composition of the cosmic radiation has been measured numerous times in the energy region above approximately 0.2 BeV/nucleon. In this region, the composition appears to be independent of energy, at least up to about 10^6 BeV/nucleon, with the possible exception of a small relative increase of the light nuclei in the 0.2 to 0.5 BeV/nucleon interval.[4–8] In particular, the helium to medium nuclei and the helium to heavy nuclei ratios are known to be the same to within about a 15 percent experimental uncertainty in tne region from 0.3 to 7.5 BeV/nucleon. The data also have revealed that there is a strong modulation of the cosmic radiation which is fairly certainly associated with the solar cycle. In the measured energy interval, the variation of cosmic ray intensity is greatest at the lowest energies.[9]

In an effort to increase our general experimental knowledge of the cosmic radiation and at the same time obtain some new insight into some of these questions, an experiment was undertaken to examine the intensity of the heavier nuclei in the cosmic radiation in the region below about 0.2 BeV/nucleon. The first question to be answered was whether or not there are any medium or heavy nuclei in this low-energy region. A cosmic ray source with a very high energy threshold for acceleration of the high charges could create a near absence of these particles, since only some particles which have been degraded in energy in their interstellar travels would be present. However, if particles are present, the measurement of their properties can provide some restraints on the combined questions of the interstellar travel of cosmic rays and the spectra at the origin.

The local solar modulation has the same effect on all the particles of primary concern in this experiment—namely, *He*, *C*, *N*, *O*, *Ne*, etc.—

*Published as *Goddard Space Flight Center document X-611-64-345*, November 1964

†NAS-NASA Research Fellow, on leave from Tata Institute of Fundamental Research, Bombay, India.

because these nuclei all have the same charge to mass ratio and hence the same velocity for a given charge.

To measure the intensity of low-energy heavy nuclei, nuclear emulsions, which are detectors particularly suited for this purpose, were exposed to the cosmic radiation above the earth's atmosphere on a sounding rocket at Fort Churchill, Canada. The use of a sounding rocket rather than a polar orbiting recoverable satellite has several advantages. First, several sounding rocket shots can be spaced at desired intervals, whereas—at least until now—it has not been possible to obtain a single emulsion exposure on a recoverable satellite under less than about 2 g/cm^2 of material in a region of space where low-energy particles are not excluded by the earth's magnetic field. Also, satellite exposures are very expensive because of the cost of the necessary modifications to an existing system and the cost of testing to meet the rigid design specifications. The design of a satellite system is complicated by the requirement that the emulsions must be protected from high temperatures and still be exposed under very little matter. Further, the fact that the geomagnetic cutoffs are uncertain demands that a time resolution device be included in a satellite experiment to obtain absolute fluxes, since emulsions themselves integrate over time. Finally, the high Van Allen belt radiation background arising from the South Atlantic anomaly is an additional disadvantage associated with a satellite exposure.

To overcome the principal difficulty associated with the sounding rocket exposure—namely, having only a short exposure time available, a large area of emulsion was extended from the side of the payload during the portion of the flight when the rocket was above the atmosphere. The rocket was fired from Fort Churchill, Canada, so that the particles of interest could reach the extended detector at full intensity without having been excluded by the earth's magnetic field.

EXPERIMENTAL PROCEDURE

The nuclear emulsion detectors used in this experiment were 600-micron-thick Ilford G–5 emulsions which were assembled in eighteen packs consisting of eighteen emulsions, 6.5 cm by 9.9 cm, placed on top of each other and covered with Mylar and black electrical tape to give a water- and light-tight package. Six of these packs were placed in each tray and held in place by means of a small metal lip. A photograph of the emulsion section of the payload is shown in Fig. 1. The trays in turn were kept inside of the payload until 61 seconds after launch of the sounding rocket, at which time extension of the trays was begun. Before reentry and 411 seconds after launch, the retraction of the trays was begun. Extension and retraction each took about 7 seconds. These events and others are indicated in the time-altitude curve in Fig. 2.

The rocket itself was an Aerobee 150, which had the capability of carrying the 171-pound payload of this experiment to an altitude of 151 miles. In addition to the standard Aerobee nose cone, there were two extension sections; the one closest to the rocket was a recovery section, and the other was

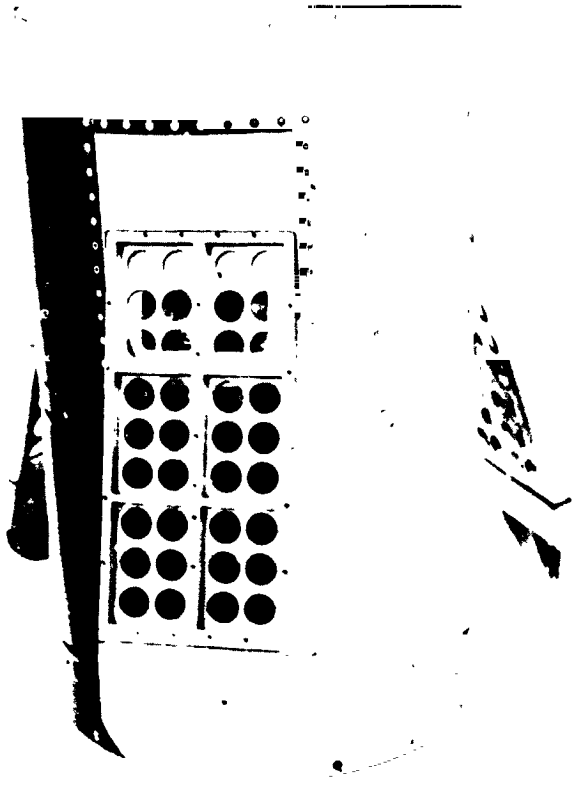

FIGURE 1.—Photograph of the rocket payload section with the emulsions removed and the emulsion trays extended. Six emulsion packs were placed in each of three symmetrically positioned trays. The angle of the trays with respect to the rocket axis was 17.5 degrees.

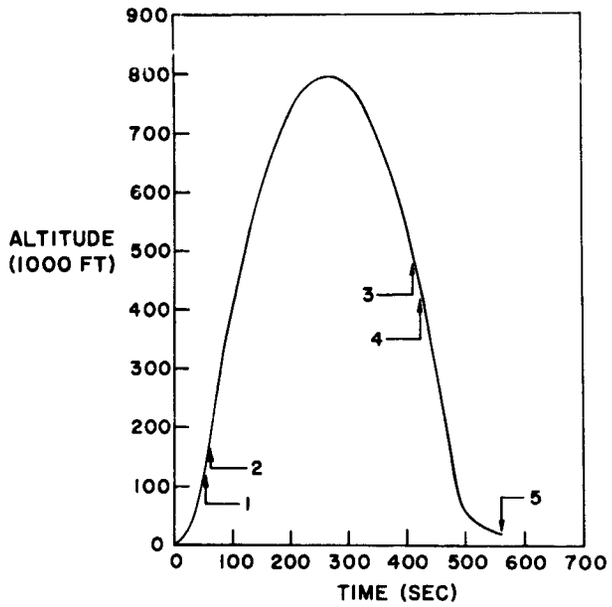

FIGURE 2.—Rocket time-altitude trajectory, showing the sequence of events: (1) rocket burnout (2) emulsion tray extension (3) emulsion tray retraction (4) payload separation (5) parachute deployment and SARAH beacon activation.

the section which housed the extension mechanisms for the emulsion trays described in the preceding paragraph. The water-tight housing for the emulsion in the retracted position extended up into the standard nose cone section. In addition, the nose cone itself contained a radar beacon, battery power for the extension and retraction motors, and a telemetry section. Magnetometer data for rocket aspect, data on the extension and retraction of the trays, and rocket parameters including acceleration and chamber pressure were telemetered.

The rocket was launched successfully at 1311 U.T. on September 4, 1963, and all parts of the payload functioned properly. It was a quiet day geophysically[10] and the Mt. Washington neutron monitor counting rate was 2318.[11] The nuclear emulsions were recovered, processed, and found to be in generally good condition. A total emulsion surface area of 821 cm^2 was available for analysis after elimination of the area held under the tray lips and the immediately adjacent area, where the clear solid angle would have been greatly reduced.

A complete area scan was made under a microscope of the top emulsion of each of the packs, as well as a complete rescan to check scanning efficiency. In the original scans, all tracks which were dark and which either had delta rays or were wider than a track formed by a single line of grains were accepted, regardless of the angle the track made in the emulsion. These tracks were then analyzed by a scientist to separate the slow proton and helium tracks from the partiles with charges greater than 2. At this point, all tracks which were within 20 degrees of the perpendicular to the emulsion were rejected. The method of charge and energy analysis is essentially the same as that used previously in other work and described in detail in a paper by Biswas, Fichtel, and Guss [12] and, therefore, will not be repeated here. Only particles which ended in the emulsion were analyzed. When this work was completed, it was found that the sample of particles, although small, was sufficiently large to permit an actual flux determination rather than simply to set an upper limit.

The calculation of the solid angle of collection involves a number of features which are indicated in Fig. 3. First, there is the restriction on the angle with respect to the plane of the emulsion (called "dip angle") mentioned above, corresponding to section A in the figure. Second, there is a very small solid angle, consisting of tracks of small dips and azimuthal angles in the emulsion which are closest to the rock t axis, which is excluded because particles would have had to pass through the rocket to enter the emulsion within this solid angle. This solid angle segment varies with position on the surface of the emulsion, but a typical segment labeled "B" is shown in Fig. 3. The final and largest portion of the solid angle which was excluded or partially excluded is made up of those angles which are forbidden to the particles by a combination of their paths along the magnetic field and the earth's atmosphere.

The method of calculating the angle of a particle with respect to the vertical for a given altitude above the earth after the particle has mirrored at a lower altitude has been discussed in an earlier paper by Biswas, Fichtel, and Guss.[12] Although the details are complicated and will not be repeated, the net effect is to increase the angle with respect to the vertical in which particles may arrive from 90 degrees to a larger angle which increases with altitude above the earth. There

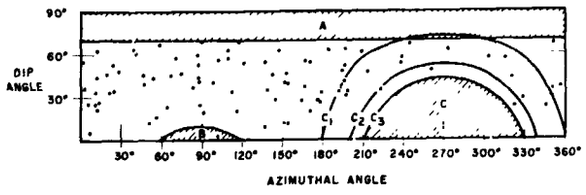

FIGURE 3.—Distribution of ending $Z \geq 6$ nuclei (indicated by black circles) in the solid angle of collection. The "dip angle" is the angle with respect to the plane of the emulsion; the "azimuthal angle" is that with respect to the perpendicular to one of the edges of the emulsion measured in the emulsion plane. The shaded area "A" was excluded from analysis because tracks in this segment had a dip too great to be analyzed. The shaded area "B" was excluded from analysis because particles at these angles had passed through the rocket material before entering the emulsion; this area varied with position in the emulsion and a typical segment is shown. The curves C_1, C_2, and C_3 are the curves for particles with space angles greater than 90°, 70°, and 60° with respect to the magnetic line of force. These curves varied somewhat as the coning angle of the rocket varied, and the ones shown are typical. The shaded area "C" is forbidden to the low-energy heavy nuclei under consideration because they would be stopped by ionization energy loss in the atmosphere between the rocket and their mirror point.

is only a very small solid angle in which particles pass through a significant amount of atmosphere, but not enough to effectively remove them from consideration. Further, the rocket was not quite vertical but had a small coning angle in addition to its spin about the principal axis; therefore, there was a small variation in the position of the set of angles in the emulsion which are at a given angle with respect to the vertical during the flight. This effect increases somewhat the solid angle in the emulsion in which primary tracks may appear but has essentially no effect on the total solid angle for collecting primary particles. Some of the curves related to this problem are shown in Fig. 3 near the area marked "C" and are labeled C_1, C_2, and C_3. The explanation of these curves is given in the figure caption. No tracks should have been observed in the shaded area C of the solid angle diagram, and none were.

The effective solid angle is then calculated from the equation

$$\Omega = \int\int (f \cdot \cos\theta) \sin\theta \, d\theta \, d\varphi,$$

where θ is the angle with respect to the perpendicular to the emulsion and φ the azimuthal angle in the emulsion: f is a weighting factor which is 0 in the shaded areas of Fig. 3 where no tracks were accepted and 1 in most of the rest of the area except around C, where it varied between 0 and 1 with position, depending on the fraction of the extended time that the primary particles could reach these angles. The cos θ factor occurs because the emulsion collecting area is a flat surface. Since the area marked "B" in Fig. 3 varies with position on the emulsion surface, Ω varies with position, but only very slightly because of the small contribution of segment B. The collection time also varies slightly with position because of the small, but finite, time required to extend the tray. With all the above factors taken into consideration, the effective primary area—collection time—solid angle factor, called "$A\,\Omega T$," was $60.7 m^2$ sr sec.

The major correction to the raw data is the one which accounts for the background tracks formed during ascent before the trays are extended and during descent after the trays are retracted. In a more recent version of this experiment flown in July 1964, this correction was eliminated by including a sliding plate mechanism which permitted separation of the tracks formed during the period that the emulsion trays were extended from those tracks made at other times. The results of this experiment will be reported later when the data reduction and analysis is complete.

The background consisted of particles of relatively large ambient energies because they had to pass through several g/cm^2 of material before reaching the emulsion, the exact amount of material depending on the angle and the height of the rocket in the atmosphere. An estimate of this background correction therefore could be made from balloon flight data because the particles composing the background had initial energies which were sufficiently great to reach balloon altitudes. For this purpose, the flux and the energy spectrum of low-energy heavy nuclei were measured in the nuclear emulsion plates carried on a balloon flight made from Fort Churchill on July 15, 1963, when the cosmic ray flux level was known to be essentially the same as on September 4, 1963, because the neutron monitor counting rates for these days differed by only 0.2 percent. The excellent

correlation between low-energy cosmic ray intensities and neutron monitor counting rates has been shown previously by McDonald and Webber.[13] In principle, the background correction could be very complex; in practice, a good approximation is obtained by simple summations because the degraded spectrum changes slowly in shape with increasing amounts of material present and, secondly, because the relative times of moving through variable amounts of residual atmosphere and remaining under a constant amount of a few g/cm² of material were about the same for the emulsions in the rocket and those on the balloon.

One final correction which had to be made to the raw data was the increase in the number of collected particles by an amount which took into account the probability that the particles might interact before ending or, in the cases of some of the higher energy particles included in the analysis, leave the stack if it entered the edge at an unfavorable angle. The upper limit to the energy was kept small in order to keep this correction small.

RESULTS AND DISCUSSION

After completion of the analysis outlined in the previous section, the results shown in Table 1

TABLE 1.—*Differential fluxes for medium nuclei and* ($10 \leq Z \leq 19$) *nuclei on September 4, 1964.*

Kinetic energy (MeV/nucleon)	$6 \leq Z \leq 9$ [p/(m² sr sec MeV/nucleon)]	$10 \leq Z \leq 19$ [p/(m² sr sec MeV/nucleon)]
50	0.0040 ± 0.0015	----------
55	----------	0.0005 ± 0.0006
90	0.0055 ± 0.0018	0.0005 ± 0.0006
130	0.0072 ± 0.0024	0.0040 ± 0.0015
170	Not measured	0.0028 ± 0.0014

were obtained. The first pointo to be made is obvious: namely, that these fluxes are quite clearly significantly different from zero. Hence, a finite flux of cosmic ray medium nuclei in an energy range as low as 30 to 70 MeV/nucleon has been observed in the vicinity of the earth. Further, there is a finite flux of heavy nuclei with energies at least as low as 110 MeV/nucleon.

In the rest of the paper, the heavy nuclei will be divided into two groups—nuclei with nuclear charges from 10 to 19, hereafter called ($10 \leq Z \leq 19$) nuclei, and very heavy nuclei ($Z \geq 20$)—because it is advantageous to keep the variation in energy loss within a charge group to within tolerable limits and because there were very few nuclei with charges of 20 or more. Comments on light nuclei ($3 \leq Z \leq 5$) will be confined to the last paragraph of this section, since they are a separate subject.

The next subject of interest is the comparison of the differential energy spectra obtained in this experiment with the differential spectra at higher energies and with the spectrum of helium nuclei. In this comparison, it is important to remember that the cosmic ray differential energy spectrum varies with the period in the solar cycle. Figure 4

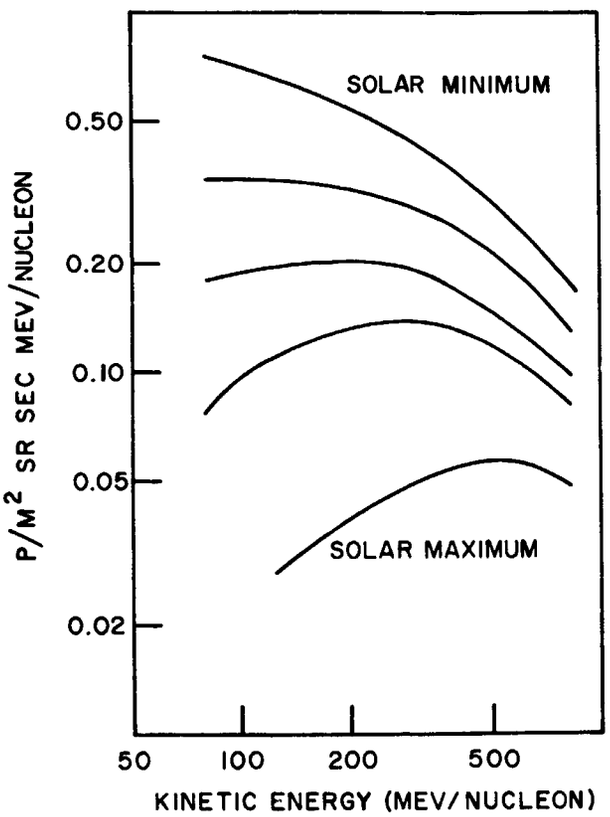

FIGURE 4.—Differential energy spectrum for helium nuclei at various times during the solar cycle. These curves were calculated from data published by Webber (see Ref. 1).

shows the differential energy spectrum for helium for various periods in the solar cycle.[1] The existing data indicate that the medium and heavy nuclei have energy spectra similar to that of the helium nuclei, only reduced in intensity.[1] The medium nuclei group, for example, is 0.063 times the helium particle intensity; and the charge group from $Z = 10$ to 19 is 0.021 times the helium particle intensity. The possibility of small differences of the order of 15 percent or less in the region from about 200 to 400 MeV/nucleon cannot be excluded; above 1.5 BeV/nucleon, they probably are correct to within 10 percent.

At the time of the firing of the sounding rocket from which the data under discussion were obtained, the cosmic ray flux had passed through the minimum value of the cycle a few years earlier and was slowly increasing. The curve in Fig. 5 shows the approximate shape of the helium particle differential spectrum at the time of the rocket shot. It has been shown[1] that the particle spectrum is a smoothly varying function of energy and that for this period in the solar cycle a 1 percent variation in the Deep River neutron monitor rate, which gives an estimate of the higher energy particle intensity, corresponds to about a 10 percent variation in the helium particle differential flux at 200 MeV/nucleon. Therefore, for purposes of correlating the measurements made here, an uncertainty of less than that will be introduced by comparing the results obtained here with helium spectra obtained when the neutron monitor was within 1 percent of the reading at the time the rocket was in the air. The authors know of four helium spectra in the energy region from about 80 to 600 MeV/nucleon that were obtained during the summer of 1963 which satisfy this condition.[14-17] An average of these spectra, which are in close agreement, was used as the basis for the curve in Fig. 5.

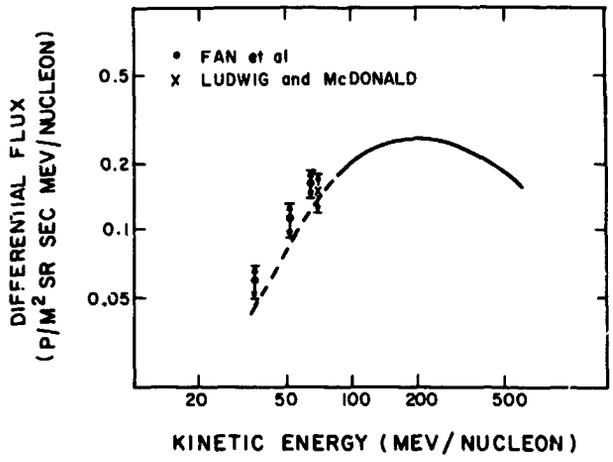

FIGURE 5.—Helium nuclei differential energy spectrum obtained as explained in the text. The low-energy points, from which the low-energy portion of the curve was deduced, are those of Fan et al, (Ref. 18) and Ludwig and McDonald (Ref. 19).

In addition, Fan et al[18] and Ludwig and McDonald[19] have obtained a helium energy spectrum in the 30 to 80 MeV/nucleon region on Explorer XVIII during the period January through March 1964, when the neutron monitor rate was typically from 1 to 2 percent higher than the rate at the time of the measurement of this experiment. To compensate for a systematic change in intensity in this region, the curve in Fig. 5 was extended below 80 MeV/nucleon by a smooth connection to data above 80 MeV/nucleon, by keeping the shape of the 30 to 80 MeV/nucleon data but reducing the intensity appropriately. This procedure could, at most, introduce a noticeable error only in the lowest medium nuclei energy interval.

Since no comparable data were available for the heavier particles at the time of writing of this paper, the helium particle curve was multiplied by the ratios mentioned above to obtain the best possible approximation of the curves for the heavier particles at higher energies.

The results displayed in Figs. 6 and 7 indicate that the low-energy spectrum of the medium nuclei observed in the vicinity of the earth falls below that of the helium nuclei multiplied by 0.063. Similarly, the $(10 \leq Z \leq 19)$ nuclei curve falls below the corresponding one for helium nuclei multiplied by 0.021. Hence, the abundance of helium nuclei relative to these higher charge groups apparently increases in the low-energy region until it is well above the fairly constant value which it has from about 400 MeV/nucleon to very high energies.

The spectra which are observed at the earth represent the source spectra after they have passed through interstellar matter and have been modulated within the solar system. Whereas

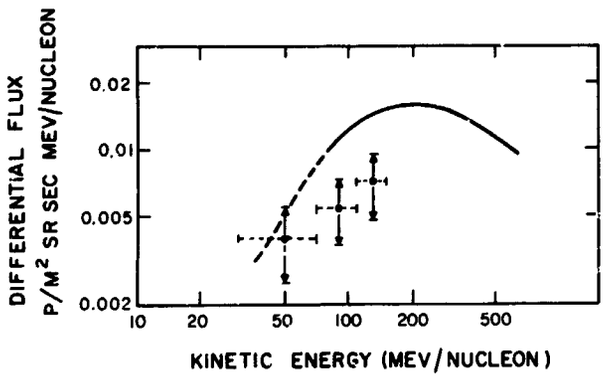

FIGURE 6.—Differential energy spectrum for medium nuclei. The curve is that for helium nuclei (Fig. 5) multiplied by 0.063.

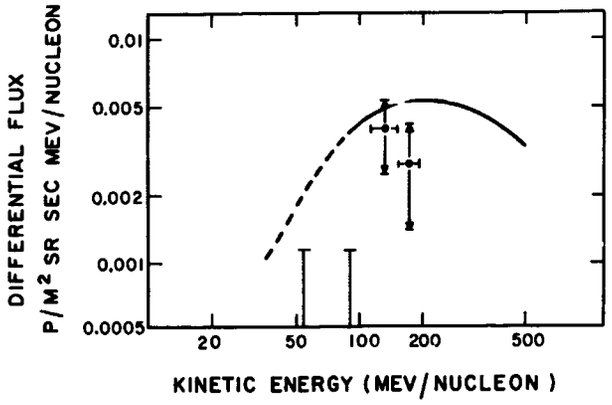

FIGURE 7.—Differential energy spectrum for $(10 \geq Z \geq 19)$ nuclei. The curve is that for helium nuclei (Fig. 5) multiplied by 0.021. For the two lowest energy points, only the upper limit corresponding to one standard deviation is shown.

the solar system modulation affects only the intensity of the increment of flux in a given energy interval, interstellar space contains enough material along the path of the particle to change appreciably the particle energy as well as the intensity. In the latter case, it normally is assumed that the intensity is changed significantly only by fragmentation in interactions and not by the complicated time-dependent magnetic effects which cause the intensity variation in the solar system. Therefore, the differential energy flux at the source for the i^{th} type of particle $j_s(i)$ is related to the differential energy flux observed in the vicinity of the earth but outside the region where the earth's magnetic field excludes, or partially excludes, particles $j_o(i)$ by the relation

$$j_o(i)[_{E=E_0} = j_s(i)]_{E=E_s(i)} \left[\frac{\Delta E_s(i)}{\Delta E_0}\right] h(v_0,R) f(i,v,\rho), \tag{1}$$

where ΔE_0 and ΔE_s represent the small energy increments containing the set of particles at the observation point and the source respectively, i is the type of particle, h the solar modulation function, f the interstellar intensity variation factor, v the particle velocity, R the rigidity (momentum/unit charge), and ρ the amount of interstellar matter traversed between the source and the earth.

The expression $f(i, v, \rho)$ is well known and is given in detail in a paper by Hayakawa.[20] However, the parameters to be substituted into the equations are not known exactly. The parameters include the mean free paths of the different elements in space, the probability of one type of particle emerging from an interaction caused by another particle and the amount of material traversed. Table 2 gives the values of the parameters used in the calculation and the references from which the parameters were obtained.[21–24] When more than one reference is given, the parameter listed in the Table is a weighted average. In Table 2, P_{ij} gives the average number of secondaries of type "j" formed in an interaction of a particle of type "i" in an interaction with a hydrogen nucleus. λ_i' is the absorption mean free path, which is given by the equation

$$\frac{1}{\lambda_i'} = \frac{1}{\lambda_i}(1 - P_{ii}), \tag{2}$$

where λ_i is the interaction mean free path.

TABLE 2.—*Parameters used for extrapolation through interstellar matter.*

	Reference		References
$\lambda_a = 14.6$ g/cm²	20	$P_{aa} = 0.07 \pm 0.07$	21–24
$\lambda_M = 6.0$ g/cm²	20	$P_{(L+M+H)a} = 1.3 \pm 0.5$	21–24
$\lambda_H = 4.0$ g/cm²	20	$P_{MM} = 0.14 \pm 0.04$	21–24
		$P_{HM} = 0.21 \pm 0.10$	21–24
		$P_{HH} = 0.40 \pm 0.15$	21–24

The above parameters are known to vary with energy; however, their exact dependence is not well known. Above approximately 100 MeV/nucleon they are thought to be nearly constant and not to vary appreciably until the energy/nucleon is below about 30 or 60 MeV.[23 25] To reach the earth at the observed energies after passing through several g/cm² of interstellar hydrogen, the particles under consideration must spend either all or almost all of their time in interstellar space at energies above 100 MeV/nucleon. Therefore, it seems reasonable to use the parameters obtained at higher energies in view of the above considerations and the lack of sufficient information to calculate more exact values. Including the generally accepted partially tested hypothesis that the energy per nucleon does not vary significantly in an interaction leads, then, to the conclusion that f is not a function of velocity in the region of interest if ρ is not a function of energy.

The true modulation function $h(v, R)$ is not known. Many models have been presented, and each seems to have some advantages and some weaknesses.[26]: For the purposes of the present discussion, it is sufficient to note that, since all the proposed modulation mechanisms involve only magnetic or electric fields and the amount of material traversed within the solar system is negligible, particles with the same charge to mass ratio and hence the same rigidity for a given velocity will be depressed by the same amount for a given velocity.

The remaining term on the right side of Eq. (1), which multiplies $j_s(i, E)$, is $(\Delta E_s(i)/\Delta E_0)$. This term arises from the change in the width of the energy interval in which particles are contained as they lose energy. Since the rate of energy loss per nucleon varies with the nuclear species, this term will affect the different nucleon groups in different ways. Further, because of the different rates of energy loss for a given E_0, $E_s(i)$ will be different for different nuclear species; and hence $j_s(i, E)]_{E=E_{s(i)}}$ can vary for a fixed E_0 even if $j_s(i, E)$ is the same for all nuclear groups.

Consider now the ratio of the differential flux values of two different nuclear types with the same charge to mass ratio. From Eq. (1), this ratio is

$$\frac{j_0(i,E)]_{E=E_0}}{j_0(k,E)]_{E=E_0}} = \frac{j_s(i,E)]_{E=E_s(i)}}{j_s(k,E)]_{E=E_s(k)}} \frac{[\Delta E_s(i)/\Delta E_0]}{[\Delta E_s(k)/\Delta E_0]} \frac{f(i,v,\rho)}{f(k,v,\rho)} \tag{3}$$

If ρ, the fragmentation parameters, and the mean free paths are independent of velocity, $f(i, v, \rho)/f(k, v, \rho)$ becomes a constant independent of velocity. Hence,

$$\frac{j_0(i,E)]_{E=E_0}}{j_0(k,E)]_{E=E_0}} = \frac{j_s(i,E)]_{E=E_s(i)}}{j_s(k,E)]_{E=E_s(k)}} \frac{[\Delta E_s(i)/\Delta E_0]}{[\Delta E_s(k)/\Delta E_0]} [K(\rho,i,k)],\ [K \neq g(V)] \tag{4}$$

Notice also that

$$\Delta E_s(i) \lambda \Delta E_0 \xrightarrow[v \to c]{} 1 \tag{5}$$

and, for reasonable spectra,

$$\{j_s(i, E)]_{E=E_s(i)}\}/\{j_s(k, E)]_{E=E_s(k)}\} \xrightarrow[v \to c]{} \text{(Const.), for a fixed } E \tag{6}$$

The implications of the experimental results now will be examined by comparing the data with the predictions based on several suggested source spectra and interstellar mean free paths. If it is assumed first that Eq. (4) is valid, the expected ratio for $j_0(i, E)]_{E=E_0}$ and $j_0(k, E)]_{E=E_0}$ can be calculated for different values of ρ and the experimental knowledge of the limiting value for the ratio at high energies, where Eqs. (5) and (6) apply.

The most commonly assumed source spectrum is a power law in the total energy with an exponent of 2.5 as given by

$$j_1(i, W) = K_1(i)/W_N^{2.5}, \tag{7}$$

where W_N is the total energy/nucleon. In Figs. 8 and 9 the observed ratios of the differential

medium nuclei and the ($10 \leq Z \leq 19$) nuclei to the differential helium nuclei spectral points obtained in the manner described earlier are plotted and compared with the ratio expected on the basis of the observed high-energy ratio and an assumed spectral shape of the form of Eq. (7). The best recent value for the estimate of the amount of interstellar matter traversed—at least for high-energy particles—is 2.5 g/cm², which is based on a calculation by Badhwar et al[23] and Badhwar and Daniel[25] with heavy emphasis on the high-energy (>1.5 BeV/nucleon) composition data of O'Dell et al.[27] The expected ratio has been calculated for both 2.5 and 5.0 g/cm² of interstellar hydrogen. Notice that this ratio is relatively insensitive to a change of a factor of 2 in interstellar matter in this range of values. Notice also that the agreement between the experimental points and the curves for these assumed conditions is satisfactory.

As a second example, a source spectrum of the form of Eq. (7) above 300 MeV/nucleon and of the form of Eq. (8) below 300 MeV/nucleon is chosen:

$$j_2(i) = K_2(i)/(E_s)^{0.67} \qquad (8)$$

The expected ratios for this source spectrum, the observed high-energy ratios, and 2.5 and 5.0 g/cm² of interstellar matter also have been calculated and are shown in Figs. 8 and 9. Here again there is a relatively small difference in the curves for 2.5 and 5.0 g/cm², and there is satisfactory agreement with the experimental data. Smooth changes in the source spectrum in general have little effect on the resultant ratios unless the variations are very large, that is, appreciably greater than those selected here.

Hence, the following conclusion can be drawn: The experimentally observed helium to medium and helium to ($10 \leq Z \leq 19$) nuclei ratios are consistent with the assumption that the source spectra are the same and that the particles have passed through the same amount of material, which is in the range of 2.5 to 5 g/cm². This conclusion is relatively independent of the exact shape of the source spectrum. On the other hand, differences in the source spectra between helium and medium nuclei would appear relatively quickly in the form of a disagreement

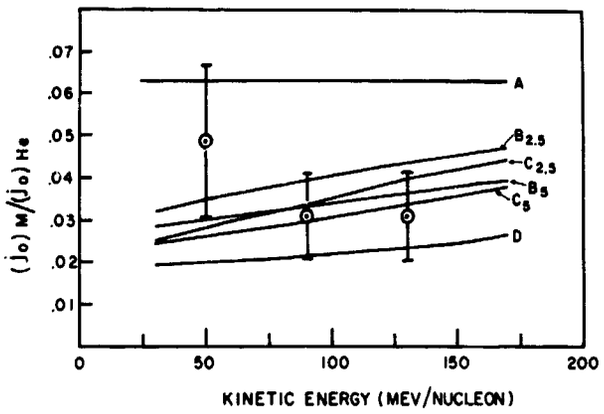

FIGURE 8. -Ratio of the differential flux of medium nuclei to helium nuclei expected after passage of the particles through various amounts of interstellar gas. Curve A: 0 g/cm² for all spectral shapes; curve $B_{2.5}$ and curve B_s: 2.5 g/cm² and 5.0 g/cm², respectively, assuming the source spectrum of Eq. (7); curve $C_{2.5}$ and curve C_s: 2.5 g/cm² and 5.0 g/cm², respectively, assuming the source spectrum of Eq. (7) for particles with kinetic energy greater than 300 Mev/nucleon and the source spectrum of Eq. (8) for particles with kinetic energy less than 300 Mev/nucleon; curve D: passage through 2.5 g/cm² for relativistic particles, 6 g/cm² for particles with kinetic energy less than 400 Mev/nucleon, assuming the source spectrum of Eq. (7).

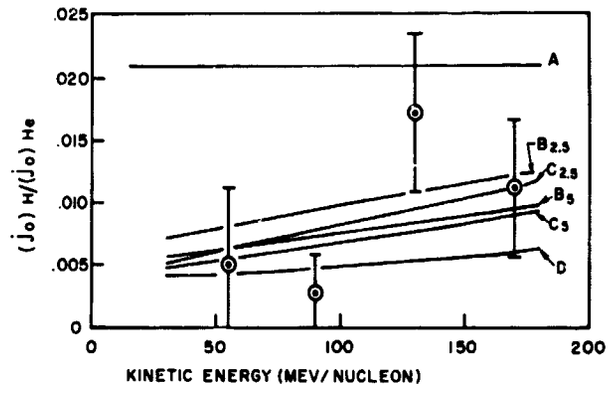

FIGURE 9.—Ratio of the differential flux of ($10 \geq Z \geq 19$) nuclei to helium nuclei expected after passage of the particles through various amounts of interstellar gas. Curve A: 0 g/cm² for all spectral shapes; curve $B_{2.5}$ and curve B_s: 2.5 g/cm² and 5.0 g/cm², respectively, assuming the source spectrum of Eq. (7); curve $C_{2.5}$ and curve C_s: 2.5 g/cm², and 5.0 g/cm², respectively, assuming the source spectrum of Eq. (7) for particles with kinetic energy greater than 300 Mev/nucleon and the source spectrum of Eq. (8) for particles with kinetic energy less than 300 Mev/nucleon; curve D: passage through 2.5 g/cm² for relativistic particles, 6 g/cm² for particles with kinetic energy less than 400 Mev/nucleon, assuming the source spectrum of Eq. (7).

between the calculated and observed helium to medium nuclei ratio as a function of energy.

The results obtained here, then, suggest there is good reason to think that above about 0.2 BeV/nucleon the source spectra of all components are at least similar. Information below this energy is not forthcoming from this approach because nuclei of the higher charges being considered must have at least this energy initially to reach the earth.

Next, assume that the particles have gone through different amounts of interstellar material depending on their energy. Dahanayake et al,[28] for example, suggest that the lower energy particles, below about 400 MeV/nucleon, have passed through more material than the high-energy ones, which are assumed to go through 2.5 g/cm^2 on the basis of the work mentioned earlier. In this case, $f(i, v, \rho)/f(j, v, \rho)$ of Eq. (3) is not a constant independent of energy. However, if the high-energy ratio of the observed fluxes is known and if the parameters of Table 2 are used, the additional expected suppression resulting from low-energy particles going through more material than high-energy ones can be calculated. The results obtained, assuming that all particles have a source spectrum of the type given by Eq. (7) and that the particles below 400 MeV/nucleon have passed through 6 g/cm^2 (as suggested by Dahanayake et al,[28]) while the high-energy ones (kinetic energy$>$1.5 BeV/nucleon) have passed through 2.5 g/cm^2, are also shown in Figs. 8 and 9. Here the agreement is poorer; further, these assumptions lead to a ratio in the 300 to 400 MeV/nucleon region which is appreciably more than one standard deviation below several measurements of the medium to heavy nuclei ratio in that region. In addition, Hildebrand and Silberberg [29] and Webber [30] now have shown that the existing experimental data on the He_3/He_4 ratio probably can be reconciled with a mean free path in the low-energy region which is the same or only slightly larger than 2.5 g/cm^2, by taking into account the properties of secondaries from interactions and the effects of the solar modulation mechanism on particles with different charge to mass ratios.

Light nuclei also were observed in the low-energy region from 30 to 110 MeV/nucleon, but no quantitative value for the differential flux will be quoted because a high scanning detection efficiency was not achieved for these particles. Since these light nuclei generally are assumed to arise from heavier nuclei, the type of theoretical analysis outlined above does not apply. There is, however, the alternate problem of interest: namely that, if the modulation effect is rigidity dependent, light nuclei might be expected to have slightly different energy spectra from the medium or heavy nuclei. If the rigidity dependence of the modulation can be determined by other means, the relative abundance of light and medium nuclei provide an independent estimate of the amount of interstellar matter traversed by the cosmic radiation at these low energies. The analysis was not pressed beyond the determination of the existence of a light nuclei flux because there was not an adequate number of particles to determine the light to medium ratio with sufficient accuracy to see a deviation from the high-energy ratio; and the additional work involved is tremendous. With an improved technique and a higher flux rate, we hope to be able to measure the relative abundance of light nuclei in the 1964 flight to be reported later.

CONCLUSIONS

The answer to the basic question of whether or not there are low-energy heavy nuclei below the energy cutoff set by material above detectors flown on balloons has been seen to be "Yes." There definitely is a finite flux of medium nuclei in an energy range as low as 30 to 70 MeV/nucleon and ($10 \leq Z \leq 19$) nuclei with energies at least as low as 110 MeV/nucleon. The abundance of medium and ($10 \leq Z \leq 19$) nuclei relative to helium nuclei in the energy regions from 30 to 150 and 30 to 190 MeV/nucleon, respectively, are less than the relative abundances at higher energies. This difference can be explained quantitatively by the higher rate of energy loss of the particles of higher charge in the interstellar matter. It also was shown that within the statistical uncertainty the resulting differential flux measurements are consistent with the helium, medium, and ($10 \leq Z \leq 19$) nuclei having the same source spectrum at least above about 0.2 BeV/nucleon for a wide range of source spectral shapes, including ones normally assumed. For a mean free path independent of energy this result also is

fairly insensitive to the values of cross sections and fragmentation parameters assumed, principally because relative values of ratios are being considered. The conclusion is independent of the solar modulation mechanism because, since all particles considered have the same charge to mass ratio, their relative abundances at a given velocity will be unaffected by the local solar modulation. No information can be obtained about the source spectrum below about 0.2 BeV/nucleon because the particles of high charge must have approximately this energy to reach the earth after passing through interstellar matter.

It has been established that there is a finite flux and that the differential flux is consistent with similar source spectra for helium, medium, and heavier nuclei and an interstellar path in hydrogen of 2.5 g/cm^2 within the relatively large uncertainties of these initial measurements. It now seems worthwhile to measure these spectra again to look for a possible variation with the period in the solar cycle and to examine the matters discussed in this paper in greater detail. This problem is being pursued.

REFERENCES

[1] W. R. Webber, Progress in Elementary Particle and Cosmic Ray Physics VI (North Holland Publishing Co., Amsterdam) p. 77 (1962).

[2] Proceedings of the International Conference on Cosmic Rays, Jaipur, India, Commercial Printing Press Limited, Bombay (1963).

[3] Proceedings of the International Conference on Cosmic Rays and the Earth Storm, Kyoto, 1961, J. Phys. Soc. Japan **17**, Suppl. A-III (1962).

[4] H. Aizu, Y. Fujimoto, S. Hasegawa, M. Koshiba, I. Mito, J. Nishimura, and K. Yokoi, J. Phys. Soc. Japan **17**, Suppl. A-III, 38 (1962).

[5] D. E. Evans, Nuovo Cimento **27**, 394 (1963).

[6] F. Foster and A. Debenedetti, Nuovo Cimento **28**, 1190 (1963).

[7] C. Fichtel, Nuovo Cimento **19**, 1100 (1961).

[8] F. B. McDonald and W. R. Webber, J. Geophys. Res. **67**, 2119 (1962).

[9] See, for example, F. B. McDonald and W. R. Webber, J. Geophys. Res. **69**, 3097 (1964).

[10] J. Virginia Lincoln, J. Geophys. Res. **69**, 525 (1964).

[11] Courtesy of the Enrico Fermi Institute for Nuclear Studies, Chicago.

[12] S. Biswas, C. E. Fichtel, and D. E. Guss, Phys. Rev. **128**, 2756 (1962).

[13] F. B. McDonald and W. R. Webber, J. Phys. Soc. Japan **17**, Supp A2, 428 (1962).

[14] V. K. Balasubrahmanyan and F. B. McDonald, J. Geophys. Res. **69**, 3289 (1964).

[15] C. E. Fichtel, D. E. Guss, D. A. Kniffen, and K. A. Neelakantan, work to be submitted to Phys. Rev.

[16] J. Ormes and W. R. Webber, Phys. Rev. Letters **13**, 106 (1964).

[17] P. S. Freier and C. J. Waddington, Phys. Rev. Letters **13**, 108 (1964).

[18] C. Y. Fan, G. Gloeckler, and J. A. Simpson, Trans. Am. Geophys. Union, Vol. **45**, 8 Sept. 1964.

[19] G. H. Ludwig and F. B. McDonald, to be submitted for publication in Phys. Rev. Letters.

[20] S. Hayakawa, Progr. Theoret. Phys. (Kyoto) **15**, 111 (1956).

[21] M. W. Friedlander, K. A. Neelakantan, S. Tokunaga, G. R. Stevenson, and C. J. Waddington, Phil Mag **8**, 1691 (1963).

[22] H. Aizu, Y. Fujimoto, S. Hasegawa, M. Koshiba, T. Mitto, J. Nishimura, and K. Yokoi, Progr. Theoret. Phys. (Kyoto), Suppl. 16 (1960).

[23] G. D. Badhwar, R. R. Daniel, and B. Vijayalakshmi, Progr. of Theoret. Phys. (Kyoto) **28**, 607) (1962).

[24] S. Hayakawa, K. Ito and Y. Terashima, Progr. Phys. (Kyoto), Suppl. **6**, 1 (1958).

[25] G. D. Badhwar and R. R. Daniel, Progr. Theoret. Phys. (Kyoto) **30**, 613 (1963).

[26] For a discussion of this problem see, for example, Ref. 9 or C. E. Fichtel, D. E. Guss, G. R. Stevenson and C. J. Waddington, Phys. Rev. **133**, B818 (1964).

[27] F. W. O'Dell, M. M. Shapiro, B. Stiller, J. Phys. Soc. Japan **17**, Suppl. A-III, 23 (1962).

[28] C. Dahanayake, M. F. Kaplon, and P. J. Lavakare, J. Geophys. Res. **69**, 3681 (1964).

[29] B. Hildebrand and R. Silberg, Regional IQSY Symposium, Buenos Aires, Aug. 3-8, 1964.

[30] W. R. Webber, Regional IQSY Symposium, Buenos Aires, Aug. 3-8, 1964.

MODULATION OF LOW ENERGY GALACTIC COSMIC RAYS*

C. E. FICHTEL, D. E. GUSS, D. A. KNIFFEN, AND K. A. NEELAKANTAN†

The exact way in which the cosmic ray energy spectrum changes with solar activity has been of particular interest because the experimental determination of this feature provides one of the most severe tests of any theory related to cosmic ray modulation. The helium and proton components in addition to being the most abundant also have the additional advantage of having charge to mass ratios which differ by a factor to two. Therefore, having a markedly different velocity for a given rigidity, these particles provide a means for separating rigidity and velocity effects.

In order to continue the study of the problem of the variation of the galactic cosmic ray proton and helium nuclei spectra, a series of balloon flights was made from Fort Churchill, Canada by Goddard beginning in 1961. It is the aim of this paper to present the results of the nuclear emulsion studies of the hydrogen and helium nuclei obtained in 1962 and 1963 and compare them to those obtained in 1961[1] and the earlier results of many experimentalists from the period of increasing solar activity.

One method of comparing the period of rising cosmic ray flux with the declining phase is to plot the integral helium nuclei flux above 250 MeV/n as a function of the neutron monitor rate which gives some measure to the higher energy cosmic rays of all charges. Figure 1 shows the smooth curve determined from many points for this period by McDonald and Webber.[2] Also shown on this figure are the points obtained by the Goddard emulsion group in 1961, 1962, and 1963. As can be seen, the points agree well with the smooth curve.

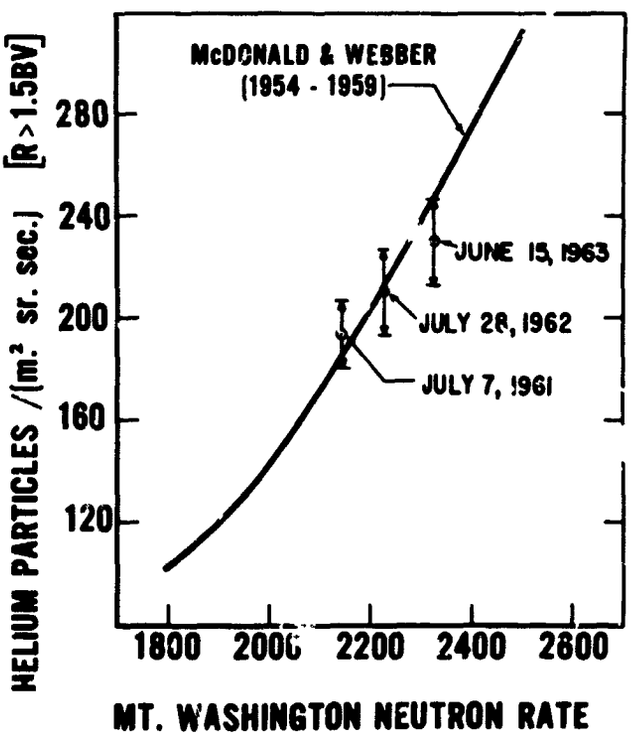

FIGURE 1.—Integral helium particle flux as a function of the Mt. Washington neutron rate.

A much more detailed and stringent comparison between the two periods is the comparison of the differential energy spectra of the helium nuclei in the present experiment with those obtained for the same neutron monitor rate during the declining phase of cosmic ray flux. Figure 2 shows the spectra for various neutron monitor counting rates during the declining phase of cosmic ray activity as given in Webber's review article.[2] These curves fit both the proton data and the helium nuclei data multiplied by seven. In general, the helium nuclei data extended down to about 1.2 BV/Nucleon and the proton data

*Published as *Goddard Space Flight Center Document X-611-64-63.*

†Goddard Space Flight Center, on leave of absence from Tata Institute of Fundamental Research, Bombay, India

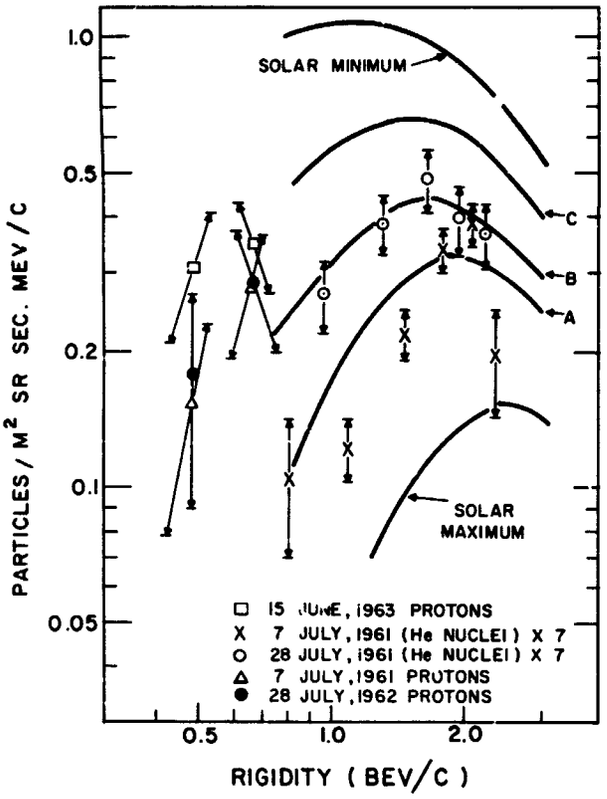

FIGURE 2.—Differential proton and helium fluxes as a function of rigidity. The solid curves are taken from figure 31a of Webber's review article and represent either the differential proton flux or the helium nuclei flux multiplied by seven for solar maximum. Curves A, B, and C correspond to times when the neutron monitor rates were the same as on July 7, 1961, July 28, 1962, and June 15, 1963, respectively.

extended from 0.8 to 1.4 BV. As can be seen, there is reasonable agreement between the helium nuclei data and the curves for the declining cosmic ray phase at the same neutron monitor rates although there is a suspicion that the helium points from this work may fall below the curve at the lowest rigidities where measurements were made. In order to obtain a more quantitative impression of the change in spectral flux from 1961 to 1962, the following numbers can be compared. The integral flux for helium nuclei with energies greater than 250 MeV/nucleon was 206 ± 13 particles/(m² sr.sec.) in 1961 and 221 ± 18 particles/(m² sr. sec.) in 1962. For the energy interval from 75 to 250 MeV/nucleon the flux was 12.7 ± 1.7 particles/(m² sr.sec.) in 1961 and 32.5 ± 4.1 particles/(m² sr.sec.) in 1962. Hence, between 1961 and 1962 there was a significant change in the helium particle flux below 250 MeV/nucleon and relatively little above.

Turning now to the protons it is known that there is a substantial secondary proton flux from interactions in the atmosphere above the detector. There is not space to describe the corrections in detail here, but the discussion of the method along with self-consistency arguments has been given in some detail in the earlier paper and will be treated further in the final publication of this work. Allowance has been made for the uncertainty in the interaction correction by drawing appropriately large errors in figure 2. This figure shows that there is a general tendency for the proton flux to increase during the period from 1961 to 1963, and that at least 1961 and 1962 the proton points lie above a reasonable extension of a smooth curve through the helium nuclei data multiplied by seven.

There is another set of data for which the analysis has just been completed which bears on this problem. Balasubraymanyan and McDonald [3] obtained a differential helium nuclei spectrum during the same period in 1963 as the proton data of this work. It agrees well with curve C above about 1.5 BV, but falls more quickly below this rigidity. These data are shown in figure 3, along with the results of this work in 1963 and

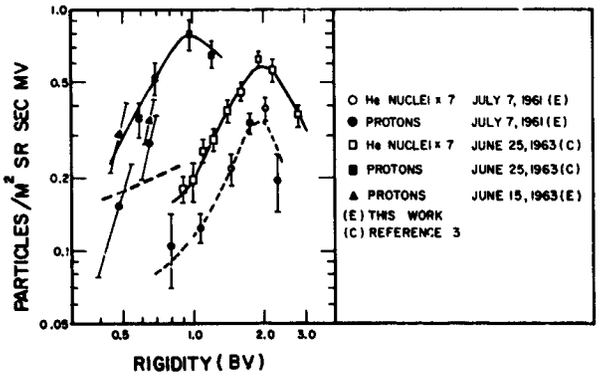

FIGURE 3.—Differential proton and helium fluxes compared to those of Balasubrahmanyan and McDonald.[3]

1961. The 1962 results lie in between those of 1961 and 1963, and were not included only to avoid unnecessarily complicating the figure. All these data are seen to be consistent with there being a difference between the proton differential

rigidity spectra and the helium one multiplied by seven below about 1.2 BV.

Hence, these combined results suggest strongly that there is a splitting of the proton differential spectrum and the helium nuclei one multiplied by seven below about 1.3 BV. This result does not contradict the earlier statements concerning the agreement in the rigidity spectra with those of the declining phase of cosmic rays because there is not sufficient helium data below 1.2 BV during this earlier period to justify a comparison in the 0.4 to 1.2 BV rigidity region. Also, although there is certainly the problem of not knowing the particle spectrum outside of the solar system, for the galactic spectra normally suggested, the splitting effect is at least qualitatively in agreement with the prediction of a modulation of the type proposed by Parker, since the protons have a higher velocity for a given rigidity than the helium nuclei and are therefore less suppressed.

REFERENCES

1. C. E. Fichtel, D. E. Guss, G. R. Stevenson, and C. J. Waddington, "Cosmic Ray Hydrogen and Helium Nuclei during a Quiet Time in 1961," to be published in the Physical Review.

2. For a summary of this work, see W. R. Webber, Progress in Elementary Particle and Cosmic Ray Physics Vol. VI, (1962). See particularly fig. 31a.

3. V. K. Balasubrahmanyan and F. B. McDonald, preceding paper, International Conference on Cosmic Rays, 1963.

MODULATION OF LOW-ENERGY GALACTIC COSMIC-RAY HYDROGEN AND HELIUM*

C. E. FICHTEL, D. E. GUSS, D. A. KNIFFEN, AND K. A. NEELAKANTAN†

A study of the energy spectrum of the cosmic-ray hydrogen and helium nuclei as a function of the period in the solar cycle provides one of the better means of gaining insight into the mechanism that modulates the galactic cosmic radiation. An examination of these nuclei in the low-energy region, where the modulation effects are greatest, has the particular merit of permitting the separation of velocity and rigidity effects, since for a given rigidity the helium nuclei have a markedly different velocity from that of the protons. Considerable information related to this problem had been obtained before 1960 for the most recent period of increasing solar activity [*Webber*, 1962].

In order to continue the study of the problem of the variation of the galactic cosmic-ray proton and helium nuclei spectrums and extend it to lower energies, a series of balloon flights, beginning in 1961, has been made from Fort Churchill, Canada. It is the aim of this letter to present the results of the nuclear emulsion studies of the hydrogen and helium nuclei obtained in 1962 and 1963 and compare them to those obtained in 1961 [*Fichtel et al.*, 1964].

The experimental data were obtained by carrying sets of nuclear emulsions aboard high-altitude skyhook balloons flown from Fort Churchill, Canada, where the earth's magnetic field allows all particles in the rigidity interval being studied to reach the top of the atmosphere. A second nuclear emulsion stack is released at the time the primary stack is rotated into the exposure position. The second stack provides the necessary information on the background particles collected during ascent and descent which must be subtracted from the particle flux measured in the primary stack, since nuclear emulsions are an integrating device.

There is not space here to describe in detail the corrections which must be applied to the data, but the discussion of the method along with self-consistency arguments has been given in some detail in an earlier paper [*Fichtel et al.*, 1964] and will be treated further in the final publication of this work. It is appropriate to mention, however, that there is a substantial secondary proton flux from interactions in the atmosphere above the detector, and allowance has been made for the uncertainty in the interaction correction in the calculation of the errors associated with the flux values that are quoted below.

In earlier work during the years 1955 through 1960, McDonald and Webber had shown that higher-energy data at higher-rigidity geomagnetic cutoffs suggested that the proton rigidity spectrum was the same as that for helium multiplied by seven [*Webber*, 1962]. Figure 1 shows that in the present data there is a general tendency for the proton points to lie above a reasonable extension of a smooth curve through the helium nuclei data multiplied by seven both in 1961 and 1962. In Figure 2 the 1963 proton data from the nuclear emulsions are plotted together with the proton and helium data of *Balasubrahmanyan and McDonald* [1964] at higher rigidity. Their data were obtained from counter experiments flown on June 24, 1963, when the high-latitude neutron monitor readings differed from those on June 15 and 16, 1963, when the emulsions were flown, by much less than 1 percent. In Figure 2 the splitting between the rigidity spectrums of the two components is quite marked. Hence, these results suggest strongly that there is

*Published in *Journal of Geophysical Research*, 69(15):3293-3295, August 1, 1964.

†Goddard Space Flight Center NAS-NASA Research Fellow, on leave from Tata Institute of Fundamental Research, Bombay, India.

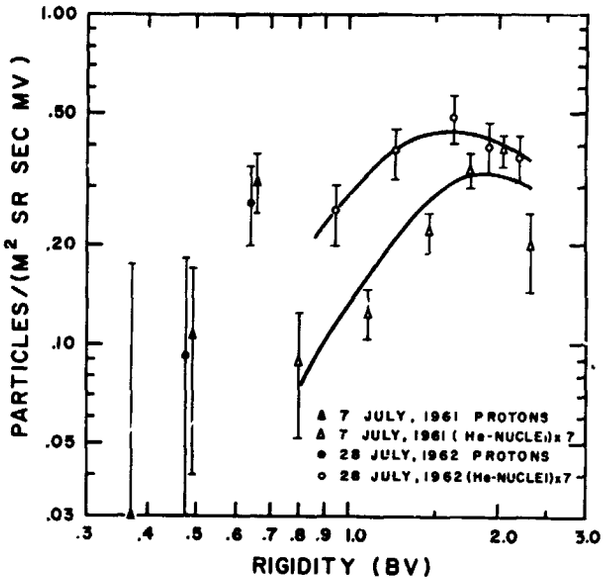

FIGURE 1.—Proton and He nuclei differential rigidity spectrums from 1961 and 1962 balloon flights at Fort Churchill.

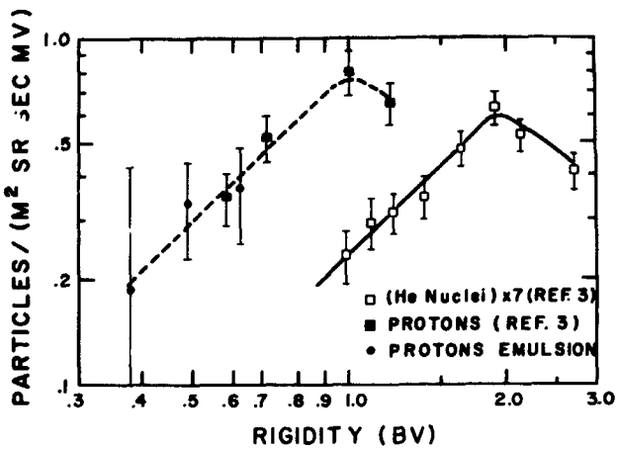

FIGURE 2.—Proton and He neclei differential rigidity spectrums from 1963 balloon flight from Fort Churchill.

a splitting below about 1.3 bv between the proton differential spectrum and that for helium nuclei multiplied by seven. This conclusion is not inconsistent with the earlier statements [*Fichtel et al.*, 1964] about the agreement in the rigidity spectrums of the proton and helium components during the declining phase of cosmic rays because there is not sufficient helium data below 1.3 bv during the earlier period to justify a comparison in the 0.4– to 1.3–bv rigidity region.

Although there is the problem of not knowing the particle spectrum outside the solar system, the splitting effect for the galactic spectrums normally suggested is at least qualitatively in agreement with the prediction of the modulation mechanisms currently proposed. Most of these models predict that protons will be less suppressed because they have a higher velocity for a given rigidity than helium nuclei. Therefore, unless the proton rigidity spectrum is very different from the helium spectrum in free space, the type of splitting in the spectrum which is observed would be predicted by these models. A more complete discussion of modulation models can be found elsewhere [*Webber*, 1962; *Fichtel et al.*, 1964].

REFERENCES

BALASUBRAHMANYAN, V. K., and F. B. MCDONALD, Solar modulation effects on the primary cosmic radiation near solar minimum, *J. Geophys. Res.*, **69**(15), August 1, 1964.

FICHTEL, C. E., D. E. GUSS, G. R. STEVENSON, and C. J. WADDINGTON, Cosmic ray hydrogen and helium nuclei during a quiet time in 1961, *Phys. Rev.*, **133**, B818, 1964.

WEBBER, W. R., *Prog. Elem. Particle Cosmic Ray Phys.*, **6**, 1962 (see particularly Figure 31*a*).

MAGNETIC EFFECTS OF THE QUIET TIME PROTON BELT*

R. A. HOFFMAN AND P. A. BRACKEN

An analysis of the magnetic effects of the quiet time proton belt has been performed with data obtained from a proton detector aboard Explorer XII. From the measured energy spectra, intensities, and pitch angle distributions of the protons with energies above 100 kev, the current density on a magnetic meridian plane was calculated using the theory of Akasofu and Chapman, modified to eliminate several simplifying assumptions. The algebraic sum of all the currents was 0.59 million amperes, and the magnetic moment of the current loop was $0.029 M_E$. From the electric current distribution the magnetic perturbations on the meridian plane were obtained. At the magnetic equator on the earth's surface the proton belt produced a 9 γ decrease in the field in comparison with the 38 γ decrease reported by Akasofu, Cain and Chapman based on some preliminary data from the same detector. The maximum perturbation appeared at $L=3.6$ on the magnetic equator, where the field attained a value of -23 γ.

I. INTRODUCTION

The various motions which a group of charged particles exhibit when trapped in the earth's magnetic field result in electric currents. The analysis of these movements yields the observation that the net currents are parallel to lines of magnetic latitude: in some regions of space they flow eastward, and in other regions westward. If one assumes longitudinal symmetry about the earth, these motions necessarily correspond to a toroidal ring current encircling the earth.

On the basis of geomagnetic evidence it has long been postulated that some type of ring current exists. The enhancement of the current at times was thought to be one cause of magnetic activity, but even during magnetically quiet times the current was never supposed to die away completely.

Thus, since the advent of the satellite era and the discovery of the earth's trapped radiation, there has been considerable expectation that the particles which constitute the ring current would be directly observed, and their species, energies and spatial distributions determined. In addition, magneticians have sought the location of the currents by attempting to measure their magnetic effects with satellite borne magnetometers. While the trapped radiation was discovered over five years ago, the endeavor to observe any significant ring current has been unsuccessful until recently.

In an initial survey of data received from a low energy proton detector aboard Explorer XII (launched August 16, 1961), *Davis and Williamson* (1963) noticed that the energy density of the 100 kev to 4.5 Mev protons amounted to an appreciable fraction of the energy density of the earth's magnetic field during a magnetically quiet period, and from 4 out to 8 earth radii the ratio of the two energy densities was almost constant. It was of obvious interest to determine the magnitude of the magnetic field produced by this population of protons. On the basis of some preliminary data furnished by Davis, *Akasofu, Cain and Chapman* (1962) calculated the magnetic disturbance for a model proton belt which resembled the measured proton distribution. The results predicted a decrease in the surface equatorial field of about 38 γ due to the quiet time belt. *Davis and Williamson* (1963) also observed a threefold increase in proton intensities at small pitch angles during a magnetic storm. Adopting the assumptions that (1) this increase was applicable to protons of all pitch angles, and (2) the average energy of the particles equalled the quiet

*Published as *Goddard Space Flight Center Document X-611-64-*. June 1964

time energy, *Akasofu and Cain* (1962a) calculated that an additional 80 γ decrease would be observed at the equator of the earth, sufficient to account for the -60 γ main phase of the aforementioned magnetic storm.

A considerably more thorough analysis of the magnetic effects of the quiet time proton belt has now been performed from the data obtained from the proton detector aboard Explorer XII, and the results are transmitted in this paper. In addition to the fact that these protons produce the greatest magnetic disturbance of any known population of trapped particles, it is also of interest to study the effects of the ring current on phenomena related to the earth's main magnetic field. The magnetic lines of force are distorted from the shapes calculated by the spherical harmonic analysis of the field at the earth's surface. There is a stretching out or strengthening of the field at distances beyond the ring current which affects the location of the magnetospheric boundary. Of interest to cosmic ray physicists is the influence of the Störmer cut-off rigidity for solar protons approaching the earth near the polar regions. Finally, the quiet time particle distributions are established in order to acquire a basis for determining storm time variations.

Thus, in this paper the proton data are also interpreted so as to determine the extent which the magnetic perturbations of the protons effect the earth's main field.

II. PROTON LIFETIMES

The proton ring current under discussion has been described as a "quiet time" current, there being arguments against consideration that its enhancement during a magnetic storm is the cause of the main phase. If one assumes that the lifetimes of these particles are limited solely by coulomb scattering and charge exchange, the decay time of an enhanced current during a magnetic storm would be an order of magnitude larger than the one day recovery time indicated by magnetograms at ground level (*Liemohn*, 1961). To obtain agreement between the observed decay time and calculated proton lifetimes, it is necessary to postulate that protons in the energy region 1 to 100 kev (below the threshold of the Explorer XII detector) constitute the storm time ring current (*Dessler, Hanson and Parker*, 1961). In light of the fact that at magnetically quiet periods the observed proton intensities remain stable to within a factor of two over a long period of time (*Davis, Hoffman and Williamson*, 1964), the electric current resulting from them is considered to exist at all times and is described as a quiet time ring current.

However, one must recognize the fact that an enhancement of the protons within the energy range of the detector might constitute the higher energy portion of the storm time particles. Since protons trapped at a given time do have finite lifetimes, there must be a source and probably an acceleration mechanism for replenishing the population. In view of the insufficiency of our knowledge concerning such processes, it is possible that the particular acceleration mechanism, and perhaps others, may influence the lifetimes of the particles. It has also been experimentally observed that during a magnetic storm some time variations do exist. For these reasons the storm time proton observations are being carefully analyzed and will be reported in a later paper.

III. ELECTRIC CURRENTS

Since the magnetic effects of the trapped protons are due to the electric currents they establish, it is first necessary to deduce the current distribution on a magnetic meridian plane from the experimental observations of the protons. For this calculation a slightly modified version of the theory developed by *Akasofu and Chapman* (1961) is used. Essentially the same notation has also been adopted and appears for reference in the Appendix.

In Alfvén's guiding center approximation describing the motion of charged particles in a strong magnetic field, the motion is analyzed into three parts: (a) the *gyration* about and in a plane perpendicular to a magnetic field line; (b) the *oscillation* essentially along a line of force between two mirror points; and (c) the east-west *drift* motion for positively charged particles on a magnetic shell. All of these motions may contribute to the flow of an electric current, i. To calculate the current produced in a gas permeated by a magnetic field, the gas pressure and the characteristics of the magnetic field must be known at every point in the gas.

We now limit the discussion to the steady state

case with a proton distribution symmetrical about the axis of the magnetic poles. While the experimental data will be analyzed in the B/B_e (or equatorial pitch angle), L coordinate system, the computations will assume a geomagnetic dipole field. If $\hat{k}$ is the eastward unit vector normal to a magnetic meridian plane at a particular point, the volume current densities arising from the three motions are obtained from the following formulae (*Parker*, 1957):

a) The current produced by the gyration:

$$\vec{i}_L=\hat{k}\left[\frac{c}{aBh_2}\left(\frac{\partial p_n}{\partial L}-\frac{1}{2}\frac{p_n}{p_m}\frac{\partial p_m}{\partial L}\right)+\frac{c}{BR_c}p_n\right] \tag{1}$$

where

$$h_2=\frac{\cos^3\varphi}{(1+3\sin^2\varphi)^{\frac{1}{2}}}=\frac{1}{\cos^3\varphi}\left(\frac{B}{Be}\right)^{-1} \tag{2}$$

and

$$\frac{1}{R_c}=\frac{3(1+\sin^2\varphi)}{aL\cos\varphi(1+3\sin^2\varphi)^{\frac{1}{2}}}. \tag{3}$$

b) The current due to the oscillations:

$$i_0=enw_s=0, \tag{4}$$

because as many particles are passing through a unit area perpendicular to B towards one mirror point as are moving towards the other mirror point, at least over a short period of time.

c) The current produced by the drift motion:

$$\vec{i}_D=\hat{k}\left(\frac{c}{2aBh_2}\frac{p_n}{p_m}\frac{\partial p_m}{\partial L}-\frac{c}{BR_c}p_s\right) \tag{5}$$

The total current is then

$$\vec{i}=-i\hat{k} \tag{6}$$

with

$$i=\frac{c}{BR_c}(p_s-p_n)-\frac{c}{aBh_2}\frac{\partial p_n}{\partial L} \tag{7}$$

The negative sign in equation 6 signifies that a positive term in i is a westward contribution to the current density, and a negative term is an eastward contribution.

Let us briefly consider just what details in the motions of the particles give rise to the three current terms of i. The first term involving p_s is due to the westward drift motion of protons which depends upon the centrifugal force mw_s^2/R_c associated with the motion along a curved field line.

The second term also arises from the curvature of the lines of force. The circular orbits due to the gyration are more crowded together on the concave side of the line than on the convex side. This is illustrated in Figure 1a, where between two

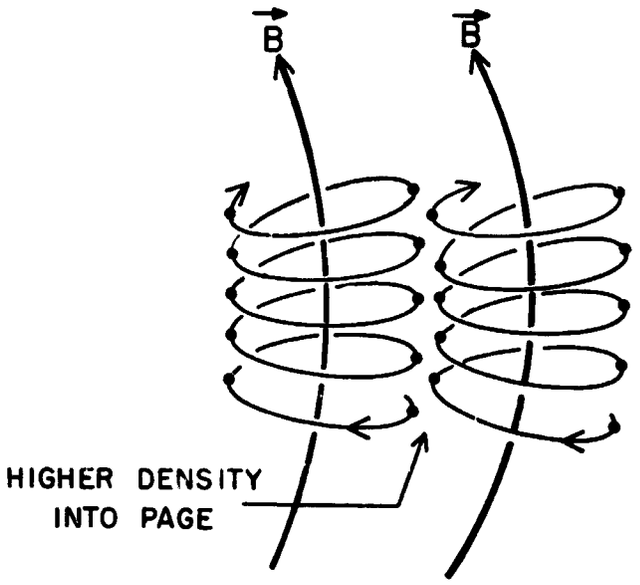

FIGURE 1a.—The source of the current due to the second term in equation 7. The eastward current between the two curved lines of force is caused by the crowding together of the circular orbits on the concave sides of the lines.

adjacent lines of force there is a higher density of particles per unit area moving into the page than out of it. For protons this results in a net eastward current at all points. Surprisingly, this term is larger than the term due to the drift motion if the pitch angle distributions are reasonably steep, as they are for the protons in the belt being discussed.

The final term is due to the fact that the radiation exists in a belt: the intensity increases with radial distance to a certain point, and then decreases. The effect in producing currents is illustrated in Figure 1b, in which the particle intensity is larger on the line of force at a greater distance from the earth, causing a more intense movement of charged particles in a direction into the page than out of it in the region between the lines of force where the two currents intersect. On the inner side of the belt the current

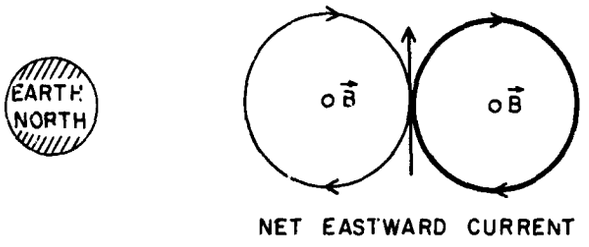

FIGURE 1b.—The source of the current arising from the last term in equation 7. If the particle intensity about the line of force further away from the earth exceeds that about the closer line, indicated by the relative weights of the gyration circles, a net eastward current results in the region between the two lines of force.

will be eastward, and on the outer side it will be westward.

The calculation of the current at all points on a meridian plane first requires the determination of the pressures p_s and p_n at each point. To simplify the equations we first consider protons of a single speed w.

The longitudinal pressure $p_s^* = Nmw_s^2$.

The lateral pressure $p_n^* = \frac{1}{2}Nmw_n^2$.

While it would be possible to calculate these pressures at each point in the magnetosphere from the experimental data, considerable simplification is obtained if they can be expressed in terms of a few parameters determined by the particle distributions. This is accomplished by first fitting the data to a special equatorial pitch angle distribution function with which the local intensities and pitch angle distributions can be obtained from the equatorial intensity and distribution by means of a single parameter depending only upon L. Then the current equation is integrated over the energy spectrum of the particles of interest at each L value; this integral turns out to be actually the total momentum flux at the equator. Hence, the local current at a given latitude depends only upon the two parameters representing the pitch angle distribution and equatorial momentum flux.

Let $F(L, s, \theta)$ denote the number density of protons at a point s on a magnetic shell L, whose speeds lie in dw at w, whose pitch angles lie in $d\theta$ at θ, and whose azimuth angle is arbitrary, since we assume symmetry in azimuth. Note that this definition of $F(L, s, \theta)$ is slightly different than that of *Akasofu and Chapman* (1961) in that it includes a differential angle in azimuth. Fortunately, we can also adopt Parker's special pitch angle distribution (*Parker*, 1957) for the functional form of the distribution in pitch angle, but with the conditions discussed in Section 4 "Proton Data" of this paper:

$$F(L,S,\vartheta, = C_\alpha\left(\frac{B_e}{B}\right)^{\frac{\alpha}{2}}\sin^\alpha\theta. \qquad (8)$$

This distribution has very useful and curious properties. It can be divided into two parts: the second part, $\sin^\alpha \vartheta$, is the local pitch angle distribution and has a form independent of B_e/B. Hence the ratio of p_n to p_s remains the same at every point on an L shell. Because the form function, $\sin^\alpha \theta$, is independent of B_e/B, the integral over all pitch angles, which would be evaluated to obtain the omnidirectional intensity at any value of B_e/B, is independent of this ratio of fields. Hence, the omnidirectional intensity varies down a line of force only as $(B_e/B)^{\frac{\alpha}{2}}$.

The constant C_α can be expressed in terms of the total density at the equator $N_e(L)$:

$$N_e(L) = C_\alpha \int_0^\pi \sin^\alpha\theta(2\pi\sin\theta)d\theta \qquad (9)$$

The integral in $N_e(L)$ will arise again in the theory and can be expressed in terms of gamma functions:

$$\int_0^\pi \sin^{\alpha+1}\theta d\theta = \sqrt{\pi}\frac{\Gamma\left(\frac{\alpha+2}{2}\right)}{\Gamma\left(\frac{\alpha+3}{2}\right)} \qquad (10)$$

Hence

$$C_\alpha = \frac{1}{2}\pi^{-3/2}\frac{\Gamma\left(\frac{\alpha+3}{2}\right)}{\Gamma\left(\frac{\alpha+2}{2}\right)}N_e(L) = A(\alpha)N_e(L) \qquad (11)$$

Therefore

$$F(L,s,\theta) = N_e(L)A(\alpha)\left(\frac{B_e}{B}\right)^{\frac{\alpha}{2}}\sin^\alpha\theta. \qquad (12)$$

Since a particle detector measures a flux rather than a density it would be well to express all equations in terms of fluxes.

$$F(L,s,\theta) = \frac{I_e(L)}{w}A(\alpha)\left(\frac{B_e}{B}\right)^{\frac{\alpha}{2}}\sin^\alpha\theta \qquad (13)$$

where $I_e(L)$ is the omnidirectional intensity at the magnetic equator as a function of L for protons of speed w. It must be noted that α is a function of L, and could also depend upon w.

Inserting this expression into the formulae for the gas pressures yields for protons with speed w:

$$p_s^* = m\int_0^{\pi} (w^2\cos^2\theta)\frac{I_e(L)}{w}A(\alpha)\left(\frac{B_e}{B}\right)^{\frac{\alpha}{2}} \sin^{\alpha}\theta(2\pi\sin\theta)d\theta \quad (14)$$

and

$$p_n^* = \frac{m}{2}\int_0^{\pi} (w^2\sin^2\theta)\frac{I_e(L)}{w}A(\alpha)\left(\frac{B_e}{B}\right)^{\frac{\alpha}{2}} \sin^{\alpha}\theta(2\pi\sin\theta)d\theta \quad (15)$$

Evaluating the integrals with the aid of equation 10, we have

$$p_n^* = \frac{1}{2}mwI_e(L)\Omega(\alpha)\left(\frac{B_e}{B}\right)^{\frac{\alpha}{2}} \quad (16)$$

where

$$\Omega(\alpha) = \frac{\alpha+2}{\alpha+3} \quad (17)$$

and

$$p_s^* = \frac{2}{\alpha+2}p_n^*, \quad (18)$$

which indicates again that the ratio of partial pressures is constant on an L shell.

The current can now be expressed in terms of $I_e(L)$ and α:

$$\begin{aligned} i^* &= \frac{c}{BR_c}\frac{\alpha}{\alpha+2}p_n^* - \frac{c}{aBh_2}\frac{\partial p_n^*}{\partial L} \\ &= -\frac{c}{BR_c}\frac{\alpha}{\alpha+3}\frac{1}{2}mwI_e(L)\left(\frac{B_e}{B}\right)^{\frac{\alpha}{2}} \\ &\quad -\frac{c}{aBh_2}\frac{1}{2}mw\left[\Omega(\alpha)\left(\frac{B_e}{B}\right)^{\frac{\alpha}{2}}\frac{\partial I_e(L)}{\partial L} + \left(\frac{B_e}{B}\right)^{\frac{\alpha}{2}}I_e(L)\right. \\ &\quad \left. +\frac{1}{2}I(L)\Omega(\alpha)\left(\frac{B_e}{B}\right)^{\frac{\alpha}{2}}\ln\left(\frac{B_e}{B}\right)\frac{\partial\alpha}{\partial L}\right] \end{aligned} \quad (19)$$

or

$$i^* = -\frac{mwc}{aH_0}\left[D^*(\alpha,\varphi)L^2I_e(L) + E^*(\alpha,\varphi)L^3\frac{\partial I_e}{\partial L}(L) + F^*(\alpha,\varphi)L^3I_e(L)\frac{\partial\alpha}{\partial L}(L)\right] \quad (20)$$

where H_0 is the field strength on the equator at the earth's surface, and

$$D^*(\alpha,\varphi) = \frac{3}{2}\left(\frac{B_e}{B}\right)^{\frac{\alpha}{2}+4}\frac{\alpha}{\alpha+3}\frac{(1+\sin^2\varphi)}{\cos^{19}\varphi},$$

$$E^*(\alpha,\varphi) = \frac{1}{2}\frac{\alpha+2}{\alpha+3}\left(\frac{B_e}{B}\right)^{\frac{\alpha}{2}}\cos^3\varphi,$$

$$F^*(\alpha,\varphi) - E^*(\alpha,\varphi)\left[\frac{1}{(\alpha+2)(\alpha+3)} - \frac{1}{2}\ln\left(\frac{B}{B_e}\right)\right] \quad (21)$$

Equation 20 corresponds to equation 52 of *Akasofu and Chapman* (1961) with the added term depending upon α (L).

It is now necessary to integrate the current over the energy range measured by the detector. Since the scintillator has a low energy cut-off near 100 kev, the current density distribution arising from protons with energies greater than 100 kev will be calculated. This low energy limit must be kept clearly in mind in what follows.

We next make another simplifying assumption: that α is independent of energy, or the energy spectrum is a function only of L, not of pitch angle. The validity of this assumption will be discussed in Section 4, "Proton Data." This allows D^*, E^*, and F^* to be independent of energy.

The only terms remaining in the current equation 20 which depend upon energy as the velocity w and the equatorial omnidirectional flux of this velocity, $I(L)$, which is actually the omnidirectional differential energy spectrum, $\frac{dN}{dE}$. Let

$$\Psi(L) = \int_{100}^{\infty} mw\frac{dN}{dE}dE = 2m\int_{100}^{\infty}\sqrt{E}\frac{dN}{dE}dE,$$

which is a momentum flux, or twice the energy density of the protons.

Then

$$i = -\frac{c}{aH_0}\left[D(\alpha,\varphi)L^2\Psi(L) + E(\alpha,\varphi)L^3\frac{d\Psi(L)}{dL} + F(\alpha,\varphi)L^3\Psi(L)\frac{d\alpha(L)}{dL}\right] \quad (23)$$

Hence, the current at any point in space, L, φ, need be expressed only in terms of the pitch angle parameter α and the momentum profile ψ at the equator.

IV. PROTON DATA

The data relating to the low energy protons from which the current distributions have been calculated were acquired from one orbit of the satellite, pass 10A (outbound) and 10B (inbound) on August 27 and 28, 1961. At this time the major axis of the orbit was lying in the meridian plane which included the sun (see Figure 2).

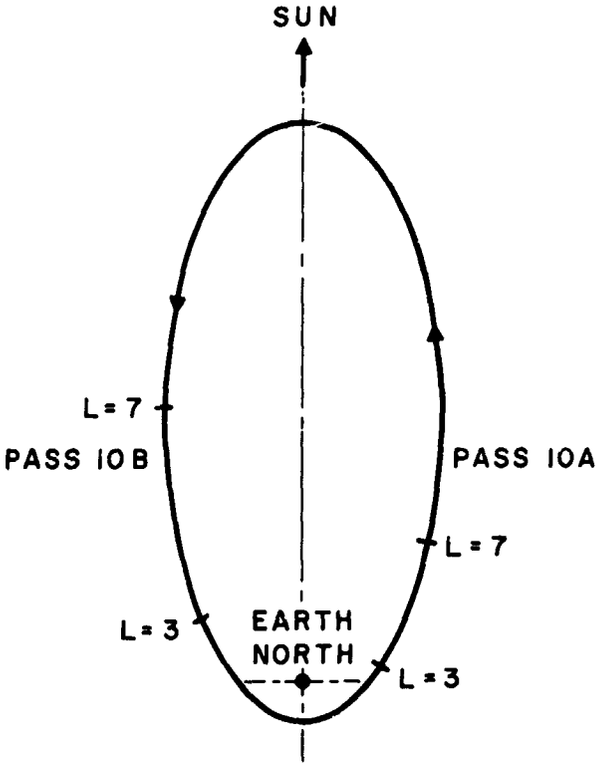

FIGURE 2.—The projection on the earth's equatorial plane of pass number 10 on August 27 and 28, 1961.

Since the heart of the proton belt ($L=3.5$) lies at a relatively low altitude in comparison with apogee ($L=13$) much of the data were collected near the twilight regions, although the outer edge of the belt was traversed on the sunlit side of the earth.

The planetary magnetic three-hour-range index K_p, plotted in Figure 3, indicated that no major disturbances were in progress. In fact the first appreciable magnetic disturbance during the lifetime of Explorer XII did not occur until pass 12.

This particular pass was chosen for thorough analysis because the orbit lay closer to the geomagnetic equator in the heart of the belt than any other orbit. Also the telemetry coverage was complete. When this study was initiated it was expected that a very typical proton distribution would be observed during the pass 10, since *Davis and Williamson* (1963) found no temporal variations larger than 30 percent during nineteen passes of Explorer VII distributed before and after this pass, but not including it. However, later comparisons with this original data indicate that the proton intensities were enhanced by as much as a factor of two at L values smaller than the maximum intensity at L of 3.5 during pass 10. The maximum was also somewhat sharper than observed on the average pass with a more rapid decrease in intensity with increasing L beyond the maximum. This means that the belt was lying at slightly smaller L values than the average belt.

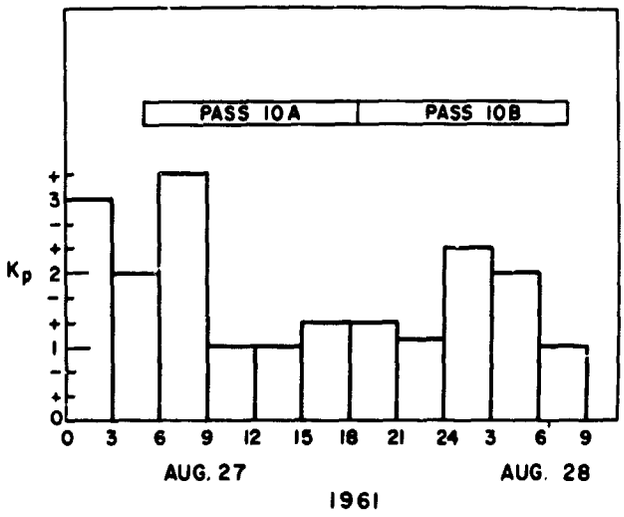

FIGURE 3.—The planetary magnetic three-hour-range index K_p for the period during which the data used in this study were acquired.

The details of the low energy proton detector have been described by *Davis and Williamson* (1963). Let it suffice here to produce a table containing the spectra employed in calculating the momentum integral (Table I), as well as some examples of pitch angle distributions. In general the energy spectrum was described as a doubly sloped exponential spectrum, illustrated in Figure 4 in the integral form which was actually measured by the detector. At L values below 2.2 the data points were best fit with power law

TABLE I.—*Proton Energy Spectra*

	30°–90° Equatorial Pitch Angles				0°–30° Equatorial Pitch Angles			
L	N_{OI}	E_0	E'	E_1	N_{OI}	E_0	E'	E_1
1.8	POWER LAW SPECTRA				POWER LAW SPECTRA			
2.0								
2.2	.....	.....	.....	662 [1]	4.69×10^{7}	625	1650	... [3,4]
2.5	2.04×10^{8}	635	1000	... [2]	1.46×10^{8}	515	1650	... [3]
2.8	2.17×10^{8}	456	1000	... [2]	3.07×10^{8}	390	900	725 [5]
3.0	4.20×10^{8}	303	900	550 [3]	4.15×10^{8}	255	900	320 [3]
3.25	5.07×10^{8}	222	1000	480	4.22×10^{8}	205	900	480
3.5	6.10×10^{8}	193	880	300	4.64×10^{8}	185	900	226
3.7	4.88×10^{8}	196	880	196	3.40×10^{8}	176	∞	.....
3.9	3.60×10^{8}	195	880	247	2.50×10^{8}	145	900	260
4.6	3.00×10^{8}	110	255	187	1.68×10^{8}	105	∞	....
5.0	2.80×10^{8}	73	255	139	1.73×10^{8}	61.5	255	90
5.5	1.62×10^{8}	68	350	[illegible]	1.14×10^{8}	52	∞	.....
6.0	2.05×10^{8}	50	375	[illegible]	2.20×10^{8}	36	∞	.....
7.05	1.35×10^{8}	33.5	.....	∞	6.13×10^{7}	33	∞	.....

Notes: All energies in kev.

[1] E_1 =662 kev from 470 to 1000 kev; for $E>1000$ kev, power law with γ for integral spectrum =4.2. From 140 to 470 kev, no protons.
[2] For $E>1000$ kev, power law with γ =4.2.
[3] For $E>1650$ kev, power law with γ =4.2.
[4] Below E =255 kev, no protons.
[5] For $E>2000$ kev, power law with γ =4.2.

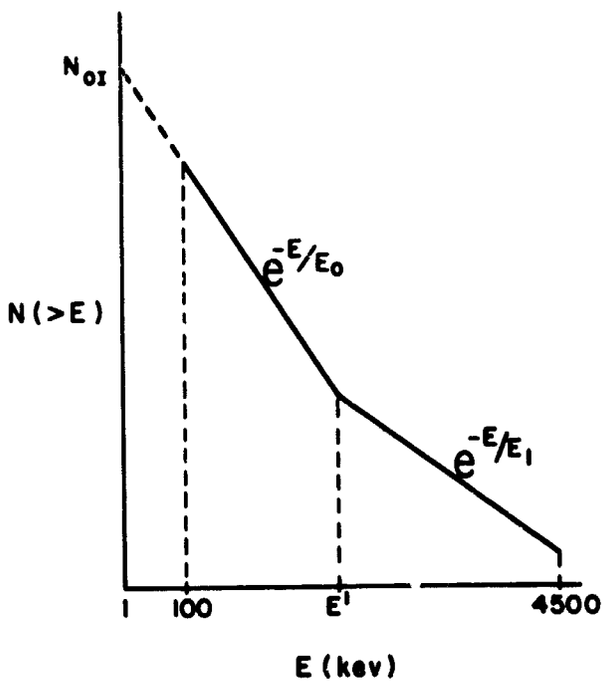

FIGURE 4.—Double sloped integral proton spectrum employed in the calculation of the momentum integral.

spectra, and up to L of 3 a steep power law spectrum was included for the higher energy protons, as suggested by the data of *Bame et al* (1963) and *Naugle and Kniffen* (1963). The spectra listed in Table I were differential before insertion into the momentum integral.

In the derivation of the formulae from which the current distributions may be computed, considerable simplification was attained by employing as the functional form of the pitch angle distribution, $\sin^{\alpha}\theta$. The measured angular distributions were found to fit this form reasonably well provided the entire range of pitch angles, 90° to 0°, was divided into two regions, 90° to 30°, and 30° to 0°, each with an independently determined value of α. Some sample fits of the data to this function appear in Figure 5.

Figure 5a illustrates the extrapolation to 90° of the distribution based on data points with pitch angles only between 30° and 56°. At low L values the orbit carried the satellite away from the magnetic equator making the measurement of protons with large pitch angles impossible. Figure 5b is an excellent example of the necessity of using the two independent values of α. An

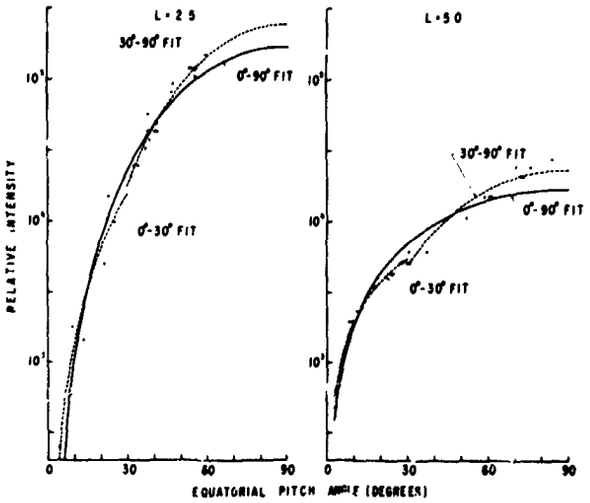

FIGURE 5.—Sample fits of the equatorial pitch angle distribution to the function sin α for the regions 90° to 30° and 30° to 0°.

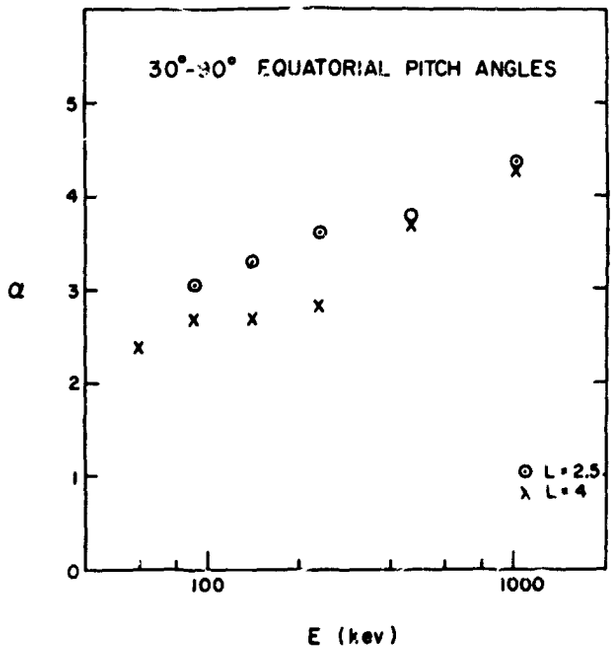

FIGURE 6.—The pitch angle parameter α as a function of energy for L values of 2 and 4.

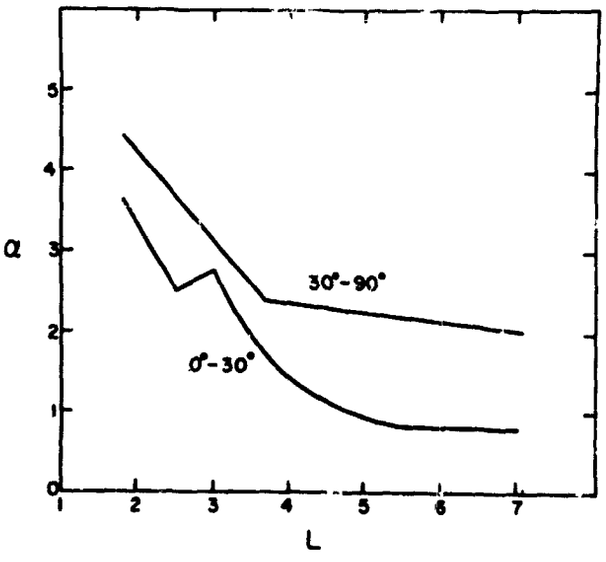

FIGURE 7.—The values of α as a function of L for the two pitch angle ranges derived for the particles having the average momentum on the given L shell.

attempt at a least squares fit of all data from 0° to 90° produced a curve (solid line) with a large hump at the middle pitch angles and a very low value at large pitch angles.

Another assumption which considerably simplified the derivation of the current distribution formulae involved the independence of α upon energy. In reality the value of α increases as a function of increasing energy, as illustrated by the data in Figure 6 for protons of equatorial pitch angles between 90° and 30°. The data in the figure were obtained from the output of the detector which measured the incident energy flux of protons rather than the particle flux. The energies at which the points are plotted are the effective low energy cut-offs for the integral energy spectrum measured at this value of L. By choosing a constant value of α for a given L, the functions D^*, E^*, and F^* (equation 21) became energy independent and could be removed from the integration over energy. Hence, the value of α (L) selected is approximately the value derived for the particles having the average momentum on the given L shell. This value of α as a function of L is plotted in Figure 7 for each of the two pitch angle ranges, 90° to 30°, and 30° to 0°.

The calculation of N_{OI}, employed in the determination of the momentum integral ψ (see Figure 4 for spectral shape of the ψ integral), required some special attention. This quantity, the integral omnidirectional intensity above zero energy, is equivalent to the directional intensities at 100 kev integrated over all pitch angles, which can be actually measured by the detector, multiplied by the factor exp $(100/E_0)$. However, the counting rates of the lowest energy channels of the detector aboard Explorer XII passed into

saturation about one earth radius on either side of the maximum intensity at 3.5 R_E, at least at large pitch angles. Hence, it was necessary to compute N_{OI} by either of two less direct methods.

If (1) a directional intensity above an energy E_c, $J(>E_c)$, is measured at a pitch angle θ_c, (2) the pitch angle distribution characterized by the parameter α is known, and (3) the energy spectrum (E_0) is measured (the latter two parameters could be determined by the current channels of the detector, which did not pass into saturation), then the value of N_{OI} can be calculated from the formulae

$$N_I(>E)=\frac{J(>E_c)}{G_0 \sin^\alpha \theta_c} 2\pi^{3/2} \frac{\Gamma\left(\frac{\alpha+2}{2}\right)}{\Gamma\left(\frac{\alpha+3}{2}\right)} \times \exp\left[(E_c-E)/E_0\right], \quad (24)$$

where G_0 is the telescope factor $=5.85\times10^{-3}$ cm^2−ster., the expression $2\pi^{3/2}$ times the gamma functions arises from integration over the pitch angles, $(\sin^\alpha \theta_c)^{-1}$ is actually an extrapolation of the directional intensity measured at θ_c to the intensity at 90° equatorial pitch angle, and $\exp[(E_c-E)/E_0]$ is an extrapolation in energy from the integral point at E_c to the energy E. The quantity N_I is then the integral omnidirection flux above the energy E, so N_{OI} would have $E=0$.

Therefore, when the counting rate channel at 100 kev was in saturation either of two extrapolations could be used to acquire N_{OI}: A higher energy channel (for example, the 880 kev step) would provide a non-saturated counting rate at a near 90° pitch angle, making $(\sin^\alpha \theta_c)^{-1}\simeq 1$ but requiring an extrapolation in energy $\exp[(E_c-E)/E_0]$, or a smaller pitch angle measurement from the 100 kev channel would provide a measurement of $J(>E_c)$ out of saturation, allowing $\exp[(E_c-E)/E_0]$ to be near one, but increasing the value of $(\sin^\alpha \theta_c)^{-1}$. Obviously the accuracy of either method depends upon how well the data can be characterized by the parameters α and E_0. The values of N_{OI} employed in the computation of ψ (L) were acquired by utilizing both methods. Table II shows a sample set of intensities calculated for an L value of 3.25 for particles with pitch angles 30° to 90°. The agreement between the various calculations of an N_{OI} at a given L value was within ±15 percent.

TABLE II

E_c(kev)	θ_c	α	E_0(kev)	N_{OI}
105	40°	2.5	222	5.01×10^8
470	30°	2.5	222	5.34×10^8
880	70°	2.5	222	4.87×10^8

From the two sets of values of α (L) necessary to describe the protons over the entire pitch angle range from 0° to 90°, a double set of N_{OI} is calculated, since this quantity is a function of α through equation 24. Hence, we obtain two independent profiles of ψ (L), one to be associated with protons having pitch angles 30° to 90°, the other with protons from 0° to 30°. These two profiles appear in Figure 8.

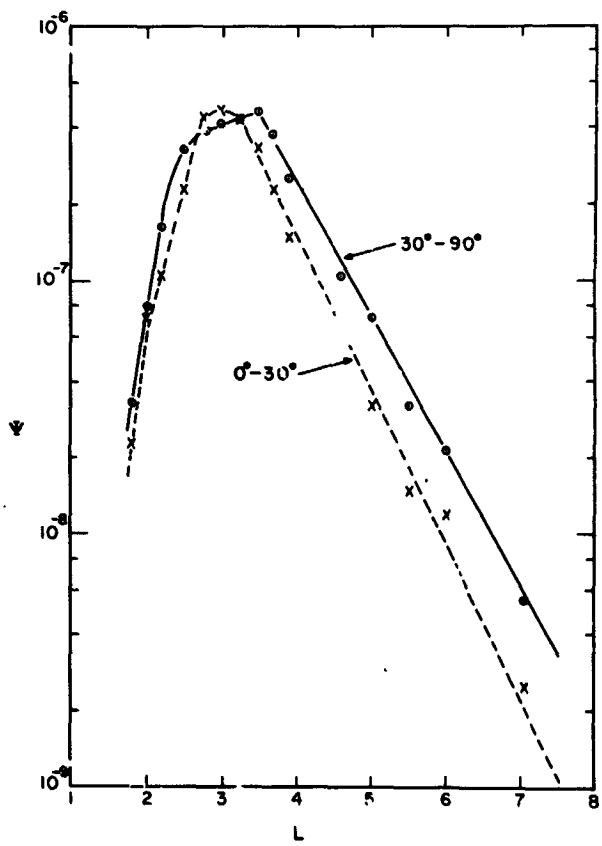

FIGURE 8.—The omnidirectional momentum flux ψ (L^3) for each of the two pitch angle ranges in units of gm/cm-sec^2 (or ergs/cm^3).

V. ELECTRIC CURRENT DISTRIBUTION

The data have now been compiled in a form sufficient for the calculation of the electric current distribution from equation 23. One must keep in mind that the current at a particular L, φ is actually a function of the local partial pressures p_s and p_n (equation 7), but we have replaced the problem of calculating them by utilizing the parameters α (L) and ψ (L). The set of these parameters which is applicable to the radiation at the point of calculation of i must be used. Since a proton with an equatorial pitch angle of 30° mirrors at a magnetic latitude of 32°, the calculation of i for latitudes less than 32° will employ the set of parameters describing protons with equatorial pitch angles from 30° to 90°, and the calculation of i for latitudes greater than 32° will utilize the parameters for protons of pitch angles 0° to 30°. There will be a discontinuity in i as a function of latitude at 32° because as this latitude is approached from the equatorial side, the parameters less accurately describe the actual radiation.

Two other discontinuities which arise in the distribution of i over a meridian plane are due to the approximation of α (L) and ψ (L) by the simple mathematical expressions listed in Table III. Except for ψ (L) in the region $L=2.25$ to 2.75 for protons with 30° to 90° pitch angles, and $L=2.75$ to 3.25 for 0° to 30° pitch angles, both α and ψ could be well approximated by either straight lines or exponentials. While the approximation curves are continuous, their derivatives contain discontinuities between the segments of the curves. Hence, since i depends upon the derivatives, it will contain discontinuities.

TABLE III

α	L Region	ψ	L Region
		30° to 90° E.P.A.	
$-1.07L+6.36$	1.5 to 3.7	$2.95\times10^{-11}\exp(L/0.256)$	1.5 to 2.4
$-0.12L+2.84$	3.7 to 10.0	$1.98\times10^{-7}\exp(L/4.12)$	2.7 to 3.5
.....	.....	$3.50\times10^{-5}\exp(-L/0.810)$	3.5 to 10.0
		0° to 30° E.P.A.	
$-1.62L+6.57$	1.5 to 2.5	$2.06\times10^{-12}\exp(5.18L)$	1.5 to 2.0
$0.52L+1.22$	2.5 to 3.0	$4.23\times10^{-10}\exp(2.52L)$	2.0 to 2.75
$27.5L^{-2.113}$	3.0 to 5.3	$5.91\times10^{-5}\exp(-1.476L)$	3.2 to 10.0
$-0.053L+1.16$	5.3 to 10.0	.....	.....

In the regions of Ψ not included by these formulae, tabulated values from the curves of Figure 8 were used.

The calculations of i in both pitch angles ranges have been performed for the region of L from 1.5 to 10 in intervals of 0.1 and latitude from the equator down an L shell to approximately 1000 km above the surface of the earth in 2° intervals by utilizing an IBM 7094 computer at Goddard Space Flight Center. Actually the calculations were terminated at a latitude within 2° of the latitude where the line of force attained a height of 1000 km. This convention was adopted so that a constant latitude increment could be used in the numerical integration involved in the magnetic field calculations. A contour plot of the current distribution on a magnetic meridian plane appears in Figure 9.

The contributions of each of the terms in equation 23 to the total current are displayed in Figure 10 for two different L shells, one on the inner side of the belt where the total current is eastward, the other on the outer side of the belt where the total current is westward. One notices from an inspection of Figures 9 and 10 that the westward portion

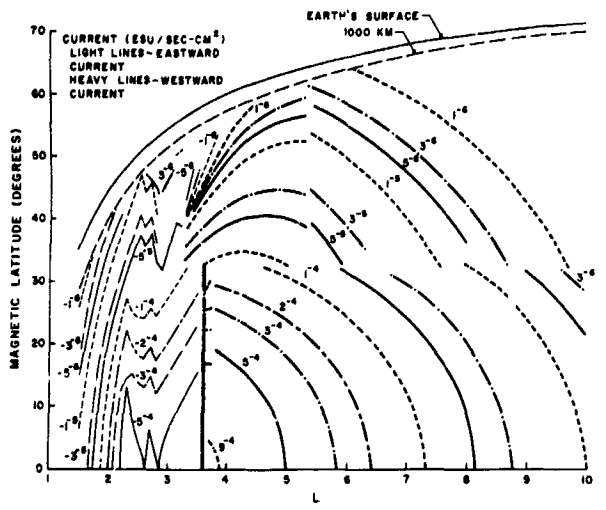

FIGURE 9.—A contour plot of the total electric current in a magnetic meridian plane derived for protons with energies above 100 kev. The currents, expressed as X^{ν} signify $X \cdot 10^{\nu}$. To convert currents from esu/cm²-sec to amps/km², multiply by three.

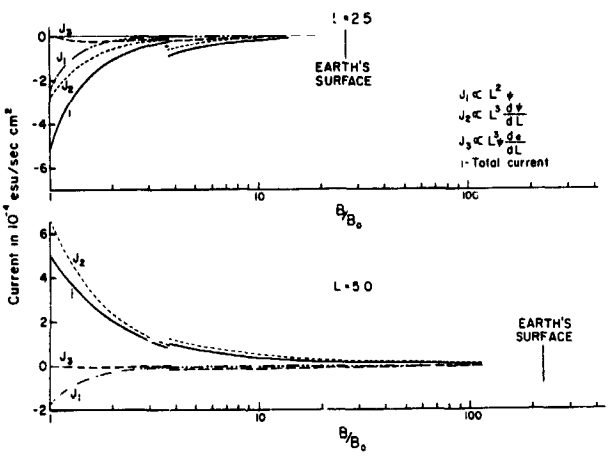

FIGURE 10.—The contributions of each of the terms in equation 23 to the total current for two different L shells.

of the ring current, producing a southward perturbing magnetic field on the earth's surface, arises from the second term J_2, which depends upon the gradiant of the momentum flux on the outer side of the belt.

Since the discontinuities in i appearing in these figures originate in the mathematical expressions used to fit the parameters appearing in the equation for i, a smoothed version of the current contour plot to illustrate the dominant features of the current distribution appears in Figure 11.

An integration has been performed to obtain the

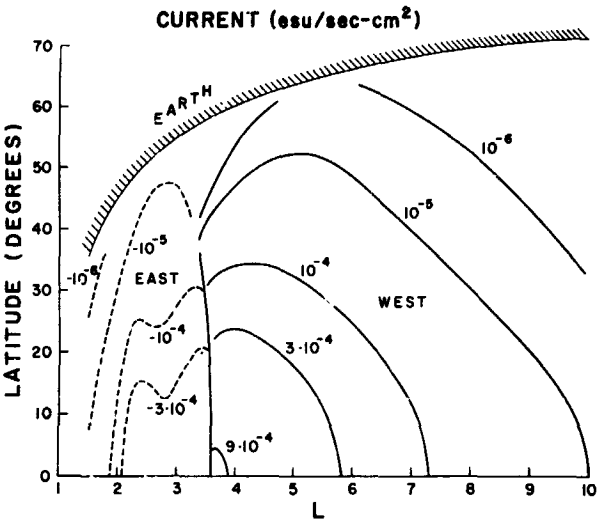

FIGURE 11.—A smoothed version of the electric current contour plot to illustrate the dominant features of the electric current distribution.

total eastward and westward currents, their algebraic sum, and the magnetic moment of the ring current. These values are tabulated in Table IV.

TABLE IV

	esu/sec	amps
Eastward Current	0.57×10^{15}	0.19×10^{6}
Westward Current	2.34×10^{15}	0.78×10^{6}
Total Current	1.77×10^{15}	0.59×10^{6}

Magnetic Moment $0.029M_E$ ($M_E=8.1\times10^{25}$ gauss-cm³)

VI. MAGNETIC FIELD OF THE RING CURRENT

The magnetic field due to the ring current may be denoted by its components H_p and H_z respectively perpendicular and parallel to the dipole axis. These components refer to a point (r, φ) specified by its polar coordinates (φ is latitude) or alternatively by a point (af, φ) in L space where $f=L\cos^2\varphi$.

The ring current region is then divided into elements dS_3 specified by (r', φ') in polar coordinates or by (af', φ') in L space, where $f'=L'\cos^2\varphi'$. Then (*Stratton*, 1941),

$$H_p=-\frac{2}{(acf\cdot\cos\varphi)}\int\int(f\sin\varphi-f'\sin\varphi')\Big[E(k^2)-K(k^2)+(2f\cdot f'\cos\varphi\cdot\cos\varphi')\frac{E(k^2)}{F_{-}^{2}}\Big](i/F)dS_3 \quad (25)$$

and

$$H_z = -\frac{2}{(ac)}\int\int\left[K(k^2)-E(k^2)+2f'\cos\varphi'(f'\cos\varphi' - f\cos\varphi)\frac{E(k^2)}{F_-^2}\right](i/F)dS_3 \quad (26)$$

Here $K(k^2)$ and $E(k^2)$ denote the complete elliptic integrals of the first and second kind respectively, and

$$k^2 = \frac{(4f\cdot f'\cos\varphi'\cos\varphi)}{F^2},$$

$$F_-^2 = f^2+f'^2-2f\cdot f'\cos(\varphi-\varphi'),$$

$$F^2 = f^2+f'^2+2f\cdot f'\cos(\varphi+\varphi').$$

An element of cross sectional area of the ring current region in the meridian, dS_3, is expressed as $dS_3 = a^2L'\cos^4\varphi' dL' d\varphi'$.

The foregoing formulae appear as in *Akasofu and Chapman* (1961) except for the correction of several misprints.

The components H_p and H_z were calculated separately at each point in the specified current region for particles in both pitch angle intervals. The results were then combined to give the total field components at each point in the current region for all ring current particles.

The integrations involved in calculating these field components were performed numerically on the IBM 7094 computer at Goddard, and the results appear in Figure 12. As with the current calculation, increments of 0.1 in L and 2° (0.0349 radian) in latitude were used.

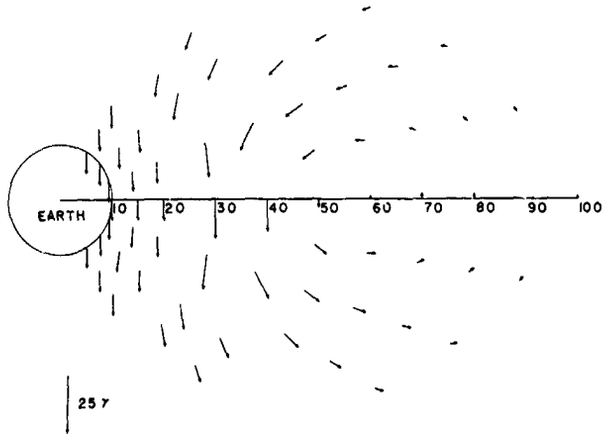

FIGURE 12.—Vector magnetic field on a meridian plane due to the proton ring current.

A discontinuity in the components H_p and H_z arises when $L=L'$ and $\varphi=\varphi'$, since in this case $F_-^2=0$, which appears in the denominator of the argument for each field component. The contribution to the components from the element of integration causing this discontinuity was taken to be zero each time such a discontinuity appeared.

The coordinate system used indicates a negative H_z is in a southerly direction and a negative H_p points toward the earth.

VII. DISCUSSION

(a) Vector Field of the Ring Current

At the magnetic equator on the surface of the earth the magnetic field due to the ring current attained a value of 9 γ in a southern direction, a value considerably smaller than the 38 γ obtained by *Akasofu, Cain and Chapman* (1962) from the preliminary data from the same detector. A reasonable error analysis on the field strength appears virtually impossible to perform. Purely an estimate would place a confidence of about 50 percent (±5 γ) on the field calculations.

The distribution of field vectors from the ring current which appears in Figure 12 indicates a field fairly uniform on the inside of the proton belt and parallel to the dipole axis as expected. In the region of the belt the field shows considerable curl and achieves a maximum value of 23 γ on the equator at an L of 3.6. Outside the belt the field becomes parallel to the earth's field, but has the extremely small value of 2.5 γ. Hence, the ring current field due to these protons above an energy of 100 kev would have little influence on the shape of the boundary of the magnetosphere.

(b) Second Order Calculation

While these protons with energies above 100 kev are showing some magnetic influence, the magnitude is not sufficient to perturb appreciably the magnetic field of the magnetosphere which arises from sources internal to the earth. In fact it appears that the distortion of the field even at the altitudes of the ring current due to the compression of the field by the solar wind is comparable to the disturbance from the ring current (*Cahill and Amazeen*, 1963). Hence the assumption of analyzing the data in the L, equatorial pitch angle coordinate system for the ring current

calculations will produce results as accurate and physically meaningful as would an attempt at a second order calculation (*Beard*, 1962; *Akasofu, Cain and Chapman*, 1961), in which the trapped protons are assumed to move in a magnetic field differing from the internal field by the field of the ring current itself.

(c) Cut-off Rigidity of Solar Protons

In order to explain the observations of low-rigidity solar protons near the earth at latitudes well below those predicted by normal Störmer theory, investigators have included the magnetic effects of a ring current as well as the termination of the geomagnetic field (*Kellogg and Winckler*, 1961; *Akasofu, Lin and Van Allen*, 1963; *Ray*, 1964). In order that a ring current contribute significantly to a reduction in the cut-off rigidity, its magnetic moment must be some appreciable fraction of the magnetic moment of the earth. However, the moment due to the quiet time protons with energies above 100 kev is calculated to be only 0.029 that of the earth, a value much too small to affect solar proton trajectories.

(d) Model Belt Parameters

On the basis of some very preliminary data from the proton detector aboard Explorer XII, the magnetic effects of a model belt that resembled the measured belt were calculated (*Akasofu, Cain and Chapman*, 1962). Since then the properties of a similar belt have been applied to various problems of a geophysical nature (see especially the later articles by Akasofu; *Vestine*, 1963). For this work the following parameters have been utilized to characterize the distribution of protons:

- r_0: distance where the number density attains its maximum value,
- g_1: Gaussian parameter for the inner side of the belt: $n=n_0 \exp(-g_1^2 z^2)$, where $z=(r-r_0)/a$,
- g_2: Gaussian parameter for the outer side of the belt,
- α: pitch angle parameter,
- n_0: maximum number density,
- E: average energy of all protons in the belt.

In table V are listed the values adopted in the literature and a set of suggested values which more accurately produce the results obtained in this more thorough study.

TABLE V

Parameter	Value in Current Literature	Revised Value
r_0	3.0 and 3.2	3.5
g_1	2.990	1.0
g_2	0.419	0.90
α	2.0	2.5
n_0	0.6/cc	0.46/cc
E	500 kev	300 kev

(e) Lower Energy Protons

One must keep clearly in mind in this discussion of the magnetic properties of the trapped protons that only those with energies above 100 kev, the low energy cutoff for the direct detection of proton particle fluxes by the detector, have been considered. However, in another mode of operation the detector could measure proton energy fluxes down to energies of some tens of kev, depending upon the steepness of the spectrum. Beginning at about an L of 5, large fluxes of protons were apparently present with energies extending down to at least 50 kev, and the ratio of the flux between 50 and 100 kev to that above 100 kev became increasingly large with range.

While a complete saturation of the field beyond five earth radii with very low energy protons would significantly contribute to a quiet time ring current, the maximum field produced at the earth's surface by such a particle distribution is insufficient to account for large magnetic storms.

For a rough estimation of this maximum field first assume that the particle energy density is limited by the energy density of the field on the magnetic equator of an L shell. Next assume that the particle intensity is isotropic ($\alpha=0$) and hence constant everywhere on an L shell to latitudes of 60°, which is essentially the surface of the earth for $L\geq 5$. Using equations 23 with $1/h_2$ add $1/R_c$ evaluated at the equator, their maximum values, and with

$$\Psi(L)=2\frac{H_0^2}{8\pi L^6}$$

the current is

$$i(L)=\frac{cH_0}{2\pi aL^4}\cos^3\varphi$$

This produces a field at the center of the earth, and approximately at the surface, of

$$H_z=-\frac{1\times10^4}{L^3}\gamma,$$

where L is the minimum distance of the belt from the center of the earth. For $L=5$, H_z is -76 γ, which is one, and probably two, factors of two too large if compared with a field derived from any realistic distribution of particles exactly calculated.

To account for a large storm of 300 γ (excluding inductive effects in the earth) the field would have to be saturated down to at least an L of 3.2, and probably more like 2.5 for a more reasonable particle distribution. The apparent necessity for such a high intensity, low altitude belt leads one to question whether the current equation 7 includes all the necessary terms to account for the ring current as it naturally occurs. One is tempted to suggest that electric fields may assist in the production of an increased westward movement of the protons already observed. It certainly would seem reasonable to attempt a measurement of electric fields in this region of space.

It is interesting to note that the lifetime of 50 kev protons at 5 earth radii is only on the order of a week (*Liemohn*, 1961). In order to sustain a quiet time belt of such particles it would be necessary to have a source which operates continually.

In passing it is perhaps well to mention that the trapped electrons observed to date produce negligible magnetic fields. Since the magnetic properties of a particle depend upon the square root of its mass, electron fluxes of the order of 10^{10} electrons/cm^2-sec would be required to produce magnetic effects equivalent to those of the protons observed. This flux is two orders of magnitude greater than any reported in the literature.

VIII. CONCLUSION

The protons with energies above 100 kev observed by the low energy proton detector flown by Davis and Williamson aboard Explorer XII are the first group of particles discovered in the trapped radiation region with intensities sufficient to produce significant magnetic effects. However, for applications to other geophysical problems, such as the distortion of field lines, the change in the Störmer cut-off rigidities, and the quiet time remains of a storm time ring current, the observed particle intensities are probably disappointingly small.

For future studies of the proton ring current two improvements in the data acquisition would be desirable. The orbit of the satellite should be more nearly equatorial over all L values, and the detectors should be capable of measuring protons down to nearly one kev in energy.

While this detector has provided information which has advanced our knowledge of the ring current problem, it appears that the complete understanding of the phenomenon will require some years of continued research with new particle detectors and possible complementary measurements of electric fields or a more complete understanding of other source mechanisms for the electric currents.

ACKNOWLEDGEMENTS

The authors appreciate the opportunity of working with the excellent data collected from the proton detector flown aboard Explorer XII by Mr. Leo R. Davis and Mr. James M. Williamson, and for very helpful discussions with them. One of us (R. A. H.) performed most of this study while the recipient of a NAS-NASA Resident Research Associateship, the support of which is gratefully acknowledged.

NOTATION

a	earth's radius, in cm.
c	speed of light, in cm/sec.
r	radial distance from the center of the earth to a point of interest, in cm.
L	McIlwain's coordinate, in earth radii.
B	magnetic field vector, in gauss.
p_m	magnetic pressure $=B^2/8\pi$.
m	mass of a trapped particle in grams.
e	magnitude of charge of a trapped particle, in esu.
w	velocity of a particle, in cm/sec.

w_s component of w along B.
w_n component of w normal to B.
E kinetic energy of a particle, in kev.
N number density of particles.
θ pitch angle of a trapped particle, i.e. the angle between w and B, or its complement if larger than 90°.
p_s pressure of the gas (trapped particles) along B.
p_n pressure of the gas normal to B.
φ geomagnetic latitude.
Note: the subscript "e" indicates that a quantity is being evaluated at the magnetic equator.

REFERENCES

AKASOFU, S. -I., and J. C. CAIN, A model storm-time proton belt, Paper presented at the 43rd annual meeting, A.G.U., Washington, April 25–28, 1962a.

AKASOFU, S. I. and J. C. CAIN, The magnetic field of the radiation belts, *J. Geophys. Research*, **67**, 4078–4080, 1962b.

AKASOFU, S. -I., J. C. CAIN, and S. CHAPMAN, The magnetic field of a model radiation belt, numerically calculated, *J. Geophys, Research*, **66**, 4013–4026, 1961.

AKASOFU, S. -I., J. C. CAIN, and S. CHAPMAN, The magnetic field of the quiet-time proton belt, *J. Geophys. Research*, **67**, 2645-2647, 1962.

AKASOFU, S. -I., and S. CHAPMAN, The ring current, geomagnetic disturbance, and the Van Allen radiation belts, *J. Geophys. Research*, **66**, 1321–1350, 1961.

AKASOFU, S. -I., W. C. Lin, and J. A. VAN ALLEN, The anomalous entry of low-rigidity solar cosmic rays into the geomagnetic field, *J. Geophys. Research*, **68**, 5327–5338, 1963.

BAME, S. J., J. P. CONNER, H. H. HILL, and F. E. HOLLY, Protons in the outer zone of the radiation belt, *J. Geophys. Research*, **68**, 55–64, 1963.

BEARD, D. B., Self-consistent calculation of the ring current, *J. Geophys. Research*, **67**, 3615–3616, 1962.

CAHILL, L. J., and P. G. AMAZEEN, The boundary of the geomagnetic field, *J. Geophys. Research*, **68**, 1835–1843, 1963.

DAVIS, L. R., R. A. HOFFMAN, and J. M. WILLIAMSON, Observations of protons trapped above 2 earth radii, Paper presented at the 45th annual meeting, A.G.U., Washington, April 21–24, 1964. To be published.

DAVIS, L. R. and J. M. WILLIAMSON, Low-energy trapped protons, *Space Research III, Proc. Third Intern. Space Sci. Symp., Washington*, 1962, ed. W. Priester, 365–375, North-Holland Pub. Co., Amsterdam, 1963.

DESSLER, A. J., W. B. HANSON, and E. N. PARKER, Formation of the geomagnetic storm main-phase ring current, *J. Geophys. Research*, **66**, 3631–3638, 1961.

KELLOGG, P. J., and J. R. WINCKLER, Cosmic ray evidence for a ring current, *J. Geophys. Research*, **66**, 3991–4001, 1961.

LIEMOHN, H., The lifetime of radiation belt protons with energies between 1 kev and 1 mev, *J. Geophys. Research*, **66**, 3593–3595, 1961.

NAKADA, M. P., J. E. MAZUR, and D. A. KNIFFEN, Variations of the proton energy spectrum with position in the inner Van Belt., *J. Geophys. Research*, **68**, 4065–4078, 1963.

PARKER, E. N., Newtonian development of the hydromagnetic properties of ionized gases of low density, *Phys. Rev.*, **107**, 924–933, 1957.

RAY, E. C., Cosmic-ray cut-offs at high latitudes, *J. Geophys. Research*, **69**, 1737–1741, 1964.

STRATTON, J. A., *Electromagnetic Theory*, McGraw-Hill Book Co., New York, 1941.

VESTINE, E. H., Low-level geomagnetic ring-current effects, *J. Geophys. Research*, **68**, 4897–4907, 1963.

N64-28...

AURORA*

BENGT HULTQVIST†

1. INTRODUCTORY DESCRIPTION

Descriptions of aurora of great antiquity are known. Some of the most famous are those by Aristotle (Meterologica, Book I, Chap. 5 (ca 340 B.C.)), Pliny (Historia Naturalis, Book II, Chaps. 27 and 33 (ca. 77 A.D.)), and Seneca (Quaestiones Naturales, Book I, Chaps. 14 and 15 (ca. 63 A.D.)). In central Europe the rare auroras were considered as warnings for coming calamities and the descriptions from the Middle Ages, especially, are characterized by superstitions and fears. In northern Europe where auroras are more common such superstitions did not influence the objective observation to the same extent. A remarkably good description can be found in the Norwegian chronicle The King's Mirror of about 1250. It is partly quoted by Störmer (1955) and he also quotes some good descriptions of auroral events of more recent time.

The name aurora borealis, or northern dawn, seems to have been first used by the French philosopher Gassendi in 1621, (Jacka and Paton, 1963) and is an appropriate description of the usual appearance of the northern lights when they are observed in medium latitudes. In analogy with aurora borealis the southern lights have been called aurora australis. "The northern dawn seen from middle latitudes is mostly the upper portion of a display which is overhead at higher latitudes. It is only when aurora moves equatorwards on the rare occasions of the great events that middle latitude observers can see those parts of the display which, being below the horizon, are so frequently concealed from them. Aurora then belies its title, since it is no longer an unspectacular glow on the horizon, like the dawn, and it is more aptly called "The Merry Dancers," the name by which it is known in the northern isles of the Britain" (after Jacka and Paton, 1963). In the last years, aurora has been made by man with the use of high-altitude nuclear explosions. The first artificial aurora was observed in 1958 (Cullington, 1958, Fowler and Waddington, 1958).

This review will concentrate on auroral characteristics which are influenced by the geomagnetic field and on results obtained in the last few years. Excellent extensive reviews of auroral phenomena have appeared, (Harang, 1951; Störmer, 1955; Chamberlain, 1961) some fairly recently, and the reader is referred to them for details on, e.g., the auroral spectrum, older morphological studies, correlations with other phenomena, etc. The emphasis here will be on the morphology, which is largely determined by the geomagnetic field. Rocket and satellite studies of primary auroral particles will also be treated in some detail, since they are not contained in the extensive treatises mentioned above. Finally, proposed theoretical models for various auroral phenomena will be briefly discussed in relation to the observations.

In this first subsection a short description of some auroral characteristics will be given.

1. Intensity and Energy Considerations

Aurora is one of the most intense luminous

TABLE 1.

Source	Flux (ergs cm^{-2} sec^{-1})
Sun	$1.4 \cdot 10^{6}$
Full moon	$3000 \cdot 10^{-3}$
Strong aurora	$1000 \cdot 10^{-3}$
Total starlight	$1.8 \cdot 10^{-3}$
Airglow (visible)	$16 \cdot 10^{-3}$
OH (infrared)	$19 \cdot 10^{-3}$
Lyman-α	$10 \cdot 10^{-3}$
Celestial sources (1230–1350Å)	$0.1 \cdot 10^{-3}$
Cosmic rays	$3.8 \cdot 10^{-3}$

*Published as *Goddard Space Flight Center Document X-611-64-97*, April 1964.

†Goddard Space Flight Center. NASA-National Academy of Sciences—National Research Council Senior Post-Doctoral Resident Research Associate on leave of absence from Kiruna Geophysical Observatory, Kiruna, Sweden.

phenomena in the sky, as is illustrated in Table 1 (after Friedman, 1960, except for the aurora value). The very strongest auroras are even more intense than the value given in Table 1. They are fully comparable to the full moon. The majority of auroras are, however, weaker and the whole scale down to the intensity of the airglow exists.

For estimation of brightness of aurora by visual observers, the following four classes of an International Brightness Coefficient (IBC) are used: I, the brightness of the aurora is equal to that of the Milky Way; II, brightness equal to that of thin moonlit cirrus clouds; III, brightness equal to that of moonlit cumulus clouds; and IV, the aurora provides a total illumination at the ground equivalent to full moonlight. These definitions are extremely crude. Seaton (1954) made a first effort to place the IBC scale on an absolute basis. His results have been slightly modified by Hunten (1955), who proposed the following definitions in terms of number of photons of λ 5577Å (generally the most important emission in aurora) per cm^2 (column) and sec.

IBC I	$10^9 = 1\ kR$
II	$10^{10} = 10\ kR$
III	$10^{11} = 100\ kR$
IV	$10^{12} = 1000\ kR$

10^6 photons/cm^2 (column) sec is called 1 Rayleigh (1R) in accordance with the proposal of Hunten et al. (1956). (For a discussion of the Rayleigh unit see also Chamberlain, 1961, Appendix II). The Rayleigh unit is not limited to a special wave length as is the IBC.

The energy influx required to produce visible aurora has been measured (McIlwain, 1960; O'Brien and Taylor, 1964) and has also been computed from optical emissions (Omholt, 1959; Chamberlain, 1961). The results show reasonable agreement. 0.2–1 percent of the input energy seems to be converted to visible light. The input energy required to produce an IBC I aurora is of the order of a few ergs/cm^2 sec (see e.g. Hultqvist, 1964c). Measurements by means of the Injun 3 satellite show that the average energy input rate required to sustain auroras around the world is of the order of 10^{18} ergs/sec (10^{11} watts) (O'Brien and Taylor, 1964). The average energy flux of the solar wind within a cylinder of radius 10 earth radii is of the order of 10^{20} ergs/sec. Thus in the average about 1 per cent of the solar wind energy has to be transformed into particle precipitation. However, during very strong auroras an appreciable fraction of the relevant solar-plasma energy flux must be converted into kinetic energy of precipitated particles, and the energy density of the solar beam may even be unsufficient on some occasions (Mogilevskiy, 1963). Large auroral events thus contribute much energy to the upper atmosphere. Most of this is probably radiated away (only some 15 percent transformed to heat according to Chamberlain, 1961). It seems quite possible that the temperature of the upper atmosphere in the auroral zones is primarily determined by the particle influx (Bates, 1960b; Chamberlain, 1961; Maeda, 1963).

Recent observations of the drag on Injun 3 indicate that the upper atmosphere temperature in the auroral zone is essentially the same as at the equator on geomagnetically disturbed days (Jacchia and Slowley, 1964). The heating accompanying geomagnetic perturbations in the auroral zones seems to be 4 or 5 times greater than the heating experienced during these perturbations in low latitudes.

2. Definition and Classification of Aurora

In connection with intensity the definition of aurora has to be considered. It has been fairly common to mean by aurora sporadic emissions of intensity at least a few times the airglow intensity but not to include emissions weaker than that. From a physical point of view this is not a good definition. Airglow and aurora, the production mechanisms of which are different, may well be thought of as being of similar brightness.

A definition based on the mechanism of excitation and emission would certainly be preferred. Along this line aurora is often defined as emissions in which the intensity ratio between the 3914 Å nitrogen band—which is produced by collision excitation—and the oxygen atom line at 5577 Å is of the order of unity. In airglow it is usually much less than unity. Unfortunately, however, the excitation mechanisms are complex and are not well-known, which makes it impractical to use them in definitions. One parameter seems to be of widely different importance for airglow and for

aurora: the geomagnetic field. Roach and Roach (1963) have defined aurora as emissions, the geographical location of which is determined by the geomagnetic field. The auroral phenomena then also include the stable red arcs, which are mostly subvisual and located in middle latitudes (see the review of Roach and Roach, 1963). We will in this review consider as aurora all emissions which are produced in one way or the other by particles of energy well above thermal and we will also include the above mentioned medium-latitude red arcs (m arcs), for which it is not known whether they are produced by particles (of very low energy) or not.

The aurora is an extremely complex phenomenon. The various types that occur can be grouped in the following six classes, for instance (due to Elvey, 1964)

1. Polar glow
2. Discrete polar cap auroras
3. High red aurora (Störmer's type III)
4. Intermediate red arcs (Störmer's type II)
5. M-arcs
6. Ordinary displays (Störmer's type I)

The polar glow aurora was discovered by Sandford (1961b). It is produced by the same solar protons in the energy range from some 10 Mev to several 100 Mev, which give rise to polar cap absorption. This type of aurora is thus fairly rare and has a pronounced maximum of occurrence frequency at solar activity maximum. The glow is distributed over the whole polar caps and is often subvisual.

The discrete polar cap auroras have several characteristics which are quite different from ordinary auroral-zone aurora (Störmer's type I). Their occurrence frequency is higher at low solar activity than at high and they also show a negative correlation with magnetic activity. The spectrum is, however, similar to that of ordinary auroral displays.

Class No. 3—high red aurora—is the most common type in low latitudes but it also occurs in the auroral zone sometimes.

The intermediate arcs are very rare. They often look grey due to faintness. The average lower height limit is 196 km (which is between the values for ordinary auroral displays and high red aurora; there-from their name). The red 6300 Å line is the most prominent spectroscopic feature. For more details see Störmer (1955).

The so-called ordinary auroral displays are, by far, the most common type of aurora and the rest of this review will deal mainly with them. Not only visual light is emitted by the aurora but emission also takes place in the ultraviolet (see for instance Chamberlain, 1961) and at radio-frequencies (cf e.g. Hartz, 1958, Murcray and Pope, 1960, Egan and Peterson 1961, and Martin and Helliwell, 1960).

In this review we will include among the auroral phenomena not only emissions of electromagnetic radiation but also the so-called radio aurora. The term radio-aurora refers to the effect on the propagation of radio waves, especially in the VHF and UHF frequency ranges, by the ionization in the atmosphere produced simultaneously with the excitation. Such ionization gievs rise to radio echoes of a special type.

3. The Development of an Auroral Display

The auroral displays show an enormous variety in their temporal development. One can, however, talk about typical sequences of events (see e.g. Heppner, 1954, Akasofu, 1963d). Equatorward of the auroral zones the display may begin with a glow along the poleward horizon. The glow then rises from the horizon and forms one or more quiet and mostly homogeneous bows of light (arc), oriented approximately east-west. An "arc" may remain relatively quiescent for hours, drifting slowly towards north or south. Suddenly it may brighten here and there and "rays" begin to appear across the arc. The arc is then likely to fold and so to lose its regular bow shape and to form an irregular "band." If the rays are very long, the band assumes the appearance of a great "drapery," waving like a curtain in the sky. Rapidly moving and fading irregular forms may appear and disappear all over the sky. As the display dies down, waves of light may surge upwards from the horizon in quick succession causing existing auroral forms to brighten as the waves pass over them (flaming aurora). A continuous glow (veil) may extend over a large part of the sky, serving sometimes as a background to the active forms. At other times, diffuse patches of light, closely resembling clouds, appear here and there in the sky. These

may come and go, often with regular pulsations, until twilight sets in. There is a tendency for reformation into arcs after the diffuse surface phase. The development pattern is closely correlated with the details of the coincident magnetic disturbance. The described sequence is typical equatorward of the auroral zone, as mentioned. On the poleward side, and especially over the central polar caps the development is quite different. This will be discussed in section 3. For some good descriptions of individual auroral events, see for instance Störmer (1955).

4. Auroral Forms

In the last few decades the auroral forms have mostly been classified in accordance with the recommendations of 1930 of the International Union of Geodesy and Geophysics. These recom-

FIGURE 1.1.—Auroral arc.

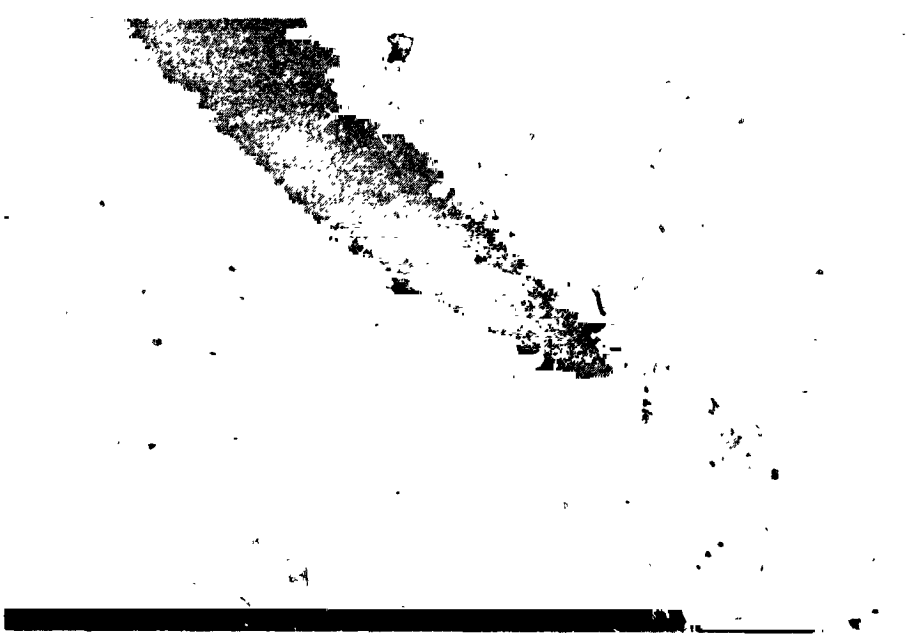

FIGURE 1.2.—A band.

mendations were worked out by Störmer (1930a, b) and are described in detail also in his book (Störmer, 1955).

The Committee for the "International Quiet Sun Year" (IQSY), 1964–1965, of the "Comité International de Géophysique" (CIG) has adopted a new scheme of nomenclature for describing auroras. It will be briefly reviewed below, following Jacka and Paton (1963).

An aurora is described in terms of 4 parameters (6 if brightness and color also are to be included).

1. Auroral forms are divided into three groups

1.1. Band-like forms: These are characterized by a continuous lower border.

(i) When the form appears as a simple, slightly curving arch (Fig. 1.1) or part of an arch, with a regular lower border it is called an arc (A).

(ii) When the lower border is irregular and contains kinks or folds (Fig. 1.2) the form is called a band (B).

1.2. Diffuse forms: These may take the form of a patch (*P*) or a veil (*V*).

(i) The patch is simply a blob of illumination with an ill-defined boundary; it often resembles an isolated cloud.

(ii) The veil refers to the uniform luminosity that may cover a large part of the sky. It may occur alone or as a background to other forms.

1.3 Rays (*R*): These are shafts of light aligned in the direction of the earth's magnetic field (cf. Fig. 1.3). There may be a single ray, a bundle of rays close together or many scattered rays (subscripts 1, 2, 3 may be added to *R* to indicate short, medium, and long rays respectively).

2. Structure is described by the following three adjectives

2.1 Homogeneous (*H*): This term implies an apparent lack of internal structure in the form. The brightness is uniform or it changes only gradually across the form. A homogeneous arc (*HA*), and horseshoe-shaped bands are shown in Fig. 1.4.

2.2. Striated (*S*): The form contains rather irregular striations or filaments aligned roughly parallel with the lower border (Fig. 1.5). Striation is usually recognizable only when the form is nearly overhead.

2.3. Rayed (*R*): Rayed forms are characterized by the appearance within them of rays which are aligned along the lines of force of the geomagnetic field (Fig. 1.6).

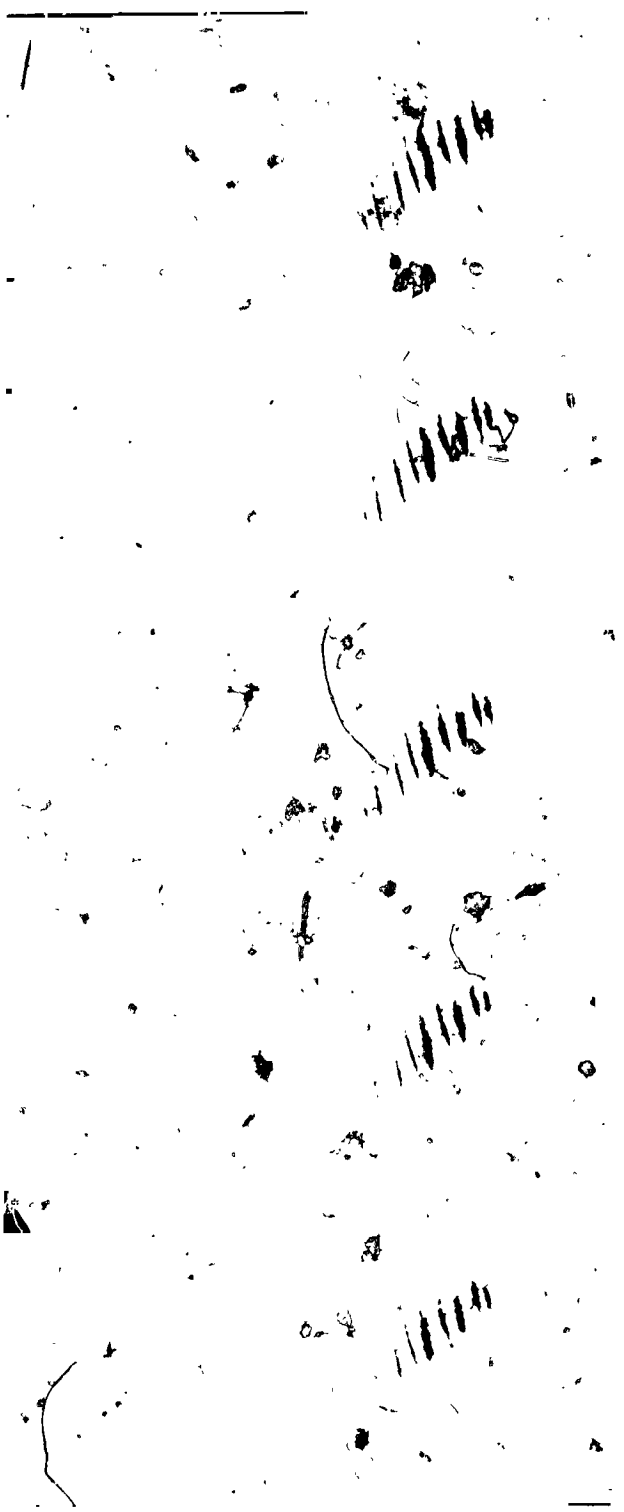

FIGURE 1.3.—Auroral rays photographed with an exposure time of 1/60 sec. 24 pictures per sec. (Courtesy T. N. Davis and G. T. Hicks).

FIGURE 1.4.—Homogeneous auroral arc and bands.

FIGURE 1.5.—Striated auroral arc.

3. *Qualifying parameters: One of three qualifying parameters may, when relevant, be added to the description*

3.1 Multiple (m): This term is used when there occur two or more associated and roughly parallel forms of the same kind. (A subscript numeral indicates the actual number of forms, e.g. m_2HB signifies two closely situated homogeneous bands).

3.2. Fragmentary (f): This term is used when only a portion of an arc or band is present.

3.3 Coronal (c): When any rayed form is viewed in the direction of the lines of magnetic force the rays appear to converge. Homogeneous forms

may also present a similar coronal appearance where they pass over the magnetic zenith.

4. *Condition describes the behavior of a form or of the whole display*

4.1 Quiet (q): The form undergoes only very slow changes in position or shape.

4.2. Active (a): is a form which moves or changes its shape rapidly. Such forms are frequently bright.

(i) a_1—refers to the movement of folds or irregularities along the boundary of a band.

(ii) a_2—refers to the rapid change of shape of the lower border of a form while the form itself may also move rapidly across the sky.

(iii) a_3—indicates the occurrence of a rapid movement of rays horizontally along a form.

(iv) a_4—refers to a display as a whole in which forms fade rather quickly, while new, similar or different forms appear in other parts of the sky. A photograph of such an event is seen in Fig. 1.7.

4.3. Pulsing (p): this describes a condition of fairly rapid and often rythmic fluctuation in brightness. The period of the fluctuation may range from a fraction of a second to the order of minutes.

(i) p_1—pulsating forms: The affected form or forms display a variation in brightness, the phase of which is uniform throughout the forms.

FIGURE 1.6.—Rayed bands.

FIGURE 1.7.—Photograph of an active aurora. The forms move and fade rapidly and new forms appear continuously in other parts of the sky.

(ii) p_2—flaming aurora. This kind of pulsing extends over a large area of the sky which appears lit by surges of light sweeping upwards over it.

(iii) p_3—flickering: A large part of the display undergoes very rapid and more or less irregular changes in brightness as if lit up by flickering flames. This occurs only rarely.

(iv) p_4—streaming: An irregular variation of brightness that progresses rapidly along the horizontal extent of homogenous forms.

Most auroras can thus be fairly well described by four symbols—or sometimes five—with subindices. For instance $a_3\,cfR_2B$ signifies a fragment (f) or a rayed band (R_2B) whose rays are of medium length (R_2) are moving rapidly in a horizontal direction along the form (a_3) and form a corona in the magnetic zenith. Symbols indicating the brightness and color may be added after the symbol for the form (for details see Jacka and Paton, 1963).

The auroral arcs and bands at the auroral zone are characterized by very long extension in east-west direction and a remarkable thinness in north-south direction. From the photographic recordings of aurora made during IGY continuous auroral arcs of lengths 4000–5000 km have been reported (Feldstein et al., 1962, Akasofu, 1963). The values mentioned were limited by the coverage of the net of recording cameras, so arcs may be still longer. Recent measurements of the thickness of 40 zenithal arcs have given values varying between 3.5 and 18.2 km with an average value of 9.1 km (Kim and Volkman, 1963). The thickness was found to increase with increasing magnetic activity. On the other hand, for an active auroral curtain the thickness has been measured to be as narrow as 150–350 m (Akasofu, 1961). No significant diurnal or seasonal variation was found. The vertical extension of the arcs and bands is generally a few ten km. It has been found to vary with solar activity, the extension being smaller and the atmospheric depth greater at the end of a solar cycle (Elvey, 1957). When the sunspot activity starts to increase again, the auroras often appear less deep in the atmosphere and have extension to great heights—the red auroras of type A.

The stable midlatitude red arcs, discovered by Barbier (1958), differ completely from ordinary auroral arcs. They cover some hundreds of kilometers in latitude and in height. Present evidence suggests that they may occur in complete rings around the world (cf. Roach and Roach, 1963).

The rays are characterized by great length and thinness. The length has been extensively studied by Störmer (1955). It may amount to several hundred km, but a more common value is between 100 and 150 km. Especially the sunlit rays can be very long and have been found to extend up to 1100 km sometimes. The diameter of the rays is of the order of 1 km (see e.g. the recent study of Akasofu, 1963b).

Wilcke (1777) first noticed that the auroral rays are aligned approximately along the earth's magnetic field lines. Vegard and Krogness (1920) found that the elevation of the "radiant point," i.e. the point towards which the rays in a corona appear to converge, is systematically one degree or so lower than the magnetic zenith. This difference is too great to be due to the curvature of the field lines. (The rays would have to be at about 1000 km to show a one degree displacement). Störmer (1938) found the auroral zenith to wander around a little in the sky. Abbott (1958) measured a rate of motion for the radiant point of at least 1° in 5 minutes of time. The radiant point was found on either side of the normal (undisturbed) magnetic zenith, but measurements of the disturbed field showed that the instantaneous magnetic zenith was 7 or 8° lower than the radiant point. No relationship between the motions of the magnetic zenith and the auroral zenith was found. Cole (1963) has studied in detail the geometry of the radiant point and found that it commonly differs by 0.5° from the "local auroral zenith," defined by him as the direction of a (hypothetical) ray, regarded as a segment of a straight line, passing through the observer. The difference may amount to as much as several degrees. Observations of the local auroral zenith have not yet been reported. Presuming the rays are oriented along the field lines such observations would give valuable information about the detailed direction of the geomagnetic field lines at auroral heights, which is difficult to obtain with comparable accuracy in other ways.

Detailed studies have shown that fine structures exist not only in auroral forms seen rayed to the eye or the camera but also in what is normally

called homogeneous forms (Nadubovich and Starkov, 1961). Dark filaments of a minimum width of 150 m and an average length of about 20 km have been found. They have been observed most often in the morning hours. The duration is several minutes.

There is a fine structure in aurora not only in space but often also in time. Rapid variations in auroral emission rate have recently been observed and studied by Campbell (1960a, b), Campbell and Rees (1961, Campbell and Leinbach (1961), Iyengar and Shepherd (1961), Omholt (1962), Skrynnikov (1962), Berger (1963), and Gustafsson (1964).

For a more detailed review of older investigations of the characteristics of various auroral forms, see e.g. Störmer (1955) and Chamberlain (1961).

5. Emission Spectrum

But for a very brief introductory survey, the auroral spectrum will not be dealt with in this review. For a detailed review see e.g. Bates (1960) and Chamberlain (1961).

The aurora seen in high latitudes is usually green to the eye. The colour is due to a forbidden transition ($'S \rightarrow 'D$) in the oxygen atom. The wavelength is 5577 Å, which is close to the maximum sensitivity of the eye. The transition probability is very low corresponding to a lifetime of the excited level of about 3/4 sec (Omholt and Harang, 1955).

In lower latitudes the aurora is often seen to be red (high red aurora in the nomenclature used). The spectral characteristic is then the 6300, 6364, 6391 Å triplett of O, which is produced in cascade ($^1D \rightarrow ^3P$) after the 5577 Å line. The 6300 line is also forbidden with a lifetime of the excited level of about 110 sec (Omholt, 1960). Due to the long lifetime, deactivation is important for this line and it is therefore mostly seen in auroras at high altitudes. The long lives of the metastable levels from which the λ 5577 Å and λ 6300 Å lines are emitted give rise to colour variations in active auroras as these lines are emitted for some time after the excitation has ceased.

There exist auroras even in high latitudes with anomalously increased 6300 Å emission. One famous example of this was the one on 11 Feb. 1958. Most other auroral spectra belong to one of three types, between which the boundaries are, however, not very sharp (Krasovskii, 1961). The first type is the low-latitude spectrum mentioned above, in which the ratio of the intensities of the 6300 Å and 5577 Å lines is high, and where these two emissions strongly dominate over e.g. the nitrogen molecule bands. In the next type, lines of neutral and ionized atoms dominate but in addition emissions of ionized and neutral nitrogen molecules are seen. This type of spectrum is observed in both high and low latitudes. Finally, the third type is characterized by numerous intense molecular bands. It is remarkable that in such spectra the green line of atomic oxygen and the first and second positive and negative band systems of N_2 are correlated in great detail. This third type of spectrum most frequently appears in high latitudes. The difference between the spectra are apparently accounted for by the depth of penetration of the exciting agent into the atmosphere, the depth increasing from the first to the third type.

Auroras located at great atmospheric depths usually have a red lower border (red aurora of type B). This is due mainly to the first positive bandsystem of the neutral nitrogen molecule. The reason for the domination of the N_2 emissions at great depths is probably that the $'S$ level of OI is deactivated by collisions to an appreciable amount.

The sunlit auroras have a spectrum different from that of the auroras located in the dark atmosphere. They have a bluish-white color which is produced by resonance emission of primarily the first negative band-system of the positively charged nitrogen molecule (N_2^+).

Of special interest are the hydrogen line emissions. They were first found by Vegard (1939). Analysis of their line contour showed that protons are entering the upper atmosphere with velocities up to 4000 km/sec (Meinel, 1951). They are seen mostly in homogeneous forms. More recently, weak hydrogen glow has been observed preceding the appearance of bright auroras (Romick and Elvey, 1958, and others). Auroras have been observed in which the $H\alpha$ line was so strong compared to other spectral emissions that this aurora might have been produced by proton impact alone (Omholt et al. 1962). In any case it appears certain that in those auroras the

protons supplied, relatively, at least one order of magnitude more energy than in other types of aurora, for which electrons are certainly the main energy contributors. The hydrogen glow is barely visible or even invisible to the eye. It occurs before the electron aurora and, when this has started, on the equatorside of it before midnight. After midnight no hydrogen emission is observed south of auroral forms but rather north of these. A distinct dark region is often seen between the proton aurora and the main forms (Stoffregen and Derblom, 1962). For more details see the reviews of Chamberlain (1961), Krasovskii (1961) and Galperin (1963).

In the midlatitude stable red arcs, mentioned earlier, no other spectroscopic feature than the 6300 Å line has been clearly identified. The location of these arcs is definitely controlled by the geomagnetic field. They are namely lined up along projections of circles from the geomagnetic equatorial plane to the earth's surface along the geomagnetic field lines. It is not clear how they can be produced by collison excitation without any other spectroscopic features being excited. According to Dalgarno (1964), the excitation may be a heating effect caused by low energy particles. On the other hand, if the excitation is chemical it is difficult to understand how the magnetic field control comes in. Megill and Carleton (1964) have proposed that local electric fields may be responsible for the excitation. A number of other proposals for excitation mechanisms are reviewed by Roach and Roach (1963).

6. Methods of Recording Visual Aurora for Morphological Studies

Almost all data concerning the morphology of aurora was taken by visual observers up to IGY. During IGY a large net of so called allsky-cameras, photographing the whole sky automatically every minute, was in operation. Various allsky-cameras have been constructed and used by Gartlein (1947), Lebedinskii (1955), Stoffregen (1955), Park (1957) and Davis and Elvey (see Elvey and Stoffregen, 1957, for a detailed description). A set of allsky-camera pictures are shown in Fig. 1.8. Most allsky films taken hitherto have been 16mm black and white film. The Soviet and Canadian cameras used, however, 35 mm film. In the last few years color film has begun to be used (Sandford and Heiser, 1959; Gadsden, 1960; Sandford, 1961). The committee for the "International Quiet Sun Year," 1964–65, of CIG has recommended the use of 35 mm film, which provides more details of the aurora. For detailed synoptic studies over large areas it is highly desirable that the net of cameras will be denser in the future than it was during IGY. Experience has shown that for most part of the polar regions the possibilities of obtaining large scale synoptic patterns from the IGY records are very limited. A most important contribution to the solution of the morphology problem may be given by very high altitude satellites, taking photographs showing most of the polar caps and auroral regions. Automatic devices for analyzing allsky-camera films have been constructed (Elvey and Belon, 1957; Nagata and Kaneda, 1961).

Davis, Deehr, and Leinbach (1960) have made an evaluation of allsky-camera observations by comparing them with simultaneous visual and photometric observations. They arrived at the following conclusions, among others.

(a) The US model allsky-camera operated during IGY (and probably most other types as well) was slightly less sensitive than an experienced visual observer in detection of very weak diffused forms and is about equal in detecting very weak but well defined forms.

(b) The allsky-camera is much superior to the visual observer in accurately locating and recording the shape of most auroral forms.

(c) The eye is more able to see the details of very bright or fast-moving forms. If the observer were to watch only a small part of the sky, his observations would, in general, be superior to those of the allsky-camera in that small region. However, if the entire sky is to be observed, the allsky-camera is superior in the sense of (b) above.

(d) A greater degree of continuity in auroral forms is often indicated in the compressed image of the sky on all-sky photographs than is apparent to the visual observer.

(e) During the times when visual observers report pulsating aurora, the over-all appearance of the display seems to be quite distinctive and often readily identified on the allsky film.

The exposure time of the ordinary allsky-cameras is generally around 20 sec. By means of image intensifier and TV camera it is possible

to take auroral pictures 24 times a second. Such films allow studies of two to three orders of magnitude more rapid time variations than has earlier been possible. An instrument for rapid filming of aurora was used successfully for the first time in the autumn of 1963 (Davis and Hicks, 1963).

It has recently become possible to observe visual aurora in daytime (Noxon, 1963).

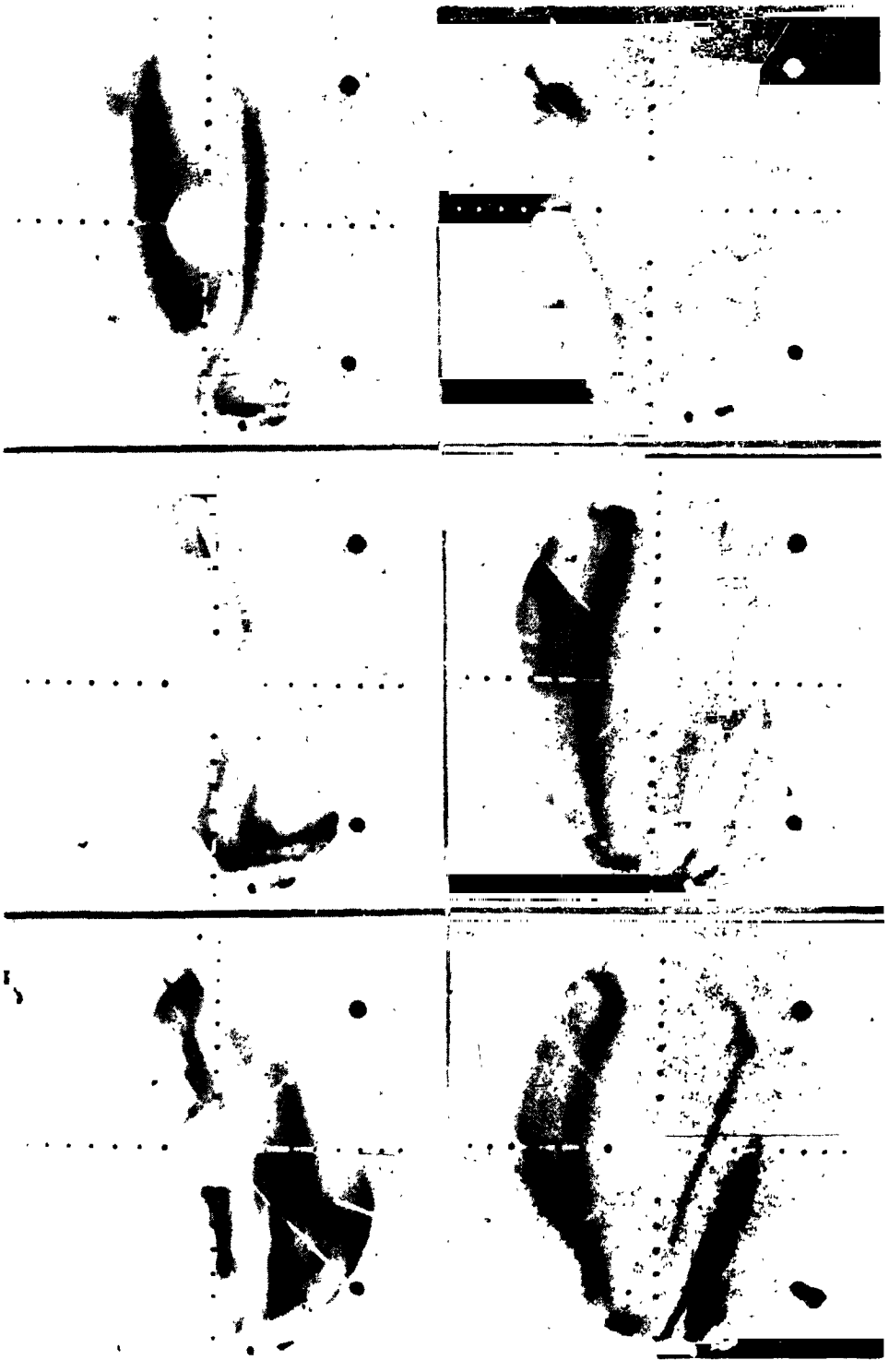

FIGURE 1.8.—Allsky camera pictures taken at Kiruna on 29 Jan. 1957. (Courtesy W. Stoffregen)

2. MORPHOLOGY OF VISUAL AURORA

1. Geographical Distribution of Auroral Activity

(a) Introduction

That the auroral activity does not increase continuously towards the poles seems to have been noted in print first by Muncke (1837). The dependence of auroral occurrence frequency on latitude was studied by Loomis (1860, 1868) in USA and by Fritz (1868, 1873, 1874, 1881) in Germany. Fritz (1881) made a detailed analysis of a large amount of data on aurora originating from very old times up to about 1878, from which he could delineate the first detailed map of the location of the northern auroral zone.

Fritz's auroral zone was defined as the locus of points where the probability of seeing an aurora in any part of the sky during any part of the night was maximal. It is thus a line, having no width. The curve connecting points with equal probability of seeing aurora in any part of sky at any time of night is called an isochasm. The auroral zone is thus the maximum isochasm. It has been recommended by Chapman (1953) and others to use the probability of seeing aurora overhead in evaluating geographical statistical distribution curves. Lines connecting points of equal probability of auroral occurrence in the zenith are called isoauroral lines or isoaurores.

It has become customary in recent years to think of the auroral zone as having a finite, but generally unspecified and variable, width. In this review, we will use the definition by which the width of the auroral zone is equaled to the distance between the points of half-maximum amplitude of a particular measure of auroral activity. The position of the peak of the auroral zone will be taken as that position at which there is maximum occurrence of overhead auroras, as determined by observations taken over a period of several months. With this definition we cannot talk about variation of the location of the auroral zone through one night or from one night to another, as is often done in the literature. One is then using the notation auroral zone for the area in which aurora exists at a given moment of time. Below, "auroral precipitation area" or "zone" or "momentaneous auroral occurrence zone" will be used for this unique-time distribution of visual auroral activity.

Both the width and the location of the center of the auroral zone is highly dependent on the type of activity-measure employed. The most commonly used measure is the occurrence frequecny of auroral activity, generally defined as the ratio of the number of half-hour (or full-hour) intervals in which aurora could be seen overhead to the total number of half-(or full-) hour intervals. The intensity of the aurora is not taken into account in this measure. Davis (1962 a, b) also employed auroral incidence, defined by the total number of auroral lower borders appearing each hour—as determined by counting the lower borders at 5-minute intervals—in a 1° latitude band passing through the station. It gives similar but somewhat sharper distributions.

The following terminology on auroral geography, suggested by Chapman, is widely used. The auroral regions (north and south) extend from geomagnetic latitudes (ϕ_m) 60° to the poles; the subauroral belts between 45° and 60° magnetic latitude; and the minauroral belt between 45° N and 45° S. The auroral regions include the aurorol zones and the auroral caps (the polar regions within the auroral zones). Alternatively, the regions on the equatorial side of the auroral zones are named cis-auroral regions, while those on the polar side which cover the polar cap, are called the transauroral regions (Jacka and Paton, 1963).

(b) Observed locations of the auroral zones and latitudinal distribution of visual auroral activity

The northern auroral zone delineation of Fritz (1881) and Vestine's (1944) modification of it are shown in Fig. 2.1 together with a zone determined by Feldstein (1960) on the basis of photographic recordings taken at 39 Arctic stations and visual observations made at three sites during the IGY, 1957–58.

While Fritz's auroral zone was based almost entirely on unsystematic auroral observations from several hundred years B.C. up to about 1878, Vestine had at his disposal more systematic observations, particularly those from the two polar years 1882–3 and 1932–3. Both delineations, however, are based on material obtained over very long periods of time with secularly changing geomagnetic field, varying solar activity, partly unknown meteorological conditions, etc. In contrast, Feldstein's curve is based on observations

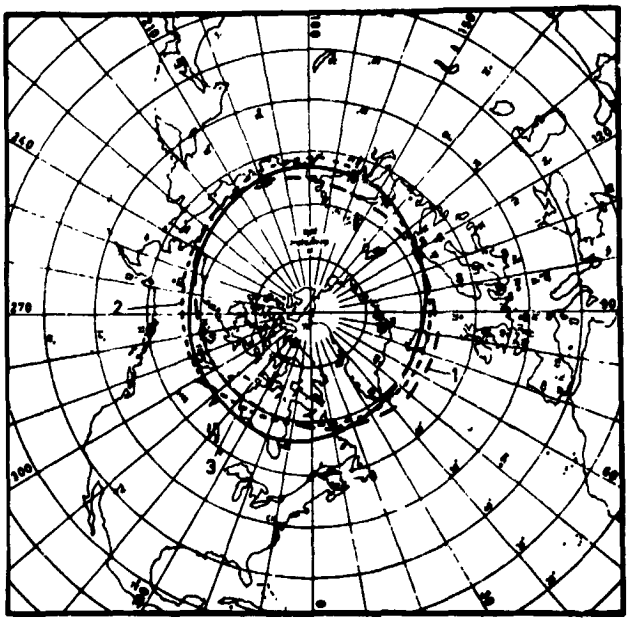

FIGURE 2.1.—Northern auroral zones determined from observations (on a map with geomagnetic co-ordinate system). Curve 1 is that of Fritz (1881), Curve 2 is Vestine's (1944) and Curve 3 Feldstein's (1960).

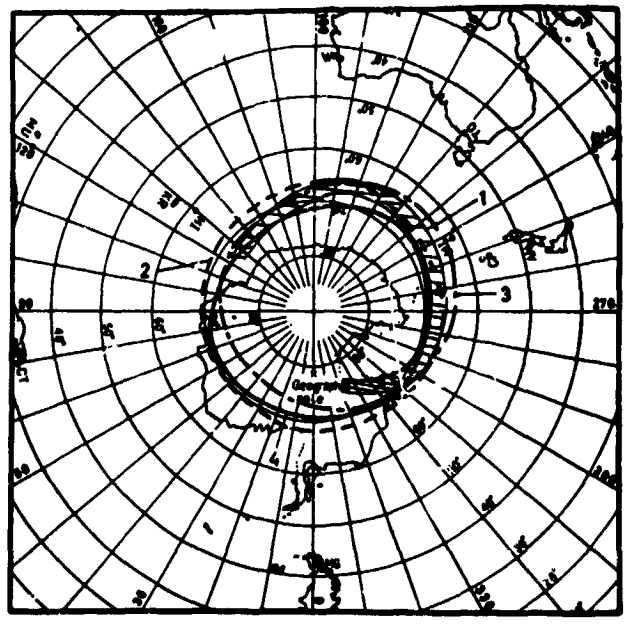

FIGURE 2.2.—Southern auroral zones determined from observations (on a map with geomagnetic co-ordinate system). Zone 1 is according to White and Geddes (1939), Zone 2 to Vestine and Snyder (1945), Zone 3 to Bond and Jacka (1960) and Zone 4 to Feldstein (1960).

made within a few years with the use of a fairly uniform technique at all stations. The auroral indices employed in his determination are more accurate than those previously used, as only the aurora in the zenith has been utilized.

The greatest difference between Vestine's and Feldstein's northern auroral zones is in the region of Hudson Bay, in North America, where Feldstein's curve reaches about 4° farther south than Vestine's.

The first attempt to investigate the auroral statistics in the southern hemisphere was made by Boller (1898). White and Geddes (1939) estimated the location of the zone on the basis of scattered visual observations of aurora australis, and Vestine and Snyder (1945) defined a zone based on geomagnetic observations in the Antarctic. These two zones are shown in Fig. 2.2 together with Bond's and Jacka's (1960) and Feldstein's (1960) zones. The IGY material used by Feldstein was taken at 20 stations on the Antarctic continent and at two stations on islands situated south of Australia. The technique employed in the evaluation was similar to that used in the Arctic.

A recent study of the detailed latitudinal variation of auroral occurrence frequency is that of

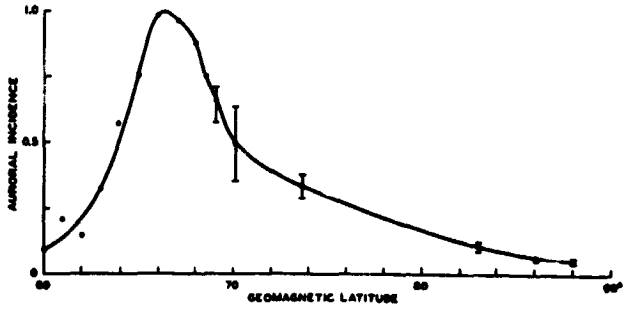

FIGURE 2.3.—(After Davis, 1962b) The incidence of auroral forms at geomagnetic latitudes 60–88°.

Davis (1962 b), shown in Fig. 2.3. It refers in time to the solar activity maximum in 1957–58. The "incidence" of auroral forms, as defined above, was deduced from allsky-camera records taken in Alaska (for the geomagnetic latitude, ϕ_m, less than 69°) and in northern Canada (for $\phi_m > 69°$). The indicated spread for the points representing incidence at high latitude is due to the uncertainty involved in connecting the Alaskan data with those of the high-latitude Canadian stations.

The curve has its maximum between 66° and 67° geomagnetic latitude in Alaska. The width of the zone, as defined above, is about 6° in latitude. The scale for the "incidence" in Fig. 2.3

is a relative one. The hourly occurrence frequency was found by Davis (1962 a) to be between 60 and 70 percent at about 66° geomagnetic latitude at solar activity maximum. Already at $\phi_m = 60°$ it was down to 10 percent, while on the inner side of the auroral zone, the decrease was slower (c.f. Fig. 2.3). Feldstein and Solomatina (1963) found that the frequency of auroral occurrence in the zenith during IGY was about 55 percent on magnetically quiet days and about 90 percent on disturbed days in the auroral zones. The index of activity used was the radio of the number of half-hour intervals with auroras in the zenith to the total number of half-hour intervals of observation, as recorded in the form of ascaplots. The last mentioned investigators also found that the probability of auroral occurrence in the boreal and austral auroral zones are very closely the same.

Nothing was known before IGY about the detailed relations between auroral phenomena in the two hemispheres, but in the last few years some results on this have appeared. They are, however, not consistant. While Jacka (1961) did not find any correlation between the occurrence of aurora at College and MacQuaire Island, which are nearly conjugate points (off by 600–700 k
and Fillius (1960) reported correlation between the general auroral activity at Ellsworth Antarctic station and the conjugate area in USA, but very small correlation (if at all significant) between the detailed pictures in the two areas, DeWitt (1962) observed good detailed correlation of form and motion and of variation of luminosity between auroral events observed at Campbell Island and MacQuaire Island in the southern hemisphere and at Farewell and Kozebue in the northern one. Breakup of the auroras was found to be simultaneous in the conjugate areas. The conjugacy of the observation points employed by DeWitt was certainly better than for any of the other two investigations quoted above. It seems therefore most probable that auroras usually occur as conjugate pairs at either end of geomagnetic field lines, as has long been suspected. More observational data would be of great value.

The occurrence of aurora in very low latitudes (subtropical and tropical) is extremely rare. Even in central Europe and southern USA the probability of seeing aurora is only a few thousandths of that at the center of the auroral zone. Instead, these medium and low latitude auroras are generally very spectacular and have often been noted and recorded also in ancient times. Recent summaries of older observations of auroras extending into the minauroral region have been made by Schove (1955), Matsushita (1956) and Chapman (1957 a, b). Several auroras occurring at very low latitudes have been described rather fully by Chapman (1953, 1957 c), Abbott (1951), and Abbott and Chapman (1959 a). A type of red auroral arcs occurring rather regularly in subauroral latitudes will be discussed later in this chapter.

(c) Comparison of observational auroral zones with various theoretical curves

There are good reasons for postulating circular symmetry in the geomagnetic equatorial plane outside the earth's surface of distance parameters representing statistical averages for corresponding variables of those processes, in and near the equatorial plane, which are associated with the occurrence of auroral phenomena in or near the two auroral zones. Only the dipole field affords a measurable contribution in the equatorial plane at a distance of several earth radii from the earth's surface, and the dipole field is circularly symmetric. Thus the configuration in the geomagnetic equatorial plane will not be influenced by the earth's rotation, provided minor effects of the different directions of the geomagnetic and the rotation axes are disregarded. The equatorial plane process will therefore be seen in the same average distance range at a given geomagnetic time from all geomagnetic meridians on the earth. It follows that—if the processes in the equatorial plane and in the auroral zones are connected by the real magnetic field lines, as seems physically plausible—the only longitudinal dependence of e.g. the averages of a great many auroral locations, observed at fixed points on the earth and equally distributed with regard to geomagnetic time, will be that introduced by the deviation of the earth's magnetic field from a dipole field. This deviation is appreciable at and near the earth's surface.

What has been said here should be true, even if the geomagnetic field is heavily distorted in its outer regions. If that is so, the distance at which the process in the equatorial plane take place may

be quite different from that of the intersection with the equatorial plane of that dipole line which intersects the earth's surface at the same place as the real field line connecting the auroral processes in the earth's atmosphere and in the equatorial plane.

According to this view the configuration in one hemisphere will correspond to the projection of the corresponding one in the other hemisphere along the geomagnetic field lines.

The only assumption made in the foregoing is that an electron or an ion moves from the equatorial plane to one of the auroral zones along a geomagnetic field line or on some surface defined by field lines. Such an assumption seems to be well founded. No other details of the actual physical processes are involved.

The projections of circles in the equatorial plane to the earth's surface along the real field lines, were calculated by Hultqvist (1958) for purposes of comparison with experimental isochasms. The projections are practically identical with the L curves of McIlwain (1961). Hultqvist used a perturbation method consisting of integration along the dipole line of the deflection from a dipole field line of the higher approximation line due to the effect of the second to the fifth terms in the spherical harmonic development of the earth's magnetic field. The calculations yielded deflection vectors for a large number of dipole lines. These gave the deflection for the point of intersection of the higher approximation field line—coinciding with the pertinent dipole line in the equatorial plane well outside the earth's surface—and the earth's surface from the corresponding point of intersection of the dipole line itself.

The calculations were carried out for 36 equidistant longitudes for each of 15 geomagnetic colatitudes, most of them less than 30 degrees. The results of Vestine's et al. harmonic analysis of the earth's magnetic field for epoch 1945, the most recent epoch for which data were then available, were used in the computation.

The projections of equatorial plane circles are ovals with the longest diameter approximately in the plane containing the 170° and 350° geomagnetic meridians. Two circle projections are shown in Fig. 2.4 (northern hemisphere) and Fig. 2.5 (southern hemisphere). They correspond to the two circles in the geomagnetic equatorial plane

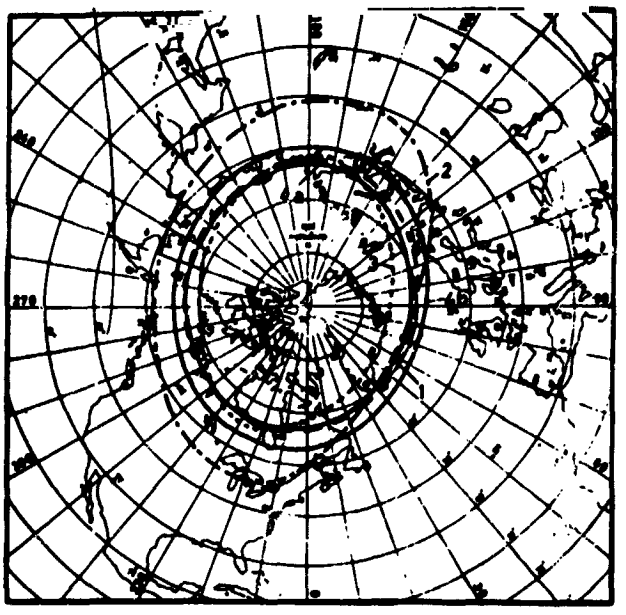

FIGURE 2.4.—Comparison of Feldstein's (1960) northern observational zone (Curve 1) with a number of "theoretical" auroral zones: 2 is according to Gartlein and Sprague (1960), 3 to Quenby and Webber (1959) and 4a and b are projections of two circles in the geomagnetic equatorial plane (corresponding to colatitudes 22 and 25 degrees respectively; Hultqvist, (1958).

having radii of 7.13 and 5.60 earth radii, for which the projections along the dipole lines are the geomagnetic colatitude circles 22° and 25° respectively.

Hultqvist pointed out that the experimental northern auroral zone of Vestine accorded well with the circle projections except over the North American continent, where the calculated curve extended about 4° farther south than the observational one. The IGY data as presented by Feldstein and illustrated in Fig. 2.4 show that the configurational agreement between the IGY northern auroral zone and the projections of circles is good. The maximal difference in latitude between Feldstein's zone and that projection which conforms best to it amounts to about one degree.

Since the network of observation stations in and near the northern auroral zone was quite dense during the IGY, it seems probable that the error in location of the experimentally determined auroral zone is only of the order of 1° in latitude. The geomagnetic data used in the calculations are for epoch 1945, which may account for minor inconsistencies with the observations of 1957–58. It is probable, however, that this error also is less than one degree of latitude. It is thus evident

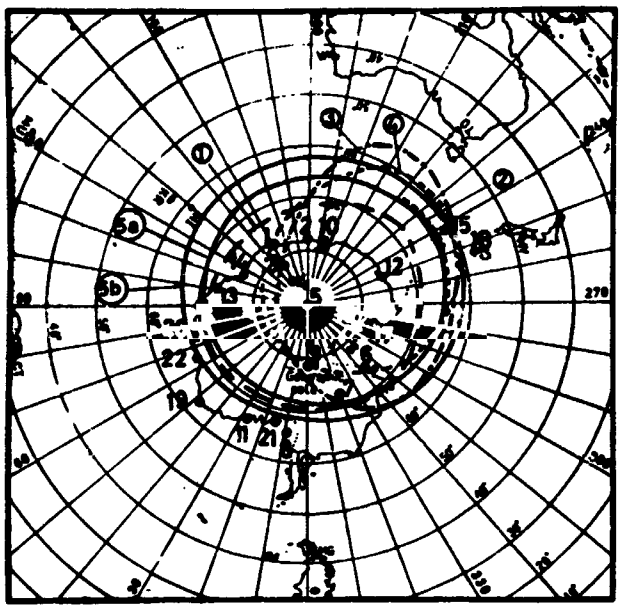

FIGURE 2.5.—Comparison of Feldstein's (1960) southern observational zone (Curve 1) and that of Bond and Jacka (1960) (Curve 2) with different "theoretical" auroral zones: 3 is according to Gartlein and Sprague (1960), 4 to Quenby and Webber (1959) and 5a and b are projections of two circles in the geomagnetic equatorial plane (corresponding to colatitudes 22 and 25 degrees, respectively; Hultqvist, 1958). The numbered points show the approximate locations of the stations at which the IGY observational material—the basis of Feldstein's auroral zone—was collected. The numbering is that of Feldstein (1960).

that the IGY northern auroral zone is, within the limits of probable error, in full configurational accord with the calculated projections of circles in the equatorial plane.

Feldstein's auroral zone in the southern hemisphere is shown in Fig. 2.5 together with the projections of the circles of radii 5.60 and 7.13 earth radii. The experimental curve differs quite significantly from the computed ones. While it follows the course of the latter in the geomagnetic longitude range of 320° E—90° E, it is much nearer to the Antarctic continent for the rest of the longitude circle where it is located over the sea. In fact, Vestine's and Snyder's (1945) auroral zone agrees better with the computed one than Feldstein's does.

A question of interest is whether the discrepancy between the IGY southern auroral zone and the projections of circles is a real one or attributable merely to inaccuracy of the observational data and/or of the computed curves. The errors of the geomagnetic data, used in the computations, are certainly greater for the Antarctic than for the Arctic. As mentioned earlier, the computations were based on Vestine's et al. harmonic analysis of the geomagnetic field for epoch 1945, when the southern hemisphere data were very sparse. Although this fact may partially account for the discrepancy, it seems likely that only a minor part of the 6 latitude degrees difference over the sea is parimarily attributable to errors in the harmonic analysis of the geomagnetic field, especially as a comparison with recent numerical computations by Dudziak et al. (1963) on the basis of the spherical harmonic coefficients for epoch 1960 by Jensen and Cain (1962) show only minor deviations.

All observational stations in the discrepant region were situated on or close to the coast of the Antarctic continent far inside the auroral zone. This means in effect that the auroras occurring in the auroral zone were visible from these stations at low elevation, a circumstance which implies considerable error in the observational results.

Indeed, since publication of Feldstein's paper, Bond and Jacka (1960) have communicated a report in which they note that the latitude of the auroral zone in the region of MacQuarie Island, south of Australia (point 15 on Fig. 2.5), is only one or two degrees more than that of the station. A small part of their auroral zone—the one near MacQuarie Island—is shown in Fig. 2.5 as curve No. 2. Taking this and the above mentioned considerations into account, it would appear that the auroral zone is fairly consistent with the computed curves, with which it shows agreement over the Antarctic continent. This seems so much the more plausible in view of the close accord between observed auroral zone and circle projections for the northern hemisphere. Indeed, it would be surprising if the two hemispheres showed entirely different degrees of agreement between the two types of curves.

Although, as mentioned above, there are good reasons for postulating circular symmetry in the geomagnetic equatorial plane for the processes producing aurora in the earth's atmosphere, it is certainly not the only possible approach. If e.g. the drift around the earth of the primary auroral particles is accordance with the adiabatic invariants is the determining process for the configuration

of auroral occurrence curves, it is perhaps reasonable to expect that the isoaurores should be identical with the lines of constant second adiabatic invariant. Vestine and Sibley (1960) computed such curves. They are very nearly identical with the projected equatorial-plane circles and it is therefore not possible to judge between the two approaches on that basis. Vestine and Sibley also calculated, using the spherical harmonic analysis of Finch and Leaton (1957), the mirror height of electrons for which the second adiabatic invariant, $J = \int_{\parallel} d\ell/v$, has the value 15.7. Their heights range from 57 km to 420 km in the northern hemisphere and from -15 km to 633 km in the southern hemisphere.

Figure 2.4 and 2.5 include, for purposes of comparison, curves showing two other types of more or less theoretical auroral zones: the zones suggested by Gartlein and Sprague (1960), which are almost identical with the isoclines 76°, and Quenby's and Webber's (1959) curves, which are based on calculations of vertical cut-off rigidities for cosmic ray particles in the earth's magnetic field, and take into account both the dipole and non-dipole parts of the internal field. Neither of these two curves conforms as closely to observed data as do the circle projections.

What conclusions can be drawn from the similarity between observed isoaurores and projections of circles in the earth's geomagnetic equatorial plane into the earth's atmosphere along the geomagnetic field lines? Not too many, in fact, since no details of the actual physical processes are involved. The geomagnetic field can be strongly distorted and we still expect to find the circular symmetry for the statistical data.

However, it can be concluded from the data presented above that local conditions close to the earth probably play a negligible role for the average auroral distribution over the earth's surface. The adiabatic drift of the primary particles around the earth seems not to be important for the shape of the insoaurores. If this process were important, one would expect the mirroring height to have a profound influence on the precipitation rate of particles and therefore on the frequence of occurrence of aurora. Since the mirror height varies very much with longitude for one $J = \text{const}$ shell, important variations in intensity and auroral occurrence frequency for various points along such a curve would be expected. This is not observed. That the drift motion is not important in this respect is also expected because of the fact that most primary auroral electrons need a time very much longer than the time scale of auroras in order to drift around the earth.

There are other statistical parameters than the isoaurores that may be expected to show circular symmetry in the equatorial plane. One is the average southern extent of the aurora a a definite degree of magnetic disturbance. Such curves have been evaluated by e.g. Gartlein et al. (1960) and Feldstein (1963). A comparison of

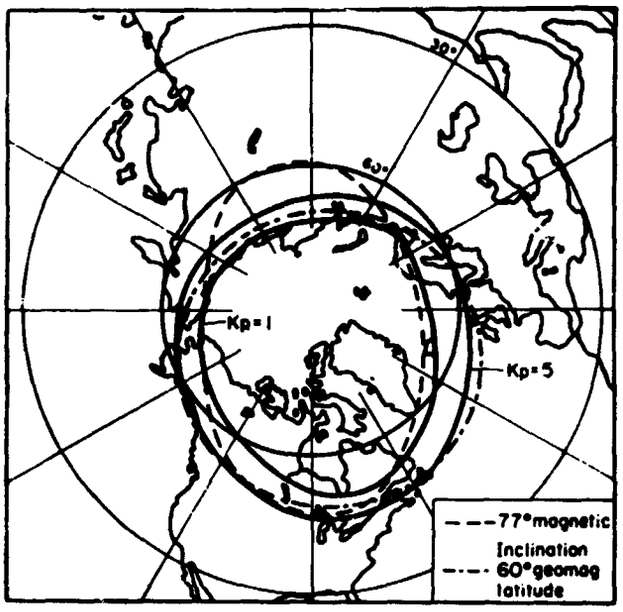

FIGURE 2.6.—Southern extent of aurora borealis for two different levels of geomagnetic activity (after Gartlein, Gartlein and Sprague, 1960).

the curves in Fig. 2.6 with the circle projections in Fig. 2.4 shows a good agreement. The southern extent increase with increasing K_p.

(d) Dependence of auroral zone location on the solar cycle

The pole distance of the auroral zone has been found to be dependent on the phase of the solar activity cycle. Sheret and Thomas (1961) made a detailed analysis of the auroral observations made at Halley Bay, Antarctica, in the years 1956–59. The position of the auroral zone, obtained from observations of quiet arcs, was the following in the four years.

TABLE 1.

Year	1956	1957	1958	1959
median south geomagn. lat	70.8	71.8	71.9	71.0

The auroral zone was thus closer to the pole at the solar-activity maximum in 1957 than before and after. This result is opposite to that of Feldstein (1962), who compared the location of the auroral zone in the Asian Arctic at solar activity maximum (1957–58) and at solar minimum (1954–55). He found the auroral zone to be 2.5—3° closer to the geomagnetic pole at the minimum of the solar cycle than at maximum. These variations in the location are discussed also in subsection 6 on motions.

(e) Auroral type effects

The distribution of auroral activity described above refers to all types and forms of aurora. Most of the basic data are obtained from black and white allsky-camera films of fairly long exposure times, which makes it impossible to distinguish between various spectroscopic characteristics as well as between quiet and rapidly varying auroral forms.

It is, however, of great theoretical interest to know whether there are significant differences in location between different types of aurora, especially between auroras caused by positive and negative primary particles. This is because relations—at least qualitative—between the locations of proton and electron precipitation areas is contained in several theoretical models. For instance, it seems difficult to think of electromagnetic acceleration processes if possitive and negative particles are precipitated together along the geomagnetic field lines.

In fact, it has been found that hydrogen line emitting aurora (see p. 13) usually is located on the equator side of the electron produced aurora before midnight (cf. the reviews of Omholt, 1963, and Galperin, 1963). (After midnight no hydrogen emission is observed south of auroral forms, but rather north of these; Stoffregen and Derblom, 1962). There is often a distinct dark region (up to 1° wide in latitude) between the "proton aurora" and the main forms. One would therefore expect the isoaurores and the auroral zone for "proton aurora" alone to be located one or a few degrees farther from the poles than the ordinary auroral zones (which certainly are the electron precipitation zones).

As mentioned in section one, there are several different types of auroral phenomena. The latitudinal distribution of the occurrence probability for high red arcs, for instance, certainly has its maximum in the subauroral regions. No detailed statistical studies of their geographical distribution exist as yet. Stoffregen (1962) has investigated the occurrence of different auroral forms in the geomagnetic latitude band 58–76° N (at the longitude of Scandinavia). His results, which he considered as a rough approximation, are shown in Fig. 2.7. As can be seen in the figure, the

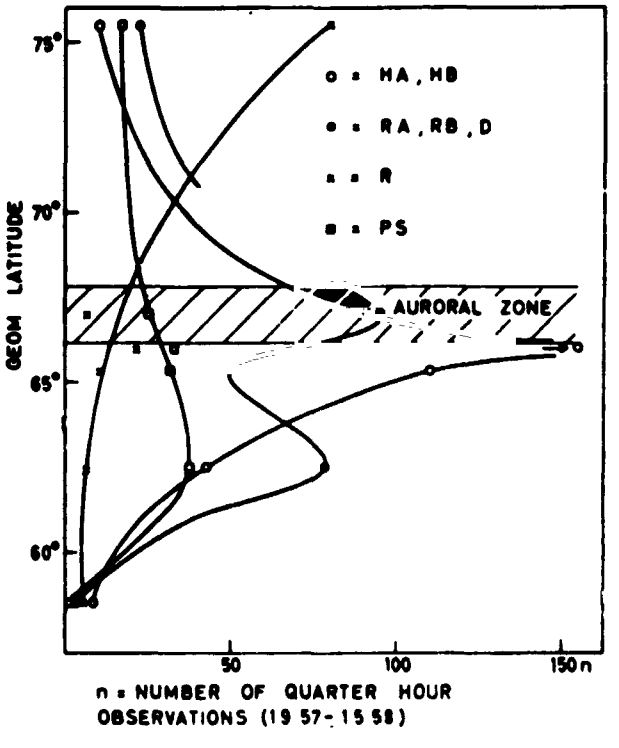

FIGURE 2.7.—(After Stoffregen, 1962) Approximate latitude distribution for different auroral types.

pulsating auroras occur most frequently some 5 degrees south of the auroral zone. This was also found by Heppner et al. (1952).

The low latitude aurora mentioned above is different from the stable subauroral red arcs described on p. 10. The red arcs populate sub-

auroral mid-latitude regions with shape very similar to the projections of circles along the field lines from the equatorial plane, described above (see Roach and Roach, 1963). The regions have their centers somewhere between the circle projections corresponding to equatorial plane circles of radii 2.5 and 3 earth radii (i.e. $L=2.5$ and 3 respectively). These red arcs seem not to exist in the auroral zones.

There certainly exist still other differences in the latitudinal distribution of the occurrence frequency for different types of aurora. The aurora inside the auroral zone has several characteristics that distinguish it from the aurora seen at and outside the auroral zone. In general, the high-latitude forms are relatively weak in intensity and more fleeting than those seen at the auroral zone. The forms consist, in part, of weak diffuse arcs and of bands that frequently show ray structure. Ray bundles are common, and these are usually arranged so as to appear as part of arcs, bands or draperies with variable intensity (cf. Davis, 1962 b).

(f) Inner auroral zones

Alfvén (1955) proposed on theoretical grounds that there should exist secondary auroral zones inside the ordinary ones, at geomagnetic colatitudes between 5 and 10 degrees. Since this proposal was made, a large number of attempts have been made to determine from observations if the inner auroral zones exist or not. At this time, it does not seem possible to draw firm conclusions. It is clear that the zone, it if exists, is much less pronounced than the main zones (which is not unexpected from Alfvén's theoretical point of view).

Observations in favor of and against the existence of the inner zones will be briefly reviewed.

Nikolskiy (1963) has discussed the Soviet data relevant to the existence of inner auroral zones. Most data is geomagnetic. What is generally found is a morning maximum in magnetic activity between 75 and 80° N geomagnetic latitude, most pronounced in the summer. The shape of the zone, found by Nikolskiy, is a spiral in a circular latitude-time coordinate system, unwinding in a clockwise direction. Meek (1957) found that the maxima of ionospheric disturbances are concentrated along a similar spiral.

On the other hand Lassen (1959), observing at Godhaven (about 80° geomagnetic latitude), could not find any magnetic evidence for an inner zone of high activity but instead he observed a type of zenithal aurora occurring around 6 h. local time, which seemed not to come up from south (i.e. from the main auroral zone) but to be produced sporadically at great elevation in the sky seen from Godhaven. The elevation did not change significantly in the course of the morning. Lassen found that the morning-type of aurora is uncorrelated not only with the local magnetic activity but with the planetary state of disturbance too. Analyzing data obtained in other parts of Greenland and in the northernmost Canada, Lassen concluded that morning aurora of the described kind is observed in the zenith only along a curve coinciding with the projection of the circle with radius 20 earth radii in the geomagnetic equatorial plane ($L=20$) on the earth's surface.

Witham et al. (1960), for instance, investigated the magnetic disturbance characteristics. They, and many other investigators of various parameters, could not reach any definite conclusion about the existence of an inner zone of high disturbance.

Davis (1962 b) analyzed allsky-camera films taken at Thule ($\phi_m=88°$), Alert ($\phi_m=86°$), Resolute Ray ($\phi_m=83°$), Baker Lake ($\phi_m=74°$) and Churchill ($\phi_m=69°$). The scaling was made by counting the number of auroral forms within zenith distance 80° on each fifteenth frame of the film from each station. The total number of forms was recorded. The result can be seen in Fig. 2.3. There is no indication from this diagram of an inner auroral zone. However, the lack of stations in the critical region between 74° and 82° prevents the making of a strong statement of the absence of a zone there. It appears that if there is an inner auroral zone, it must lie between 76° and 81° latitude over northern Canada, and that the enhancement of the number of auroral forms within this zone must not be great.

2. Diurnal Variation of Visual Auroral Activity

As does the geographical distribution of aurora, the diurnal variation of auroral activity varies considerably with the measure of the activity

used. In addition, it depends on the type of auroral display and perhaps on season and phase of the sunspot cycle. Very much still remains to be done before our knowledge of the diurnal variation of auroral activity is consistent and complete.

The most widely used measures of auroral activity are "occurrence frequency" and "incidence," defined in the previous subsection. Fig. 2.8 (after Davis, 1962 a) shows the occurrence

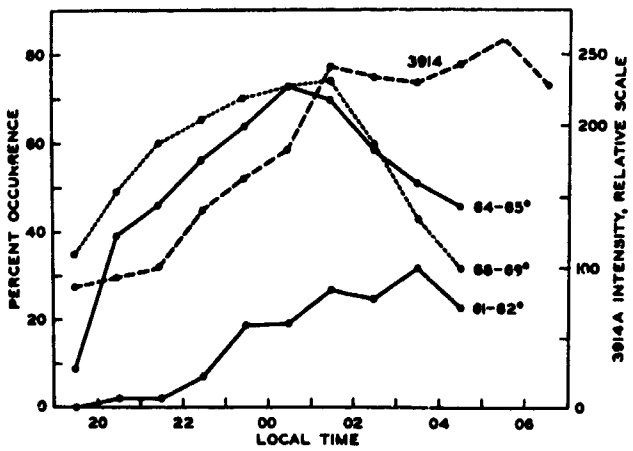

FIGURE 2.8.—(After Davis, 1962a) Percentage hourly occurrence in a latitude belt of width 1° centered over each of the stations: Barrow (68°–69°), College (64°–65°), and Farewell (61°–62°). The curve (3914) is drawn from data by Murcray (1959) and represents relative all-sky 3914Å intensity over College during 1955 and 1956.

frequency of visual aurora in a latitude belt of width 1° centered over each of the Alaskan stations Barrow (68–69°), College (64–65°), and Farewell (61–62°). Geomagnetic midnight occurs 1 to 2 hours after local midnight, the displacement from local midnight being largest for Barrow and smallest for Farewell. These curves demonstrate a shift of the auroral occurrence toward earlier local time with increasing latitude. In Fig. 2.8 there is also a curve marked 3914. It is drawn from data by Murcray (1959) and represents relative allsky 3914 Å intensity over College during 1955 and 1956. As can be seen in the figure, this curve has its point of gravity located several hours later than the others. This is due to an important difference between the auroral intensity distribution in premidnight and postmidnight hours. Before midnight the auroral forms stand out sharply above the low intensity of the background, but after midnight the intensity of the background is enhanced so that individual auroral forms are not easily distinguished.

Davis and DeWitt (1963) have evaluated the per cent of hours in which aurora was observed at Byrd, Antarctica, close to the southern auroral zone, for every hour of day and night in a two-months period of southern winter. Their result is shown in Fig. 2.9. The auroral occurrence

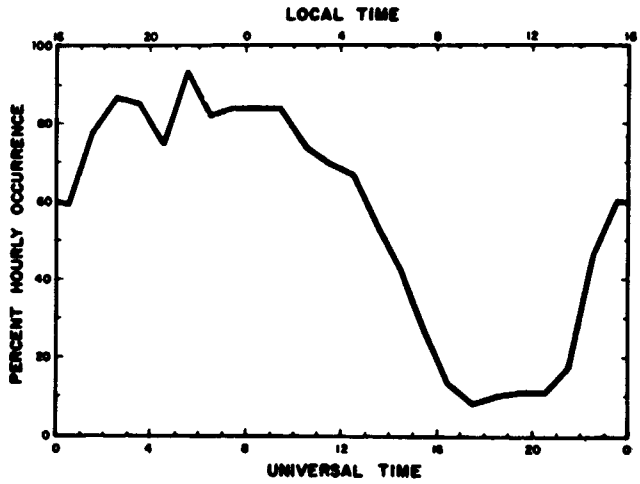

FIGURE 2.9.—(After Davis and DeWitt, 1963) Diurnal variations of hourly occurrence of visual aurora within 150 km of Byrd Station for all clear, dark hours in May and June 1960.

frequency has a maximum around geomagnetic midnight (at about 2200 local time) and a deep minimum around geomagnetic noon.

Reports on diurnal variation of aurora have also been given by Tromholt, 1882; Carlheim-Gyllenskiöld, 1886; Paulsen, 1893; Vegard, 1912; Chree, 1927; Sverdrup, 1927; Lee, 1930; Fuller, 1933, 1935; Currie and Edwards, 1934; Davies, 1935 a, 1950; Stagg, 1937; Stetson and Brooks, 1942; Jacka, 1953; Elvey et al., 1955; Murcray, 1959; Hale, 1959; Lassen, 1959, 1961; Malville, 1959; Chamberlain and Thorson, 1960; Feldstein, 1960; Feldstein and Solomatina, 1961; Loginov, et al., 1962 and others. A large number of these investigators have found diurnal variation curves similar to the occurrence curves in Fig. 2.8 and 2.9 with miximum fairly close to geomagnetic midnight.

There have been many suggestions of a less pronounced, secondary maximum in the early morning hours but it has not been possible to

find at some stations (Hulbert, 1931). Studies of ascaplots for IGY by Feldstein (1960) and Feldstein and Solomatina (1963) have resulted in the curves of Fig. 2.10 showing the geomagnetic time of maximum auroral occurrence frequency as function of the distance of the observation place from the observed auroral zone (curve 3 in Fig. 2.1), which distance is an approximately linear function of the geomagnetic latitude, corrected for the higher terms in the spherical harmonic expansion. There are two spiral-shaped curves in Fig. 2.10 unwinding in opposite directions. At the auroral zone, Feldstein found only one maximum (around geomagnetic midnight). Also, at geomagnetic latitudes around 78° only one maximum occurred (on the dayside) and at latitudes in between there were two maxima. The same result has been presented by Malville (1964). Similar functions of latitude have been found for the time of maxima of various other disturbance measures: e.g. for geomagnetic distrubances by Meek (1955), Burdo (1957) and Nikolskiy (1957), for sporadic-E ionization by Hagg et al. (1959), for redio aurora by Forsyth et al. (1960) and Egeland et al. (1962) and for radio wave absorption by Thomas and Piggot (1960).

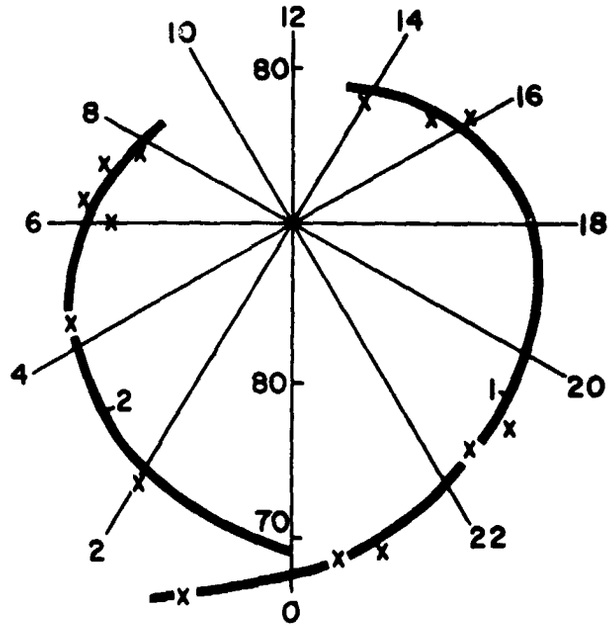

FIGURE 2.10.—(After Feldstein and Solomatina, 1963) Geomagnetic times of maximum frequency of auroral occurrence in the zenith as function of geomagnetic latitude corrected for the non-dipole part of the geomagnetic field.

On the basis of their observational results, Feldstein and Solomatina (1961) and Khorosheva (1961, 1962) (see also Feldstein, 1964) have proposed that the precipitation curve for aurora at a given time has the shape of the two combined spirals in Fig. 2.10. An instantenous auroral zone of a similar shape has been proposed by Akasofu, (1963 d). Support for this shape are among other observations those of Khorosheva (1961), who mapped 17 cases of momentary auroral distribution over the eastern hemisphere and found parts of oval-shaped curves similar to that in Fig. 2.10. However, the simple regularity of Fig. 2.10 was not found by Davis (1962 b) and the results of the case studies of some strong auroral events made by Akasofu (1960, 1962, 1963) and Akasofu and Chapman (1962) gave instantaneous configurations of the aurora, which were very closely similar to the projections of equatorial-plane circles on the earth's surface along the geomagnetic field lines (see previous subsection). The extensive auroral studies by Morozumi (1963) at the South Pole (geomagnetic latitude 78° S) did not show one, but two peaks in the diurnal variation curve for auroral occurrence. Instead for a maximum at magnetic noon there was a minimum.

A theoretical motivation for an oval auroral zone, being at higher latitude at noon than at midnight, is obtained when one considers the drift motion of particles around the earth in a magnetosphere, which is compressed by the solar wind on the dayside. The mirror points are at lower latitudes in the night than in the day. On this theoretical basis oval instantaneous auroral zones have been proposed by Rees and Reid (1959) and by Liemohn (1960). Detailed calculations by Malville (1960) show, however, that the expected effect is much less than the observed (less than 2° as compared with 8° observed). O'Brien (1963) therefore, concludes that if the diurnal variations are related at all, it is only in the sense that they are effects of a common and as yet unknown cause. More observational data are evidently needed before a conclusion about the existence or nonexistence of the oval instantaneous auroral zone can be reached.

That the main maximum in the diurnal distribution of auroral activity occurs close to geomagnetic noon at geomagnetic latitudes of about 78°, as Feldstein found, need not necessarily mean

that the corresponding processes in, or close to, the equatorial plane take place on the dayside, namely if the topology of the geomagnetic field is the one proposed by Johnson (1960) and others. A fairly evident hypothesis is that the neutral points or lines of that model are responsible for the daytime maximum in auroral occurrence.

Two spiral arcs of a kind described above are incorporated in the qualitative model for magnetic disturbances and associated phenomena proposed by Axford and Hines (1961).

That the diurnal variation differs for different auroral forms has been found by e.g. Fuller (1935) at College, Alaska, which is close to the auroral zone (cf. Fig. 2.11). Strong and brilliant forms have some predominance during the evening hours, and the faint and quiet forms in the morning. The hydrogen glow generally precedes the appearance of bright auroras, as first found by Romick and Elvey (1958) near the auroral zone, and the diurnal variation curve for this type of aurora therefore has its maximum well before midnight. Pulsating aurora occurs most often in the morning hours (Heppner, 1954).

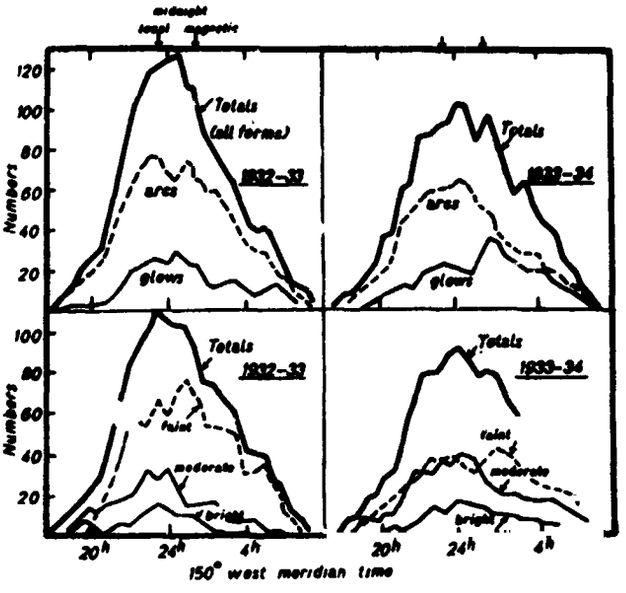

FIGURE 2.11.—(After Fuller, 1953) Diurnal variation of different auroral forms and of auroras of different intensitities at College, Alaska.

3. Other Time Variations of Visual Auroral Activity

(a) 27 day recurrence tendency

Auroras tend to repeat with a period of about 27 days, which is the synodic rotation period of the sun. As the moon considerably influences the possibilities of observing aurora, the apparent repetition tendency of auroral activity is enforced by the synodic lunar period (29.5 days), which is fairly close to the solar one. When the analysis is corrected for the lunar effect, a small but definite indication of a recurrence maximum around 26 and 27 days remains, which evidently is due to the rotation of the sun (Meinel et al., 1954). By the second and third solar rotations, no recurrence tendency remains.

(b) Seasonal variation

In the subauroral regions the annual curve of auroral occurence frequency has two maxima at the equinoxes. Fig. 2.12 shows the monthly aurora occurrence frequency distribution found by Meinel et al., (1954) at Yerkes Observatory.

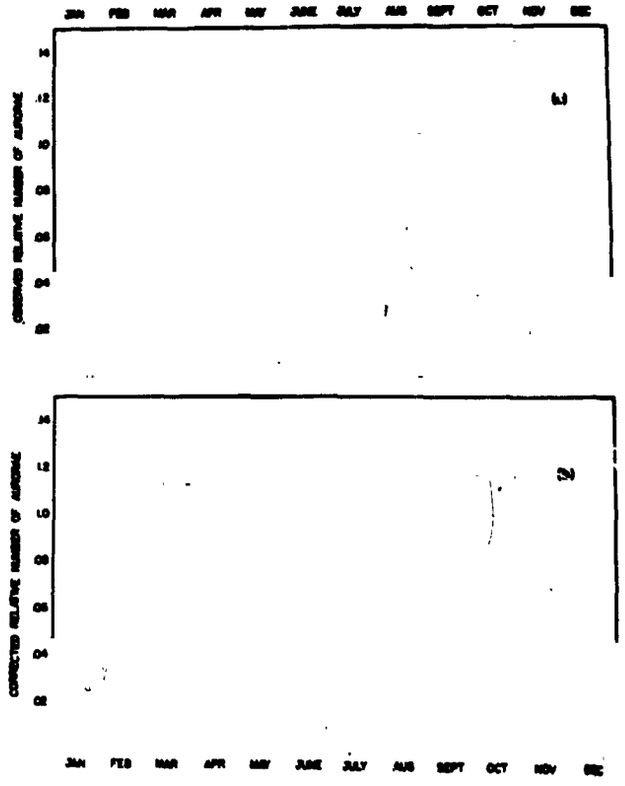

FIGURE 2.12.—(After Meinel et al., 1954) (a) Fraction of all auroras observed in each calendar month at Yerkes Observatory; (b) monthly frequency distribution corrected for cloudiness and number of dark hours in each month.

The existence of spring and fall maxima were known already to Mairan (1733). It was proposed by Cortie (1912) that the similar maxima in geomagnetic disturbances are due to the earth being at highest heliographic latitudes in March and September. If this is true, the angular diameters of the solar plasma beams do usually not exceed about 5° as seen from the sun. This is certainly not so for the very largest solar events, however.

The dependence of the seasonal variation on latitude is obscured by the change with latitude of the ratio of the lengths of day and night. If this change is ignored, as it usually is, then the summer minimum becomes progressively deeper with increasing latitude, while the winter minimum becomes progressively shallower, disappears and is replaced by a maximum, which is then the only one in the distribution (cf. e.g. Chree, 1911). Gartlein and Moore (1953) found that the ratio of the mean of the numbers of overhead auroras in North America occurring in June and December to that for auroras in March and September is a steadily increasing function of geomagnetic latitude. Between about 58 and 60° N the level of activity appears to be constant throughout the year. Feldstein and Shevnina (1961) investigated the seasonal variation in auroral occurrence frequency in two hours centered on local midnight—thereby eliminating the influence of the diurnal variation—for six stations between 63 and 83° geomagnetic latitude in the northern hemisphere and for five stations between 66° and 90° geomagnetic latitude in the southern one. They found the same seasonal variation as described above at and close to the auroral zones, but no perceptible seasonal variation in auroral frequency on the central auroral caps.

(c) Sunspot cycle variation

Fig. 2.13, after Tromholt (1902), shows the correlation between the number of days with aurora per year, observed in Norway between 1761 and 1877 and the sunspot number. The correlation is good and the maxima seem to coincide. Meinel et al., (1954) found a similar correlation when analyzing auroral observations made at Yerkes Observatory between 1897 and 1951. The maximum auroral activity occurred, however, during those 5 eleven year sunspot cycles some 2 years after the sunspot maximum. Egedal (1937) too, found a time delay of the maximum occurrence frequency of aurora in relation to the solar activity in Denmark during the 3 solar cycles from 1897 to 1929, but the delay was only 1 year.

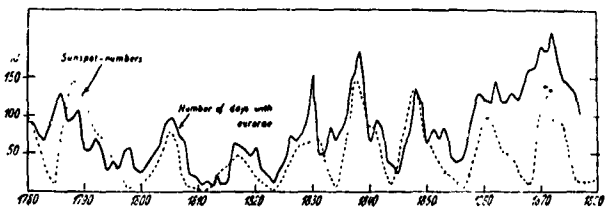

FIGURE 2.13.—(After Tromholt, 1902) Variation of the number of auroral days, N, in each year, observed in Norway, and the sunspot number between 1761 and 1877.

4. Orientation of Auroral Arcs

Hitherto various characteristics or auroral "activity," i.e. of statistical parameters describing the probability of occurrence of aurora, have been described. Now we will go somewhat more into detail. In this section the orientation of auroral arcs, which can be readily measured from photographic recordings, will be discussed.

(a) Average orientation

There exist fairly much data on the average orientation of auroral arcs. Even the very early studies of aurora showed that quiet auroral arcs tend to be oriented in a preferred direction, approximately perpendicular to the horizontal component of the geomagnetic field. A number of these early investigations were discussed by Fritz (1881). Vegard and Krogness (1920) referred the directions to the geomagnetic meridian and the Norwegian school made a large number of accurate direction determinations in northern Scandinavia.

In the majority of the pre-IGY investigations average values of all observed quiet arcs and bands were estimated. The fact that the observations were often made only during a certain period of the night—and in different periods for different investigations—was not considered.

A fairly extensive collection of such data is contained in Fig. 2.14 (after Hultqvist, 1962 b). Also included are a number of computed projections of circles in the equatorial plane on the earth's surface along the geomagnetic field lines (Hultqvist, 1958).

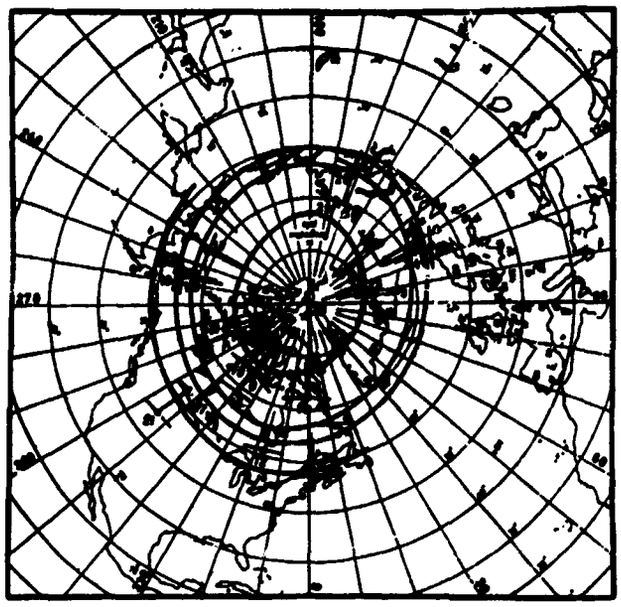

FIGURE 2.14.—Directions of quiet auroral arcs in the northern hemisphere. 1. Haldde and Bossekop; 2. Cap Thordsen; 3. Jan Mayen; 4. Nain; 5. Kingua Fjord; 6. Fort Rae; 7. Sagastyr (the data for points 1-7 are after Vegard and Krogness, 1920); 8. Chesterfield; 9. Coppermine; 10. Cape Hope's Advance; 11. Saskatoon; 12. Coral Rapids; 13. Aroostook; 14. Gjöahavn (the data for points 8-14 are taken from Currie and Jones, 1941; the dotted lines at Chersterfield and Coppermine refer to all types of aurora); 15. Baker Lake; 16. Churchill; 17. Barrow; 18. Fort Yukon; 19. College; 20. Farewell; 21. Choteau (the data for points 15-21 are after Davis, 1961; the values are averages for the hour around geomagnetic midnight); 22. Godhavn (the data are after Lassen, 1959, and refer to the early morning hours); 23. the region of Micardbu (approximate data after Störmer, 1944); 24. Tromsö (the data are after Harang, 1945, and refer to geomagnetic midnight); 25. Wiese; 26. Dixon; 27. Cape Schmidt (data for points 25-27 are after Feldstein, 1960, and refer to local midnight); 28. Thule (data of Harang, taken from Störmer, 1955); 29. Kiruna (refers to geomagnetic midnight). The map has a geomagnetic coordinate system.

Despite the above-mentioned reservations concerning the observational material, it is evident from Fig. 2.14 that, in general, the alignment of the arcs conforms to the direction of the relevant circle projection quite closely, and that the agreement with the circle projections is better than with the geomagnetic latitude circles. The observed arc azimuth is in most cases, greater than 90° in those quadrants where the azimuth of the circle projections exceeds 90°, and less than 90° in quadrants where this is under 90°. Thus, it has been verified experimentally that on the eastern and western coasts of Greenland the observed average azimuths deviate in opposite directions from 90°, as do the azimuths of the circle projections.

Starkov and Feldstein (1960) and Evans and Thomas (1959) investigated the alignment of arcs at two places where the isoclines and the geomagnetic latitude circles differ greatly (Dixon near the northern auroral zone and Halley Bay near the southern one). They found that the preffered direction of alignment is far more consistent with geomagnetic latitude circles, and therefore with the higher approximation circle projections, than with the isoclines.

The available observational results for the southern hemisphere are relatively exiguous. A collection of IGY and subsequent data is contained in Fig. 2.15. The arrows indicate results of

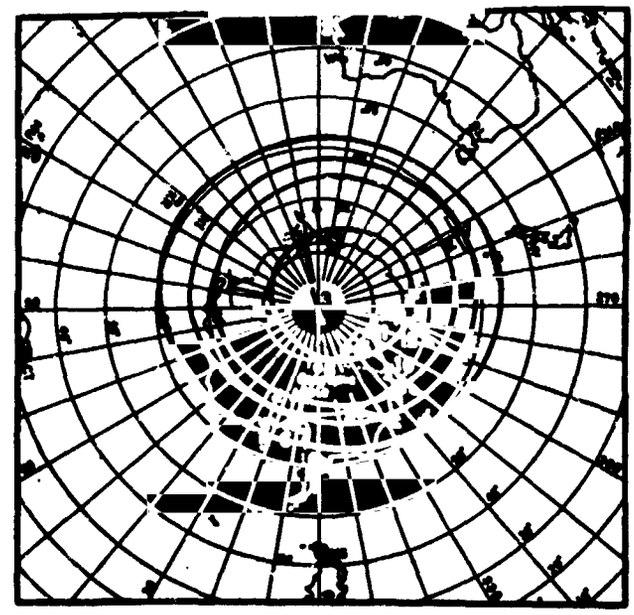

FIGURE 2.15.—Directions of quiet auroral arcs and sighting directions to the highest points of quiet arcs and bands (arrows) in the southern hemisphere. 1. Macquarie Island. 2. Mawson (data taken from Bond and Jacka, 1960); 3. Vastok; 4. Oasis (The data, after Feldstein, 1960 refer to local midnight); 5. Halley Bay; 6. Shackleton (data from Evans and Thomas, 1959); 7. Ellsworth; 8. South Pole; 9. Byrd; 10. Little America; 11. Scott Base (the long arrows at points 11 and 12 are after Hatherton and Thomas, 1959); 12. Hallett (short arrow); 13. Wilkes (the data for points 7-13 are from Gartlein et al., 1960, the two arrows at points 8 and 13 show the average directions for the two years 1957 and 1958, the 1957 arrow being the one nearest the meridian at both points); the map has a geomagnetic coordinate system.

TABLE 2

No.	Station	Geomagn. Coord. °N	Geomagn. Coord. °E	Observed azimuth (degr.)	Approx. measure of deviation	Azimuth of circle projection ("theor. azimuth")	Diff. obs. azimuth and "theor. azimuth"
1	Baker Lake	73.8	314.8	94	Diff. max-min ~60°	93	1
2	Churchill	68.8	322.5	99	Diff. max-min ~60°	95	4
3	Barrow	68.6	241.2	92	Diff. max-min ~60°	84	8
4	Fort Yukon	66.6	256.8	90	Diff. max-min ~80°	87	3
5	College	64.6	256.5	86	Diff. max-min ~60°	87	−1
6	Farewell	61.4	253.2	83	Diff. max-min ~60°	86	−3
7	Choteau	55.5	306.0	88	Diff. max-min ~70°	95	−7
8	Schmidt	62.6	226.6	80	Diff. max-min ~30°	80	0
9	Dixon	63	162	98	Stand. deviat. $< \pm 10°$ for magn. quiet periods	98	0
10	Vise	69	176	103	$\sim \pm 15°$	100	3
11	Pyramid	---	---	111	$\sim \pm 15°$	113	−2
12	SP-7 1957–58	---	---	96	---	96	0
13	SP-7 1958–59	---	---	0	---	0	0
14	Tromsö	67	117	98	Diff. max-min ~27°	106	−8
15	Kiruna	65.3	115.6	106	Stand. deviat. ±5°	105	1

observations of directions, as sighted to the auroral point of highest elevation. Two arrows for any single station represent the results of observations during each of the two years 1957 and 1958. The differences in direction of the arrows for the two years demonstrate the uncertainty of the results.

As will be seen from Fig. 2.15, the agreement between observed directions with those of the projected equator plane circles is fairly good for all places except Byrd (No. 9), and the agreement is certainly better than for the geomagnetic latitude circles.

Because of the existence of a diurnal variation in the orientation of the auroral arcs, increased accord between the directions of the arcs and of the circle projections is to be expected if values for a short period (e.g. 1 hr.) of the night are compared. The results of such a comparison for local midnight at twelve stations, most of them in or near the northern auroral zone, are presented in Table 2 and Fig. 2.16. A comparison with Fig. 2.14 clearly shows that the concordance of the arc directions with the circle projections is better for the selected material of Fig. 2.16 than for the unselected values of Fig. 2.14.

Table 2 contains azimuths of quiet auroral arcs at local midnight in the northern hemisphere (measured from northern geomagnetic meridian towards the east). The observed azimuths for stations 1–7 are after Davis (1961), those for stations 8–13 are after Feldstein (1960), and that for Tromsö is after Harang (1945).

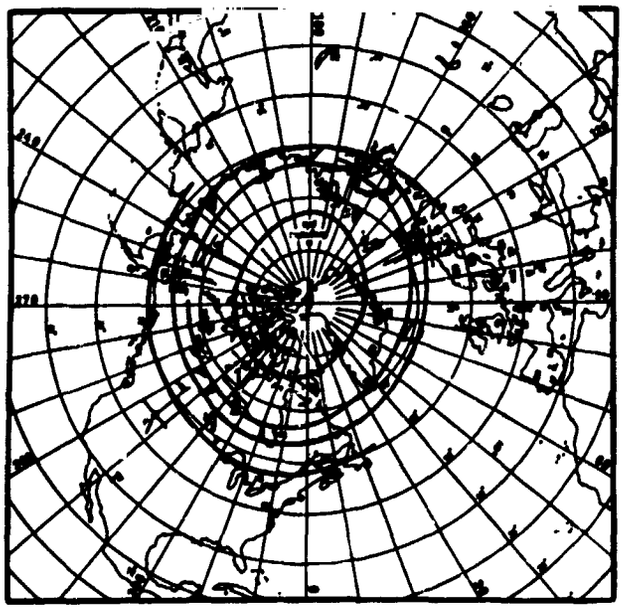

FIGURE 2.16.—Directions of quiet auroral arcs and bands at local midnight in the northern hemisphere. 1. Baker Lake; 2. Churchill; 3. Barrow; 4. Fort Yukon; 5. College; 6. Farewell; 7. Choteau (data for points 1-7 taken from Davis, 1961); 8. Cape Schmidt; 9. Dixon; 10. Wiese (data taken from Feldstein, 1960); 11. Tromsö (after Harang, 1945); 12. Kiruna. The map has a geomagnetic coordinate system.

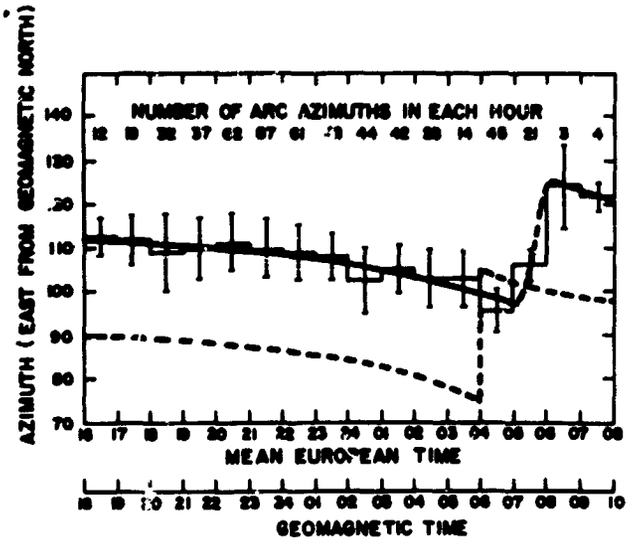

FIGURE 2.17.—Observed directions of quiet auroral arcs at Kiruna as function of MET and of approximate geomagnetic time. For each hour the average direction and the standard deviation are given. The lower, dashed curve is Alfvén's theoretical diurnal variation curve (see Alfvén, 1950).

(b) Diurnal variation in the orientation in and near the auroral zones

Although it was evident from the observations of Bravais at Bossekop in northern Norway as early as 1938–40 that the directions of the arcs and bands show a diurnal variation, very little attention was paid to this phenomenon until the nineteen-thirties, and even now only few studies exist.

From allsky-camera recordings taken at Kiruna ($\phi_m = 65.3°$ N) in the period December 1958 to end of 1962, the directions of 559 quiet auroral arcs were estimated. Only arcs reaching from horizon to horizon or, in the case of the most distant ones, covering an azimuth angle of view of about 100° were used in the analysis. The error in the measured direction of an arc probably does not exceed 4°.

The result of the alignment investigations is shown in Fig. 2.17.

For each hour of Mean European Time (MET) the average direction and the standard deviation were computed, for which procedure the direction value of each arc was weighted with the arc's duration. The durations vary over a wide range—from less than a minute to about an hour.

The total average azimuth for the whole material is 109°. A typical standard deviation for a 1 hr. period is 5°.

At the top of Fig. 2.17 is shown the number of arcs used for each hour. The number is maximal around geomagnetic midnight. In the morning hours the aurora is usually unsuitable for direction determination; as a rule, it is diffuse and situated far to the north. That is the reason why the observational material is smallest for that part of the night.

The azimuth charge in the morning is so rapid as to resemble a discontinuity of the type predicted by the Alfvén theory (see e.g. Alfvén, 1950).

In fact, the "discontinuity" can probably be observed only in longitudes where geomagnetic time runs ahead of local time, since daylight will preclude auroral observations in or close to the auroral zones until 8 or 10 o'clock geomagnetic time in other longitudes.

A number of similarly obtained diurnal variation curves for auroral arc orientation, based on observations in or fairly near the northern auroral zone (up to a geomagnetic latitude of 80°), are shown in Fig. 2.18.

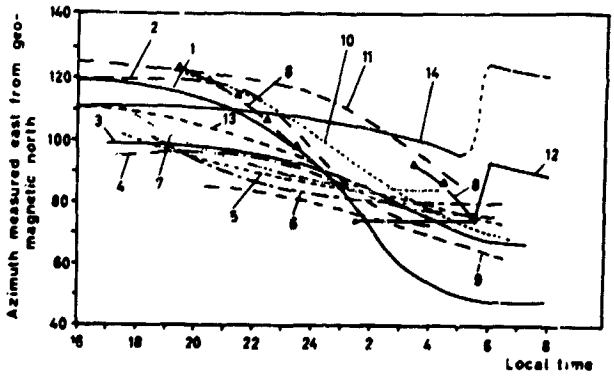

FIGURE 2.18.—Observed (smoothed) diurnal variation curves for the orientation of quiet auroral arcs and bands in and near the northern auroral zone. 1. Baker Lake (geom. lat. 74°); 2. Churchill (geom. lat. 69°); 3. Barrow (geom. lat. 69°); 4. Fort Yukon (geom. lat. 67°); 5. College (geom. lat. 65°); 6. Farewell (geom. lat. 61°); 7. Choteau (geom. lat. 56°) (curves 1-7 are after Davis, 1962b); 8. Dixon (geom. lat. 63°); (after Starkov and Feldstein, 1960); 12. Godhavn (geom. lat. 80°) (after Lassen, 1959); 13. Tromsö (geom. lat. 67°) (after Harang, 1945); 14. Kiruna (geom. lat. 65°).

The wide dispersion of the location and form of the different diurnal variation curves is striking. The amplitude of the diurnal variation also varies greatly. Here a regularity emerges, the amplitude increasing rapidly with latitude. Thus, the auroral arc direction varies at Baker Lake (geomagnetic latitude 74°) over a range of 70°, while at Choteau (geomagnetic latitude 56°) the range is only 20° (and at Kiruna, 65° N, 15°, if the final rapid increase in azimuth is ignored).

A "discontinuity" in the morning hours has been observed only at Godhaven and at Kiruna. As mentioned above, observation is likely to be possible only in the eastern geomagnetic hemisphere, where the geomagnetic time is running ahead of the local time. The difference between geomagnetic and local times is greatest in the region of northern Scandinavia (about 2 hours), where it is possible to observe aurora up to 1000 hrs. geomagnetic time. The reason why such "discontinuity" has not been observed at the Siberian stations could be that the geomagnetic times differs less from local time at those sites than it does at Godhavn and Kiruna.

For the southern hemisphere there is still a paucity of published observational data concerning the diurnal variation of arcs in and near the auroral zone. One such diurnal variation curve, of Evans and Thomas (1959) for Halley Bay, is shown in Fig. 2.19. From this curve it can be seen that at the southern auroral zone the azimuth —measured east from geomagnetic north—increases with time instead of diminishing as in the northern hemisphere. The range of variation (about 15°) is similar to that for the stations of lowest latitude in Fig. 2.18. This lends support to the assumption that the northern and southern momentaneous auroral occurrence curves are geomagnetically conjugated.

Comparison of the curve for Halley Bay in Fig. 2.19 (No. 1) with that for Oasis (No. 2 in Fig. 2.19) of geomagnetic latitude 78° shows that the range of variation increases with latitude in the southern hemisphere also.

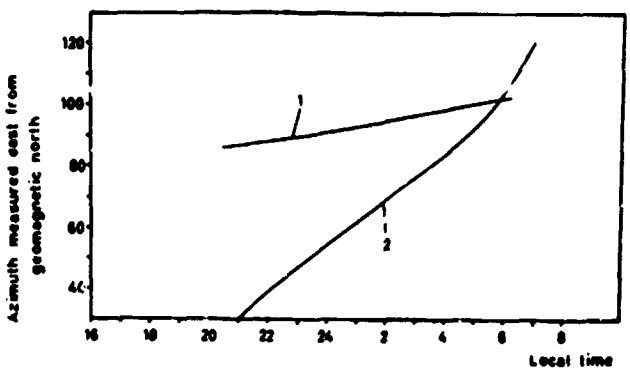

FIGURE 2.19.—Observed (smoothed) diurnal variation curves for the orientation of quite auroral arcs in the southern hemisphere. 1 Halley Bay (geom. lat. 66°S; outside the auroral zone) (after Evans and Thomas, 1959); 2. Oasis (geom. lat. 78°S; far inside the auroral zone) (after Feldstein, 1960).

(c) Discussion of the diurnal variation near the auroral zones

In order to ascertain the degree to which the differences between the curves in Fig. 2.18 could be attributed to referral of the direction of the geomagnetic meridian, i.e. to overlooking of the effect of the non-dipole part of the geomagnetic field, Hultqvist (1962 b) made a correction for this factor in respect of several stations near the northern auroral zone. The direction, instead of being referred to the geomagnetic meridian, was referred to the perpendicular to the projection of circles in the geomagnetic equatorial plane on to the earth's surface along higher approximation geomagnetic

field lines. The azimuths of these circles at a number of stations are given in Table 2. By changing the time scale to the geomagnetic one, the curves of Fig. 2.20 were obtained.

A comparison of Figs. 2.18 and 2.20 shows that the agreement between the North American stations on the one hand and Cape Schmidt and Kiruna on the other, was much improved by this modification.

Fig. 2.20 also includes the theoretical curve of Alfvén (1939, 1940, 1950). A comparison shows that the time derivative sign is the same, but that all the experimental azimuths are higher than the theoretical ones before midnight and that the amplitude of the diurnal variation for most stations is greater than theoretically expected.

The "discontinuity" observed at Kiruna has the same amplitude as that on the theoretical curve but is displaced about 1½ hour in the positive time direction.

From the observed diurnal variation curves of Fig. 2.20, a third type of auroral precipitation curve can be evaluated by integration according to formula (1)

$$\theta = \theta_0 \exp\left(-\int_{\lambda_0}^{\lambda} \cot a \, d\lambda\right) \qquad (1)$$

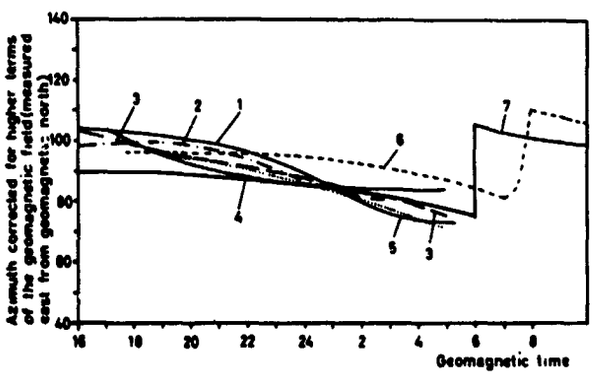

FIGURE 2.20.—Observed diurnal variation curves (smoothed) for the direction of quiet arcs, corrected for the non-dipole part of the geomagnetic field, given as a function of geomagnetic time for a number of stations situated in or near the northern auroral zone. 1. Barrow (geom. lat. 69°); 2. Fort Yukon (geom. lat. 67°); 3. College (geom. lat. 65°); 4. Farewell (geom. lat. 61°); (curves 1-4 are based on data taken from Davis, 1961); 5. Cape Schmidt (geom. lat. 63°) (based on a curve presented by Feldstein, 1960); 6. Kiruna (geom. lat. 65°); 7. Alfvén's theoretical diurnal variation curve (cf. e.g. Alfvén, 1950).

where θ is the geomagnetic colatitude,
λ is the geomagnetic time angle,
a is the azimuth of the auroral arcs measured from geomagnetic north towards east,
λ_0 is the geomagnetic time angle at the start of the observational curve, and
θ_0 is an integration constant that determines the polar distance of the curve.

This curve is Alfvén's theoretical I curve. It is defined by the orientation of the auroral arcs around the auroral zone, considered to be fixed in relation to the sun.

From the Kiruna diurnal variation curve of Fig. 2.20 the I curve of Fig. 2.21 has been derived. The whole curve is situated outside the circle with which it coincides at 1800 hours, in contrast to Alfvén's theoretical curve, which is inside the circle. The difference is due to the fact that the observation curve in Fig. 2.20 is situated almost completely above azimuth 90°. The difference between the experimental and theoretical curves

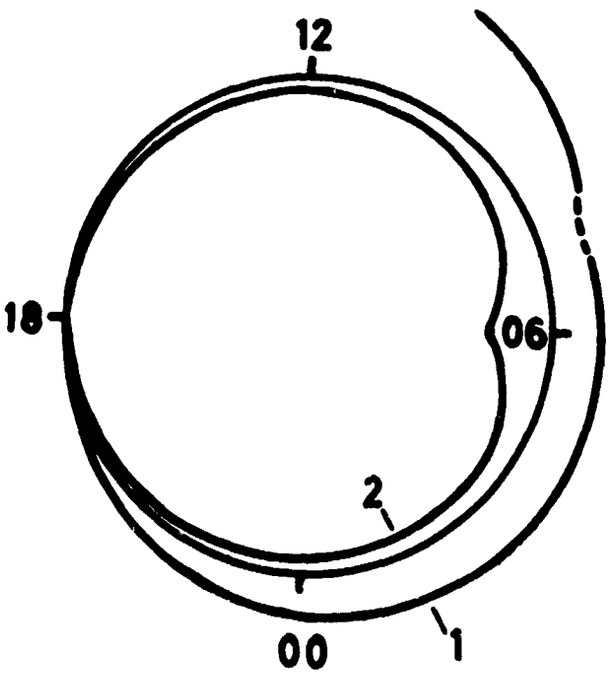

FIGURE 2.21.—Curve 1 is the auroral zone corresponding to Alfvén's I curve, evaluated from the Kiruna curve of Fig .17 for diurnal variation in the orientation of quiet auroral arcs. It is corrected for the non-dipole part of the geomagnetic field. Curve 2 is Alfvén's theoretical I curve (see Alfvén, 1950).

varies between 7 and 9°, which means that the theoretical curve is situated outside the standard deviation "region" of the observational material.

The very high amplitudes of the diurnal variations found for high latitude stations are not contained in Alfvén's model, according to which the greatest deviation of the arc azimuth from 90° should be at 0600 hours geomagnetic time, where the I curve has a singular point and the azimuth changes from 105° to 75° in the auroral zone.

Even for L = 70 earth radii, corresponding to a geomagnetic auroral latitude of above 80°, the azimuth is only 76° at 0600 hours.

Khorosheva (1961, 1962) investigated recordings of aurora made simultaneously at widely different longitudes in the arctic of the eastern hemisphere and found that the auroras form a single, physically related band which changes synchronously in brightness, width and latitude over its entire extension. On the basis of these observations, Khorosheva and Feldstein proposed that the momentaneous auroral precipitation zone forms an oval-shaped curve around the geomagnetic axis pole, at the normal distance of the auroral zone (about 23°) on the night side but only 10–12° from the pole on the day side, i.e. the zone is similar in shape to the combination of two spiral arcs shown in Fig. 2.10. The proposal (Feldstein, 1964) also implies that the auroral arcs are lined up along the momentaneous precipitation zone of the described shape. This would explain the existence of two maxima in the diurnal variation curve for auroral occurrence at latitudes inside the ordinary auroral zones. It would, however, mean that the aximuth of the auroral arcs, measured from the perpendicular to the auroral zone (curve 3 in Fig. 1), would be smaller than 90° after midnight, with the most rapid change in direction around midnight. That is usually not observed.

(d) Diurnal variation on the central auroral caps

On the central auroral caps (inside about 80° geomagnetic latitude) the diurnal variation of the orientation of quiet auroral arcs has been reported to be entirely different from the one described above. Observed (smoothed) diurnal variation curves are shown in Fig. 2.22 for both the northern and southern central caps. Curve 2 in Fig. 2.19 also belongs to this category.

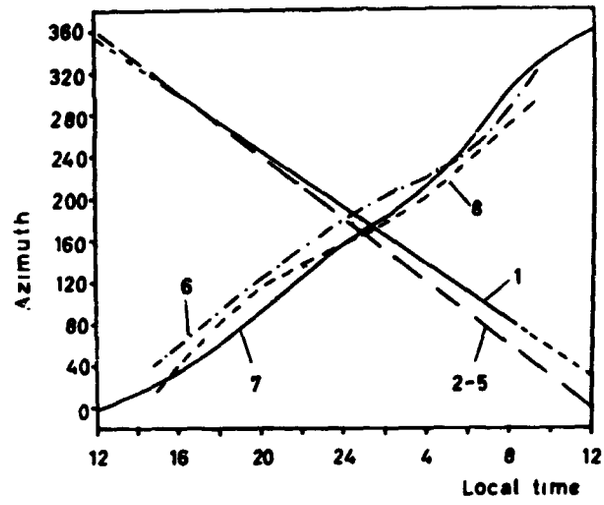

FIGURE 2.22.—Observed diurnal variation curves (smoothed) for the direction of quiet arcs at stations deep inside the auroral zones. The azimuth is measured towards the east from geographic north for curves 1-5 and from geomagnetic north for curves 6-8. 1. Dumon d'Urville (geom. lat. 76°S) (after Weill, 1958); 2. Wilkes (geom. lat. 77°S); 3. Dumont d'Urville; 4. Scott Base (geom. lat. 79°S); Hallet (geom. lat. 74°S) (the curves for points 2-5 are after Denholm and Bond, 1961); 6. Thule (geom. lat. 88°N); 7. Alert (geom. lat. 86°N); 8. Resolute Bay (geom. lat. 83°N) (the curves for points 6-8 are after Davis, 1961).

If the azimuth in Fig. 2.22 is taken from geographic north, the diurnal variation curves imply that the arcs are continuously pointing to the sun while the earth rotates below the auroral pattern. The first to report such a 360° diurnal variation of the auroral arc direction seems to have been Mawson (1914), but it was forgotten and rediscovered by Weill (1958). In the last few years it has also been reported by Davis (1960, 1961, 1962 b), Feldstein (1960), and Denholm and Bond (1961). Consistent data showing this 360 degrees rotation of the arcs during the 24 hours of day and night have thus been presented by several investigators and there seems to be no doubt that the effect is real. There are, however, a number of inconsistencies between observational results found by different observers (see Hultqvist, 1962 b) and there is, therefore a need for more observations.

It has been suggested by Cole (1959, 1960) and Davis (1960, 1961, 1962 b) that the geometric pattern of aurora over the polar caps is the same as the pattern of the ionospheric current system which is equivalent to the local-time-dependent

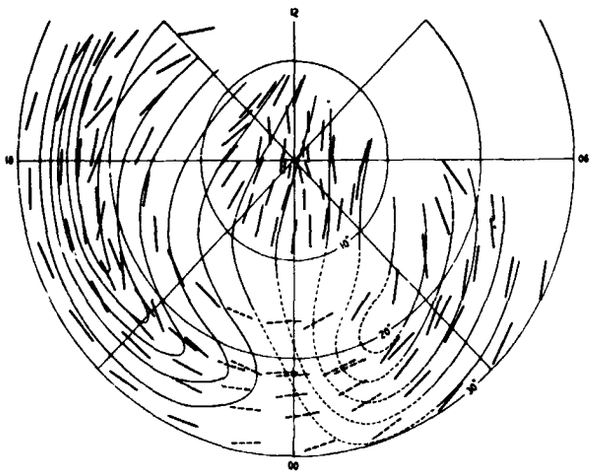

FIGURE 2.23.—(After Davis, 1962b) The alignment of auroral forms in a polar coordinate system with geomagnetic colatitude and approximate geomagnetic time as polar and azimuthal coordinates. The dashed lines represent the discontinuous post break-up aurora.

component of the geomagnetic disturbance—the DS current system (see Fig. 2.23). These views were incorporated as important constituents of the qualitative model of geomagnetic storms and associated phenomena by Axford and Hines (1961). According to this model the DS currents and the auroral arcs should have the same direction over the auroral caps.

The angle between auroral arcs and the direction of the horizontal currents, corresponding to the observed magnetic disturbance, has been evaluated by Sobouti (1961), Davis and Kimball (1962), Pudovkin and Yevlashin (1962), Feldstein (1964) and others for auroral and transauroral latitudes. Near the auroral zone, all investigators found the directions being identical within measuring accuracy. While Feldstein's results in the near polar regions were that the directions mentioned form an angle of, in the average, about 50°, Sobouti (1961) did not see any difference at Resolute Bay (geomagnetic latitude 83.2° N). A disagreement between directions of auroral arcs and the ionospheric current lines has also been found in the Antarctic (see Cole, 1963). A difference between the two directions introduces difficulties for theoretical models which require that the geographical pattern of auroral arcs and of the DS current system should be identical (like the model of Axford and Hines, 1961). It is, however, to be remembered that the horizontal geomagnetic disturbance component shows the direction of the ionospheric current only for simple current patterns.

(e) Other variations in arc orientation

Jensen and Currie (1963) found a pronounced seasonal variation in the auroral arc orientation in the years 1949–51 at Saskatoon (lat. 52.1° N) and Chesterfield (lat. 63.3° N) Canada. The peak to peak variation in azimuth over a year amounted to about 30°, with a maximum azimuth of 115° in February at Saskatoon and minima in October-November and April-May. The seasonal-variation investigation of Jensen and Currie (1953) seem to be the only one made.

Those authors also studied the dependence of the arc direction on the activity of the auroral display. No significant difference between quiet and active displays could be found. When grouping their observational material for auroral arc orientation with regard to magnetic disturbance level, Jensen and Currie obtained for Saskatoon an average azimuth of $93° \pm 1°$ (standard deviation) for the highest degree of activity, $100° \pm 1°$ for median disturbance and $100° \pm 2°$ for the lowest degree of disturbance. More investigations of the kinds undertaken by Jensen and Currie, made for different geomagnetic longitudes, would be of great value.

No theoretical models of aurora contain any seasonal variations in the auroral activity at all. The difference in direction between the earth's rotation axis and the dipole axis has been neglected so far.

5. The Height and Vertical Extent of Visual Aurora

The height of auroras was studied extensively especially in the first two to three decades of this century by the Norwegian school of auroral physics, with Störmer as the originator. Detailed reports of the methods used and the results obtained can be found in the books by Harang (1951) and Störmer (1955). Observations in Canada and Alaska have been reported by McLennan et al. (1931), Currie (1934, 1955), Fuller and Bramhall, (1937), and McEwen and Montalbetti (1958). Southern hemisphere observations have been published by Geddes (1939). Only a very short review will be given here.

The height can be measured only if the auroral form contains some well defined features which can be identified on photographs taken from two places at a distance from each other comparable to the height of the aurora (paralactic photography).

In most auroras the lower border is well defined and the height given in most reports is the height of the lower limit of the aurora, as seen on photographic pictures. Fig. 2.24 shows the height distribution of lower limits for different auroral forms (after Vegard and Krogness, 1920). The differences between the various types represented in the figure are fairly small.

The dependence of the heights of the lower borders of auroral arcs on their intensity is shown in Fig. 2.25 (after Harang, 1951). As can be seen from Fig. 2.25, there is a difference of 20 km

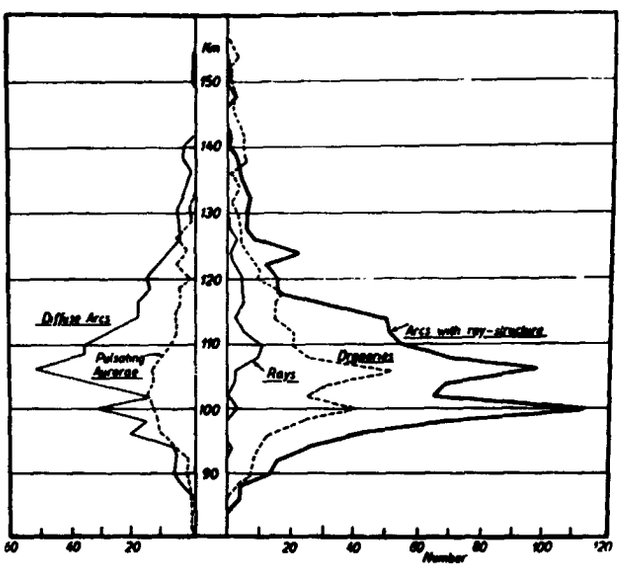

FIGURE 2.24.—(After Vegard and Krogness, 1920) Distribution of lower limits for different auroral forms.

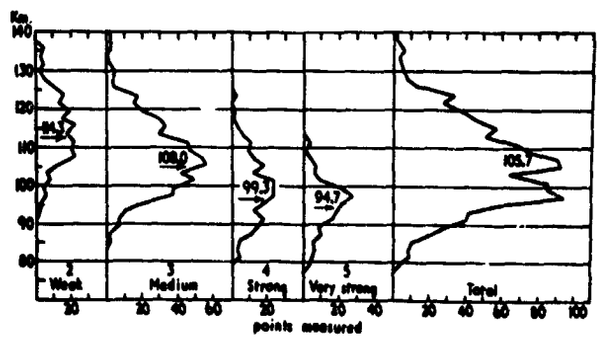

FIGURE 2.25.—(After Harang, 1944) Lowering of the heights of arcs with increasing intensities, as observed from Tromsö 1929-1938.

in height between weak and very strong arcs. Harang found a similar but less strong dependence on intensity also for other forms.

The results described above were obtained in or close to the northern auroral zone. The height of subauroral zone aurora has been extensively studied by Störmer (cf. Störmer, 1955) over southern Scandinavia. Compared with the auroral heights determined in the vicinity of the auroral zones the height diagram for southern Norway shows a far greater extension towards increasing heights. The lower limits are, however, the same in both cases. According to Barbier (1963) the majority of auroras seen over central Europe have lower limits situated above 250 km altitude.

In addition to the type effects shown in Fig. 2.24, there are a number of others. Störmer (see Störmer 1955) determined the height of the lower limit of sunlit auroras and found a height distribution completely different from those in Fig. 2.24. The distribution was very extended in height, with its maximum of probability at about 300 km.

Aurora of type B, i.e. aurora with the lowest part red due to emissions from the first positive band system of N_2 and first negative system of O_2^+, usually occurs at altitudes for the lower border of between 80 and 100 km. The lowest height of aurora reported was found by Harang and Bauer (1932) for a type B display. Numerous measurements were made on an intense arc and they obtained some points extending down as low as 95 km with an average height of 70 km.

On the other hand, red aurora of type A (with the 6300 Å O line dominating) is observed mostly at heights greater than those shown in Fig. 2.24. The medium latitude aurora mentioned above, which has a lower limit greater than 250 km, is mostly of this kind.

Störmer has reported a type of homogeneous arc, lying in the dark atmosphere near 200 km, which may be of a different kind from the aurora observed at 100 km level (Barbier, 1963; see also p. 6).

Finally, the quiet mid-latitude red arcs have been found to occur at heights between 390 and 560 km, but most often in the interval 400-450 km (see the review by Roach and Roach, 1963).

The extent along the field lines of an auroral form is quite different for different forms. Fig. 2.26 (after Vegard; cf. Harang, 1951, p. 35) shows

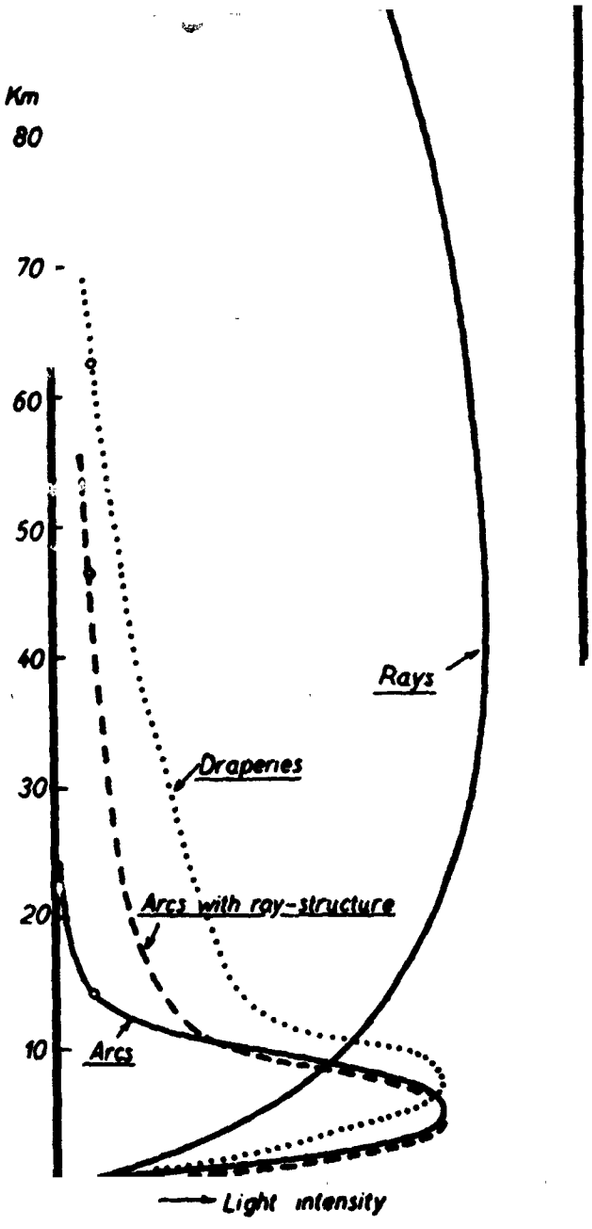

FIGURE 2.26.—(After Harange, 1951) Distribution of light intensity along different auroral forms.

the mean variation of light intensity in vertical direction for different auroral forms. An ° indicates the upper limit of photographic impression. Some average numerical parameters have been collected in Table 3 (after Vegard and Krogness, 1920).

Here l_1, l_2 and l_3 are the distances from the lower limit to the height of maximum luminosity, the upper limit of strong luminosity, and the upper limit of faint luminosity, respectively. It is evident from Fig. 2.26 and Table 3 that the rays differ entirely from the other auroral forms in respect of luminosity distribution with height.

There is a solar-cycle variation in the height of the lower boundary of aurora as well as in vertical extent (Elvey, 1957). Both height and vertical extension are lower in years with solar-activity-minimum than at high solar activity.

TABLE 3

Type	l_1	l_2	l_3
arcs	6.4 km	14.0 km	14.0 km
arcs with ray-structure	5.8 km	13.6 km	46.7 km
draperies	9.1 km	16.3 km	63.4 km
rays			137.0 km

6. Motions

There are many different types of motions associated with the auroral activity and individual auroral forms. Some of the motions for which observational data are available will be discussed here. From the point of view of the theoretical models of aurora, we are interested in how the auroral precipitation zones change location with time under various conditions as well as in how individual complete forms, or irregularities in the forms, move. These types of motion will be discussed in this subsection, where we will deal with the statistical properties. In subsection 7 examples of motion in connection with changes of momentaneous auroral geographical distributions will be discussed.

(a) Changes in the geographical pattern of auroral activity

It has been mentioned already before in this review that the location of the auroral zone shifts towards lower latitudes when the solar activity increases (although inconsistency exists in the available data). The first one who deduced this motion from observational data seems to have been Tromholt (1882). Davies (1950) evaluated a change of about 3 degrees of latitude between solar maximum and solar minimum. Tromholt

(1882) and Davies (1950) also arrived at a seasonal variation in the polar distance of the auroral zones. This is large around the equinoxes and small at solstizes. This is supported also by the recent study by Feldstein and Shevnina (1961), but the opposite result was found by Sheret and Thomas (1961).

With the statistical definition of the auroral zone adopted earlier in this section, seasonal variation in its location are the shortest that can exist. We will, however, now consider briefly the average behavior of the momentaneous auroral precipitation zone as a function of geomagnetic disturbance level (this momentaneous region of auroral activity is often called the auroral zone in the literature). There exist two types of data of relevance in this respect: those which concern the equator-ward boundary of the region where auroras occur, and those referring to the region of maximum occurrence frequency for the aurora at a given moment of time.

Gartlein et al. (1960) found the southern boundary of aurora in the northern hemisphere to be at almost 10° lower latitude for $K_p=5$ than for $K_p=1$, the $K_p=5$ boundary passing through Stockholm, southernmost Alaska and the Great Lakes in North America (see Fig. 6). Akasofu and Chapman (1963) found the southern limit of latitude of northern quiet auroral arcs to be approximately a linear function of Dst(H), i.e. of the ring current field, for 16 magnetic storms studied. The latitude variation with the ring current amounted to more than 10°, the southern limit reaching 49° geomagnetic latitude for the strongest storms investigated.

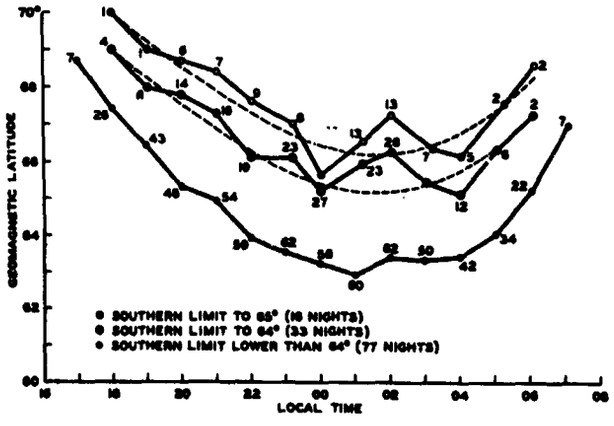

FIGURE 2.27.—(After Davis, 1962a) Diurnal variation of average southern extent for each of three groups of displays extending to geomagnetic latitudes 65°, 64°, and beyond 64°. The number beside each point gives the number of displays contributing to that particular mean position.

The southern border of auroral activity in Alaska, taken to be the lowest latitude position at which defined auroral forms appear, was found by Davis and Kimball (1960) to move regularly in the course of the night in the manner shown in Fig. 2.27. The extreme southern extent of the smoothed curves occurs, as can be seen in Fig. 2.27, around geomagnetic midnight (which is 1-2 hours after local midnight in Alaska). Davis (1962 b) states that the decrease in the number of discrete forms in low latitudes in the morning must be due to the actual disappearance of the forms in place—either because of a decrease of auroral luminosity or to a tendency for the forms to diffuse —and not to withdrawing to the north.

Jacka (1953) studied the location of the region of maximum auroral occurrence around MacQuarie Island in the southern hemisphere. He found that the southern auroral precipitation zone moves towards the equator with increasing K_p as $\Delta\phi = 2.95 - 0.605\,K_p$, where $\Delta\phi$ is the latitude departure of the homogeneous arcs from MacQuarie Island. From Jacka's relation, it can be seen that the latitude of the auroral precipitation zone can vary with as much as 5–6°. This is the same amount as found by Feldstein and Solomatina (1961).

A question of interest is the following: is the detailed shape of the distribution of auroral activity within the auroral precipitation zone changed when its center or southern boundary moves in latitude. Studies of this have been reported in the last few years. Some investigations of individual events will be reviewed in subsection 7, below. Here the average behavior will first be discussed.

Feldstein and Solomatina (1961) reported that at the same time as the auroral precipitation zone withdraws from the pole, there is an expansion of the zone, also towards higher latitudes, but they did not present quantitative results. Davis and Kimball (1960) and Davis (1962 b) give some details. Fig. 2.28, after Davis (1962 b) shows several measures of auroral activity vs. geomagnetic latitude for weak and strong displays. For curve A the maximum K index at College during

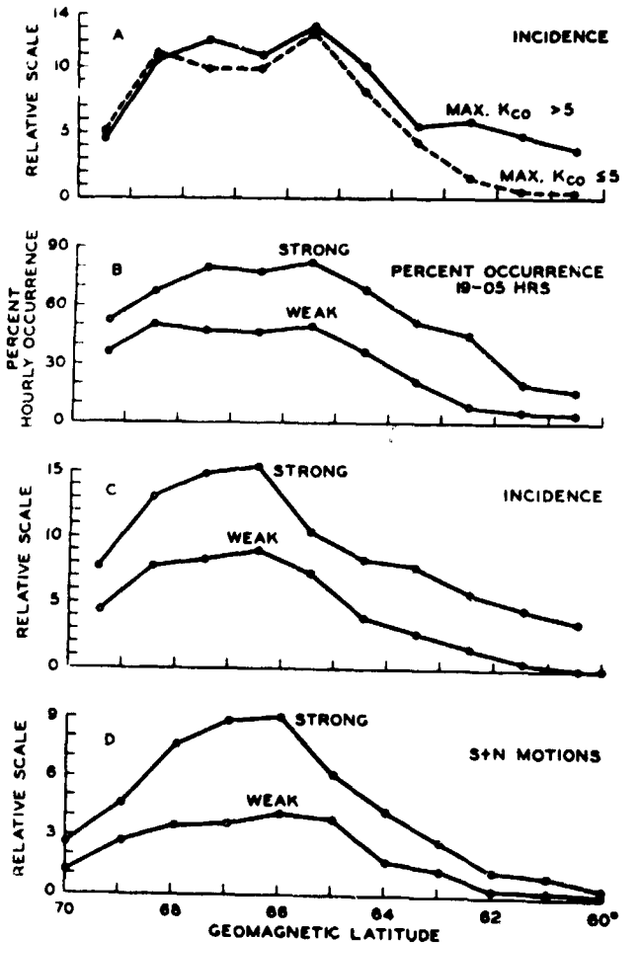

FIGURE 2.28.—(After Davis, 1962b) Several measures of auroral activity versus latitude for weak and strong displays observed in Alaska in the season 1957-58. (A) Curves of total incidence for 25 displays during which the maximum K-index for College did not exceed 5 (dashed line) and for 25 displays for which it exceeded 5 (solid line). (B) Average percentage hourly occurrence of overhead auroras (local time interval 19-05[h]) during 24 strong and weak displays. (C) Total incidence of forms during the 24 strong and 24 weak displays used to draw curves B. (D) Total south and north moving forms observed throughout 31 strong and 30 weak displays.

the display has been the criterion for classing. Davis points out that the small difference between strong and weak events at high latitudes, shown in Fig. 2.28, does not mean that there is no connection between magnetic and auroral activity in those latitudes, but only that the highest K index achieved during a display at an auroral-zone station is a poor indicator of the auroral activity at the auroral zone. In Fig. 2.28 B, C, and D the division of the displays into strong and weak was made on the basis of the total number of forms observed in Alaska between geomagnetic latitudes 60° and 70° during each display. In Fig. 2.28 D the total number of auroral forms moving north or south through the zenith of the station has been taken as measure of auroral activity.

Fig. 2.28 clearly indicates that the position of the maximum activity is at essentially the same geomagnetic latitude (66° to 67°) for both small and large displays, but at the lower latitude positions the relative increase of activity for the large displays is considerably greater than at higher latitudes.

(b) Motion of individual auroral forms

A drift of distinct luminous auroral features must be due either to a drift or change of the source of the impact particles or to a change in the electric and magnetic fields experienced by the particles on their way to the atmosphere. The studies of the drift motion of auroral forms is therefore, of course, of considerable interest.

The available observational data in general give the motion in N–S and E–W direction. Considering the deviation from the E–W direction of both geomagnetic isolatitude lines and the average orientation of the auroral forms, it would be preferable in the future to have the motions measured parallel and perpendicularly to the observed auroral zone or to the individual auroral arcs. In this review the motion will, however, have to be divided into N–S and E–W direction.

With regard to the motions of individual auroral forms there are two cardinal observations, which are valid irrespective of direction. First, all parts of rays, which can be several hundred km long, appear to move at the same velocity, aligned with the geomagnetic field in the first approximation, and secondly, auroral forms and inhomogeneities have not been reported to overtake one another.

(i) *Meridional Motion*

The motion of individual auroral forms varies with latitude and local time.

Davis and Kimball (1960) found, when scaling allsky-camera films from Alaska to determine the meridional motions, that the direction of first motions observed each evening at the various latitude positions followed definite trends. On many nights, there existed a geomagnetic latitude

between 60° and 70°, north of which the first motions were to the north, and south of which the first motions were to the south. This latitude they referred to as the "latitude position of origin." According to Davis (1962 b), the auroral forms do not necessarily form at this latitude. Rather, they seem to develop within a few degrees of the "latitude position of origin" and have a direction of first motion determined by whether the forms develop on the poleward or equatorward side of the "latitude position of origin." Davis and Kimball found the "latitude position of origin" to be between 60° and 70° on 86 of the 180 nights when aurora was observed over Alaska during the 1957–1958 season. On 58 other nights the aurora first moved south across the whole latitude band 60°–70°. Approximately 10 nights were found on which either the first motions were without pattern or there were more than one latitude of origin.

The regularity mentioned was for the first direction of motion seen in the evening. Later on in the night both northward and southward moving forms are observed. In fact, Davis and Kimball (1960) and Davis (1962 b) found that during IGY the number of auroral forms moving southward within the geomagnetic latitude band 60° to 70° over Alaska was greater than the number of north-moving forms at any time in the night. Bhattacharyya (1961) observed near Ottawa, well to the south of the auroral zone, that the number of equatorward moving forms outnumbered those in the reverse direction only up to 0200 hours (75th meridian time). Fillius, Gartlein and Sprague found a similar result at the southern auroral zone (according to Cole, 1963). The data presented by Davis (1962 b) differs from those of Bhattacharyya and Fillius et al, in that Davis gave the number of forms within a 10° latitude range, whereas the others presented observations from one place.

Older observational results of local time dependence of meridional motion in subauroral latitudes have been reviewed by Harang (1951) and Störmer (1955.) They can be roughly summarized in the following way: the motion is on the average equatorwards before midnight and polewards after. The apparent discrepancy between the results of Davis and Kimball (1960) and most older results may be due to the difficulty to distinguish, without the use of allsky films, between motion of the equatorward boundary of auroral activity and actual meridional movement of individual forms.

Kim and Currie (1958) analyzed the N–S motion south of the northern auroral zone with regard to velocity. They found the velocity to be greatest (about 160 m/sec) at the latitude of the auroral zone. The number of occasions of equatorward movement exceeded those polewards in every 50 m/sec speed range up to 670 m/sec except in the range 0–50 m/sec.

(ii) *Longitudinal Motion*

At the auroral zones and in subauroral latitudes both east and west longitudinal motions of auroral forms occur during the night, westerly predominating early in the night and easterly in the morning. (Meinel and Schulte, 1953; Meek, 1954; Bless et al., 1955; Malville, 1959; Evans, 1959, 1960; Kim and Currie, 1960; Bond, 1960; Stoffregen, 1961; Davis and DeWitt, 1963). Most investigators are agreed that east–west motions are in general much faster—by at least a factor of 3—than north-south motions, amounting to several hundred m/sec for average disturbance levels. Kim and Currie (1960) observed a general increase of speed with proximity to the auroral zone and also with increasing geomagnetic disturbance level.

Davis (1962 b) and several before him found that during the simplest type of auroral display, one accompanied by positive disturbance of the horizontal magnetic field in the evening and negative disturbance in the morning, the auroral motion is westward during the positive disturbance and eastward during the negative. The reversal from westward to eastward auroral motion is abrupt to within 30 minutes and occurs at the time of, or some minutes after, the change of sign of the horizontal magnetic disturbance.

Mawson (1914) and Stoffregen (1961 b) observed inside the southern and northern auroral zones, respectively, that the longitudinal motion in auroras was, in general, from the daylight to the dark side of the earth, i.e. opposite the general trend outside the zone.

According to Davis (1961, 1962 b), the moderate evening aurora at the auroral zone is typified by the existence of a partial or complete array of west-opening loop structures along which clockwise (as seen from above) motions of irregularities occur. These motions are superimposed on the

general westward drift of the auroral forms. Following the change from positive to negative horizontal disturbance, broken forms are prevalent, but now counter clockwise motions occasionally can be seen. Auroral displays accompanied by magnetic disturbance of variable sign have correspondingly complicated auroral motion.

The motion pattern observed by Davis agrees with Mawson's and Stoffregen's observations inside the auroral zones and it also fits well to the theoretical model of Axford and Hines (1961).

Recently, Omholt (1962) has reported east–west speeds of rays in a very active auroral curtain as high as 30 km/sec. These observations were made with a new technique. The data reported are only preliminary and more measurements of this kind will certainly add much to our knowledge about the auroral mechanisms. Still higher velocities of irregularities along auroral forms (up to 124 km/sec) have been observed by Davis and Hicks (1963) with the use of image amplifier technique, permitting 30 exposures/sec or more.

7. Dynamic Morphology of Individual Auroral Displays

A few synoptic studies of auroral displays have been published since IGY (but much fewer than would be desirable). This type of investigation is certainly one of the most important that can be made at the present stage of our knowledge about aurora. Those published have revealed several previously unknown characteristics of the auroral morphology. A brief review will be given here.

Khorosheva (1963) found that auroras observed simultaneously at different longitudes in the eastern hemisphere form a single, physically related band, which changes synchronously in brightness, width, and latitude over its entire extension.

Davis (1962 b) and Davis and Kimball (1962) analyzed synoptic auroral maps for Alaska and evaluated the results reviewed earlier concerning auroral motion and auroral configurations. Cood evidence for the configuration pattern of aurora being similar to that of the DS current system was found.

Synoptic maps covering still larger areas than those of Davis (1962 b), namely eastern Siberia, Alaska, and western and central Canada; have been prepared and analyzed by Akasofu (1960, 1962, 1963) and Akasofa and Chapman (1962). The disturbance periods studied are the very great ones. (Sept. 22–23, 1957, Feb. 11, 1958, Feb. 13, 1958; March 24, 1958).

A short report of the time history for the Feb. 13, 1958 aurora, given by Akasofu (1963), will be included here, because it illustrates better than has been done before the development of a large aurora on a world-wide scale. Fig. 2.29, a-e, shows snapshots of the situation at five different moments of time.

Three arcs extended across Alaska at 0830 UT but only one to the north of eastern Siberia (Fig. 2.29 a). Five minutes after the break-up, the auroras over Alaska were completely disrupted. A few arcs rapidly moved northward and one of them went to the north of Barrow (Fig. 2.29 b). To the west of Alaska a remarkable loop formation can be seen in Fig. 2.29 b. It seemed to be produced at the time of the breakup over Bering Strait. There is a great difference in the latitude range of the aurora between Alaska and Canada in Fig. 2.29 b. This is because the zone with aurora did not expand simultaneously over the longitude range shown. It started over Alaska. There was, however, a strong increase in brightness also over Canada when the breakup began in Alaska.

At 0900 UT the expansion had spread to central Canada (Fig. 2.29 c). A new breakup started at 0907 UT in Alaska and the broken bands became much brighter also in central Canada. At 1030 UT the auroral forms in Alaska and the Siberian Arctic Sea were quiet again and there were several faint arcs. The aurora was, however, still irregular in Canada and did not recover to this quiet phase, although it became fainter. The auroral precipitation zone was still expanding to the north there.

Some of the observations made by Akasofu in analyzing synoptic sequences similar to the one in Fig. 2.29 are summarized here.

(1) The auroral precipitation zone starts to move away from the pole when the ring current starts to build up. It may reach latitudes 10° (or more) less than that of the auroral zone. The width of the precipitation zone in quiet periods (between polar magnetic (DP) substorms) is not increased (5° wide or less).

(2) The breakup occurs when a DP substorm starts. It is characterized by a sudden increase

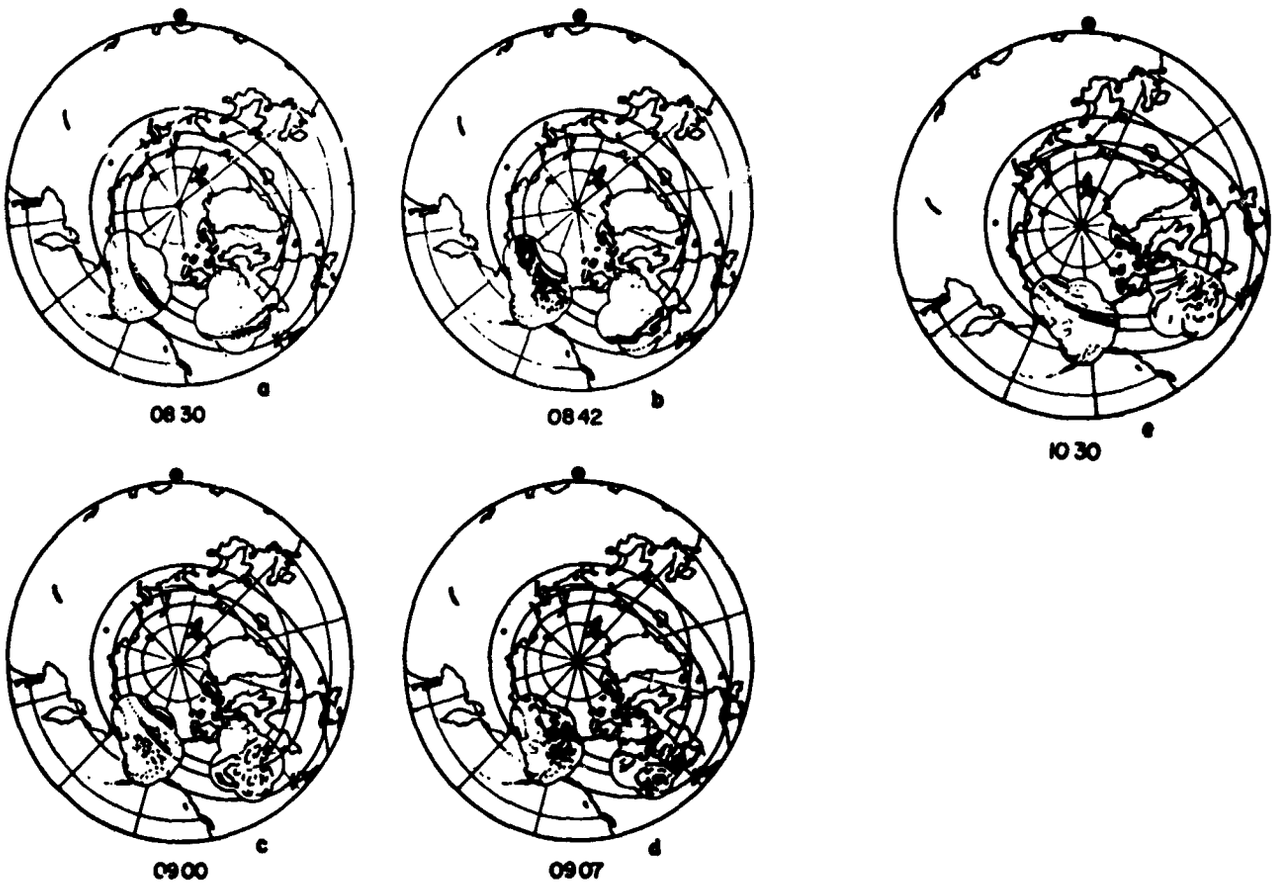

FIGURE 2.29.—(After Akasofu, 1963) The distribution of the auroras on February 13, 1958. The field of view of each allsky camera station is indicated by a circle of radius 500 km. The dark dot on the top of each map shows the direction of the sun. L-curves 4, 6 and 8 are also shown.

of the brightness and rapid and complicated folding or wavy motions of all arcs and bands over a large area on the morning side, together with a rapid expansion polewards of the precipitation zone. The northward expansion often starts around midnight or in the early morning and propagates into the morning side. It may amount to more than 10°.

(3) Breakup with poleward expansion has been observed in the auroral zone already 4 minutes after the sudden commencement.

(4) At the breakup, westward traveling folds are often formed. They propagate with velocities of 300–600 m/sec and have characteristic lengths of a few hundred km. Akasofu thinks it is possible the folds are identical with those observed and studied by Davis (1962 b).

(5) Some of the auroral forms in the auroral caps move up there from auroral zone latitudes during and after the breakups.

(6) Complete breakup of the quiet auroral forms are not so common on the auroral caps as in the auroral zones or on their equatorward side.

(7) An arc extending at least 5000 km in E–W direction was seen on March 24, 1958.

It is evident that a large number of the characteristics found by Akasofu do not fit into any theoretical model, in most cases because the existing models are not detailed enough. Some of the results presented above seem to disagree with some proposed models. The disrupted auroral forms shown in Fig. 2.29 are not similar to the DS-current pattern to be expected on the basis of Axford's and Hines' (1961) model for magnetic storms and aurora, just to mention one of the most recent ones. Also, the observation of large scale activation of aurora, with breakup and northward expansion of the auroral precipitation zone already 4 minutes after a sudden commencement, seems not fit their model.

Akasofu (1963 d) has worked out a model of simultaneous auroral activity over the entire polar region in terms of the auroral substorm, which corresponds to the polar geomagnetic substorm (DP).

3. CORRELATION WITH SOLAR AND GEOPHYSICAL PHENOMENA

In this section observed statistical relations between visual aurora and solar and geophysical phenomena will be briefly reviewed.

1. Solar Disturbances

Except for the investigations of the variation of the occurrence frequency of aurora with the solar cycle, which have been mentioned in Section 2 (see page 32), detailed investigations of the correlation between visual aurora and solar disturbances seem not to have been made. A large number of studies of relations between solar events and geomagnetic disturbances exist in the literature and are reviewed in Chapter 00 of this book. Since the correlation between occurrence of aurora and planetary magnetic activity is good (cf. below), most of the relevant conclusions reached for magnetic storms are also valid for aurora. The 27-day recurrence tendency seems to be less pronounced for aurora than for magnetic disturbances (Chamberlain, 1961).

2. Geomagnetic Disturbances

That worldwide magnetic disturbances occur at the times when aurora can be observed was discovered in 1741 by Celsius and Hiorter in Uppsala, Sweden (cf. Chapman and Bartels, 1940).

A detailed investigation of the correlation between the occurrence of aurora and the planetary magnetic activity has been made by Bartels and Chapman (1958). It has been known for long to aurora investigators that the start of a magnetic storm in the day almost invariably leads to the occurrence of aurora in auroral zone latitudes in the following night. This is true in subauroral latitudes only when the storm is a strong one—in which cases very little aurora may be seen in the auroral zone (see Section 2).

Over the central polar caps (geomagnetic latitude above 80°) the visual aurora is negatively correlated with the local as well as with the planetary K indices (Davis, 1963). In the region between geomagnetic latitudes 75 and 80° the relationship between auroral occurrence and geomagnetic activity is more complicated and of a transitional nature. Feldstein (1962 b) found that auroras are observed in the zenith at Murchison Bay (geomagnetic latitude 75°N) most frequently when there is a weak magnetic disturbance ($K=2$–3). When auroras appearing to the south were also taken into account the auroral occurrence frequency increased with the K-index up to high values of it. Morozumi (1963) found positive correlation between auroral occurrence and magnetic disturbance even at 78° geomagnetic latitude (at the South Pole).

There is not only a correlation between the general occurrence of aurora, but a fairly detailed relationship exists between the development of the visual aurora, as seen in auroral zone latitudes, and the development of the associated geomagnetic disturbance. These relations have been studied by Meek (1953, 1954b), Heppner (1954a, b, 1955), Zaborshchikov and Fediakina (1957), Fan (1958), Bless et al. (1959) and Akasofu (1963d).

Heppner (1954b) summarizes his observations at College (geomagn. lat. 64.5°N) in the following way. The magnetic disturbance and simultaneous auroral activity on a large majority of, and perhaps all, nights may be represented by means of two patterns, which apply individually or in combination. This is a consequence of recognizing that magnetic disturbances are made up of individual bay disturbances and that coincident with each bay there is a distinct sequence of auroral activity. The two patterns differ in respect to what happens when the disturbance in the horizontal component of the geomagnetic field changes from being positive to being negative. In the first pattern the aurora undergoes a distinct change in form and in the second it disappears at this time or recedes very far northward. The first pattern is more frequent than the second.

In the early part of the night the aurora is generally far north as seen from College and has quiet forms (arcs and glow). The luminosity advances slowly equatorwards. A positive magnetic bay is generally observed in this period. Close to the moment when a negative bay sets in, the aurora becomes active, moves southward and breaks up (first pattern) or disappears (second

pattern). In the first pattern of Heppner the recovery of the horizontal component takes place during the appearance of diffuse and pulsating aurora. In the majority of cases there is a short period following the negative bay in which the horizontal magnetic disturbance component is positive. A homogeneous arc is frequently formed again during this period.

A close correlation between rapid variations in the auroral luminosity and geomagnetic micropulsations has been found by Campbell and Nebel (1959), Campbell (1960 a,b,c), Campbell and Rees (1961) and Berger (1963) (see also Chapter).

3. Earth Currents

The occurrence during the day of induced voltages in long telegraph wires was used by Störmer in his extensive program for paralactic height measurements on aurora with good success for many years as a warning that aurora would occur in the next night. As the electric conductivity of the ground is generally not known with adequate precision it is difficult to relate the details of the induced electrical field and the resulting earth currents to the aurora in individual cases. The correlation of occurrence of the two phenomena is, however, good (cf. e.g. Hessler and Wescott, 1959). Freier (1961) has reported evidence for the accumulation of negative charges at the earth's surface during auroras, corresponding to an influx of negative charges into the upper atmosphere.

4. Radio Aurora

Reflections of radio waves of frequencies well above the critical frequencies of the ionosphere from ionization associated with aurora—radio aurora—were first investigated in 1938 by Harang and Stoffregen (1938, 1940). That radio wave propagation via auroral ionization is possible was, however, discovered earlier in the 1930's by amateur radio operators. After the second world war and particularly during the last ten years radio aurora has been studied by a number of researchers in North America, Britain, Norway, Sweden, Germany, Russia, New Zealand and the Antarctic. For a review of radio aurora with detailed references, see for instance Egeland (1962), Huitqvist and Egeland (1964) and Leadabrand (1964).

The diurnal variation of radio aurora as observed in the auroral zone has an afternoon maximum as well as a night maximum (Fig. 3.1). The seasonal variation in the auroral zone has maxima at the equinoxes. The long term occurrence frequency variation has its maximum about 2 years after the solar activity, as is the case with visual aurora.

Radio aurora is observed in the same general regions as optical aurora. With high power radars auroral type echoes can be recorded very often even in latitudes far from the auroral zones.

The reflection process has been found to take place in a fairly narrow height interval with mean value between 90 and 110 km, i.e. in the same height range as the lower border of visual aurora, by a large number of investigators. Also the motions of radio aurora correlate quite well with those of visible aurora, described in Section 2 (see p. 44). Fig. 3.2 shows an example of simultaneous recording of visual and radio aurora. As can be seen, there is a significant but not perfect correlation. The correlation is, however, good only at low elevation angles in a sector centered somewhere around geographic or geomagnetic north, in the northern hemisphere, and south in the southern hemisphere (cf. Fig. 3.3). Even extremely strong aurora overhead does not give any echoes at all.

The mentioned limitations of the regions in which auroral echoes are found is due to the fact that the reflection mechanism is aspect sensitive: reflections occur predominantly from a direction perpendicular to the magnetic field lines at the reflection point. This can be understood if the reflection mechanism is one of weak scattering from small irregularities strongly elongated along the lines of force, as well as if it is a critical reflection from larger magnetic-field-aligned irregularities. Recently it has been suggested that the irregularities may be ion sound waves (Buneman, 1963). The fine structure of the received echoes shows that a large number of reflecting centers are active at the same time.

As radio aurora has been observed for frequencies up to 2850 Mc/s (Groth et al., 1964) it seems most probable that weak scattering from small irregularities in the electron density distribution is the most important process at higher frequencies, whereas critical reflection—i.e. reflection

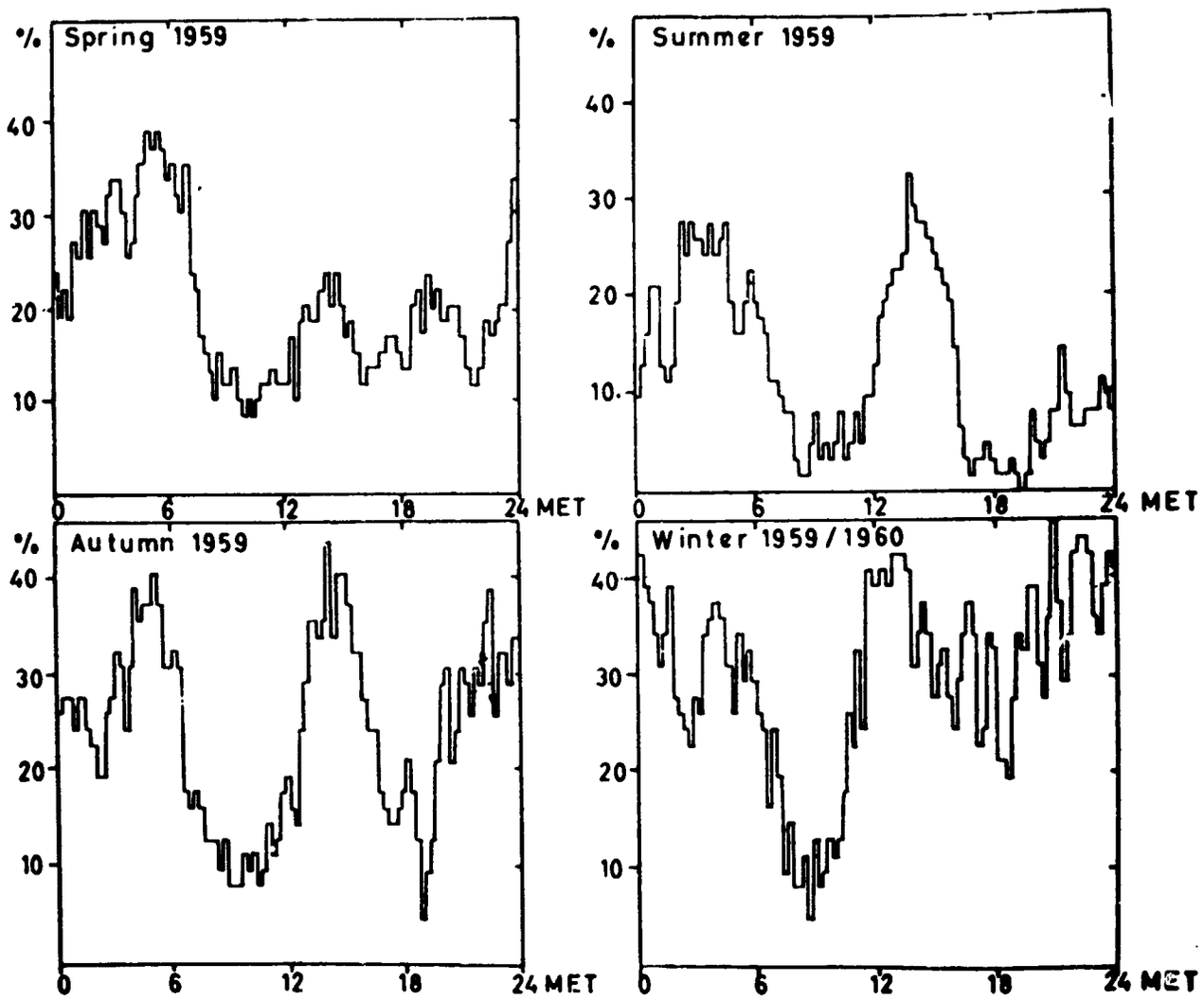

FIGURE 3.1.—Diurnal variation of the occurrence frequency for radio aurora at about 90 Mc/s, observed at Kiruna Sweden (geomagnetic latitude 65.3°). After Egeland (1962a).

from an electron density so large that the refractive index is zero—may be of importance in the lowermost part of the VHF band. How the irregularities are produced is far from clear. See the above mentioned review papers for more details.

5. Bremsstrahlung X-rays at Balloon Altitudes

In the auroral zone the probability of occurrence of x-rays has been found to be fairly well correlated to large scale magnetic activity. But the detailed correlation between aurora and precipitation of the energetic electrons, which generate bremsstrahlung, is in general quite poor there (cf. Anderson, 1960, 1962; Anderson and Enemark, 1960). It does, however, happen that auroral luminosity and x-ray flux follow each other extremely well (see Fig. 3.4, after Anderson and DeWitt, 1963). This seems to be fairly exceptional in auroral zone latitudes.

In subauroral latitudes strong x-ray events occur almost only during strong magnetic storms, and the correlation between the occurrence of visual aurora and bremsstrahlung at balloon heights is quite good (see the review by Winckler, 1962, for instance).

The balloon observations thus show that the high-energy electrons responsible for the bremsstrahlung production in general do not constitute the high energy tail of the electron spectrum producing the visible aurora in auroral zone latitudes, whereas they usually do in subauroral latitudes. The spectrum of the primary electrons is discussed in some more detail in Section 4.

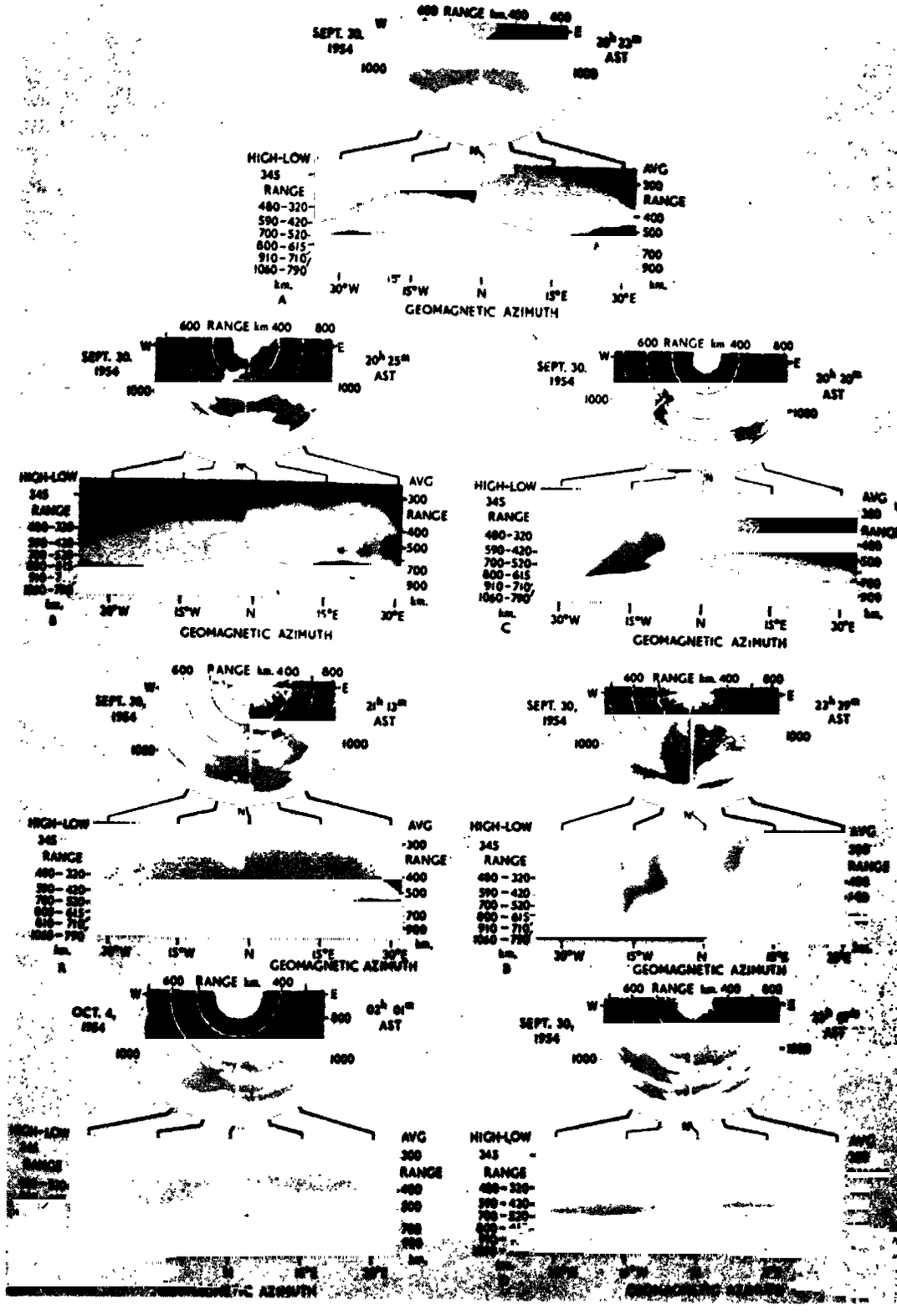

FIGURE 3.2.—Allsky-camera photographs of visible aurora compared with simultaneous 106 Mc/s radar echoes obtained at College, Alaska. After Bowles (1954).

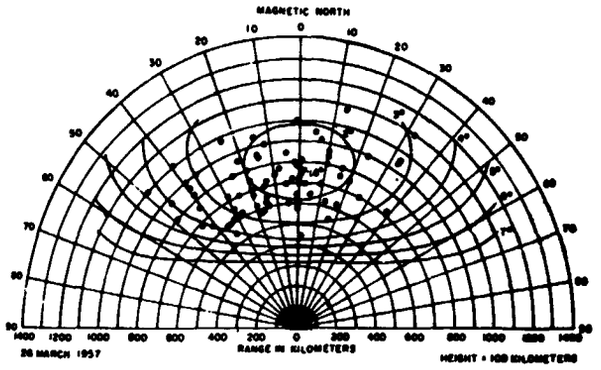

FIGURE 3.3.—Mass plot of 398/Mc/s echoes as a function of range and azimuth, College, Alaska, March 26, 1957. The points represent observations. The numbers attached to the various curves give the off-perpendicular angle with regard to the geomagnetic field lines at the reflection point. After Leadabrand, et al. (1959).

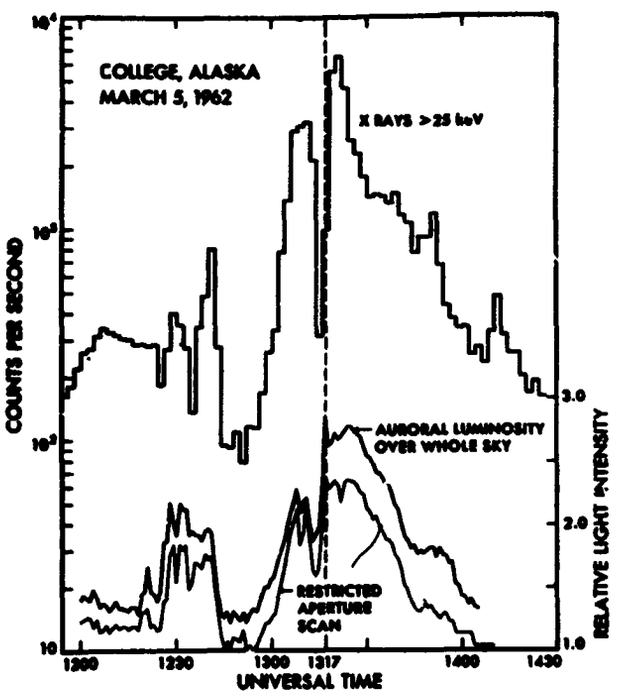

FIGURE 3.4.—Comparison of auroral luminosity obtained from allsky-camera pictures with x-ray flux at balloon altitude. After Anderson and DeWitt (1963).

6. Auroral Absorption

During aurora and magnetic storms the ionospheric absorption of radio waves recorded by means of riometers most often shows an irregular time structure. Although the period of absorption may last several hours, individual peaks often have durations of only a few minutes. Rates of increase and decrease may be as high as 3–2 db/minute, and the magnitude of the absorption can be 8–10 db at about 30 Mc/s for short periods. The character of the record differs definitely from that seen during SIDs or polar cap absorption events (PCA) (cf. Chapter). This type of absorption is usually called auroral absorption. Thus, the auroral absorption (AA) is defined as all absorption observed when there is no SID or PCA. It is then not surprising that Ansari (1963) has been able to show that AA consists of more than one type of absorption phenomenon, different with regard to the energy spectrum of the ionizing particles. One type, primarily occurring in the pre-breakup phase of aurora, is well correlated with the visual aurora (see also Gustafsson, 1964). It is limited approximately to the luminous forms and its intensity is generally fairly low ($\lesssim$1 db at about 30 Mc/s). During the break-up of the visual aurora the AA is intensified and is still mostly limited to the luminous forms.

After break-up, and practically only after magnetic midnight at College, strong fairly slowly varying absorption often occurs. It is sometimes associated with faint and diffuse aurora all over the sky, but there is no detailed correlation between light intensity and AA.

Even if there, thus, is a good statistical correlation between auroral absorption and visible aurora, bright coronas may appear without being associated with any measurable amount of absorption (see e.g. Kavadas, 1962). Ansari (1964) reported cases in which the absorption even decreased when an auroral form brightened up.

The auroral absorption has been found to have its maximum average value in a zone located a few latitude degrees further from the pole than the visual aurora (Gorbushina, 1962; Hartz, 1963; Holt, 1963; Basler, 1963).

The height where the auroral absorption takes place is a parameter of great importance for the understanding of the electron reactions in the lowermost ionosphere (see Hultqvist 1963b, 1964). The observation that the effect of sunrise and sunset on AA is much lower than expected on the basis of existing models (see e.g.Hultqvist,1963a) has been interpreted as indicating that all AA takes place above 90 km (Brown and Barcus, 1963). Such an interpretation is, however, in

contradiction with a large body of other experimental data (see Hultqvist, 1963b). Recent extensive multi-frequency riometer measurements (Little et al., 1963) which provide height information for the AA in the interval 35-75 km, have shown that in some 40 percent of 112 studied cases the height distribution of the absorption per km had its maximum at or below 72 km. In some 10 percent of the cases the peak was even at or below 60 km.

The multi-frequency riometer technique cannot tell about possible existence of appreciable AA in the *E*-layer in the presence of AA also below the *D*-layer, for instance. Analysis of recent satellite measurements of electron precipitation has shown that most of the auroral absorption in general is located between 60 and 90 km (Hultqvist 1964a, b) in good agreement with the riometer measurements mentioned. The satellite data show that AA is due mainly to electrons of energy above 40 kev, whereas the visual aurora is caused by electrons of energies between a few kev and a few ten kev (see the review by Hultqvist 1964c). This is illustrated by Figures 3.5 and 3.6.

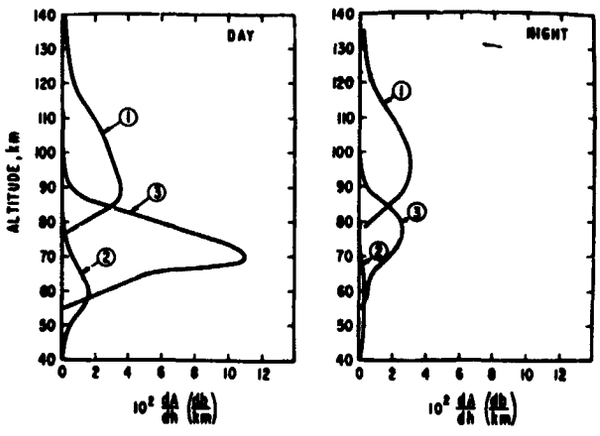

FIGURE 3.5. —Curves 1 show the height distribution of the absorption produced by the differential energy spectrum $N(E)=5.10^9\ e^{-E/5}$ electrons (cm² sec ster kev)$^{-1}$. The total absorption under the curve amounts to 1.04 db in the day and to 0.89 db at night. Curves 2 give the absorption due to the bremsstrahlung of the mentioned electron spectrum. Total absorption in the day is 0.27 db and in the night 0.061 db. Curves 3, finally, represent the absorption distribution produced by the differential energy spectrum $N(E)=7.10^4e^{-E/41}$ electrons (cm² sec kev)$^{-1}$ coming in along the field lines. Total daytime absorption is 1.9 db and the nighttime one is 0.52 db. After Hultqvist (1964a).

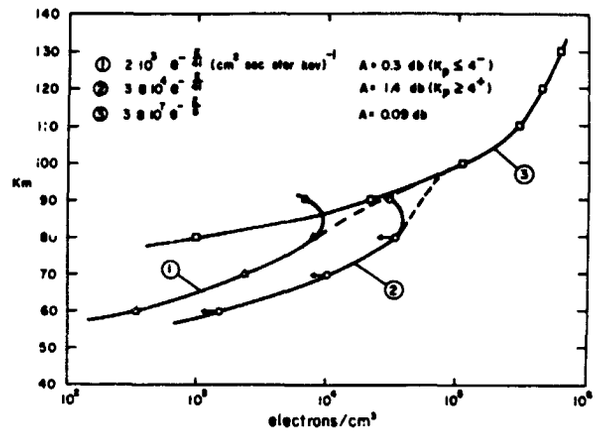

FIGURE 3.6.—Equilibrium electron density profiles due to three energy spectra of precipitated electrons. The spectra as well as the total absorption, A, at 27.6 Mc/s are given in the figure. Curve No. 2 gives an upper limit for the equilibrium electron density distribution produced by the spectrum $3.8\cdot10^4e^{-E/30}$ electrons (cm² sec ster kev)$^{-1}$ which is the equivalent spectrum for the average fluxes when $K_p>4$ as found by McDiarmid et al. (1963) a lower limit for this spectrum is curve No. 1. After Hultqvist (1964b).

Fig. 3.5 shows an estimation of the height distribution of the absorption produced by the primary electrons of a strong visible aurora of International Brightness Coefficient (IBC) between III and IV (curves nos. 1; spectrum of the electrons being that observed by McIlwain, 1960). The absorption due to the bremsstrahlung of those primary electrons (curves 2) and the absorption due to high energy electrons observed in the auroral zone with satellites by Mann et al. (1963) (curves 3). In Fig. 6 the equilibrium electron density profiles produced by the average precipitation fluxes of electrons in the auroral zone, as observed by means of the satellite Alouette (McDiarmid et al., 1963) and Injun 3 (O'Brien, 1964) are shown. For electrons of energy above 40 kev data are available for low ($K_p<4$) and high ($K_p>4$) magnetic activity. Curve 1 gives the average distribution for low magnetic activity, while curve 2 gives only an upper limit for the electron density profile when $K_p>4$. Curve 3 finally is due to the average electron flux in the energy range 1–40 kev.

The total absorption values computed from the satellite measured electron fluxes (0.3 db, <1.4 db, and 0.09 db for curves 1, 2, and 3, respectively) for the two ranges of magnetic activity are in quite

good accordance with the average absorption during the five most disturbed days and five most quiet days in each month, as observed over several years at College by Basler (1963). For the disturbed days he found a daily average of about 1 db in the summer and between 1 and 2 db in the winter and at equinoxes. This should be compared to the value $\sim$ 1 db of Fig. 3.6. For the quiet days the daily average observed by Basler was 0.3 db, which is identical to the value obtained from the satellite data.

The bremsstrahlung x-rays are most probably always negligible as compared to the primary electrons for producing AA (Ansari 1963, Hultqvist 1963, 1964, Brown, 1964).

The fluxes of the high-energy electrons causing AA and the low energy electrons producing aurora vary independently of each other. This explains the variable degree of correlation between aurora and AA. One can expect to observe aurora without AA and AA without aurora and all combinations in between. Ansari's (1963) results indicate that the electrons of energy above 40 kev are precipitated mainly after magnetic midnight. In the same way it is also understandable why auroral absorption has its maximum in the morning (Fig. 3.7), while aurora is most frequent in the middle of the night. The good correlation that has been found between AA and bremsstrahlung x-rays (see Brown, 1961, and Pfotzer et al., 1962, for instance) fits also well into the picture.

From the data presented above it seems reasonable to conclude that the absence of a significant influence of sunlight on the auroral absorption cannot be explained by the absorbing ionization being located, as a rule, above 90 km altitude.

For a discussion of other aspects of auroral absorption see e.g. the reviews of Ansari (1963), Holt (1963), and Hultqvist (1963c) and Chapter 0 of this book.

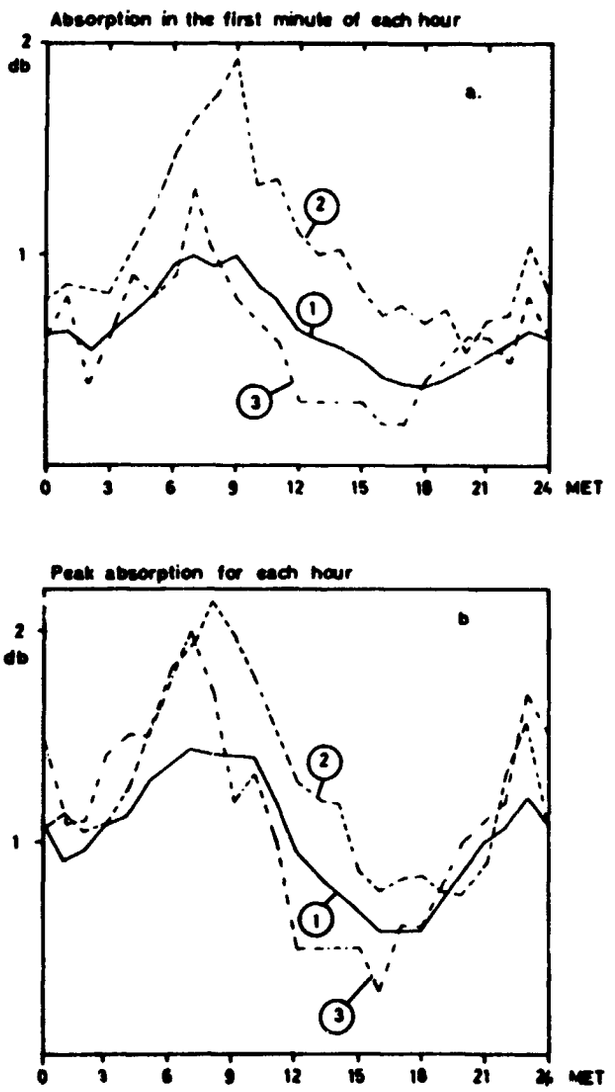

FIGURE 3.7.—Diurnal variation of the average intensity of 27.6 Mc/s cosmic noise absorption for the equinoxes at Kiruna. Months in which PCA's occurred are excluded. Curve 1 represents the average for the following months: April 1959, September 1959, October 1959, March 1960, October 1960, March 1961, April 1961, September 1961, and October 1961. Curve 2 is for September 1961 alone and curve 3 for September 1959. After Hultqvist (1963a).

7. Other Ionospheric Disturbances Associated with Aurora

The first phase of an auroral situation in the ionosphere is usually characterized by increasing height of the $F2$-layer. In about 100–110 km height an auroral sporadic E-layer is formed, which is quite similar to the daytime E-layer but has greater vertical extension. The critical frequency of this layer may rise up to 7–8 Mc/s and has usually well pronounced ordinary and extraordinary components. Multiple reflections are quite common, thus little absorption below this layer is often observed. In the second phase more absorption takes place, the minimum frequency of the E-layer increases and less multiples are recorded. Auroral forms with ray structure is often seen at this time. The third phase is characterized by high absorption of radio-waves,

often resulting in black-out and strong aurora with ray-structure (after Stoffregen, 1958).

During the second and third phases low-frequency reflections are often observed at abnormally low altitudes of down to 60 km (Stoffregen, 1958; Stoffregen et al., 1960; Gregory, 1961; Pedersen, 1962; and others.)

Only few detailed studies of the correlation between visual aurora and sporadic *E* in the auroral zones have been reported (Heppner et al., 1952; Knecht, 1956; Hunsucker and Owren, 1962). The most recent one is that of Hunsucker and Owren. They compared auroral type sporadic-*E* recorded with ionosondes in Alaska during the IGY with simultaneous allsky camera observations and other data for times of auroral activity. They found a high correlation between zenithal aurora and the critical frequency of the sporadic-*E* layer (*fEs*). From detailed studies of simultaneous visual aurora and ionospheric sounding data Hunsucker and Owren drew the following conclusions:

The motion of an auroral arc or band from a low elevation angle to a position near the zenith is accompanied by an increase in the value of *fEs*.

fEs is more than two times as great when there is aurora in the zenith as when there is not.

The highest value of *fEs* is observed when an auroral arc or band is present at the astronomical zenith (not the magnetic zenith).

A general survey of existing knowledge concerning sporadic-*E* phenomena of all kinds can be found in the paper by Thomas and Smith (1959). For other ionospheric disturbance effects associated with aurora, see Chapter 0.

8. Scintillation of Radio Waves from Radio Stars and Satellites

Although no statistical studies of the correlation between auroral occurrence and scintillation of radio-waves from point sources outside the ionosphere have been made, it can be said that a good correlation certainly exists. A correlation exists namely between scintillation and geomagnetic activity (cf. e.g. Little et al. 1962, and Liszka, 1963), as well as between occurrence of visual aurora and geomagnetic activity (see above) and a few detailed studies of situations in which the radio waves have propagated through an observed visual aurora have shown that the scintillation is higher when the waves pass through the aurora than when they do not. This has been found both for ordinary aurora (Little and Maxwell, 1952a; Benson 1960; Morcroft and Forsyth) and for the subauroral-latitude red arcs (Roach, 1963).

9. Radio-Noise Emission

There is some evidence for VHF radio noise being emitted by the auroral primary electrons. The situation is still somewhat unclear. If the reported emissions are of auroral origin, a strong solar cycle variation in their occurrence frequency seems to exist. Observations have been reported only for solar activity maximum. Leadabrand (1964) has given a review of published observational results. Synchrotron radiation from the auroral primaries seems to be a possible mechanism of generation (Hower, 1963).

Whereas, thus, the association of aurora with significant VHF noise emission still must be considered as somewhat doubtful or at least as of rare occurrence, observational results showing a close relationship between visual aurora and a type of very-low-frequency noise emissions, the so-called auroral hiss, have recently appeared. Hiss differs from the other types of VLF emissions in that discrete emissions are not distinguishable in the emission spectra. A class of hiss known as "auroral hiss" has been shown to be closely associated with the occurrence of aurora on the basis of ground observations (Martin and Helliwell, 1960; Jörgensen and Ungstrup, 1962; Morozumi, 1962) although VLF hiss emission is sometimes undetectable on the ground even in the presence of an intense and active aurora. Morozumi (1963) has found that VLF hiss usually occurs in the prebreakup phase of aurora and is well correlated with homogeneous auroral arcs and bands. He observed, however, also that intense auroral hiss sometimes occurs unaccompanied by auroras. Fig. 3.8 shows simultaneous records of VLF noise, visual emission, and precipitated electrons obtained on board Injun 3 (Gurnett and O'Brien, 1964). The agreement between the time functions of the various variables is quite good. The satellite was between 250 and 350 km while the records in Fig. 3.8 were taken. The photometer was looking along the field lines, and the measured electrons were on their way down into the atmosphere. The antenna on the satellite received the

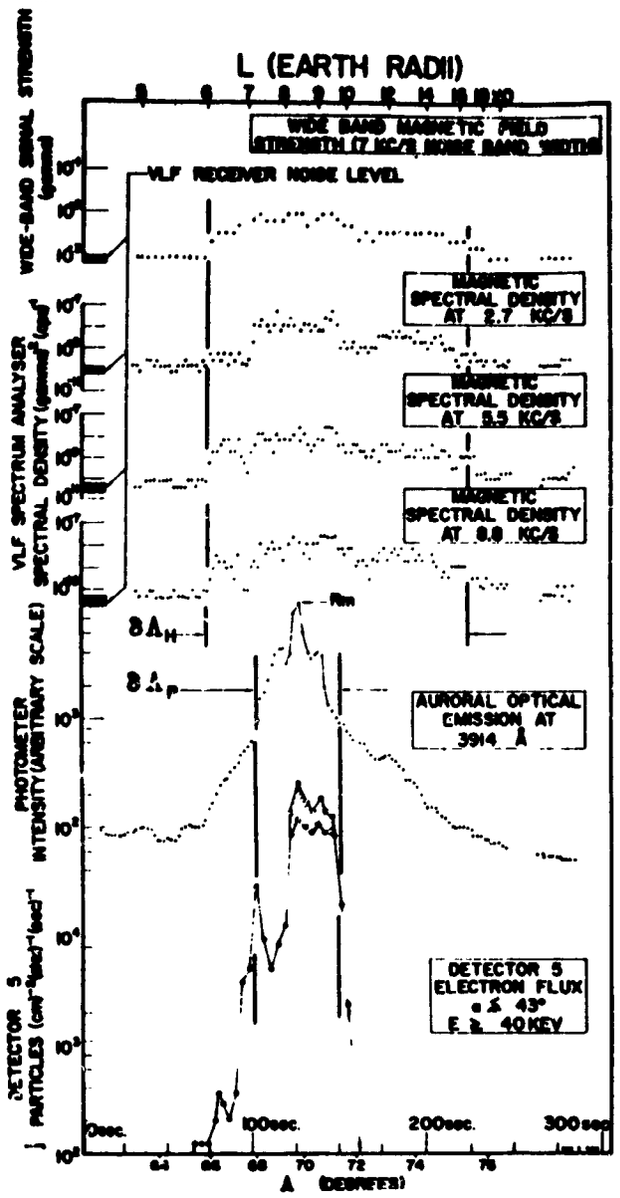

FIGURE 3.8.—A simultaneous observation of VLF electromagnetic emission, auroral luminosity and precipitated electrons on board Injun 3 on March 3, 1963, 0720-0725 UT. After Gurnett and O'Brien (1963).

VLF magnetic component perpendicular to the geomagnetic lines of force. The emission spectrum of the auroral hiss record in Fig. 3.8 is essentially a flat noise spectrum starting below 2.7 kc/s and extending above 8.8 kc/s. The Injun 3 measurements suggest that, at least sometimes, the same precipitated electrons cause both visual aurora and VLF hiss emission.

10. Auroral "Sound"

A large number of reports of aural observations of sound in connection with aurora exist. A review has recently been presented by Campbell and Young (1963). According to these reports, some of which have been given by experienced auroral researchers, a sound is heard in a few per cent of the active auroras, mainly in the years of maximum in the eleven-year solar activity cycle. The sounds are said to be at the upper frequency limit of the observers' auditory response.

Chapman (1931, 1932) has pointed out that the mean free path in the height interval where aurora occurs is too large compared with the wave length of sound waves in the audible frequency range, for transmission down to the earth's surface to be possible. The aurora has to reach down below 65 km for the sound waves to be able to propagate to the earth's surface. But if this occurred, the variations in luminous and acoustic intensity could not be simultaneous, as has been reported, because of the low sound propagation velocity (unless the aurora extended to the ground level). It seems probable that the reported acoustic effects are due to the electric fields that are induced in any suspended wire connected to the earth by the geomagnetic variations associated with strong auroras, as proposed by Harang (1951), Störmer (1955) and others. During very strong auroras these voltages may be of sufficient magnitude to produce discharges.

For infrasonic waves in the period range 10–110 seconds the ratio of wavelength to mean free path is large, and propagation to the ground from the auroral altitudes is physically possible. Such waves have also been observed (Chrzanowski et al., 1961, 1962). Maeda and Watanabe (1964) have pointed out that auroral activity is expected to be associated with the appearance of infrasonic waves due to periodic heating of the ionosphere by the primary auroral particles. Such correlation was found by Campbell and Young (1963) in Alaska, where they observed that every night of bright visual aurora, or ionospheric evidence of aurora, was associated with 10–110-sec-period pressure oscillations of about 1 to 10 dynes/cm^2 amplitude. Nights of no auroral activity showed no infrasonic effects.

4. DIRECT OBSERVATIONS OF ENERGETIC PARTICLES ASSOCIATED WITH AURORA

1. Introduction

The first definite observational evidence for fast charged particles entering the earth's upper atmosphere along the geomagnetic field lines was obtained from a spectrogram taken by Meinel (1950a, b, 1951). He pointed his instrument toward the magnetic zenith during a strong aurora and obtained an $H\alpha$ profile that was shifted—as well as broadened—with its peak corresponding to a doppler velocity of roughly 500 km/sec, but the short wavelength tail of the profile extended to more than 2000 km/sec. In the direction of the magnetic horizon the profile was not shifted but only broadened to about 500 km/sec on either side of the center. The broadening on the red side arises probably in part from scattering of light from other parts of the sky and in part from motions of protons away from the observer. The latter may be due to many small-angle scatterings of protons that initially were moving nearly perpendicularly to the magnetic field.

Proton fluxes as high as 10^8 $(cm^2\ sec)^{-1}$ with velocities below 500 km/sec have been deduced from spectroscopic measurements (Malville, 1960). That proton velocities much above 2000 km/sec have not been observed, does not mean that higher velocities do not exist in the incoming proton beam. The observed limit is due to the effect that much more rapid protons cannot take up electrons to form neutral hydrogen atoms which then can emit the hydrogen lines on its continued way.

In this section will be given a brief review of some recent direct measurements of particles related to aurora which have been made by means of balloon-, rocket-, and satellite-borne instruments.

2. Observed Fluxes and Energy Spectra of Electrons Precipitated Into the Upper Atmosphere

In the summer of 1953 a group from the State University of Iowa when carrying out a program for study of the low-energy end of the primary cosmic-ray spectrum recorded an anomalous soft radiation by means of rockoons launched from a ship west of Greenland (Meredith et al., 1955). The radiation was identified as x-rays of energy 10–100 kev. Some two dozen rockoon launchings at various latitudes showed that the latitude dependence of the radiation intensity was very similar to that for the occurence of visual aurora (Van Allen, 1957).

X-rays directly coincident with auroras were first observed at balloon levels in 1957 (Winckler et al., 1958). A few rockets were launched through visible auroral forms in 1958 (Davis et al., 1960; and McIlwain, 1960). The first proof that electrons are precipitated into the atmosphere from altitudes of 1000 km or more was obtained from Sputnik 3 in a period of about one minute on May 15, 1958, by Krasovskii et al. (1962). A number of reports of measurements on electrons precipitated into the atmosphere have been collected in Table 1. Nos. 1–3 are rocket measurements, no. 4 refers to the rockoon results of the Iowa group, nos. 5–9 are measurements obtained by means of balloons (only x-ray maesurements for which the existence, or nonexistence, and characteristics of visual aurora in the period of measurement have been reported are included in Table 1), nos. 10–21, finally are satellite results.

The early rocket measurements (Davis et al., 1060; McIlwain, 1960) as well as the satellite results (e.g., O'Brien, 1962a, 1964) have verified the conclusions of Omholt (1957, 1959) based on spectroscopic observations of aurora that the protons play a very minor role in the excitation of most auroras.

The first somewhat detailed satellite studies of particles that were definitely precipitated into the atmosphere were made by means of Injun 1 (O'Brien, 1962a, b). O'Brien and others working with satellite data define precipitated particles as such which would mirror at or below 100 km altitude (if the atmosphere had not been present). The satellite results have also shown that electrons on the average carry much more of the energy to the lower ionosphere than do protons (O'Brien, 1962b).

(a) Latitudinal Distribution and Other Spatial Characteristics

The recent simultaneous measurements on Injun 3 (O'Brien and Taylor, 1964) of flux of precipitated electrons and of auroral light emission below the satellite have shown that above auroras there are electron fluxes several orders of

TABLE 1.—*Precipitated Electrons*

No.	Reference	Flux (above the atmosphere)		Spectrum or energy range	Time of obs.	Place of observat. geomagn. lat.	Visible aurora		Magn. disturb.	Radio-wave absorpt.	Method of measur.	Remarks
		Number of particles	Energy				Intens.	Location with regard to part. measurement				
1a	Davis et al. (1960)	$N(E \geq 10$ kev$) = \geq -6 \cdot 10^7$ (cm^2 sec ster)$^{-1}$	0.5 –2.5 erg (cm^2 sec ster)$^{-1}$ 8 kev $<E<100$	$N(>E) \propto E^{-1}$ for 5 kev $<E<50$ kev	Jan. 26, 1958 0421 UT	Churchill, A = 68.8°N	Fading rayed structure and const. diffuse surface of IBC ~1; after break-up.	Passed through rayed structure during ascent, and through diffuse surface on both ways. Peak altit. 178 km.			Rocket scintill	Protons present. El. flux isotropic within ±15% between magn. zenith angles 9° and 81°
1b	Davis et al. (1960)		<0.01 erg (cm^2 sec ster)$^{-1}$	8 kev $<E<$ 100 kev	Mar. 16, 1958 0454 UT	Churchill, A = 68.8°N		No penetrat. Weak arc moved to the north.			Rocket scintill.	Protons present.
1c	Davis et al. (1960)		<0.06 erg (cm^2 sec ster)$^{-1}$	8 kev $<E<$ 100 kev	Mar. 22, 1958 0641 UT	Churchill, A = 68.8°N		No penetrat. Fading arc moved to south.			Rocket scintill.	Protons present.
1d	Davis et al. (1960)		<0.02 erg (cm^2 sec ster)$^{-1}$	8 kev $<E<$ 100 kev	Nov. 16, 1958 0658 UT	Churchill, A = 68.8°N		No penetrat. Bright arc just to the north.			Rocket scintill.	Protons present.
1e	Davis et al. (1960)	$<10^9$ (cm^2 sec ster)$^{-1}$ 30 ev $<E<$ 1000 ev			During 1a, b, c, d	Churchill, A = 68.8°N						
2a	McIlwain (1960)	$N(>3$ kev$) = 2.1.10^8$ (cm^2 sec ster)$^{-1}$*	1.7 erg (cm^2 sec ster)$^{-1}$ $E>3$ kev	$N(>E) = 3.9 \cdot 10^{6}$* exp ($-E/5$ kev) electrons (cm^2 sec ster)$^{-1}$	Feb. 22, 1958 0537 UT	Churchill, A = 68.8°N	Faint glow	Passed through the aurora. Peak altitude 120 km.			Rocket scintill.	Protons present.
2b	McIlwain (1960)	$N(E=6$ kev$) = 5.10^{10}$ (cm^2 sec ster)$^{-1}$	2000 erg cm^{-2} sec^{-1}	Approx. mono-energetic $E=6$ kev	Feb. 25, 1958 0551 UT	Churchill, A = 68.8°N	Bright arc; after break-up	Passed through the aurora. Peak altitude 120 km.	$\Delta X > 1000\gamma$		Rocket scintill.	No protons present.
3	McDiarmid et al. (1962)	$\leq 2.10^5$cm^{-2}sec^{-1} for $E>30$ kev		$N(>E) \propto \exp$ ($-E/22$ kev) $E>30$ kev	Oct. 28, 1960 1223 UT (about sunrise)	Churchill, A = 68.8°N			$\Delta Z > 1000$ before and after	~3 db (30 Mc/s)	Rocket GM-tube.	Protons present. El. flux very irregular. Peak alt. 150 km.
4	Van Allen (1957)	$10^3 - 10^4$ cm^{-2} sec^{-1}	0.01 –1 erg/cm^2 sec^1	10 –100 kev	Summers of 1953–1955	A = 54 –88°					Rockoons	Lat. dep. as for visual aurora.

TABLE 1.—*Precipitated Electrons—Continued*

No.	Reference	Flux (above the atmosphere)		Spectrum or energy range	Time of obs.	Place of observat. geomagn. lat.	Visible aurora		Magn. disturb.	Radio-wave absorpt.	Method of measur.	Remarks
		Number of particles	Energy				Intens.	Location with regard to part. measurement				
5	Anderson & Enemark (1960)	$\leq 2.10^8$ cm^{-2} sec^{-1} for E > 25 kev 10^9 cm^{-2} sec^{-1} for E > 25 kev	0.1 erg cm^{-2} sec^{-1} for E > 25 kev	$N(>E) \propto e^{-E/8}$ for E > 25 kev	Aug. 18, 1959 0745 UT	Churchill, A = 68.8°N	Strong active auroral forms overhead		$\Delta Z = -250\gamma$	≤ 1.5 db at 30 Mc/s	Balloon x-rays	X-rays present 40% of time. Poor correl. with visible aurora. Time average over days.
6	Winckler (1960)	8.10^9 cm^{-2} sec^{-1} for E > 40 kev			Sep. 23, 1957 1050 UT	Minneapolis A = 55°N	Very strong ray structure at 30° elevation		Weak dist. (during recovery phase of storm)		Balloon x-rays	
7	Bhavsor (1962)	$\leq 10^9$ cm^{-2} sec^{-1} for E > 22 kev		$N(>E) = 0.66.10^{15}$. E^{-4} cm^{-2} sec^{-1} for E > 22 kev	May 12, 1959	Minneapolis A = 55°N	Strong overhead aurora				Balloon x-rays	
8	Anderson (1962)	$\leq 10^7$ cm^{-2} sec^{-1} for E > 25 kev			Mar. 27-28, 1961 1100 UT	Fairbanks A = 64.5°N	No apprec. visual aurora				Balloon x-rays	No correl. visual aurora x-rays.
9	Anderson & DeWitt (1963)	5.10^7 cm^{-2} sec^{-1} for E > 25 kev	3 erg cm^{-2} sec^{-1}	$N(>E) = E^{-4}$	Mar. 5, 1962 1320 UT	Fairbanks A = 64.5°N	Strong glow over entire sky; aver. int. ~60 kR			~6 db (riometer)	Balloon x-rays	Very good correl. visual aurora x-rays
10	Krasovskii et al. (1962)		10^{-3} to > 20 erg/cm^2 sec ster	Equivalent energy most often 14 kev	1958	Over a very wide latitude range					Sputnik 3	Neither energy flux nor spectrum depend significantly on pitch angle.
11	O'Brien (1962a)	Aver. 10^8 (cm^2 sec ster)$^{-1}$ for E > 40 kev	$\geq 0.6.10^{-3}$ erg (cm^2 sec ster)$^{-1}$ for E > 40 kev		June 30–July 2, 1961	L = 2 –10			$K_p = 0 - 4$ No correl. with magn. act.		Injun 1, 12 passes during period of rapid spin	Occurs more on day side than on night side; uncorrel. with lat. and long. of observ.
12	O'Brien & Laughlin (1962)	6.10^7 (cm^2 sec ster)$^{-1}$ for E > 40 kev [10^{10} (cm^2 sec ster)$^{-1}$ for E > 10 kev]	400 erg (cm^2 sec ster)$^{-1}$ for E > 1 kev	$N(E) \propto E^{-4}$ for E > 10 kev	Sep. 25, 1961 2237:10 UT LT 1835	Lat. 59.0° Long. 303° L 8.82 Alt. 1011 km			Magn. disturbance		Injun I	Measured part. were not precip. but there is evidence that electron flux was isotropic.
		3.10^9 (cm^2 sec ster)$^{-1}$ for E > 40 kev [6.10^{10} (cm^2 sec ster)$^{-1}$ for E > 0]		$N(E) \propto \exp(-E/6)$ Very rapid variat. in spectrum	Sep. 25, 1961 2236:25 UT LT 1835	Lat. 57.3 Log 300° L 8.04 Act. 1011 km						

TABLE 1.—*Precipitated Electrons—Continued*

No.	Reference	Flux (above the atmosphere)		Spectrum or energy range	Time of obs.	Place of observat. geomagn. lat.	Visible aurora		Magn. disturb.	Radio-wave absorpt.	Method of measur.	Remarks
		Number of particles	Energy				Intens.	Location with regard to part. measurement				
13	O'Brien (1962b)	4.10^3 (cm² sec ster)$^{-1}$ 8.10^3 (cm² sec ster)$^{-1}$ 4.10^4 (cm² sec ster)$^{-1}$ 10^5 (cm² sec ster)$^{-1}$ 7.10^4 (cm² sec ster)$^{-1}$ 6.10^4 (cm² sec ster)$^{-1}$		E > 40 kev	June 29–Sep. 6, 1961	$\cos^{-1}(L^{-1/3})$ = 45–50° 50–55° 55–60° 60–65° 65–70° 70–75°					Injun I	Aver. intens. at 1000 km altitude. Only order of magnitude significant.
14	O'Brien et al. (1962)	3.10^3 (cm² sec ster)$^{-1}$ for E > 40 kev	~1 erg (cm² sec ster)$^{-1}$ for E > 40 kev	$N(E) \propto E^{-3}$	July 21, 1961 ~1600 UT	L ~ 5.3					Injun I	
		[$\sim 10^5$ (cm² sec ster)$^{-1}$ for E > 5 kev]	~9 erg (cm² sec ster)$^{-1}$ 1 kev < E < 40 kev	$N(E) \propto E^{-3}$							Injun I	
15	Mann et al. (1963)	$4 \cdot 10^3$ (cm² sec ster)$^{-1}$ for 80 < E < 106 kev		$N(E) \propto \exp(-E/5$ kev)	1500 UT Sep. 1—0130 UT Sep. 2, 1961	1/4 to 1/3 of a great circle; in high latitudes			Correl. with magn. disturb.		Discoverer 29 magnetic el. spectromet.	Polor orbit with altitude varying between 160 and 610 km. Directional measurements along radius vector from earths center.
		$2 \cdot 10^3$ (cm² sec ster)$^{-1}$ for E > 80 kev		Two groups of spectra: $N(E) \propto \exp(-E/25 \pm 5)$ and $N(E) \propto \exp(-E/42 \pm 3)$	Aug. 30–Sep. 3, 1961	In the auroral zones			Correl. with magn. disturb.		Discoverer 29 magnetic el. spectromet.	
16	Stilwell (1963)	$\sim 10^3$ (cm² sec ster)$^{-1}$ for E > 10 kev	~2 erg (cm² sec ster)$^{-1}$ for E > 10 kev	$N(E) \propto \exp(-E/4)$ E > 10 kev Mean energy < 10 kev	Mar. 3, 1963 0721 UT LT-2220	L = 8 – 10	~20kR of γ3914Å	Along the field line the satell. is on			Injun 3 Rev. 994	Angular distrib. isotropic

TABLE 1.—*Precipitated E[illegible]s—Continued*

No.	Reference	Flux above the atmosphere		Spectrum or energy range	Time of obs.	Place of observat. geomagn. lat.	Visible aurora		Magn. disturb.	Radio-wave absorpt.	Method of measur.	Remarks
		Number of particles	Energy				Intens.	Location with regard to part. measurement				
17	McDiarmid et al. (1963)	$3 \cdot 10^8$ (cm² sec ster)$^{-1}$ for E > 40 kev	Aver. value correspond to exponential equival. mean spectrum at A = 65°	Equiv. mean spectrum at A = 65° $N(E) = 2.10^8 \cdot e^{-E/kT}$ el (cm² sec ster kev)$^{-1}$ or	Oct. 1962–Jan. 1963	Invariant lat. A = 65°			$K_p \leq 4^-$		Alouette	Average values at peak of latitude distribution.
		$1.9 \cdot 10^8$ (cm² sec ster)$^{-1}$ for E > 250 kev	0.03 erg (cm² sec)$^{-1}$	$N(E) = 8 \cdot 10^8 E^{-2.8}$ el (cm² sec ster)$^{-1}$ for 40 < E < 250 kev)	Oct. 1962–Jan. 1963	Invariant lat. A = 60°			$K_p \leq 4^-$		Alouette	Average values at peak of latitude distribution.
		$3 \cdot 10^8$ (cm² sec ster)$^{-1}$ for E > 40 kev	Aver. value correspond to exponential equival. mean spectrum at A = 65°	Equiv. mean spectrum at A = 65° $N(>E) = 4 \cdot 10^4 e^{-E/38}$ el (cm² sec ster kev)$^{-1}$ or	Oct. 1962–Jan. 1963	Invariant lat. A = 65°			$K_p > 4^+$		Alouette	Average values at peak of latitude distribution.
		$2.6 \cdot 10^8$ (cm² sec ster)$^{-1}$ for E > 250 kev	0.3 erg (cm² sec)$^{-1}$	$N(>E) = 4.4 \cdot 10^{11} \cdot E^{-3.0}$ el (cm² sec ster)$^{-1}$ (for 40 < E < 250 kev)	Oct. 1962–Jan. 1963	Invariant lat. A = 60°			$K_p \geq 4^+$		Alouette	Average values at peak of latitude distribution.
18	O'Brien (1964) O'Brien and Taylor (1964)	Average: $4 \cdot 10^8$ cm^{-2} sec^{-1} for E > 40 kev	Average: 4 erg cm^{-2} sec^{-1} for E > 1 kev	Equiv. mean spectrum at A = 65° $N(E) = 7.8 \cdot 10^7 e^{-E/5.7}$ el (cm² sec kev)$^{-1}$ or $N(>E) = 1.4 \cdot 10^8 E^{-2.3}$ el. cm^{-2} sec^{-1} (for 1 < E < 40 kev)	First months of 1963	Invariant lat. A ~ 65°	$2\binom{+4}{-1.5}$ kR	On the same field line where the port. were measured			Injun 3	Average values at peak of latitude distribution. 100–1000 times less at subauroral lat. Variations of a factor of 10^3 in auroral zone.
19a	Sharp et al. (1964a)	Max. 10^8 el/cm² sec ster above 2 kev		$N(E) \propto e^{-E/a}$ in burst	March 1, 1962 10:40 UT	Over Alaska		Homogeneous arc			Total energy scint. detect on board a short-lived polar orbiting satellite.	Very little contribution from protons to energy flux
19b	Sharp et al. (1964b)	Max $8 \cdot 10^9$ el/cm² sec ster above 2 kev	Max. ~100 ergs/cm² sec ster above 2 kev	$N(E) \propto e^{-E/E_0}$ with $E_0 = 4 - 9$ kev	March 2, 1962 0918 UT	Over Alaska		Auroral arc				
19c	Sharp et al. (1964b)		Max. ~100 ergs/cm² sec ster above 2	$N(E) \propto e^{-E/E_0}$ with $E_0 = 3 - 5$ kev	March 2, 1962 1048 UT	Over Alaska					"	Very little contribution from protons to energy flux

TABLE 1.—*Precipitated Electrons—Continued*

No.	Reference	Flux (above the atmosphere)		Spectrum or energy range	Time of obs.	Place of observat. geomagn. lat.	Visible aurora		Magn. disturb.	Radio-wave absorpt.	Method of measur.	Remarks
		Number of particles	Energy				Intens.	Location with regard to part. measurement				
20a	Sharp et al. (1964c)		0.60 erg/cm² sec ster above 0.18 kev 0.035 erg/cm² sec ster above 10 kev 0.0087 erg/cm² sec ster above 31 kev	$N(E) \propto e^{-E/E_0}$ with E_0=2.2 kev between 0.18 and 10 kev	May 1963 LT~05	61.3°N 124.9°W geographic coord.					Total energy scint. detector and electrostatic retard. detector with postacceleration on board a short-lived polar orbiting satellite.	"Typical Orbits"
20b	Sharp et al. (1964c)		0.83 erg/cm² sec above 0.18 kev 0.065 erg/cm² sec ster above 10 kev	E_0=2.4 kev between 0.18 and 10 kev	May 1963 LT~05	65.3°N 141.3°W geographic coord.					"	"Typical Orbits"
20c	Sharp et al. (1964c)		0.21 erg cm² sec ster above 0.18 kev 0.084 erg/cm² sec ster above 10 kev	E_0=4.9 kev between 0.18 and 10 kev	May 1963 LT~05	68.7°N 156.5°W geographic coord.					"	"Typical Orbits"
20d	Sharp et al. (1964c)		0.34 erg/cm² sec ster above 0.18 kev 0.096 erg/cm² sec ster above 10 kev	E_0=4.0 kev between 0.18 and 10 kev	May 1963 LT~05	62.3°N 131.4°W geographic coord.					"	"Typical Orbits"
21a	Sharp et al. (1964c)		4.4 ergs/cm² sec ster above 0.080 kev 4.4 ergs/cm² sec ster above 1.5 kev 0.25 erg/cm² sec ster above 21 kev	E_0=4.6 kev between 1.5 and 21 kev Cutoff above 1.5 kev	2 Nov 1963 ~20 UT	60.5°S 76.4°E geographic coord.					"	Sample of a "representative orbit."

TABLE 1.—*Precipitated Electrons—Continued*

No.	Reference	Flux (above the atmosphere)		Spectrum or energy range	Time of obs.	Place of observat. geomagn. lat.	Visible aurora		Magn. disturb.	Radio-wave absorpt.	Method of measur.	Remarks
		Number of particles	Energy				Intens.	Location with regard to part. measurement				
21b	Sharp et al. (1964c)		1.1 erg/cm² sec ster above 0.080 kev 1.1 erg/cm² sec ster above 1.5 kev 0.04 erg/cm² sec ster above 21 kev	E_0 =4.1 kev between 1.5 and 21 kev Cutoff above 1.5 kev	2 Nov. 1963 ~20 UT	54.5°S 76.1°E geographic coord.					Total energy scint. detector and electrostatic retard detector with postacceleration on board a short-lived polar orbiting satellite.	Sample of a "representative orbit."
21c	Sharp et al. (1964c)		1.2 erg/cm² sec ster above 0.080 kev 1.2 erg/cm² sec ster above 1.5 kev 0.86 erg/cm² sec ster above 21 kev	E_0 =20 kev between 1.5 and 21 kev Cutoff above 1.5 kev	2 Nov. 1963 ~20 UT	71.5°N 68.6° E geographic coord.					"	Sample of a "representative orbit."
21d	Sharp et al. (1964c)		0.63 erg/cm² sec ster above 0.080 kev 0.45 erg/cm² sec ster above 1.5 kev 0.44 erg/cm² sec ster above 21 kev	E_0 =95 kev between 1.5 and 21 kev	2 Nov. 1963 ~20 UT	62.1°N 114 7°W geographic coord.					"	Sample of a "representative orbit."

*This value is obtained from the energy flux value in the way described by McIlwain (196C). It is, however, a factor of about 2π smaller than the value given by McIlwain himself.

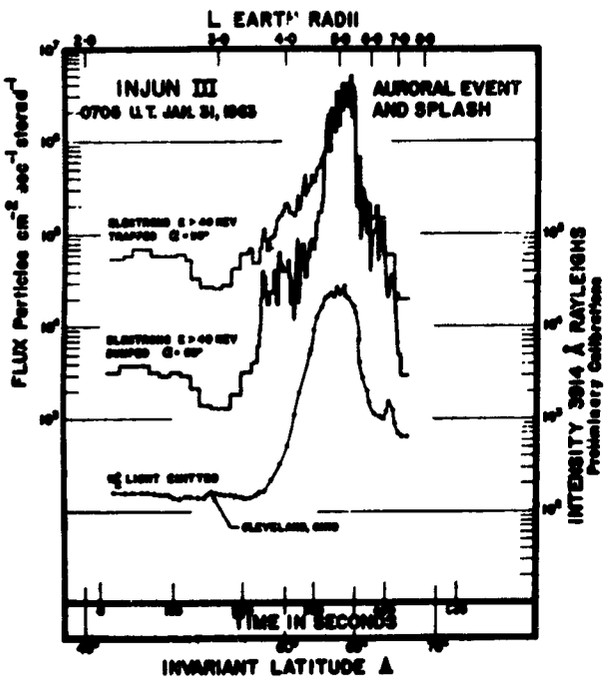

FIGURE 4.1.—Data from a northbound pass of Injun 3 over North America, which shows simultaneous detection of an aurora, of the precipitated electrons (pitch angle ~50°) partially responsible for causing it, and of trapped electrons. Note the approach to isotropy of the particle flux over the aurora. No attempt has been made to subtract the low-latitude contamination of the photometer signal, part of which was the detection of Cleveland, Ohio, and its surrounds. (After O'Brien and Taylor, 1964.)

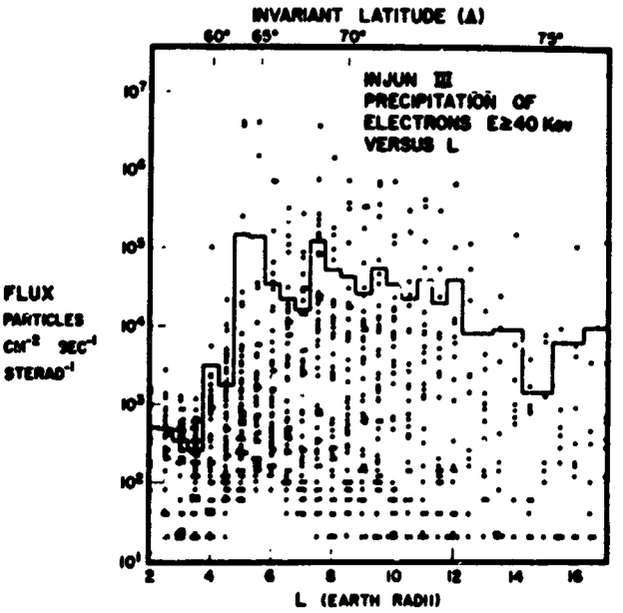

FIGURE 4.2.—Samples of precipitated fluxes over North America in January 1963. Each point is an 8-sec average of thirty-two measurements made at half-integral values of L. The solid line gives the average flux. (After O'Brien, 1964.)

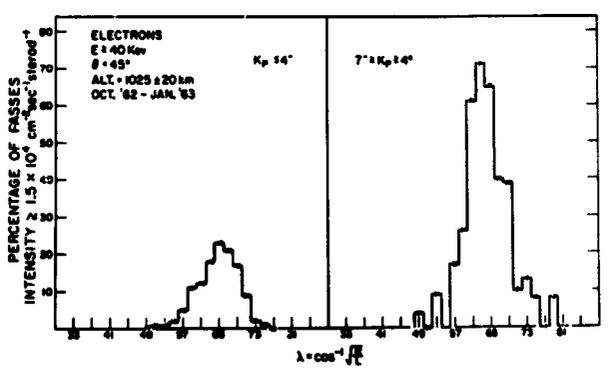

FIGURE 4.3.—Percentage of passes in which the intensity of precipitated electrons with energies greater than 40 kev is greater than 1.5 x 10^4 cm^{-2} sec^{-1} plotted against invariant latitude. (After McDiarmid et al., 1963.)

magnitude larger than outside the aurora (see Fig. 4.1).

Fairly extensive statistical data on the spatial characteristics of precipitated electrons have recently been published by O'Brien (1962a, b, 1964) and McDiarmid et al. (1963). Fig. 4.2 shows the scatter diagram of the Injun 3 observations of precipitated electrons of energy above 40 kev for the range of the invariant latitude Λ (defined by $\Lambda = \cos^{-1}(1/L)^{1/2}$ and at the most a few degrees different from geomagnetic latitude in the latitude range of interest here) between 45 and 76 degrees. As can be seen from the figure, the precipitated flux of electrons of $E \gtrsim 40$ kev has a maximum of about 10^5 (cm^2 sec ster)$^{-1}$ for Λ between 60 and 70 degrees. The flux is 2–3 orders of magnitude lower in subauroral latitudes. Fig. 4.2 also shows that some 10 degrees inside the auroral zone the precipitation rate is down by 1–2 powers of ten. Similar results have been found by McDiarmid et al. (1963) for electrons of energies above 40 kev and above 250 kev. Fig. 4.3 shows their data presented in a manner different from that of O'Brien (1964).

The histograms give, for two different ranges of magnetic activity, the percentage of passes in which the intensity of precipitated electrons with $E \gtrsim 40$ kev was above $1.5 \cdot 10^4$ (cm^2 sec ster)$^{-1}$ (corresponding to 0.2 db absorption at about 30 Mc/s). The flux of $1.5 \cdot 10^4$ (cm^2 sec ster)$^{-1}$ was one half of the maximum average intensity for

$K_p<4$ and 1/20 for $K_p>4$. Fig. 3 shows that during quiet geomagnetic conditions the precipitated intensity was greater than half the average value during some 25 percent of the passes through $\Lambda=65°$, while for moderately disturbed conditions —there were no strong storms represented in the data—the intensity exceeded 1/20 of the average value in about 72 percent of the passes over that latitude.

Simultaneous observations on two satellites indicate that at least sometimes the area of precipitation has a fairly limited longitudinal extent (O'Brien and Laughlin, 1962). On the other hand the precipitated flux seems on occasions to be uniform over as much as 80 degrees of longitude, i. e., over more than 4000 km (O'Brien, 1964).

The flux of precipitated electrons has its maximum close to the poleward boundary of the region of trapped electrons, as observed on the same satellite (McDiarmid et al., 1963, O'Brien, 1964).

Electron precipitation occurs simultaneously in magnetically conjugate areas at least sometimes, according to balloon observations of x-rays (Brown et al., 1963). This is in accordance with observations of aurora (cf. e.g. DeWitt, 1962).

A 100 fold change in the flux over two km has often been observed by Injun 3, which is in agreement with results of rocket measurements in aurora by Davis et al. (1960). They found the electron flux being concentrated in the visible auroral forms, whereas protons were found over a much larger volume than that occupied by the aurora.

The statistical latitude profile of the intensity of dumped electrons with $E\gtrsim 40$ kev has been found by O'Brien and Taylor (1964) to have its maximum at a few degrees lower latitude than the frequency of occurrence of visual aurora as observed on the same satellite. Sometimes the visual emission has been found to extend to higher latitudes than the precipitation of electrons with energy greater than 40 kev, indicating electrons of $E<40$ kev are being precipitated up to higher latitudes than the higher energy ones. The lower latitude limit of the aurora coincides with the lower latitude limit of appreciable precipitation (O'Brien, 1964; O'Brien and Taylor, 1964).

Precipitation was found all the time in the auroral zone by Injun 3 (O'Brien, 1964). It can be seen in Fig. 4.2 that at $L=6$ there was never

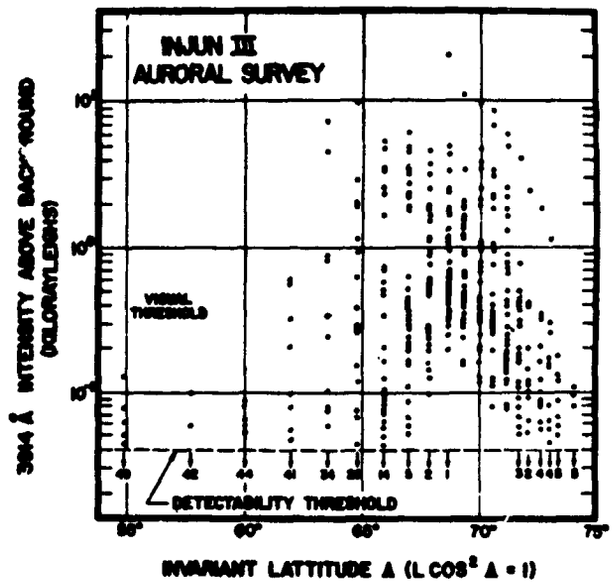

FIGURE 4.4.—Intensity of 3914 Å auroral light averaged over 4 sec at half-integral values of L in about fifty passes of Injun 3 early in 1963. (After O'Brien and Taylor, 1964.)

observed any flux lower than about 80 electrons $(cm^2\ sec\ ster)^{-1}$.

The corresponding continuous photon emission in the auroral zone is evident from Fig. 4.4. The minimum emission rate is, however, below visual threshold even in the auroral zone.

Figs. 4.2 and 4.4 also give a good impression about the enormous variability of precipitation and photon emission at all latitudes, but especially near the auroral zone. At $L=6$ there are values of about $6\cdot 10^6$ electrons $(cm^2\ sec\ ster)^{-1}$ shown in the figure. This is some 10^5 times the minimum value observed there

The latitudinal extent of the precipitation can be very restricted (e.g., over $L\sim 1$ earth radius) or very extensive (over $L>20$ earth radii). This is illustrated in Fig. 4.5.

(b) Time Characteristics of Precipitation

It is not possible to differ between time and space variations in satellite measurements. Balloon observations show, however, that time variations as rapid as of periods of a tenth of a second can occur in the electron flux (Winckler et al., 1962).

No systematic variation in the intensity of electron precipitation over periods as long as a day could be found by O'Brien (1964) from the

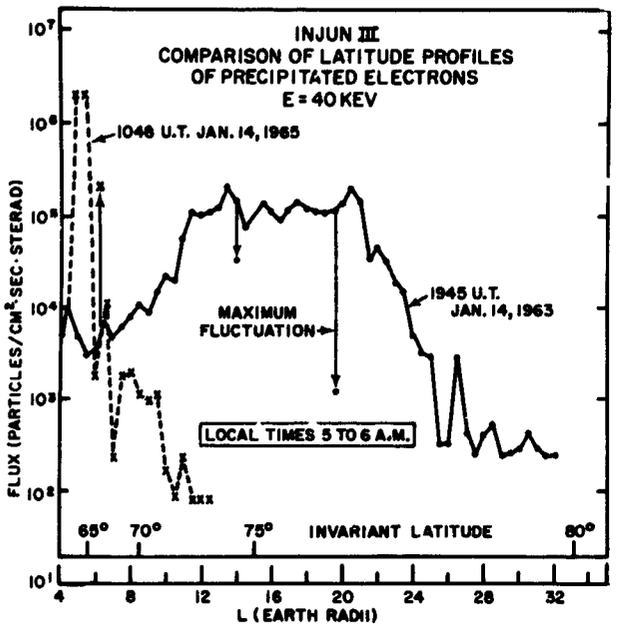

FIGURE 4.5.—Comparison of the latitude, or L profile, of precipitation for two successive passes at about the same local time. Arrows illustrate range of fluctuation of intensities at given locations. (After O'Brien, 1964.)

Injuns 1 and 3 measurements, in contrast with the case for trapped electrons. Sharp et al. (1964) observed a higher nighttime than daytime precipitation flux of electrons in the energy range 0.08–24 kev—as well as of protons—during the 5 days lifetime of an oriented polar-orbiting satellite. They also found the energy distribution of the electrons to be harder on the dayside than on the nightside of the earth (Johnson et al., 1964). With the enormous variability of the precipitation phenomenon a large amount of data seems, however, necessary for deducting statistically significant diurnal variation curves.

(c) Pitch Angle Distribution

Figure 4.1 shows that over the aurora, where the precipitation is intense the directional flux of precipitated electrons becomes equal to the flux of trapped electrons, which also is increased over the aurora. Figure 4.1 illustrates a general rule that has been found by O'Brien (1962a, b, 1964) namely that for electrons of $E \geq 40$ kev the pitch angle distribution approaches isotropy in the regions of intense precipitation. An isotropic pitch angle distribution in regions of strong precipitation has also been observed by Krasovsk" et al. (1962) at an energy of about 10 kev. No cases have been found in which the directional flux of precipitated electrons has been higher than the corresponding value of trapped electrons. The mentioned observations were made fairly close to the earth's atmosphere.

The tendency to isotropy seems to indicate that the acceleration of the electrons—if it is directed along the field lines—takes place far away from the atmosphere. This, as well as the mentioned observations of precipitation of electrons from above 1000 km in auroras, suggest that the role of the ionosphere in the production of the energetic electrons is not important. O'Brien (1964) found a flux upwards along the field lines, which was some 10 percent of the precipitated electron flux. He interpreted these observations as backscattering of electrons from the atmosphere.

(d) K_p Dependence of Precipitation

The K_p dependence of the precipitation of electrons of energy above 40 kev is illustrated in Fig. 4.3. The average intensity was ten times higher near the auroral zone when K_p was above 4 than when it was below 4. The data material for the higher K_p range in Fig. 4.3 does not contain data from any strong magnetic storm, so still higher values may be expected.

O'Brien (1964) found that the flux of precipitated electrons above 40 kev increased on the average by a factor of 5 for every step of K_p. A close correlation between precipitation intensity was also observed for the 0.8–24 kev energy range by Sharp et al. (1964). O'Brien's results, obtained on Injun 3 in a low orbit, are shown in Fig. 4.6

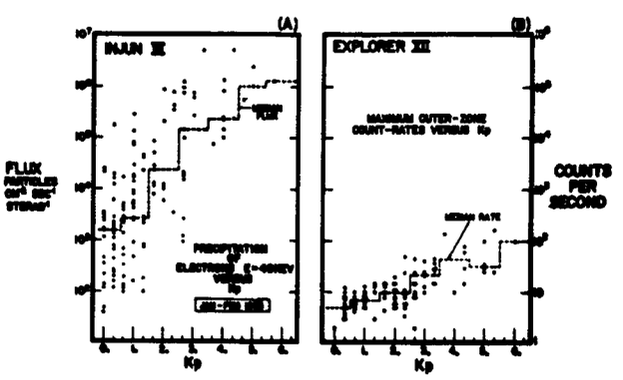

FIGURE 4.6.—Illustration that the flux of precipitated electrons (in A) varies more with K_p than does the omnidirectional flux (mainly of trapped electrons) in the equatorial plane (in B). Each point shows the maximum respective flux encountered on an outer-zone pass. (After O'Brien, 1964.)

together with the dependence of the omnidirectional flux above 40 kev as observed in the eqautorial plane far from the earth by Explorer 12 (Freeman, 1963). As can be seen, the K_p dependence is very much larger close to the earth (at one end of the field line) than in the equatorial plane (at the middle of the field line). If one assumes that both increases are due to a common acceleration mechanism it follows that it acts preferentially parallel to the geomagnetic field lines (O'Brien, 1964).

The change of omnidirectional flux above 40 kev with K_p, shown in Fig. 4.6b, is opposite to what has mostly been observed for electrons of $E \gtrsim 2$ Mev (Arnoldy et al., 1960; Hoffman et al., 1962).

The dependence of the poleward boundary of precipitation on magnetic activity has been studied by Maehlum and O'Brien (1963). They used data for trapped electrons, but since O'Brien (1964) has shown that the precipitation has its maximum close to the poleward boundary of the region of trapped electrons, their results may be interpreted in terms of possible extension of precipitated electrons.

Maehlum and O'Brien (1963) found that during magnetic storms there was a very sharp boundary of the region where trapped electrons of energy above 40 kev could be observed at about 1000 km altitude. For this boundary, measured in L, they used the symbol L_n. It can be seen as a function of the K_p index during one geomagnetic storm in Fig. 4.7. When K_p reached its maximum value of 9, L_n had its minimum value of 4. Maehlum and O'Brien (1963) also found that the poleward edge of strong radio wave absorption followed the L_n quite closely during the storm.

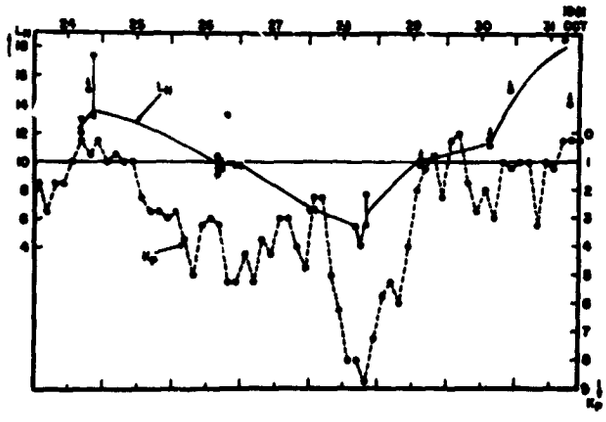

FIGURE 4.7.—Variation of the northern boundary of trapping with K_p during a geomagnetic storm, as observed by Injun 1 at a height of about 1000 km. (After Maehlum and O'Brien, 1963.)

The effect of K_p on L_n is similar to the equatorward movement of the region of visual aurora during strong magnetic storms, which has been studied in the last few years in detail for some storms by Akasofu (1962, 1963a,b) Akasofu and Chapman (1962) and Davis and Kimball (1962).

(e) The Spectrum of Precipitated Electrons

Up to now only rough measurements of the energy spectrum of the precipitated electrons have been reported. In most cases the proposed spectra have been obtained from two instruments with different energy characteristics. They thus are to be considered as rough equivalent spectra for measurements made in a defined way. In addition, it has been found that the equivalent spectrum is highly variable both in space and time (cf. O'Brien et al., 1962). Nonetheless the available spectral data are of great interest at the present stage of knowledge in the field, and they even make it possible to draw some interesting conclusions about ionospheric effects of the precipitated electrons (see Section 3).

Most spectra that have been reported hitherto can be divided in two categories if they are expressed in an exponential form. On one hand, the e-folding value, b, in the spectrum of precipitated electrons, written in the form $\alpha \exp(-E/b)$, has been found often to be in the range 2–8 kev (McIlwain, 1960; Stilwell, 1963; Sharp et al. 1964 a,b,c.) This is a very steep spectrum, but even steeper ones have been observed. McIlwain interpreted his rocket measurements in a strong aurora as indicating a monoenergetic flux of electrons with an energy of about 6 kev. Krassovskii et al. (1962) has observed steep spectra for precipitated electrons with a most common equivalent energy value of 14 kev.

The majority of the existing measurements have been made with Geiger tubes, for which the minimum detectable electron energy is about 40 kev. These measurements have mostly given e-folding values much higher than those mentioned above namely between 20 and 45 kev. (Davis et al. 1960; McDiarmid et al. 1960; O'Brien et al. 1962; Mann et al. 1963; McDiarmid et al. 1963; O'Brien and Taylor, 1964). Mann et al. (1963) found

from measurements during only some 20 orbits that the values within this range were grouped in two classes, 25 ± 5 kev and 42 ± 3 kev.

The balloon measurements of x-rays at 30–35 km altitude also, in general, give spectra of a fairly flat type, corresponding to e-folding energies in the range 20–45 kev mentioned (see e.g., Anderson and Enemark, 1960), although power law spectra often are found to fit the observations somewhat better than exponential spectra.

Recently the first direct measurements of precipitated electrons below 1 kev energy have been reported (Sharp et al. 1963, 1964c; Evans et al. 1964). They showed that there is generally not very much energy flux below 1 kev. This is also evident from observations of the luminosity distribution with height in aurora. (O'Brien and Taylor, 1964). It therefore seems probable that the spectrum, in general, does not increase very fast below 1 kev, which means that it is not of the power law type at these low energies.

Sharp et al. (1964c) reported a significantly harder spectrum on the dayside than on the nightside of the earth. This observation agrees with multifrequency riometer measurements of auroral absorption by Lerfald et al. (1964) according to which the absorbing ionization is located lower down in the atmosphere in the day than in the night.

Of special interest are the statistical data on electron precipitation, published recently. As mentioned earlier the precipitation is most intense near the auroral zone. O'Brien (1964) found an average flux of 4.10^5 electrons/cm^2 sec in the precipitation cone at an invariant latitude of 65°. Injun 1 had a CdS detector, measuring electrons of energy above about 1 kev (O'Brien, 1962b). O'Brien and Taylor (1964) stated that the flux of 4.10^5 electrons/cm^2 sec of energy greater than 40 kev was associated with an energy flux of 4 erg/cm^2 sec for electrons of $E \gtrsim 1$ kev. These data should be considered as accurate to a factor of about three. Using these two values an equivalent electron spectrum in the range 1–40 kev can be duduced. It is found to be $n(E) = 7.8 \cdot 10^7 e^{-E/5.7}$ electrons (cm^2 sec kev)$^{-1}$

For the energy values 40 and 250 kev similar average fluxes have been obtained from the Alouette measurements reported by McDiarmid et al. (1963). While the flux above 40 kev had its maximum at an invariant latitude of 65 degrees, the flux above 250 kev was maximal at about 60 degrees. McDiarmid et al. (1963) did not present any details for the latitudinal variation of this latter integral flux. By applying a rough correction factor of 0.1 for the latitude variation of the average flux above 250 kev from 60 to 65 degrees invariant latitude the following approximate equivalent spectra for the energy range 40–250 kev can be derived for two ranges of magnetic activity in the auroral zone, if isotropy is assumed for the upper hemisphere:

$$K_p < 4 : n(E) = 1.2 \cdot 10^4 e^{-E/41}$$

electrons (cm^2 sec kev)$^{-1}$,

$$K_p > 4 : n(E) = 2.4 \cdot 10^5 e^{-E/30}$$

electrons (cm^2 sec kev)$^{-1}$

(cf. Hultqvist 1964b). The applied latitude correction is probably too large and the resulting spectra are thus too steep rather than too flat. As mentioned, the spectra of precipitated electrons are very variable. There is also an important latitude variation in the steepness which increases with latitude (O'Brien et al. 1962; McDiarmid et al. 1963; O'Brien, 1964). On the other hand there seems to be no significant dependence of the spectrum on pitch angle or on the intensity of precipitation (O'Brien, 1964). The averaging on which the equivalent spectra given above are based has been made over a large number of measured fluxes. With a variation of a factor of 10^5 the use of averages may be questioned. It is also questionable whether average integral fluxes are the best values to use when the interest is in the average electron density produced by the particle influx. The average electron density is then defined by the averaging process, and this method of averaging is not identical with the averaging made in measuring the ionospheric absorption, for instance. It can, however, be shown that the average electron density produced by the precipitated electrons can be expressed in the average integral fluxes measured on satellites (Hultqvist, 1964). Since only two experimental integral flux values are available one has to fit a two-parameter energy relation for the average flux to these experimental data, as has been done above.

3. Observed Fluxes and Energy Spectra of Protons Precipitated Into the Atmosphere

The number of observations of protons on their way down into the atmosphere is much less than that for electrons. Some rocket results observed in passing through aurora or close to distinct auroral forms, or from launchings made under quite disturbed upper atmosphere conditions with no auroral information available, are collected in Table 2.

While electrons were observed only within the auroral form in the case of no. 1a, protons were found over much larger volumes. In the flights 1b, c, and d, when no auroral form was penetrated and no electrons were recorded, protons (and/or heavier ions) were found in appreciable amounts. The proton precipitation thus seems to have that wide spread and diffuse character that the hydrogen emissions generally show. This may possibly be due to protons taking up an electron also well outside the atmosphere. As a neutral atom it is not locked to the magnetic field lines and the particle flux may be spread out before reaching the atmosphere (Shklovskii, 1958). In all cases of Tables 1 and 2 in which both electrons and protons were measured, the energy flux of the electrons was about two orders of magnitude, or more, greater than the proton energy flux.

The satellites Injun 1 and Injun 3 did not measure any auroral event in which the electrons were not the dominant constituent in radiation of a given penetrability (O'Brien and Taylor, 1964). The possibility that there were as many protons/cm² sec with an energy about 40 kev, say, as there were electrons/cm² sec with the same energy could, however, not be excluded on the basis of the Injun measurements. Such protons would be stopped above the normal auroral heights and one would expect hydrogen emissions well above the ordinary aurora. They could, however, be quite weak, especially as the protons flux generally is spread out over a much larger surface than the electron flux, as mentioned above. It seems difficult to judge on these things on the basis of ground observations, as the hydrogen emissions are mostly diffuse and therefore unsuitable for height determination with standard ground techniques. Rocket measurements of the height distribution of the hydrogen emissions would be valuable.

4. Quantitative Relations Between Electron Precipitation and Photon Emission in Aurora

There are two direct measurements reported of the quantitative relations between precipitation and photon emission which will be discussed here, namely those of McIlwain (1960) and O'Brien and Taylor (1964). It is of interest to compare their results with what is expected on theoretical grounds.

McIlwain did not use any filter, but measured the photon flux integrated over the transmission curve of the photomultiplier. If we assume that ⅕ of the light was λ3914 Å, the measured photon flux corresponds to an emission rate of about 3 kilorayleigh at this wavelength. The fraction ⅕ is fairly arbitrary, but it seems reasonable (cf. e.g. Dalgarno, 1964) and is probably in error by less than a factor of 2 and ½, respectively, for an ordinary auroral-zone aurora. McIlwain's (1960) measured electron flux corresponds to an energy flux of 20 erg/cm² sec if the spectrum obtained was extrapolated to $E=0$. Thus, the resulting electron energy flux required per unit of λ3914 Å emission rate is 7 ergs cm^{-2} sec^{-1} per kR.

O'Brien and Taylor (1964) reported an average λ3914 Å intensity of $2\binom{+4}{-1.5}kR$ at the maximum of the latitude distribution i.e. in the auroral zone. As mentioned before the electron measurements gave a corresponding average of the electron flux above 40 kev of $4\cdot10^5$cm^{-2} sec^{-1} and an average energy flux for $E\gtrsim1$ kev of about 4 ergs cm^{-2} sec^{-1}, which values they consider as accurate to a factor of about three. In order to get a value directly comparable with that of McIlwain one would have to extrapolate the energy spectrum from 1 kev down to $E=0$ and evaluate the total energy flux. Using the equivalent exponential spectrum, we find 5 ergs cm^{-2} sec^{-1} for $E>0$. Thus the Injun 3 results give 2.5 ergs cm^{-2} sec^{-1} per kR. Considering the uncertainties in measurements and the method of evaluation, this is a good agreement.

What energy flux per kR does one expect on the basis of existing knowledge about the emission processes? Omholt (1957, 1959) Chamberlain (1961), Rees (1963) and Dalgarno (1964), among others, have discussed this. It has been shown by Stewart (1956) that the ratio between the

TABLE 2.—*Precipitated Protons (and other ions)*

No.	Reference	Flux (above the atmosphere)		Spectrum or energy range	Time of observ.	Place of observ. Geomagn. lat.	Visible aurora intensity and location with regard to part. measurement	Magn. disturb.	Radio-wave absorp.	Method of observ.	Remarks
		Number of particles	Energy								
1a	Davis et al. (1960)	$1.2 \cdot 10^5$ (cm² sec ster)$^{-1}$ $100 < E < 800$ kev	$3 \cdot 10^{-3}$ erg (cm² sec ster)$^{-1}$	$N(>E) = E^{-2.2}$	Jan. 26, 1958 0421 UT	Churchill, A = 68.8°	Passed through fading rayed structure during ascent and through diffuse surface of IBC 1 on both ways.			Rocket Scintill.	Definitely protons.
1b	Davis et al. (1960)	$4 \cdot 10^5$ (cm² sec ster)$^{-1}$ $100 < E < 800$ kev	$1.5 \cdot 10^{-3}$ erg (cm² sec ster)$^{-1}$	$N(>E) \propto E^{-1}$	Mar. 16, 1958 0454 UT	Churchill, A = 68.8°	No penetrat. of aurora. Weak arc moved to the north.			Rocket Scintill.	
1c	Davis et al. (1960)	$\sim 3 \cdot 10^5$ (cm² sec)$^{-1}$ ster)$^{-1}$ $100 < E < 800$ kev	$\sim 1.2 \cdot 10^{-3}$ erg (cm² sec ster)$^{-1}$	$N(>E) \propto E^{-1.7}$	Mar. 22, 1958 0641 UT	Churchill, A = 68.8°	No penetrat. of aurora. Fading arc moved to the south.			Rocket Scintill.	
1d	Davis et al. (1960)	$8.5 \cdot 10^5$ (cm² sec ster)$^{-1}$ $100 < E < 800$ kev	$2 \cdot 10^{-3}$ erg (cm² sec ster)$^{-1}$	$N(>E) \propto E^{-2.2}$	Nov. 16, 1958 0658 UT	Churchill, A = 68.8°	No penetrat. Bright arc just to the north.			Rocket Scintill.	
2a	McIlwain (1960)	$2 \cdot 10^5$ (cm² sec ster)$^{-1}$ for $E > 80$ kev		$N(>E) = 2.5 \cdot 10^5 \cdot \exp(-E/30)$ (cm² sec ster)$^{-1}$ for $80 < E < 200$ kev	Feb. 22, 1958 0537 UT	Churchill, A = 68.8°	Passed through a faint glow			Rocket Scintill.	Most probably protons.
2b	McIlwain (1960)	$< 4 \cdot 10^5$ (cm² sec ster)$^{-1}$ for $E > 100$ kev			Feb. 22, 1958 0551 UT	Churchill, A = 68.8°	Passed through bright arc (after break up of aurora)				
3	McDiarmid et al. (1962)	$3 \cdot 10^5$ cm^{-2} sec^{-1} for $E > 500$ kev			Oct. 28, 1960 1223 UT	Churchill, A = 68.8°		$\Delta Z > 1000\gamma$	~3 db (30 Mc/s)	Rocket GM tube	

excitation cross section for the λ3914 Å band of N^{2+} and the total ionization cross section is constant at least up to 200 ev energy and has the value 0.02. Assuming that this value is true over the whole energy range of interest, one finds that 50 electrons-ions pairs are produced for each 3914 Å photon. Since the mean energy expended by fast electrons in nitrogen per electron ion pair is 35 ev (at least for energies down to a few hundred ev; it is assumed the figure is correct down to zero energy) we find that $50 \times 35 = 1750$ ev is dissipated per 3914 Å photon. Since each photon has an energy of 3.2 ev, the efficiency with which energy is converted into 3914 Å radiation is $1.80 \cdot 10^{-3}$. When the initial energies of the fast electrons fall below perhaps 100 ev, these efficiencies must decrease sharply (Dalgarno and Griffing, 1958; Dalgarno, 1964). 1*kR* of 3914 Å photons corresponds to an energy influx of 2.8 erg/cm² sec, if the efficiency figure $1.8 \cdot 10^{-3}$ is employed. Dalgarno (1964) has used the value $1 \cdot 10^{-3}$. With this conversion efficiency we find the energy flux requirement to be 5.1 erg cm^{-2} sec^{-1} per *kR*. The agreement between these values and the experimental ones of McIlwain (1960) and O'Brien and Taylor (1964) is much better than expected, when the uncertainties in the analysis are taken into account.

The total efficiency of converting particle energy into photons of any energy is expected to be about 1 percent on theoretical basis (cf. Chamberlain, 1961). McIlwain found from his rocket measurements a value of only 0.2 percent, while preliminary Injun 3 results point towards 1 percent (O'Brien and Taylor, 1964).

5. Relation of Precipitated Electrons to the Outer Radiation Belt

The idea about the relations between the electrons that are precipitated into the atmosphere in auroras and elsewhere and the trapped radiation in the radiation belts, which was prevailing one or two years ago, was roughly that the precipitated particles were dumped from the large storage of energetic trapped particles in the magnetosphere through the influence of disturbing effects caused by the solar plasma, as, for example the magnetic disturbances. The number of trapped particles was thought to be sufficiently large to allow the precipitation rates observed to occur with only weak and perhaps independent processes of injection and acceleration required to replenish the particles in the radiation belt, and the occurrence of which is necessary to be assumed in any case for understanding the existence of the trapped radiation. This picture has been completely changed recently, through the investigations by O'Brien (1962b, 1964) of the measuring results of Injun 1 and Injun 3 and also through a number of balloon studies of x-ray fluxes in the lower atmosphere (Winckler et al., 1962; Anderson, 1964).

O'Brien (1962b) estimated the lifetime of the trapped electrons in the outer radiation belt assuming that the source was stopped but the loss mechanisms operated at the same rate as observed by Injun 1. He found that the outer zone beyond $L \sim 2$ would drain empty of electrons in a few hours. Similar average lifetimes have also been evaluated from x-ray measurements (cf. e.g. Winckler et al. 1962 and Anderson, 1964). Sometimes precipitation rates several orders of magnitude above the average (more than 1000 ergs/cm² sec) have been observed (Krasovskii et al. 1961; O'Brien and Laughlin, 1962, Winckler et al., 1962). Thus Winckler et al. (1962) recorded an electron burst reaching 10^{11} electrons $(cm^2\ sec)^{-1}$, a flux which would have used up the total energy of trapped particles in the field tube in half a second, but yet it persisted for about 100 seconds.

O'Brien (1964) has also shown that the flux of trapped radiation increases when precipitation takes place instead of diminishing, which would be expected if the trapped particles were simply dumped into the atmosphere. An acceleration mechanism seems to influence precipitated and trapped particles simultaneously.

Finally, O'Brien (1964) has demonstrated that the precipitation is highly energy dependent. There was no significant (<10 percent) precipitation or change in the flux of electrons of energy greater than 1.5 Mev observed in the middle of a strong burst of electrons of energy above 40 kev. This demonstrates that the precipitation could not be due simply to a lowering of the mirror point through a decrease in the geomagnetic field, since such a mechanism would be active over the whole spectrum.

Taken together, this new evidence clearly demonstrates that the precipitated electrons which produce aurora and ionospheric ionization are not

produced by simple dumping of trapped electrons into the atmosphere. An acceleration machanism must be involved. This mechanism must be one that can act with full strength very quickly (in a fraction of a second) and it should not change the flux of Mev electrons more than 10 percent when the simultaneous changes for trapped electrons of energy above 40 kev is a hundredfold, and of the precipitated electron flux above 40 kev is more than three orders of magnitude.

5. THEORETICAL MODELS

1. Introduction

In the last few years many new observational facts have been added to the picture of the aurora. Important new information has been obtained primarily from satellites, but also through detailed synoptic studies of individual auroral storms on the basis of allsky camera recordings taken during IGY.

Some important examples of such new information, some of which have been mentioned earlier in this review, are the following. Electrons are precipitated into the atmosphere over a very wide latitude range, with the maximum intensity in the auroral zone where some precipitation always takes place. The flux of trapped electrons of energy above 40 kev increases simultaneously with the precipitated flux. The increase is such that isotropy over the upper atmosphere is approached. The precipitated flux has never been found to be greater than the trapped flux.

The precipitation mechanism has been found to be energy dependent. During strong precipitation of electrons of energy greater than 40 kev the flux of Mev electrons was not significantly changed. During strong storms the poleward boundary, L_N, of the precipitation zone is very distinct and may be located at L-values as low as 4. During the quiet phase no aurora is seen on the poleward side of a certain L-value, probably identical with the L_N boundary. Following the break up, the aurora may extend rapidly polewards from the pre-break-up position as far as 10° of latitude or even more. Then it returns slowly toward the low L boundary again. It has also been definitely established that the energy content of the particles precipitated into the atmosphere in a period of the order of a minute may be orders of magnitude greater than the total energy content of the particles trapped in the corresponding field tube. Both virtually monoenergetic electrons and exponential and power law spectra have been observed in aurora. Evidence has accumulated that the local properties of the geomagnetic field in the upper atmosphere is not very important for the aurora. This indicates that drift motion around the earth of the particles which at some stage are precipitated into the atmosphere is not an important process. It has been proven that discharge acceleration within the ionosphere is not necessary for auroral production (O'Brien, 1962b).

Special chapters in this book are devoted to the description of some theoretical models of the relations between solar disturbances and geophysical effects, thereamong aurora. The reader is referred to them for details about the models.

The development of our experimental knowledge about the aurora and of our understanding of the physical processes in it is very rapid at present. It is, therefore, not a suitable stage for summing up and comparing experimental data with theoretical models. In this section only a very short summary of some main lines of proposed theories will be given in connection with a comparison of the models with some observational data which seem to be significant today.

2. Some Specifications of the Theoretical Problem

There is a general agreement that auroras, as well as magnetic storms, are caused by plasma streams which are emitted from disturbance centers on the sun. The problem of the interaction between the solar plasma and the geomagnetic field is one of great complexity, which has not as yet been solved in quantitative detail in a rigorous way. Simplified models have been used and the broad picture obtained differs very much depending on the theoretical approach.

Observations by Mariner II (Snyder and Neugebauer, 1963) and other space vehicles have shown that the interplanetary space usually has a number density, N, of charged particles of the order 10 cm^{-3}, the equivalent temperature, T, obtained from the velocity dispersion of the plasma, for instance, is typically a few times 10^5 degrees Kelvin, there exists a magnetic field, B, of

the order of a few gamma, mostly directed about 45° from the sun-earth line in the equatorial plane (see e.g. Ness, 1964). This means that the mean free path for Coulomb collision is a few astronomical units (see e.g. Parker, 1962, Kellogg, 1962, and Alfvén and Fälthammar 1963). In the plasma beams from disturbance centers on the sun somewhat higher values (but less than one order of magnitude higher) of N, B and T have been observed. A plasma of the mentioned characteristics is a "low density plasma" when the system sun-earth is considered (cf. e.g. Alfvén and Fälthammar, 1963). For such a plasma the ordinary fluid theory cannot be applied, as the statistically defined parameters have no meaning. Especially, the electric conductivity is not defined and the hypothesis that the magnetic field lines are "frozen" into the plasma may possibly not be applicable. Electric fields may exist along the geomagnetic field lines (Persson, 1963, Alfvén and Fälthammar, 1963). No macroscopic theory for the interaction of a low density plasma with the geomagnetic field seems to have been developed.

The plasma contained in the magnetosphere is probably also a low-density plasma, at least during disturbed conditions according to Alfvén and Fälthammar (1963) and Alfvén et al. (1964).

Although the theoretical basis for fluid-dynamic models of the interaction between the solar plasma and the geomagnetic field, which have been proposed, thus must be considered as weak at the present time, some of the characteristics of these models agree well with observations. They all require that the geomagnetic field shall be enclosed in a finite region around the earth, the so-called magnetosphere. A discontinuity in the magnetic field has been observed by Explorers XII, XIV and XVIII (Cahill and Amazeen, 1963; Freeman et al., 1963; Ness, 1964) at distances of about 10 earth radii on the side facing the sun, where it is expected to be according to the fluid-theory models.

The discussion below will be limited to a comparison of some observations with results of two fundamentally different types of theoretical approach, namely the fluid-dynamic (macroscopic) one, leading to a closed magnetosphere, and a microscopic model in which the plasma penetrates into the geomagnetic field to some extent.

3. Closed Magnetosphere Models

Chapman and Ferraro (1930, 1931, 1932, 1933) first discussed a model containing a confinement of the geomagnetic field lines in a finite volume around the earth. They considered a neutral unmagnetized plasma beam approaching the earth with a velocity of about 1000 km/sec and applied the boundary condition that the magnetic pressure is equal to the dynamic pressure of the plasma. Their model did not contain any details about the generation of aurora. The basic concept treated by Chapman and Ferraro has in recent years been further developed. Accurate calculations of the shape of the boundary of the magnetosphere have been made, the most recent and accurate one being that of Mead and Beard (1964). Extensive qualitative models of the geophysical effects caused by the solar plasma have been worked out on the basis of the Chapman-Ferraro model. The most comprehensive one is that of Axford and Hines (1961). In this model the acceleration of the particles is due to the plasma in the interface between magnetosphere and solar beam being convected into the interior of the magnetosphere, during which process it is adiabatically compressed. The theory is described in detail in Chapter

The closed magnetosphere models are characterized by a distinct boundary between the magnetosphere and the interplanetary medium. No model contains any details about how particles can enter the magnetosphere. For stable flow no particles can pass the boundary, except possibly at the neutral points. As the energy of the particles precipitated into the atmosphere with all probability must originate in the solar beam, one has made hypothesis about how the energy transport takes place over the boundary. Magnetohydrodynamic waves have been proposed. Axford and Hines assumed that some type of viscous interaction takes place at the boundary of the magnetosphere. Other types of instabilities have also been invoked (cf. e.g. Gold, 1962). It seems to be common to all of the proposed ways of energy transport over the magnetospheric boundary that only a minor fraction of the energy content in the solar wind is transferred to the magnetospheric plasma.

The existing fluid theories all are based on the assumption that the magnetic field lines are

equipotential lines and are "frozen" into the plasma. Therefore, acceleration of particles inside the magnetosphere must in these models be due to other effects than electrostatic fields along the lines of force. Of known acceleration processes the Fermi and betatron mechanisms and possibly electromagnetic radiation in the VLF band may be of importance in the magnetosphere (see Kaufmann, 1963, for a review). All these mechanisms require a large number of acceleration steps, and therefore fairly long time, and they produce a wide energy spectrum due to statistical fluctuations in the process. It has also been proposed that electric fields perpendicular to the magnetic field lines may cause acceleration of electrons and ions along neutral lines, i.e. lines where the geomagnetic field is zero (see Kaufmann, 1963). The existence of neutral lines has been proposed and their properties discussed by Dungey (1958, 1961, 1963) and Akasofu and Chapman (1961).

Since the discovery of the radiation belts and up till recently it was fairly generally believed that the trapped radiation was the source of those particles which produce the aurora, as was mentioned in the previous section. The density of trapped radiation was then thought to be three or four orders of magnitude greater than now (cf. e.g. O'Brien, 1963b). It was considered possible that some of the slow acceleration mechanisms mentioned above might be responsible for the acceleration of the particles from their energy in the solar wind to that observed inside the magnetosphere, although no quantitative theories existed neither for the particle transport into the magnetosphere nor for the acceleration of the particles in the outer radiation belt. An important unsolved problem was and is still how the electrons, which are most important in aurora, are energized, since most of the mentioned acceleration mechanisms give most energy in the ions.

The precipitation of the primary aurora particles into the atmosphere was thought to be produced by more or less transient instabilities of various kinds. A number of such were proposed by Akasofu and Chapman (1961), Chamberlain (1961, 1963), Kern (1962) and others. Other studies of possible auroral effects associated with adiabatically invariant motions of trapped charged particles, some of which are scattered into the atmosphere, were those of Chamberlain et al. (1960), Kern and Vestine (1961) and others.

The recent observations mentioned in the introduction to this section have completely changed the picture in regard to the importance of the trapped radiation as source for the aurora.

The fact that precipitated energies have been found sometimes to be several orders of magnitude greater than the total particle energy in the corresponding magnetic field tube (see previous section) shows that dumping without acceleration cannot be the important process for precipitation of electrons into the atmosphere, at least on some occasions. The observations of O'Brien (1964) that the flux of trapped particles always increases when precipitation takes place and is never less than the precipitated flux demonstrates clearly that the trapped radiation is not the source of the precipitated ones but is rather produced by the same acceleration mechanism that accelerates the precipitated electrons.

The observation of energy dependence of the precipitation mechanism (O'Brien, 1964) demonstrates that the precipitation is not due to a lowering of the mirror point by some geomagnetic disturbance, since such a lowering would affect the whole energy spectrum, contrary to what has been observed.

The acceleration mechanism responsible for the production of trapped as well as precipitated particles according to this mentioned picture is unknown. An electrostatic voltage of the order of 10 kilovolt along the magnetic field lines was mentioned as a possible source of acceleration by O'Brien (1964). That electrostatic field acceleration is important in aurora is supported by the observation by McIlwain (1960) of monoenergetic electrons of 6 kev energy in strong aurora. In the closed magnetosphere models that have been presented electrostatic fields along magnetic field lines cannot exist. The mechanism must therefore be an unknown one.

In the described "splash-catcher" model of O'Brien (1962b, 1964) the precipitated electrons are "fresh," i.e. they have existed with the energy they have at precipitation only for a very short time. This means that drift motion around the earth of the source of auroral primaries is not important, which is in agreement with the earlier

mentioned independence of the isoauroral curves on the mirror height.

The recent observations described above have thus modified the early closed magnetospheric models considerably. Some of the observations are even difficult to accommodate in such models. This is true for the very high energy fluxes of precipitated electrons which have been observed. While, in the average, only of the order of one percent of the solar wind energy has to be converted into kinetic energy of precipitated electrons (O'Brien and Taylor, 1964) an appreciable fraction of the solar wind energy has to be given off in electron precipitation during strong magnetic storms. This is difficult to associate with a closed magnetosphere, where energy is transported over the boundary by second order effects.

Another important difficulty with models of the closed magnetosphere type which have been proposed hitherto, is that the solar plasma is supposed to be unmagnetized, whereas observations by a number of space vehicles have shown that the interplanetary plasmas are magnetized. Alfvén (1964) has pointed out that the difference between the two cases with unmagnetized and magnetized solar plasma is more than a question of mathematical method. As the magnetic flux passing through a certain mass of gas must be fairly constant during the motion, a plasma with an initial magnetization may be brought into a stronger field if it is compressed. Thus a plasma with any value of the initial magnetization may be brought into a strong magnetic field. If the initial magnetization is zero this is not the case. The assumption $B=0$ leads therefore to conclusions which are fundamentally different from the assumption $B\neq 0$ even if B is very near zero.

The entire surface of the closed magnetosphere maps into one neutral point in each hemisphere. These are not in the auroral zones and there are no obvious reasons for the precipitation of particles taking place preferably in the auroral zones. Some complicated mechanism, like the one devised by Axford and Hines (1960), is needed to get the aurora in the proper regions of the earth.

The topology of the magnetospheric field lines is very complicated in some regions of the closed models. Aurora shows a fairly high degree of order on the earths surface with arcs often being aligned along L-curves (see e.g., Akasofu, 1963; Akasofu and Chapman, 1962 and Hultqvist, (1962). This corresponds to high degree of order also in the equatorial plane with the processes taking place at about constant distance from the earth, if the field is axisymmetric. If such an auroral arc is projected to the equatorial plane along the field lines in the closed magnetospheric model, the equatorial cross section of which is shown in Fig. 5.1, curves are found which seem to have no relation to simple physical processes. They differ significantly from particle drift surfaces, for instance (Hones, 1964).

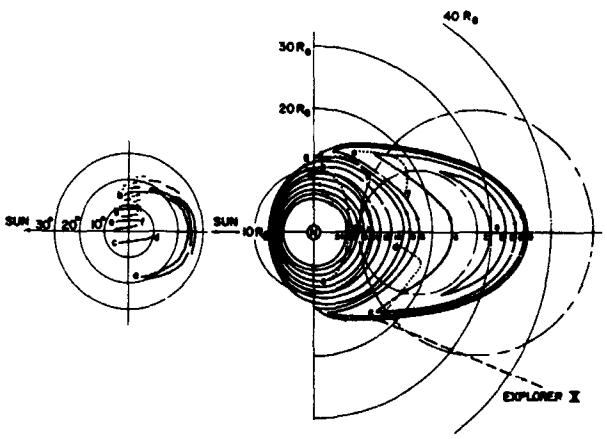

FIGURE 5.1.—Projections of auroral arcs along the geomagnetic field lines to the equatorial plane in a closed magnetosphere model. The letters a-h in the two figures indicate corresponding points in the earth's atmosphere and in the geomagnetic equatorial plane (Courtesy, Dr. E. W. Hones, Jr.).

4. Model with the Solar Plasma Penetrating into the Geomagnetic Field

Alfvén (1939, 1940, 1950, 1955; Alfvén and Fälthammar, 1963; Alfvén et al., 1964) has pointed out that a low-density magnetized plasma can penetrate into the geomagnetic field through the action of the electric field that is associated with a moving magnetic field. The depth of penetration is determined by the electric and magnetic fields and the temperature in the incoming plasma and not by the dynamic pressure as in hydromagnetic models. The penetration is stopped at a forbidden region, from which electrons and protons may be accelerated down into the atmosphere by an electric field. The acceleration field is thought to be due to charge separation,

which takes place during the invasion of the geomagnetic field. The particles from the forbidden zone moving along the field lines reach the auroral latitudes, if the properties of the plasma are in agreement with space vehicle observations. The particles may be accelerated to energies of tens or hundreds of kev.

In the first model of Alfvén it was assumed that no space charges are collected around the earth, but that immediate discharging takes place along the magnetic lines of force as soon as space charges start to build up. Karlsson (1963) has investigated the case of maximal space charge accumulation. He assumed that no discharging at all takes place along the field lines. In that way he found the general picture derived by Alfvén is preserved when space charges are taken into account. The forbidden zone is, however, smaller and more nearly circular than in the case studied by Alfvén. The general picture is thus not influenced very much by the amount of space charge accumulation.

There seems to be no basic difficulties in incorporating the above mentioned large fluxes of precipitated particles, observed by Winckler et al. (1962) and others, in the Alfvén model. This mechanism may well be active in the presence of simultaneous dumping of trapped particles due to disturbances of the geomagnetic field. For the mechanism to meet the requirements that O'Brien (1962b) has derived from the Injun 1 data, it is necessary that a rapid diffusion of particles scattered into trapped orbits takes place from the forbidden zone into the inner part of the radiation belt. If the quantitative requirements can be met is not known to this author.

Together with other large-scale charge-separation mechanisms, Alfvén's has the difficulty that electrons and protons are expected to be precipitated in two distinctly separated areas over the earth. Spectral observations from the ground as well as satellite observations of particle precipitation (Evans et al., 1964) show that electrons and protons often are precipitated simultaneously in the same auroral form.

Electrostatic acceleration of electrons and protons into the atmosphere is an inherent feature of Alfvén's model. The observations of O'Brien (1962b, 1964) thus fit well into his model in this respect. On the other hand it does not contain the observed discontinuity in the geomagnetic field at about 10 earth radii from the center of the earth, which have been observed by means of Explorers XII, XIV, and XVIII. Alfvén's model was made with the magnetic field of the solar plasma parallel to the earth's magnetic field in the equatorial plane. This direction was originally chosen in order to have the model fit observed diurnal variations in auroral occurrence. Dungey (1961, 1963) has discussed the case with the magnetic field of the solar plasma being antiparallel to the geomagnetic field in the equatorial plane. In that case neutral points or lines occur. The plasma does not penetrate further than to the neutral line and is precipitated from there along the field lines into the atmosphere. Recent laboratory experiments with magnetized plasma beams moving towards and interacting with a dipole magnetic field (Alfvén et al., 1963) have verified that there is a fundamental difference between the cases with parallel and antiparallel magnetic fields in the equator plane.

The observed discontinuity in the magnetic field may thus be due to Dungey's mechanism. Magnetic field measurements on space vehicles seem, however, to indicate that the interplanetary magnetic field lines mostly form only a small angle with the geomagnetic equatorial plane and the component parallel or antiparallel to the geomagnetic field lines is generally small and variable in magnitude and sign (Ness, 1964). In spite of this the discontinuity in the field seems always to have been observed by Explorer XVIII, at least on the side of the earth facing the sun. This does not seem to fit Dungey's model.

It is probable that within the near future space vehicles will provide experimental information that will make it possible to determine which of the two above-mentioned types of approach is relevant to nature—if any.

The theories discussed concern the large scale configuration of the auroral precipitation pattern. For the breakup of aurora and the extremely complicated phenomena that then occur on a global scale (see p. 49) no comprehensive theoretical models exist. The theories for this certainly will have to be sought in the realm of plasma instabilities, a field where the theoretical understanding of many basic phenomena still is poor.

ACKNOWLEDGEMENT

I am grateful to many colleagues at Goddard Space Flight Center for having read the manuscript, or part of it, and proposed improvements.

REFERENCES

ABBOTT, W. N., The aurora of August 19, 1950, photographed in Greece, J. Atm. Terr. Phys., 1, 343–344, 1951.

ABBOTT, W. N., Displacement of the radiant point during the auroral disturbance of September 22, 1957, Can. J. Phys., 36, 643–648, 1958.

ABBOTT, W. N. and S. CHAPMAN, On the aurora of August 19, 1950, photographed from Greece, J. Atm. Terr. Phys., 14, 111–122, 1959.

AKASOFU, S. I., J. Atm. Terr. Phys., 19, 10, 1960.

AKASOFU, S. I., J. Atm. Terr. Phys. 21, 287, 1961.

AKASOFU, S. I., Large-scale auroral motions and polar magnetic disturbances–II. The changing distribution of the aurora during large magnetic storms, J. Atm. Terr. Phys., 24, 723–727, 1962.

AKASOFU, S. I., The dynamical morphology of the aurora polaris, J. Geophys. Res., 68, 1667–1673, 1963.

AKASOFU, S. I., The auroral rays, J. Atm. Terr. Phys., 25, 163–165, 1963 b.

AKASOFU, S. I., Deformation of magnetic shells during magnetic storms, State University of Iowa, Report SUI, 63–16, 1963 c.

AKASOFU, S. I., The development of the auroral substorm. Paper presented at the American Geophysical Union, Third Western National Meeting, Boulder, Dec. 1963, 1963 d.

AKASOFU, S. I. and S. CHAPMAN, A neutral line discharge theory of the Aurora Polaris, Phil. Trans. Roy. Soc. London, A, 253, 359–406, 1961.

AKASOFU, S. I. and S. CHAPMAN, Large-scale auroral motions and polar magnetic disturbances–III. The aurora and magnetic storm of February 11, 1958, J. Atm. Terr. Phys. 24, 785–796, 1962.

AKASOFU, S. I. and S. CHAPMAN, The lower limit of latitude (US sector) of northern quiet auroral arcs, and its relation to Dst (H), J. Atm. Terr. Phys., 25, 9–12, 1963.

ALFVÉN, H., Theory of magnetic storms, I. Kungl. Sv. Vet.–Akademiens Handl. (3), 18, No. 3, 1939.

ALFVÉN, H., Theory of magnetic storms. II, III. Kungl. Sv. Vet.–Akademiens Handl. (3), 18, No. 9, 1940.

ALFVÉN, H , "Cosmical Electrodynamics.", The Clarendon Press, Oxford, 1950.

ALFVÉN, H., On the electric field theory of magnetic storms and aurora, Tellus 7, 50–64, 1955.

ALFVÉN, H., Personal communication, 1961.

ALFVÉN, H., Hydromagnetics of the magnetosphere, Space Science Reviews (in print), 1964.

ALFVÉN, H. and C. A. FÄLTHAMMAR, Cosmical electrodynamics (2nd. ed.) The Clarendon Press, Oxford, 1963.

ALFVÉN, H., L. DANIELSON, C. A. FÄLTHAMMAR, and L. LINDBERG, On the penetration of interplanetary plasma into the magnetosphere, Paper presented at the Plasma Space Science Symposium at the Catholic University, Washington, D.C., 1963.

ALFVÉN, H., L. DANIELSON, C. A. FÄLTHAMMAR, L. and LINDBERG, On the penetration of interplanetary plasma into the magnetosphere (in print), 1964.

ANDERSON, K. A., Balloon observations of x-rays in the auroral zone I, J. Geophys. Res. 65, 551–564, 1960.

ANDERSON, K. A., Relation of balloon x-rays to visible auroras in the auroral zone, J. Phys. Soc. Japan, 17, Suppl. A–I, 237–241, 1962.

ANDERSON, K. A., Balloon measurements pertaining to the dynamics of the outer radiation belt above the auroral zone. Paper presented at the Lockheed Symposium on Auroras, Palo Alto, January, 1964.

ANDERSON, K. A. and D. C. ENEMARK, Balloon observations of X-rays in the auroral zone II, J. Geoph. Res., 65, 3521–3538, 1960.

ANDERSON, K. A. and R. DEWITT, Space-time association of auroral glow and X-rays at balloon altitude, J. Geoph. Res., 68, 2669–2675, 1963.

ANSARI, Z. A., The spatial and temporal variations in high latitude cosmic noise absorption and their relation to luminous aurora, University of Alaska Sci. Rep., No. 4, NSF Grant No. G14133, 1963.

ARNOLDY, R. L., R. A. HOFFMAN, and J. R. WINCKLER, Observations of the Van Allen Radiation Regions during August and September, 1959, Part I, J. Geoph. Res., 65, 1361–1376, 1960.

ARNOLDY, R. L., R. A. HOFFMAN, J. R. WINCKLER, and S. I. AKASOFU, Observations of the Van Allen radiation regions during August and September, 1959, J. Geoph. Res. 67, 3673–3686, 1962.

AXFORD, W. T and C. O. HINES, A unifying theory of high-latitude geophysical phenomena and geomagnetic storms, Can. J. Phys., 39, 1433–1464, 1961.

BARBIER, D., Ann. Geophys., 14, 334, 1958.

BARBIER, D., Introduction à l'étude de la luminesence atmosphérique et de l'aurore polaire. In Geophysics, the Earth's environment (Eds. DeWitt, Hieblot and Lebeau) Gordon and Breach, New York pp. 303–372, 1963.

BARTELS, J. and S. CHAPMAN, Geomagnetic activity data, in connection with the aurora in lower latitudes. Akad. der Wiss-Göttingen, Beiträge zum Internationalen Geophysikalischen Jahr, Heft 1, 1958.

BASLER, R. P., Radio wave absorption in the auroral ionosphere, J. Geophys. Res., 68, 4665–4681, 1963.

BATES, D. R., The auroral spectrum and its interpretation, in "Physics of the upper atmosphere" (Ed. Ratcliffe) pp. 297–353, Academic Press, Inc., New York, 1960.

BENSON, R. F., Effect of line-of-sight aurora on radio star scintillations, J. Geophys. Res., 65, 1981–1985, 1960.

BERGER, S., Giant pulsations in the magnetic field and pulsating aurora, Planet Space Sci., 11, 867–868, 1963.

BHATTACHARYYA, B. K., Can. J. Phys., 39, 350, 1961.

BHAVSAR, P. D., Scintillation-counter observations of auroral X-rays during the geomagnetic storm of May 12, 1959, J. Geoph. Res., 66, 679–690, 1961.

BLESS, R. C., C. W. GARTLEIN and D. S. KIMBALL, East-west motions in the aurora, Astrophys, J., 122, 205–206, 1955.

BLESS, R. C., C. W. GARLTEIN and D. S. KIMBALL, and G. SPRAGUE, Auroras, magnetic bays, and protons, J. Geoph. Res., 64, 949–953, 1959.

BOLLER, W., Das Südlicht, Beitr. angew. Geophys., 3, 56–130, 1898.

BOND, F. R., Austral. J. Phys., 13, 477, 1960.

BOND, F. R., and F. JACKS, Distribution of auroras in the southern hemisphere, Austral. J. Phys., 13, 611–612, 1960.

BOWLES, K. L., Doppler shifted radio echoes from aurora, J. Geoph. Res., 59, 553–555, 1954.

BROWN, R. R., Balloon observations of auroral-zone X-rays, J. Geoph. Res., 66, 1379–1388, 1961.

BROWN, R. R., Features of the auroral electron energy spectrum inferred from observations of ionospheric absorption. Arkiv för Geofysik (in print), 1964.

BUNEMAN, O., Excitation of field aligned sound waves by electron streams, Phys. Rev. Letters, 10, 285–287, 1963.

BURDO, O. A., Canadian Defence Research Board Translation by E. R. Hope T321 R (1959), 1955.

CAHILL, L. J., and P. G. AMAZEEN, The boundary of the geomagnetic field, J. Geophys. Res., 68, 1835–1843, 1963.

CAMPBELL, W. H., Magnetic micropulsations and the pulsating aurora, J. Geoph. Res., 65, 784, 1960 a.

CAMPBELL, W. H., Magnetic micropulsations, pulsating aurora, and ionospheric absorption, J. Geoph. Res., 65, 1833–1834, 1960 b.

CAMPBELL, W. H., Natural electromagnetic energy below the ELF range, J. Res. Nat. Bur. Standards, 64D, 409–411, 1960 c.

CAMPBELL, W. H., and B. NEBEL, Micropulsation measurements in Alaska, Nature, 184, 628, 1959.

CAMPBELL, W. H., and H. LEINBACH, Ionospheric absorption at times of auroral and magnetic pulsations, J. Geoph. Res., 66, 25–34, 1961.

CAMPBELL, W. H., and J. M. YOUNG, Auroral-zone observations of infrasonic pressure waves related to ionospheric disturbances and geomagnetic activity, J. Geophys. Res., 68, 5909–5916, 1963.

CAMPBELL, W. H., and M. H. REES, A study of auroral coruscations, J. Geoph. Res., 66, 41–55, 1961.

CARLHEIM-GYLLENSKIÖLD, Expl. int. polaires 1882–83. Exp. Suédois. Aurore boreale, Stockholm, 1886.

CHAMBERLAIN, J. W., and H. M. THORSON, The nightly variation of aurora at a subauroral station, J. Geophys. Res., 65, 133–136, 1960.

CHAMBERLAIN, J. W., Theory of auroral bombardment, Astrophys. J. 134, 401–424, 1961.

CHAMBERLAIN, J. W., Plasma instability as a mechanism for auroral bombardment, J. Geoph. Res., 68, 5667–5674, 1963.

CHAMBERLAIN, J. W., J. KERN, and E. H. VESTINE, Some consequences of local acceleration of auroral primaries, J. Geoph. Res. 65, 2535–2537, 1960.

CHAPMAN, S., The audibility and lowermost altitude of the aurora polaris, Nature 127, 341–342, 1931.

CHAPMAN, S., Low altitude aurora, Nature 130, 764–765, 1932.

CHAPMAN, S., Polar and tropical aurorae and the isoauroral diagram, Proc. Indian Acad. Sci. 37, 175–188, 1953.

CHAPMAN, S., The aurora in middle and low latitudes, Nature 179, 7–11, 1957 a.

CHAPMAN, S., Aurora in middle and low latitudes, Ann. IGY, Pt. II, 25–40, 1957 b.

CHAPMAN, S., Auroral observations in India and Pakistan, Bull. Natl. Inst. Sci. India, No. 9, 180–192, 1957 c.

CHAPMAN, S., and V. C. A. FERRARO, A new theory of magnetic storms, Nature, 126, 129–130, 1930.

CHAPMAN, S., and V. C. A. FERRARO, A new theory of magnetic storms, Terr. Magn., 36, 77–97, 171–186, 37, 147–156, 421–429, 38, 79–96, 1931, 1932, 1933.

CHAPMAN, S., and J. BARTELS, "Geomagnetism," Clarendon Press, Oxford, 1940.

CHREE, C., Aurora Polaris, in "Encyclopedia Britannica," 11th. edn., Vol. 2, p. 927, New York, 1911.

CHREE, C., Proc. Phys. Soc., 39, 389, 1927.

CHRZANOWSKI, P., G. GREEN, K. T. LEMMON, and J. M. YOUNG, Traveling pressure waves associated with geomagnetic activity, J. Geoph. Res. 66, 3727–3733, 1961.

CHRZANOWSKI, P., et al., Infrasonic pressure waves associated with magnetic storms, J. Phys. Soc. Japan, 17, Suppl. A-2, 9–13, 1962.

COLE, K. D., Proc. Antarctic Sympos., Buenos Aires, Nov. 1959.

COLE, K. D., Austral. J. Phys. 13, 484, 1960.

COLE, K. D., The directions of auroral rays, Austral. J. Phys. 16, 32–39, 1963.

COLE, K. D., Motions of the aurora and radio-aurora and their relationships to ionospheric currents, Planet. Space Sci., 10, 129–164, 1963.

CORTIE, A. L., Sunspots and terresterial magnetic phenomena, 1898–1911, The cause of the annual variation in magnetic disturbances, Monthly Nat. Roy. Astr. Soc. 73, 52–60 and 136, 1912.

CULLINGTON, A. L., A man-made or artificial aurora, Nature 182–1365, 1958.

CURRIE, B. W., Summary of some auroral height measurements and observations at Chesterfield, Terr. Magn. 39, 293–297, 1934.

CURRIE, B. W., Auroral heights over west-central Canada, Can. J. Phys. 33, 773–779, 1955.

CURRIE, B. W., and H. W. EDWARDS, Summary of some auroral height-measurements and observations at Chesterfield, Canada, Terr. Magn. 39, 293–297, 1934.

CURRIE, B. W., and C. K. JONES, Directional and diurnal characteristics of auroras at some places in Canada, Terr. Magn. 46, 269–278, 1941.

DALGARNO, A., Ann. de Géophys. (in print), 1964.

DALGARNO, A., and W. G. GRIFFING, Proc. Roy. Soc. A248, 415, 1958.

DAVIES, F. T., The diurnal variation in magnetic and auroral activity at three high-latitude stations, Terr. Magn. 40, 173–182, 1935.

DAVIES, F. T., Visual auroral observations in Canada, 1943–47, Bull. Intern. Assoc. Terr. Magn. Elec., Intern. Un. Geod. Geoph. No. 13, 255–273, 1950.

DAVIS, L. R., O. E. BERG, and L. H. MEREDITH, Direct measurements of particle fluxes in and near auroras, Space Research (Ed. H. K. Kallmann Bijl), pp. 721–735, North-Holland Publ. Co., Amsterdam, 1960.

DAVIS, T. N., An investigation of the morphology of the auroral displays of 1957–58, Geophysical Institute, College, Sci. Rep. No. I, NFS Grant No. G14782, 1961.

DAVIS, T. N., The morphology of the auroral displays of 1957–1958, I, Statistical analyses of Alaska data, J. Geoph. Res. 67, 59–74, 1962 a.

DAVIS, T. N., The morphology of auroral displays of 1957–1958, 2. Detail analyses of Alaska data and analyses of high-latitude data, J. Geoph. Res. 67, 75–110, 1962 b.

DAVIS, T. N., Negative correlation between polar-cap visual aurora and magnetic activity, J. Geophys. Res. 68, 4447–4453, 1963.

DAVIS, T. N., and D. S. KIMBALL, Incidence of auroras and their north-south motions in the northern auroral zone, Geophys. Insti. College, Alaska, Sci. Rept. No. 4, NSF Grant No. Y/22.6/327, 1960.

DAVIS, T. N., and D. S. KIMBALL, The auroral display of February 13–14. 1958, Univ. of Alaska, Sci. Rep. No. 2, NSF Grant No. 14782, 1962.

DAVIS, T. N. and R. N. DEWITT, Twenty-four hour observations of aurora at the southern auroral zone, J. Geophys. Res. 68, 6237–6241, 1963.

DAVIS, T. N., and G. T. HICKS, Cinema photography of variations in auroral forms with an image Orthicon Television System. Paper presented at AGU Third Western National Meeting, Boulder, 26–28 Dec. 1963.

DENHOLM, J. V., and F. R. BOND, Orientation of polar auroras, Austral. J. Phys. 14, 193–195, 1961.

DEWITT, R. N., The occurrence of aurora in geomagnetically conjugate areas, J. Geophys. Res. 67, 1347–1352, 1962.

DUDZIAK, W. F., D. D. KLEINECKE, and T. J. KOSTIGEN, Graphic displays of geomagnetic geometry, RM 63TMP–2, DASA 1372, General Electric Co., Santa Barbara, Calif., 1963.

DUNGEY, J. W., "Cosmic electrodynamics," Cambridge University Press, Oxford, 1958.

DUNGEY, J. W., Phys. Rev. Letters, 6, 47–48, 1961.

DUNGEY, J. W., Interactions of solar plasma with the geomagnetic field, Planet. Space Sci. 10, 233–237, 1963.

EGAN, R. D., and A. M. PETERSON, Auroral noise at HF, J. Geophys. Res. 65, 3830–3832, 1960.

EGEDAL, J., Observations of aurorae from Danish light-vessels during the years 1897–1937, Publ. Det Danske Meteorol. Inst., Tillaeg, Copenhagen, 1937.

EGELAND, A., Studies of auroral reflections in the VHF band. I. Experimental investigations, with special regard to time variations, fading rate, azimuthal distributions and polarization characteristics, Arkiv för Geofysik 4, 103–169, 1962 a.

EGELAND, A., Studies of auroral reflections in the VHF band. II. Comparison of experimental results with theoretical models, Arkiv för Geofysik 4, 171–209, 1962 b.

EGELAND, A., J. ORTNER, and B. HULTQVIST, A study of the statistics of VHF oblique auroral reflections, Ann. Géoph. 18, 23–44, 1962.

ELVEY, C. T., Aurora borealis, in "Advances in electronics and electron physics," Vol. IX, pp. 1–42, Academic Press, Inc., New York, 1957.

ELVEY, C. T., Auroral morphology. Paper presented at the Lockheed Symposium on auroras at Palo Alto, January, 1964.

ELVEY, C. T., H. LEINBACH, J. HESSLER, and J. NOXON, Preliminary studies of the distribution of auroras in Alaska, Trans. Am. Geoph. Un. 36, 390–394. 1955.

ELVEY, C. T., and A. BELON, Description of the allsky-camera, its method of operation, an instrument (Ascagraph) for measuring the film. Sci. Rept. No. 1, IGY Project No. 1.1, NSF Grant No. Y/1.1/44, Geophys. Inst., College, Alaska, 43 pp., 1957.

ELVEY, C. T., and W. STOFFREGEN, Auroral photography by allsky-camera, Ann. IGY 5, Pt. II, 117–151, 1957.

EVANS, S., J. Atm. Terr. Phys. 16, 191, 1959.

EVANS, S., Proc. Roy. Soc. A 256, 234, 1960.

EVANS, S., and G. M. THOMAS, The southern auroral zone in geomagnetic longitude sector 20° E, J. Geophys. Res. 64, 1381–1388, 1959.

EVANS, J. E., R. G. JOHNSON, R. D. SHARP, and J. B. REAGAN, Precipitated proton fluxes at 300 km altitude over the auroral zones. Paper presented at the American Geophysical Union, Spring meeting in Washington, D.C., April 1964.

FAN, C. Y., Time variation of the intensity of auroral hydrogen emission and the magnetic disturbance, Astroph. J. 128, 420–427, 1958.

FELDSTEIN, Y. I., Geographical distribution of aurora and azimuth of auroral arcs. Investigation of the aurora, The Academy of Sciences of the USSR, Moscow, No. 4, 61–78, 1960.

FELDSTEIN, Y. I., Changes in the auroral zone location in connection with solar activity cycle, Geomagnetism and Aeronomie (English transl.), 2, 476–478, 1962.

FELDSTEIN, Y. I., Auroras and magnetic activity in the neighborhood of the pole, Geomagnet. and Aeronomie (English Transl.) 2, 706–708, 1962 b.

FELDSTEIN, Y. I., Auroral morphology. I. The location of the auroral zone, Tellus (in print), 1964 a.

FELDSTEIN, Y. I., Auroral morphology. II. Aurora and geomagnetic disturbances, Tellus (in print), 1964 b.

FELDSTEIN, Y. I., and N. F. SHEVNINA, Seasonal variations in auroral frequency, Geomagn. and Aeromonie (US transl.) 1, 812–814, 1961.

FELDSTEIN, Y. I., and E. K. SOLOMATINA, Auroras in the southern hemisphere, Geomagn. and Aeron. (US transl.) 1, 475–479, 1961.

FELDSTEIN, Y. I., O. V. KHOROSHEVA, and A.T. LEBEDINSKY, Investigations of auroral phanetary distributions, J. Phys. Soc. Japan 17, Suppl. A–1, 249–254, 1962.

FELDSTEIN, Y. I., and N. F. SHEVNINA, The position of the auroral zone in the southern hemisphere, Geomagn. Aeronomie (US transl.) 2, 240–242, 1962.

FILLIUS, R. W., IGY General Report No. 12, 8, 1960.

FINCH, H. F., and B. R. Leaton, The earth's main magnetic field—epoch 1955.0, Monthly Notices Roy. Astron. Soc., Geophys. Suppl., 1, 314–317, 1957.

FORSYTH, P. A., F. GREEN, and W. MAH, Can. J. Phys. 38, 770, 1960.

FOWLER, P. H., and C. J. WADDINGTON, An artificial aurora, Nature 182, 1728, 1958.

FREEMAN, J. W., State Univ. of Iowa Publ. SUI-63-20, 1963.

FREEMAN, J. W., J. A. VAN ALLEN, and L. J. CAHILL, Explorer 12 observations of the magnetospheric boundary and the associated solar plasma on September 13, 1961, J. Geoph. Res. 68, 2121-2130, 1963.

FREIER, G. D., Auroral effects on the earth's electric field, J. Geophys. Res. 66, 2695-2702, 1961.

FRIEDMAN, H., The sun's ionizing radiations, in "Physics of the upper atmosphere" (Ed Ratcliffe) pp. 133-218, Academic Press, Inc., New York, 1960.

FRITZ, H., Die Gewitter and Hydrometeore in ihrem Verhalten gegenüber den Polarlichten, Vierteljahrschrift der Naturforschenden Gesellschaft in Zürich 13, 337-373, 1868.

FRITZ, H., Verzeichnis beobachteter Polarlichten, Akad. Wissenschaffen, Wien, 1873.

FRITZ, H., Die geographische Verbreitung des Polarlichtes, Petermanns Geographische Mitteilungen 20, 347-358, 1874.

FRITZ, H., Das Polarlicht, Brockhaus, Leipzig, 1881.

FULLER, V. R., Auroral observations at the Alaska Agricultural College and School of Mines for the years 1931-1932, Terr. Magn. 38, 207-238, 1933.

FULLER, V. R., A report of work on the aurora borealis for the years 1932-1934. Terr. Magn. 40, 269-275, 1935.

FULLER, V. R. and E. H. BRAMHALL, Auroral research at the University of Alaska, 1930-1934, Misc. Publ. Univ. Alaska, Vol. III, 1937.

GADSDEN, M., Colour photography of the aurora. J. Atm. Terr. Phys. 17, 347-49, 1960.

GALPERIN, Y. I., Proton bombardment in aurora. Planet. Space Sci. 10, 187-193, 1963.

GARTLEIN, C. W., Unlocking secrets of the northern lights. Nat. Geograph. Mag. Nov., pp. 673-704, 1947

GARTLEIN, C. W., Ann. Géophys. 15, 31, 1959.

GARTLEIN, C. W., and R. K. MOORE, J. Geoph. Res. 56, 85, 1953.

GARTLEIN, C. W., A. E. GARTLEIN, and G. SPRAGUE, The aurora and the local magnetic field. IGY, WDC, A, U.S. National Academy of Sciences, IGY General Report No. 12, 57-67, 1960.

GARTLIEN, C. W., B. NACK, and G. SPRAGUE, IGY, WDC, A, U.S. Nat. Acad. Sci., IGY General Rept. No. 12, 38, 1960.

GARTLEIN, C. W., and G. SPRAGUE, Auroral occurrence, IGY, WDC, A, U.S. National Academy of Sciences, IGY General Report No. 12, 68-73, 1960.

GEDDES, M., The photographic determination of the height and position of aurorae observed in New Zealand during 1937. New Zealand J. Sci. Tech. 20, No. 6B, 1939.

GOLD, T., Magnetic Storms, Space Sci. Rev. 1, 100-114, 1962.

GORBUSHINA, G. N., The geographical distribution of anomalous absorption in the northern hemisphere. Geomagnetism and Aeronomi (English translation), 2, 225-231, 1962.

GREGORY, J. B., Radio wave reflections from the mesosphere, J. Geophys. Res. 66, 429-445, 1961.

GROTH, L. H., L. J. ANDERSON, C. C. EASTERBROOK, and L. R. BURDETTE, S-Band auroral radar returns, J. Geophys. Res. 69, 194-196, 1964.

GURNETT, D. A., and B. J. O'BRIEN, High-latitude geophysical studies with satellite Injun 3 5. Very-low-frequency electromagnetic radiation, J. Geophys. Res. 69, 65-89, 1964.

GUSTAFSSON, G., Ionization in the D-region during auroral break-up events., Planet. Space Sci., (in print), 1964.

GUSTAFSSON, G., and J. ORTNER, Kiruna Geophysical Observatory, Sci. Rep. No. 2, Contract No. AF61(052)-288, 1962.

HAGG, E. L., D. MULDREW, and E. WARREN, J. Atm. Terr. Phys. 14, 345, 1959.

HALE, D. P., Characteristics of the visual aurora at Byrd Station, Antarctica, during 1957, J. Atm. Terr. Phys. 17, 65-70, 1959.

HARANG, L., A study of auroral arcs and draperies, Geofys. Publikasj. 13, No. 14, 1-15, 1944.

HARANG, L., A study of auroral arcs and draperies, Terr. Magn. 50, 296-306, 1945.

HARANG, L., The aurorae, John Wiley and Sons, Inc., New York, 1951.

HARANG, L., and W. BAUER, über einen Nordlichtbogen in weniger als 80 km Höhe über der Erde, Gerl. Beite. Geophys. 37, 109-115 1932.

HARANG, L., and W. STOFFREGEN, Scattered reflections of radiowaves from a height of more than 1000 km. Nature, 142, 832-833, 1938.

HARANG, L., and W. STOFFREGEN, Echoversuche auf Ultrakurzwellen. Hochfreq. und Elektroak. 55, 105-108, 1940.

HARTZ, T. R., Auroral radiation at 500 Mc. Can. J. Phys. 36, 677-682, 1958.

HATHERTON, T., and G. M. THOMAS, J. Geogh. Res. 64, 1381, 1959.

HEPPNER, J. P., Time sequences and spatial relations in auroral activity during magnetic bays at College, Alaska, J. Geoph. Res. 59, 329-338, 1954 a.

HEPPNER, J. P., A study of relationships between the aurora borealis and the geomagnetic disturbances caused by electric currents in the ionosphere. Thesis, California Institute of Technology, Pasadena, 1954 b.

HEPPNER, J. P., Note on the occurrence of world-wide S.S.C.'s during the onset of negative bays at College, Alaska, J. Geoph. Res. 60, 29-32, 1955.

HEPPNER, J. P., E. C. BYRNE, and A. E. BELON, The association of absorption and E_s ionization with aurora at high latitudes. J. Geoph. Res. 57, 121-134, 1952.

HERLOFSON, N., Particle diffusion in the radiation belts. J. Phys. Soc. Japan 17, Suppl. A2, 151-153, 1962.

HESSLER, V. P., and E. M. WESCOTT, Correlation between earth-current and geomagnetic disturbance. Nature 184, 627, 1959.

HOFFMAN, R. A., R. L. ARNOLDY, and J. R. WINCKLER, J. Geophys. Res. 67, 4543, 1962.

HOLT, O., Some experimental studies of the ionospheric D region at high latitudes. Norwegian Defence Res. Establ. Report No. 46, 1963.

HOLT, O., and A. OMHOLT, J. Atm.Terr. Phys. 24, 467, 1962.

HONES, E. W., JR., Personal Communication, 1964.

HOWER, G. L., Synchrotron emission as the source of uhf auroral noise. Stanford Electronics Laboratories, Stanford University, No. SEL-62-149-(SUP), Technical Rept., (1403-1), Sci. Rept. (1), 1963.

HULBERT, E. O., On the diurnal variation of the aurora polaris. Terr. Magn. 36, 23-40, 1931.

HULTQVIST, B., The geomagnetic field lines in higher approximation. Arkiv för Geofysik 3, 63-77, 1958.

HULTQVIST, B., On the orientation of auroral arcs. J. Atm. Terr. Phys. 24, 17-30, 1962.

HULTQVIST, B., Circular symmetry in the geomagnetic equatorial plane. Planet. Space Sci., 8, 142-150, 1962 b.

HULTQVIST, B., Sunrise and sunset effects on cosmic noise absorption associated with aurora and magnetic storms. Planet. Space Sci. 11, 371-383, 1963 a.

HULTQVIST, B., On the height distribution of the ratio of negative ion and electron densities in the lowest ionosphere. J. Atm. Terr. Phys., 25, 225-240, 1963 b.

HULTQVIST, B., Studies of ionospheric absorption of radio waves by the cosmic noise method. In "Radioastronomical and Satellite Studies of the Atmosphere (Ed. J. Aarons), North-Holland Publishing Co., Amsterdam, 1963 c.

HULTQVIST, B., On the height of auroral absorption. Planet. Space Sci., (in print), 1964 a.

HULTQVIST, B., On the height of auroral absorption II. Planet. Space Sci., (in print), 1964 b.

HULTQVIST, B., Aurora and the lower ionosphere in relation to rocket and satellite measurements of precipitated particles. Paper presented at the COSPAR Fifth International Space Science Symposium in Florence, May 1964. (1964 c).

HULTQVIST, B., and A. EGELAND, Radio aurora. Space Science Review, (in print), 1964.

HUNTEN, D. M., Some photometric observations of auroral spectra. J. Atm. Terr. Phys. 7, 141-151, 1955.

HUNTEN, D. M., F. E. ROACH, and J. W. CHAMBERLAIN, A photometric unit for the airglow and aurora. J. Atm. Terr. Phys. 8, 345-346. 1956.

IYENGAR, R. S., and G. G. SHEPHERD, Observations of auroral luminosity fluctuations. Can. J. Phys. 39, 1911, 1961.

JACCHIA, L. G., and J. SLOWLEY, Atmospheric heating in the auroral zones: A preliminary analysis of the atmospheric drag of the Injun 3 satellite. J. Geophys. Res. 69, 905-910. 1964.

JACKA, F., Austral. J. Phys. 6.2, 1953.

JACKA, F., The southern auroral zone as defined by the position of homogeneous arcs. Austral. J. Phys. 6, 219-228, 1953.

JACKA, F., Ann. IGY 11, 145, 1961.

JACKA, F., and J. PATON, IQSY Instruction Manual No. 3 Aurora, CIG-IQSY Committee, London, 1963.

JENSEN, R. E., and B. W. CURRIE, Orientations of auroral displays in west-central Canada. J. Geophys. Res. 58, 201-208, 1953.

JENSEN, D. C., and J. C. CAIN, Unpublished, presented at April 1962 meeting of the American Geophysical Union, Washington, D.C., 1962.

JOHNSON, F. S., The gross character of the geomagnetic field in the solar wind. J. Geoph. Res. 65, 3049-3051, 1960.

JOHNSON, R. G., J. E. EVANS, R. D. SHARP, and J. B. REAGAN, Paper presented at the American Geophysical Union Meeting in Washington, D.C., April 1964. (1964).

JÖRGENSEN, T. S., and E. UNGSTRUP, Ionosphere Laboratory, Royal Techn. Univ. Denmark, Copenhagen, Sci. Rept., 1962.

KAISER, T. R., Radio investigations of aurorae and related phenomena. In "The Airglow and the Aurora" (E. B. Armstrong and A. Dalgarno, eds.), pp. 156-173, Pergamon Press, London, 1956.

KARLSSON, E., Streaming of a plasma through a magnetic dipole field. Phys. Fluids, 6, 708-722, 1963.

KAUFMAN, R., Experimental tests for the acceleration of trapped particles. J. Geoph. Res. 68, 371-386, 1963.

KAVADAS, A., J. Atm. Terr. Phys. 23, 170. 1962.

KELLOGG, P. J., Flow of plasma around the earth. J. Geophys. Res., 67, 3805-3811, 1962.

KERN, J. W., A charge separation mechanism for the production of polar auroras and electrojets. J. Geoph. Res. 67, 2649-2665, 1962.

KERN, J. W., and E. H. VESTINE, Theory of auroral morphology. J. Geoph. Res. 66, 713-723, 1961.

KHOROSHEVA, O. V., The space and time-distribution of auroras and their relationship with high-latitude geomagnetic disturbances. Geomagn. Aeronomi (U. S. translation), 1, 615-621, 1961.

KHOROSHEVA, O. V., The diurnal drift of the closed auroral ring. Geomagn. and Aeronomie (English translation) 2, 696-705, 1962.

KIM, J. S., and B. W. CURRIE, Horizontal movements of aurora. Can. J. Phys. 36, 160-170, 1958.

KIM, J. A., and B. W. CURRIE, Can. J. Phys. 38, 1366, 1960.

KIM, J. S., and R. A. VOLKMAN, Thickness of zenithal auroral arcs over Fort Churchill, Canada. J. Geophys. Res. 68, 3187-3190. 1963.

KNECHT, R. W., Relationships between aurora and sporadic E-echoes at Barrow, Alaska. J. Geoph. Res. 61, 59-69, 1956.

KRASOVSKII, V. I., Some results of investigations of aurora and night airglow during the IGY and IGC. Planet. Space Sci. 8, 125-141, 1961.

KRASOVSKII, V. I., YU. M. KUSHNIR, G. A. BORDOVSKII, G. F. ZAKHAROV, YE. and M. SVETLITSKII, Detection of corpuscular fluxes by means of the Third Soviet earth satellite. Ann. IGY, Vol. XII, Part II, 722-724. (Published in "Artificial Earth Satellites" Issue No. 2, Moscow, 1958.)

KRASOVSKII, V. I., I. S. SHKLOVSKII, YU. I. GALPERIN, E. M. SVETLITSKII, YU. M. KUSHNIR, and G. A. BORDOVSKII, The detection of electrons with energies of approximately 10 kev in the upper atmosphere. Planet. Space Sci. 9, 27-40. 1962.

LASSEN, K., Existence of an inner auroral zone. Nature, 184, 1375-1377, 1959.

LASSEN, K., Day-time aurorae observed at Godhavn 1954-56, Det Danske Meteor. Inst., Meddel. No. 15, 1961.

LEADABRAND, R. L., Electromagnetic measurements of auroras. Paper presented at the Lockheed Symposium on Auroras, Palo Alto, January 1964.

LEADABRAND, R. L., L. DOLPHIN, and A. M. PETERSON, Preliminary results of the 400-Mc radar investigations of auroral echoes at College, Alaska. IRE Trans. Antennas and Prop., AP-7, 127–136, 1959.

LEBEDINSKII, A. I., On certain applications of wide-angle mirror cameras (translated title), Doklady Akad. Nauk. SSSR, 102, 473–475, 1955.

LEE, A. W., Auroral observations at Lerwick Observatory, 1924–29. Meteorology Office Professional Notes, No. 56, London, 1930.

LERFALD, G. M., C. G. LITTLE, and R. PARTHASARATHY, D-region electron density profiles during auroras. J. Geophys. Res. (in print), 1964.

LIEMOHN, H., The outer radiation belt and aurorae. Nature, 188, 394–395, 1960.

LISZKA, L., Satellite cintillation observed in the auroral zone. Arkiv for Geophysik. 4, 211–225, 1963.

LITTLE, C. G., and A. MAXWELL, Scintillation of radio stars during aurora and magnetic storms. J. Atm. Terr. Phys. 2, 356–360. 1952.

LITTLE, C. G., and H. LEINBACH, Some measurements of high-latitude ionospheric absorption using extraterrestrial radio waves. Proc. Inst. Radio Engrs. 46, 335–348, 1958.

LITTLE, C. G., G. C. REID, E. STILTNER, and R. P. MERITT, An experimental investigation of the scintillation of radio stars observed at frequencies of 223 and 456 Mc/s from a location close to the auroral zone. J. Geoph. Res. 67, 1763–1884, 1962.

LITTLE, C. G., G. M. LERFALD, and R. PARTHASARATHY, Personal communication, 1963.

LOGINOV, G. A., M. I. PUDOVKIN, and R. A. SKRYNNIKOV, Diurnal variation of the intensity of aurorae and S_D variation. Geomagnetism and Aeronomy (English translation) 2, 709–713, 1962.

LOOMIS, E., The great auroral exhibition of August 28 to September 4, 1859 and the geographical distribution of auroras and thunder storms. Am. J. Sci. and Arts. 30, 79–100, 1860.

LOOMIS, E., Sciences physiques et naturelles. Arch. Sci. Phys. et Nat. 31, 273–285, 1868.

MAEDA, K., Auroral dissociation of molecular oxygen in the polar mesosphere. J. Geophys. Res. 68, 185–197, 1963.

MAEDA, K., and T. WATANABE, Pulsating auroral and infrasonic waves in the polar atmosphere. J. Atm. Sci. 21, 15–29, 1964.

MAEHLUM, B., and B. J. O'Brien, Study of energetic electrons and their relationship to auroral absorption of radio waves. J. Geoph. Res. 68, 997–1010, 1963.

MAIRAN, J. J. D. DE, Traité Physique et Historique d l'Aurore Boréale. Imprimerie Royale, Paris (2nd ed. 1754), 1733.

MALVILLE, J. M., Antarctic auroral observations. Ellsworth Station, 1957. J. Geophys. Res. 64, 1389–1393, 1959.

MALVILLE, J. M., Narrow hydrogen emissions in the aurora. Planet. Space Sci. 2, 130–132, 1960.

MALVILLE, J. M., The effect of the initial phase of a magnetic storm upon the outer Van Allen belt. J. Geophys. Res. 65, 3008, 1960.

MALVILLE, J. M., Diurnal variation of high-latitude auroras. J. Geophys. Res. 69, 1285–1292, 1964.

MANN, L. G., S. D. BLOOM, and H. I. WEST, Jr., The electron spectrum from 90 to 1200 kev as observed on Discoverer satellites 29 and 31. Space Research III (Ed., W. Priester), pp. 447–462, North-Holland Publ. Co., Amsterdam, 1963.

MARTIN, L. H., and R. A. Helliwell, Association between aurorae and very-low frequency hiss observed at Byrd Station, Antarctica. Nature, 187, 751, 1960.

MATSUSHITA, S., Ancient aurorae in Japan. J. Geophys. Res. 61, 297–302, 1953.

MAWSON, D., Scientific Report Australasian Antarctic Expedition 1911–14, Vol. 11, Part 1: Records of the Aurora Polaris, 1914.

McDIARMID, I. B., D. C. ROSE, and E. BUDZINSKI, Direct measurement of charged particles associated with auroral zone radio absorption. Can. J. Phys. 39, 1888–1900, 1961.

McDIARMID, I. B., J. R. BURROWS, E. E. BUDZINSKI, and M. D. WILSON, Some average properties of the outer radiation zone at 1000 km. Can. J. Phys. 41, 2064–2079, 1963.

McEWEN, D. J., and R. MONTALBETTI, Parallactic measurements on aurorae over Churchill, Canada. Can. J. Phys. 36, 1593–1600, 1958.

McILWAIN, C. E., Direct measurement of particles producing visible auroras. J. Geoph. Res. 65, 2727–2747, 1960.

McILWAIN, C. E., Coordinates for mapping the distribution of magnetically trapped particles. J. Geophys. Res. 66, 3681–3691, 1961.

McLENNAN, J. C., H. S. WYNNE-EDWARDS, and H. J. C. IRETON, Height of the polar aurora in Canada. Can. J. Res. 5, 285–296, 1931.

MEAD, G. D., and D. B. BEARD, The shape of the geomagnetic-field solar-wind boundary. Goddard Space Flight Center, Rep. X-640-63-239, 1963.

MEEK, J. H., Correlation of magnetic auroral and ionospheric variations at Saskatoon. J. Geoph. Res. 58, 445–456, 1953.

MEEK, J. H., Correlation of magnetic auroral and ionospheric variations at Saskatoon. Part 2. J. Geoph. Res. 59, 87–92, 1954 b.

MEEK, H. H., The location and shape of the auroral zone. J. Am. Terr. Phys. 6, 313–321, 1955.

MEEK, J., J. Am. Terr. Phys., Suppl. 120, 1957.

MEINEL, A. B., On the entry into Earth's atmosphere of 57 kev protons during auroral activity. Phys. Rev. 80, 1096–1097, 1950 a.

MEINEL, A. B., Evidence for the entry into the upper atmosphere of high-speed protons during auroral activity. Science 112, 590, 1950 b.

MEINEL, A. B., Doppler-shifted auroral hydrogen emission. Astrophys. J. 113, 50–54, 1951.

MEINEL, A. B. and D. H. SCHULTE, A note on auroral motion. Astrophys. J. 117, 454–455, 1953.

MEINEL, A. B., B. J. NEGAARD, and J. W. CHAMBERLAIN, A statistical analysis of low-latitude aurorae. J. Geoph. Res. 59, 407–413, 1954.

MEREDITH, L. H., M. B. GOTTLIEB, and J. A. VAN ALLEN, Direct detection of soft radiation above 50 kms in the auroral zone. Phys. Rev. 97, 201–205, 1955.

MOGILEVSKIY, On the nature of the action of solar corpuscular flux upon the Earth's magnetosphere (translated title) Geomagnetism i Aeronomiya 3, No. 6, 1002, 1963.

MOORCROFT, D. R., and Forsyth, P. A., On the relation between radio star scintillations and auroral and magnetic activity. J. Geoph. Res. 68, 117–124, 1963.

MOROZUMI, H. M., A study of the aurora australis in connection with and association between VLFE hiss and auroral arcs and bands observed at the South Geographic Pole. Thesis, State University of Iowa, 62–14, 1962.

MOROZUMI, H. M., Semidiurnal auroral peak and VLF emissions observed at the South Pole, 1960. IG Bulletin No. 73, July 1963, pp. 16–23. (Paper presented at the Second Western National Meeting of the American Geophysical Union at Stanford Univ., Dec. 1962).

MUNCKE, G. W., Nordlicht. Physikalisches Wörterbuch 7, 113–268, 1837.

MURCRAY, W. E., Some properties of the luminous aurora as measured by a photoelectric photometer. J. Geophys. Res. 64, 955–959, 1959.

MURCRAY, W. B., and J H. Pope, Radiation from protons of auroral energy in the vicinity of the earth. J. Geoph. Res. 65, 3569–3574, 1960.

NADUBOVICH, Y. A. and G. V. STARKOV, The fibrous structure of faint auroral homogeneous arcs. Geomagn. Aeron. (U. S. transl.) II, 57–61, 1961.

NAGATA, T. and E. KANEDA, A photoelectric analyzer of all-sky camera auroral photographs. J. Geophys. Res. 66, 2259–2261, 1961.

NESS, N. F., Personal communication, 1964.

NIKOLSKIY, A. P., The world-wide distribution of magneto-ionospheric disturbance and aurora (translated title). Doklady Akad. Nauk. SSSR, 115, 84–87.

NIKOLSKIY, A. P., Experimental proof of the existence of a second zone of magnetic disturbance in the east Arctic. Geomagnetism and Aeronomy (U. S. transl.) 1, 833–837, 1963.

NOXON, J. F., Observation of daytime aurora. J. Am. Terr. Phys. 25, 637–645, 1963.

O'BRIEN, B. J., Direct observations of dumping of electrons at 1000-km altitude and high latitudes. J. Geoph. Res. 67, 1227–1233, 1962 a.

O'BRIEN, B. J., Lifetimes of outer-zone electrons and their precipitation into the atmosphere. J. Geoph. Res. 67, 3687–3706, 1962 b.

O'BRIEN, B. J., A large diurnal variation of the geomagnetically trapped radiation. J. Geoph. Res. 68, 989–995, 1963.

O'BRIEN, B. J., Review of studies of trapped radiation with satellite-borne apparatus. Space Science Reviews 1, 415–484, 1963.

O'BRIEN, B. J., High-latitude geophysical studies with satellite Injun 3.3. Precipitation of electrons into the atmosphere. J. Geophys. Res. 69, 13–43, 1964.

O'BRIEN, B. J. and C. D. LAUGHLIN, An extremely intense electron flux at 1000-km altitude in the auroral zone. J. Geoph. Res. 67, 2667-2672, 1962.

O'BRIEN, B. J., C. D. LAUGHLIN, J. A. VAN ALLEN, and L. A. FRANK, Measurements of the intensity and spectrum of electrons at 100-km altitude and high latitudes. J. Geoph. Res. 67, 1209–1225, 1962.

O'BRIEN, B. J., and H. TAYLOR, High-latitude geophysical studies with satellite Injun 3.4. Auroras and their excitation. J. Geophys. Res. 69, 45–63, 1964.

OMHOLT, A., Astrophys. J. 126, 461, 1957.

OMHOLT, A., Geoph. Publikasjoner 20 (11), 1, 1959.

OMHOLT, A., The time delay of the red (OI) lines in the aurora. Plan. Space Sci. 2, 246–48, 1960.

OMHOLT, A., Velocities of very active auroral rays. Planet. Space Sci. 9, 285–286, 1962.

OMHOLT, A., Observations and experiments pertinent to auroral theories. Planet. Space Sci., 10, 247–262, 1963.

OMHOLT, A. and L. HARANG, Measurement of the mean lifetime of the metastable ^1S-state of the oxygen atom in the upper atmosphere during auroral displays. J. Atm. Terr. Phys. 7, 247–253, 1955. J. Geophys. Res. 61, 161, 1956.

OMHOLT, A., W. Stoffregen, W., and H. DERBLOM, Hydrogen lines in auroral glow. J. Atm. Terr. Phys. 24, 203–209, 1962.

PARK, F. R., An all-sky camera for auroral research. Bull. Radio and Electr. Eng. Div., Nat. Res. Council, Ottawa, 7, 1–3, 1957.

PARKER, E. N., Kinetic properties of interplanetary matter. Planet. Space Sci. 9, 461–475, 1962.

PAULSEN, A., Obs. int. polaires 1882–83. Exp. Danois, Copenhague, 1893.

PEDERSON, A., Time, height, and latitude distribution of D layers in the subauroral zone and their relation to geomagnetic activity and aurorae. J. Geophys. Res. 67, 2685–2694, 1962.

PERSSON, H., Electric field along a magnetic line of force in a low-density plasma. Phys. of Fluids 6, 1756–1757, 1963.

PFOTZER, A., A. EHMERT, H. ERBE, E. KEPPLER, B. HULTQVIST, and J. ORTNER, a contribution to the morphology of X-ray bursts in the auroral zone. J. Geophys. Res. 67, 575–585.

PUDOVKIN, M. T. and L. S. YEVLASHIN, Spatial relationship between auroras and electric currents in the ionosphere. Geomagnetism and Aeronomy, (English translation), 2, 557–560, 1962.

QUENBY, J. J., and W. R. WEBBER, Cosmic ray cut-off rigidities and the earth's magnetic field. Phil. Mag. (8), 4, 90–113, 1959.

REES, M. H., Auroral ionization and excitation by incident energetic electrons. Planet. Space Sci. 11, 1209–1218, 1963.

REES, M. H., and G. C. REID, Nature 184, 539, 1959.

ROACH, J. R., Effects of radio wave propagation through mid-latitude 6300Å auroral arcs. J. Res. Nat. Bur. Standards, 67D, 263–271, 1963.

ROACH, F. E., and J. R. ROACH, 6300Å auroral arcs in mid-latitudes. Planet. Space Sci. 11, 523–545.

ROMICK, C. J., and C. T. ELVEY, J. Atm. Terr. Phys. 12, 283, 1958.

ROSSER, W. G. V., B. J. O'BRIEN, J. A. VAN ALLEN, L. A. FRANK, and C. D. LAUGHLIN, Electrons in the earth's outer radiation zone. J. Geoph. Res. 67, 4533-4542, 1962.

SANDFORD, B. P., Aurora and airglow from colour film observations. J. Atm. Terr. Phys. 21, 177.

SANDFORD, B. P., Nature 190, 245. Arctic Inst. of North America, Res. Paper No. 18, August 1961, 1961b.

SANDFORD, B. P., and P. HEISER, Colour photography of the aurora. Nature 184, 541, 1959.

SCHOVE, D. J., The Sunspot cycle, 649, B.C. to A.D. 2000. J. Geophys. Res. 60, 127–146.

SEATON, M. J., Excitation processes in the aurora and airglow. I. Absolute intensities, relative ultraviolet intensities, and electron densities in high latitude aurorae. J. Atm. Terr. Phys. 4, 285–294, 1954.

SHARP, R. D., J. E. EVANS, R. G. JOHNSON, and J. B. REAGAN, Paper presented at American Geophys. Union Third Western Nat. Meeting, Boulder, December 1963.

SHARP, R. D., J. E. Evans, R. G. Johnson, and J. B. REAGAN, Paper presented at COSPAR Fifth Space Sci. Symp. Florence, May 1964 a.

SHARP, R. D., J. E. EVANS, W. L. IMHOF, R. G. JOHNSON, J. B. REAGAN, and R. V. SMITH, Satellite measurements of low-energy electrons in the northern auroral zone, submitted for publication to J. Geophys. Res., 1964 b.

SHARP, R. D., et al., Personal communication, 1964 c.

SHERET, M. A., and G. M. THOMAS, Auroral observations at Halley Bay, Antarctica, during 1959. Nature 189, 826, 1961.

SHKLOVSKII, I. S., Ann. Geophys. 14, 414, 1958.

SKRYNNIKOV, Short-period variations of the intensity of auroral luminosity. Geomagnetism and Aeronomy (Engl. transl.) 2, 894–896, 1962.

SNYDER, C. W., and M. NEUGEBAUER, Interplanetary solar-wind measurements by Mariner II. Paper presented at the fourth COSPAR Space Science Symposium, Warsaw, June 1963.

SOBOUTI, Y., The relationship between unique geomagnetic and auroral events. J. Geophys. Res. 66, 725–737, 1961.

STAGG, J. M., British Polar Year Expedition, Fort Rae, N. W. Canada, 1932-33, Vol. 1, p. 127, Royal Soc., London, 1937.

STARKOV, G. V., and Y. I. FELDSTEIN, Investigations of the Aurora, No. 4, p. 56. Academy of Science of the USSR, Moscow, 1960.

STETSON, H. T., and C. F. BROOKS, Terr. Magn. 47, 21, 1942.

STEWART, D. T., Proc. Phys. Soc. A69, 437, 1956.

STILWELL, D. E., Observations of intense, low energy electron fluxes in the outer zone during January and March, 1963. Thesis, State University of Iowa, SUI-63-28, 1963.

STOFFREGEN, W., All-sky camera auroral research during the Third Geophysical Year 1957–1958. Tellus 7, 509–517, 1955.

STOFFREGEN, W., Radio reflections on low frequencies from 75–90 km height during intense aurora activity. J. Atm. Terr. Phys. 13, 167–169, 1958.

STOFFREGEN, W., Results quoted by Harang, L. and J. TRÖIM, Studies of auroral echoes. Planet. Space. Sci. 5, 33–45, 1961.

STOFFREGEN, W., The east-west drift of auroral forms determined from all-sky camera films. J. Atm. Terr. Phys. 21, 257–260, 1961b.

STOFFREGEN, W., H. DERBLOM, and A. OMHOLT, Some characteristics of the D-region ionization during auroral activity. J. Geophys. Res., 65, 1699–1704, 1960.

STOFFREGEN, W. and H. DERBLOM, Auroral hydrogen emission related to charge separation in the magnetosphere. Planet. Space Sci. 9, 711–716, 1962.

STÖRMER, C., "Photograph c Atlas of Auroral Forms and Scheme for Visual Observations of Aurorae", 1st. ed., A. W. Bröggers Boktrykkeri, Oslo. Publication sponsored by the International Union of Geodesy and Geophysics.

STÖRMER, C., Photography of polar aurora. In "Supplement to the Photographic Atlas of Auroral Forms" pp. 4–11, A. W. Bröggers Boktrykkeri, Oslo. Publication sponsored by the International Union of Geodesy and Geophysics.

STÖRMER, C., Photographische Höhenmessungen und Spectra des grossen Nordlichtes vom 25. bis 26. January 1938. Naturwissenschaffen 26, 633–638, 1938.

STÖRMER, C., Results of the photogrammetric measurements of the aurora borealis during the Norwegian-French polar expedition to North-East Greenland, 1938–1939. Geophys. Publ. XII, No. 13, 1944.

STÖRMER, C., The Polar Aurora, Oxford at the Clarendon Press, 1955.

SVERDRUP, H. V., Auroral results, Maud-expedition, 1918–1925. Rep. Dept. Terr. Magn., Carnegie Inst. Wash. 6, No. 175, 1927.

THOMAS, J. A. and E. K. Smith, A survey of the present knowledge of sporadic-E ionization. J. Atm. Terr. Phys. 13, 295–314,1959.

THOMAS. L. and W. R. PIGGOTT, Some aspects of the incidence of polar blackout during IGY. In "Some ionospheric results obtained during the IGY" (Ed. Beynon), Elsevier Pub. Co., pp. 62–71.

TROMHOLT, S., Sur les periodes des aurores boréales. Danish Meteor Inst. Yearbook for 188?, 1882.

TROMHOLT, S., Katalog der in Norwegen bis Juni 1878 beobachteten Nordlichter. Kristiania (Oslo), 1902.

VAN ALLEN, J. A., Direct detection of auroral radiation with rocket equipment. Proc. Natl. Acad. Sci. 43, 57–62, 1957.

VEGARD, L., On the properties of the rays producing aurorae borealis, Phil. mag. 23, 211–237, 1912.

VEGARD, L., Hydrogen showers in the auroral region. Nature 144, 1089–1090, 1939.

VEGARD, L. and KROGNESS, O., The position in space of the aurora polaris from observations made at the Haldde Observatory 1913–191? Geophys. Publik. 1, 1–172.

VESTINE, E. H., The geographic incidence of aurora and magnetic disturbance, northern hemisphere. Terr. Magn. 49, 77–102, 1944.

VESTINE, E. H., J. Geophys. Res. 65, 260–262, 1960.

VESTINE, E. H., and E. J. SNYDER, The geographic incidence of aurora and magnetic disturbance, southern hemisphere. Terr. Magn. 50, 105–124, 1945.

VESTINE, E. H., and W. L. SIBLEY, The geomagnetic field in space, ring currents and auroral isochasms. J. Geophys. Res. 65, 1967–1979, 1960.

WEILL, G. W., Aspects de l'Aurore observeé à la base Dumont d'Urville on Terre Adélie. Compt. Rendus, 246, 2925–2927, 1958.

WHITE, F. W. G., and M. Geddes, The Antarctic zone of maximum auroral frequency. Terr. Magn. 144, 367–377, 1939.

WILCKE, J. C., Von den jährlichen und täglichen Bèwegungen der Magnetnadel in Stockholm. Svensk. Vet. Akad. Handl. pp. 273–300, 1777.

WINCKLER, J. R., Balloon study of high-altitude radiations during the IGY. J. Geoph. Res. 65, 1331–1359, 1960.

WINCKLER, J. R., Atmosphere phenomena, energetic electrons, and the geomagnetic field. J. Res. Nat. Bur. Standards 66D, 127–143, 1962.

WINCKLER, J. R., L. PETERSON, R. ARNOLDY, and R. HOFFMAN, X-rays from visible aurorae at Minneapolis. Phys. Rev. 110, 1221–1231, 1958.

WINCKLER, J. R., P. D. BHAVSAR, and K. A. ANDERSON, A study of the precipitation of energetic electrons from the geomagnetic field during magnetic storms. J. Geoph. Res. 67, 3717–3736, 1962.

WITHAM, K., E. LOOMER, and E. NIBLETT, J. Geophys. Res. 65, (1960)

ZABORSCHIKOV, F. VA., and N. T. FEDIAKINA, Interrelations of aurora, radiowave propagation, magnetic and ionospheric disturbance (translated title). Preblemij Arktiki 2, 149–159, 1957.

N65-33705

AURORA AND THE LOWER IONOSPHERE IN RELATION TO SATELLITE OBSERVATIONS OF PARTICLE PRECIPITATION*

BENGT HULTQVIST†

The direct observations of electron precipitation by means of rockets and satellites is reviewed. Upon comparison of the observed energy fluxes with those expected on the basis of optical measurements of aurora, the agreement is found to be good. It is demonstrated that the satellite observations make understandable the observed variable degree of correlation between visual aurora and auroral absorption of radio waves. The precipitated electrons contribute significantly to the night time ionosphere not only in the auroral zone but also over the polar caps and in sub-auroral latitudes. It does not seem impossible that the observed precipitation of electrons is the main source of nighttime ionization in the lower ionosphere. The airglow is briefly discussed in relation to observed particle precipitation. Finally, the recent demonstrations of the insufficiency of the Van Allen belt as a source for the precipitated electrons is briefly reviewed.

INTRODUCTION

The first rocket investigations of particles precipitated into the atmosphere were made by the Iowa group in the early 1950's. In IGY and thereafter a few more direct rocket measurements of high energy particles in auroral altitudes have been reported. Although of extreme value as exploratory studies, these few rocket measurements suffer from the weakness of being very limited in space and time. Some data about the rate of precipitation of electrons having energies greater than about 25 kev have been obtained from balloon observations of X-rays, but it is only in the last two years that systematic satellite measurements of precipitated particles, primarily by the two Injun satellites (O'Brien, 1962, a, b, 1964) and Alouette (McDiarmid, et al., 1963) have provided statistical data, on the basis of which some rough estimates of the average influence on the ionosphere can be made. In addition to precipitated electrons Injun 3 also measured the emission rate below the satellite of 3914Å and 5577Å photons along the magnetic field line upon which the satellite was located. The measurements have recently given very valuable information about detailed relations between electron precipitation and photon emission rate (O'Brien and Taylor, 1964).

One primary purpose of this review is to summarize some of the knowledge about relations between particle influx into the atmosphere and the resulting aurora and ionospheric effects. It should be said, however, that most reports on satellite observations published hitherto concern particles of fairly high energies (greater than 40 kev for electrons). For particles in the lowest energy range (i.e., from a fraction of 1 kev for electrons and some tens of kev for protons) the available experimental results are still scanty. What is going to be said about the influence of observed precipitation on the ionosphere above 100 km will therefore be most preliminary.

OBSERVATIONS OF PRECIPITATED ELECTRONS

The early rocket measurements (e.g., Davis et al., 1960; McIlwain, 1960) as well as the satellite results (e.g., O'Brien, 1962a, 1964) have verified the conclusions of Omholt (1957, 1959), based on spectroscopic observations of aurora, that the protons play a very minor role in the excitation of most aurorae and in producing ionization in the

*Published as Goddard Space Flight Center Document X-611-64-107, May 1964.

†Goddard Space Flight Center, NASA—National Academy of Sciences—National Research Council Senior Post-Doctoral Resident Research Associate on leave of absence from Kiruna Geophysical Observatory, Kiruna, Sweden.

lower ionosphere. Therefore only electrons will be discussed in this review.

The first somewhat detailed satellite studies of particles that were definitely precipitated into the atmosphere were made by means of Injun 1 (O'Brien, 1962a, b). O'Brien and others working with satellite data define precipitated particles as those particles which would mirror at or below 100 km altitude (if the atmosphere had not been present).

(a) Latitudinal Distribution and Other Spatial Characteristics

The recent simultaneous measurements on Injun 3 (O'Brien and Taylor, 1964) of flux of precipitated electrons and of auroral light emission below the satellite have shown th... above aurorae there are electron fluxes several orders of magnitude larger than outside the aurora. (Fig. 1).

Fairly extensive statistical data on the spatial characteristics of precipitated electrons have recently been published by O'Brien (1962a, b, 1964) and McDiarmid et al. (1963). Figure 2 shows the scatter diagram of the Injun 3 observations of precipitated electrons of energy above 40 kev for the range of the invariant latitude Λ (defined by $\Lambda = \cos^{-1}(1/\sqrt{L})$ and at the most a few degrees different from geomagnetic latitude in the latitude range of interest here) between 45 and 76 degrees. As can be seen from the figure, the precipitated flux of electrons of $E \gtrsim 40$ kev has a broad maximum of about 10^5 electrons/cm² sec ster for Λ between 60 and 70 degrees. The flux is 2–3 orders of magnitude lower in subauroral latitudes. Figure 2 also shows that some 10 degrees inside the auroral zone the precipitation rate is down by 1–2 powers of ten.

Similar results have been found by McDiarmid et al. (1963) for electrons of energies above 40 kev and above 250 kev. Figure 3 shows their data presented in a manner different from that of O'Brien (1964). The histograms give, for two different ranges of magnetic activity, the percentage of passes in which the intensity of precipitated electrons with $E \lesssim 40$ kev was above $1.5 \cdot 10^4$ electrons/cm² sec ster (corresponding to 0.2 db absorption at about 30 Mc/s). The flux of $1.5 \cdot 10^4$/cm² sec ster was one-half of the maximum

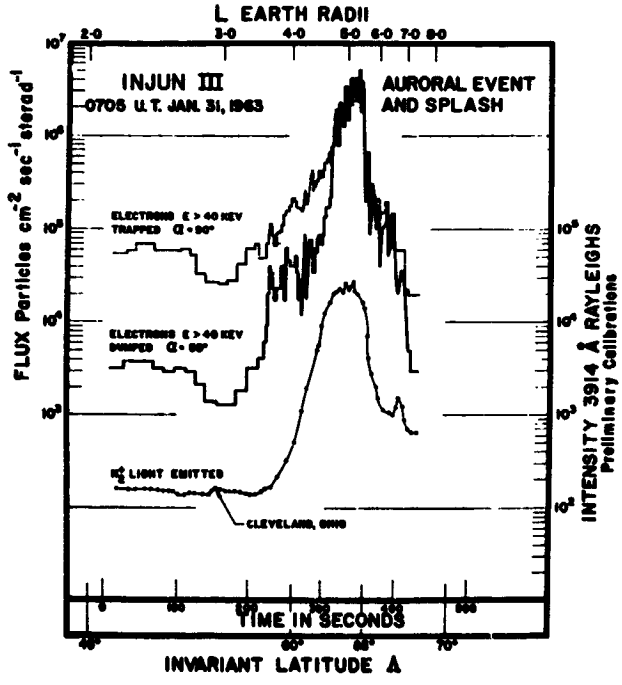

FIGURE 1.—Data from a northbound pass of Injun 3 over North America, which shows simultaneous detection of an aurora, of the precipitated electrons (with pitch angle 50°) partially responsible for causing it, and of trapped electrons. Note the approach to isotropy of the particle flux over the aurora. No attempt has been made to subtract the low-altitude contamination of the photometer signal, part of which was the detection of Cleveland, Ohio, and its surroundings. (After O'Brien and Taylor, 1964.)

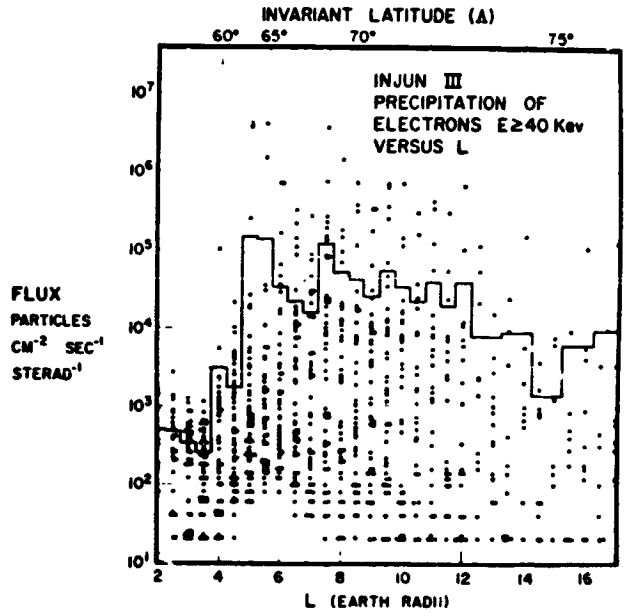

FIGURE 2.—Samples of precipitated fluxes over North America in January 1963. Each point is an 8-sec average of thirty two measurements made at half-integral values of L. The solid line gives the average flux. (After O'Brien, 1964.)

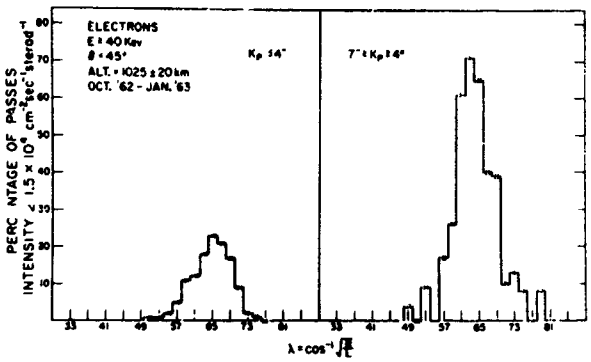

FIGURE 3.—Percentage of passes in which the intensity of precipitated electrons with energies greater than 40 kev was greater than 1.5×10^4cm^{-2} sec^{-1} sterad^{-1} corresponding to 0.2 db of 30 Mc/s absorption, plotted against invariant latitude. (After McDiarmid et al., 1963.)

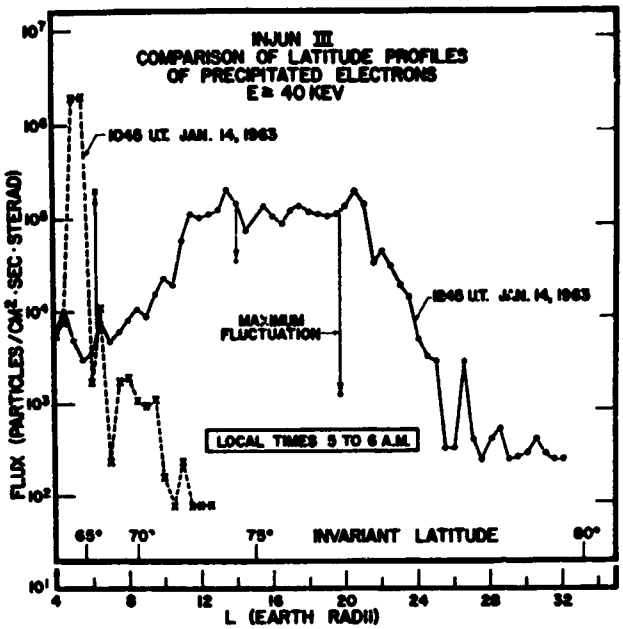

FIGURE 4.—Comparison of the latitude, or L profile, of precipitation for two successive passes at about the same local time. Arrows illustrate range of fluctuation of intensities at given locations. (After O'Brien, 1964.)

average intensity for $K_p<4$ and 1/20 for $K_p>4$. Figure 3 shows that during quiet geomagnetic conditions the precipitated intensity was g[illegible] than half the average value during some 2[illegible] percent of the passes through $\Lambda=65°$, while for moderately disturbed conditions—there were no strong storms represented in the data—the intensity exceeded 1/20 of the average value in about 72 percent of the passes over that latitude.

Simultaneous observations on two satellites indicate that at least sometimes the area of precipitation has a fairly limited longitudinal extent (O'Brien and Laughlin, 1962). On the other hand the precipitated flux seems on occasions to be uniform over as much as 80 degrees of longitude, i.e., over more than 4000 km (O'Brien, 1964).

The latitudinal extent of the precipitation can be very restricted (e.g., over a range of $L\backsim1$ earth radius) or very extensive (over an L interval >20 earth radii). This is illustrated in Figure 4.

The flux of precipitated electrons has its maximum close to the poleward boundary of the region of trapped electrons, as observed on the same satellite (McDiarmid et al., 1963; O'Brien, 1964).

Electron precipitation occurs simultaneously in magnetically conjugate areas at least sometimes, according to balloon observations of X-rays (Brown et al., 1963). This is in accordance with observations of aurora (cf. e.g. DeWitt, 1962).

A 100 fold change in the flux over two km has often been observed by Injun 3 which is in agreement with results of rocket measurements in aurora by Davis et al. (1960). They found the electron flux being concentrated in the visible auroral forms whereas protons were found over a much larger volume than that occupied by the aurora.

The statistical latitude profile of the intensity of dumped electrons with $E\gtrsim40$ kev has been found by O'Brien and Taylor (1964) to have its maximum at a few degrees lower latitude than the frequency of occurrence of visual aurora as observed on the same satellite. Sometimes the visual emission has been found to extend to higher latitudes than the precipitation of electrons with energy greater than 40 kev, indicating electrons of $E<40$ kev are being precipitated up to higher latitudes than the higher energy ones. The lower latitude limit of the aurora coincides with the lower latitude limit of appreciable precipitation (O'Brien, 1964; O'Brien and Taylor, 1964).

Precipitation was found all the time in the auroral zone by Injun 3 (O'Brien, 1964). It can be seen in Figure 2 that at $L=6$ there was never observed any flux lower than about 80 electrons (cm^2 sec ster)$^{-1}$.

The corresponding continuous photon emission in the auroral zone is evident from Figure 5. The

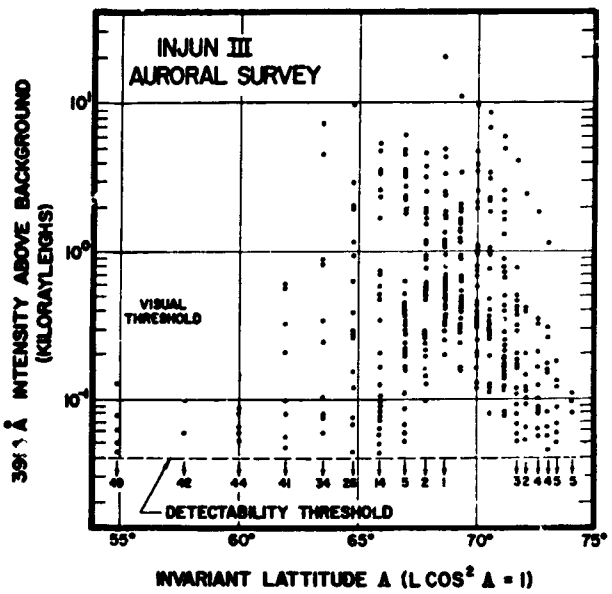

FIGURE 5.—Intensity of 3914Å auroral light average over 4 sec at half-integral values of L in about fifty passes of Injun 3 early in 1963. (After O'Brien and Taylor, 1964.)

minimum emission rate is, however, below visual threshold even in the auroral zone.

Figures 2 and 5 also give a good impression about the enormous variability of precipitation and photon emission at all latitudes, but especially near the auroral zone. At $L=6$ there are values of about $6 \cdot 10^6$ electrons/cm^2 sec ster shown in the figure. This is some 10^5 times the minimum value observed there.

(b) Time Characteristics of Precipitation

It is not possible in satellite measurements to differ between space variations and time variations short compared to the period of revolution. Balloon observations show, however, that time variations as rapid as of periods of a tenth of a second can occur in the electron flux (Winckler et al., 1962).

No systematic variation in the intensity of electron precipitation over periods as long as a day could be found by O'Brien (1964) from the Injun 1 and 3 measurements in contrast with the case for trapped electrons. Sharp et al. (1964) observed a higher nighttime than daytime precipitation flux of electrons in the energy range 0.08–24 kev—as well as of protons—during the 5 days life time of an oriented polar-orbiting satellite. They also found the energy distribution of the electrons to be harder on the dayside than on the nightside of the earth (Johnson et al., 1964). The Iowa group has recently reported the existence of a diurnal variation in the precipitated flux of electrons of energy above 40 kev at high latitudes. The maximum in the diurnal variation curve was reported to be on the dayside of the earth (Frank et al., 1964). It is not clear if the difference in the results found by various observers is due to the diurnal variation being different for different energy ranges or if it is due to some of the results being not statistically significant because of the enormous variability of the precipitation phenomenon.

(c) Pitch Angle Distribution

Figure 1 shows that over the aurora, where the precipitation is intense, the directional flux of precipitated electrons becomes equal to the flux of trapped electrons, which also is increased over the aurora. Figure 1 illustrates a general rule that has been found by O'Brien (1962a, b, 1964), namely that for electrons of $E \geq 40$ kev the pitch angle distribution approaches isotropy in the regions of intense precipitation. An isotropic pitch angle distribution in regions of strong precipitation has also been observed by Krasovskii et al. (1962) at an energy of about 10 kev. No cases have been found in which the directional flux of precipitated electrons was higher than the corresponding value for trapped electrons. The mentioned observations were made fairly close to the earth's atmosphere.

The tendency to isotropy seems to indicate that the acceleration of the electrons—if it is directed along the field lines—takes place far away from the atmosphere. This, as well as the mentioned observations of precipitation of electrons from above 1000 km in aurorae, suggest that the role of the ionosphere in the production of the energetic electrons is not important.

O'Brien (1964) found a flux upwards along the field lines, which was some 10 percent of the precipitated electron flux. He interpreted these observations as backscattering of electrons from the atmosphere.

(d) K_p—Dependence of Precipitation

The K_p dependence of the precipitation of electrons of energy above 40 kev is illustrated in

Figure 3. The average intensity was ten times higher near the auroral zone when K_p was above 4 than when it was below 4. The data material for the higher K_p range in Figure 3 does not contain data from any strong magnetic storm, so still higher values may be expected.

O'Brien (1964) found that the flux of precipitated electrons above 40 kev increased on the average by a factor of 5 for every step of K_p. A close correlation between precipitation intensity has also been observed for the 0.08–24 kev energy range by Sharp et al. (1964). O'Brien's results, obtained on Injun 3 in a low orbit, are shown in

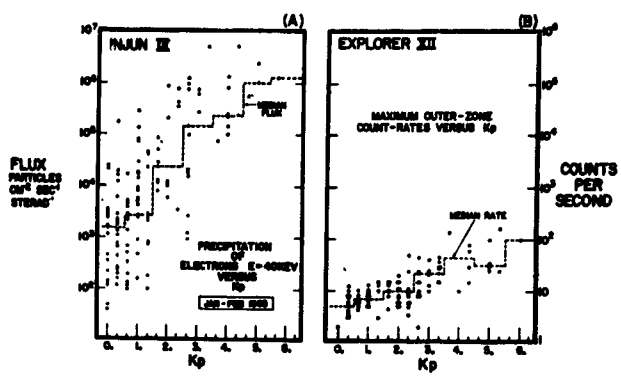

FIGURE 6.—Illustration that the flux of precipitated electrons (in A) varies more with K_p than does the omnidirectional flux (mainly of trapped electrons) in the equatorial plane (in B). Each point shows the maximum respective flux encountered on an outer-zone pass. (After O'Brien, 1964.)

Figure 6 together with the dependence of the omnidirectional flux above 40 kev as observed in the equatorial plane far from the earth by Explorer 12 (Freeman, 1963). As can be seen, the K_p dependence is very much larger close to the earth (at one end of the field line). If one assumes that both increases are due to a common acceleration mechanism it follows that it acts preferentially parallel to the geomagnetic field lines (O'Brien, 1964).

The change of omnidirectional flux above 40 kev with K_p, shown in Figure 6b, is opposite to what has mostly been observed for electrons of $E \gtrsim 2$ Mev (Arnoldy et al., 1960; Hoffman et al., 1962).

The dependence of the poleward boundary of precipitation on magnetic activity has been studied by Maehlum and O'Brien (1963). They used data for trapped electrons, but since O'Brien (1964) has shown that the precipitation has its maximum close to the poleward boundary of the trapped electrons, their results may be interpreted in terms of possible extension of precipitated electrons.

Maehlum and O'Brien (1963) found that during magnetic storms there was a very sharp boundary of the region where trapped electrons of energy above 40 kev could be observed. For this boundary, measured in L, they used the symbol L_n. It can be seen as a function of the K_p index during one geomagnetic storm in Figure 7. When K_p

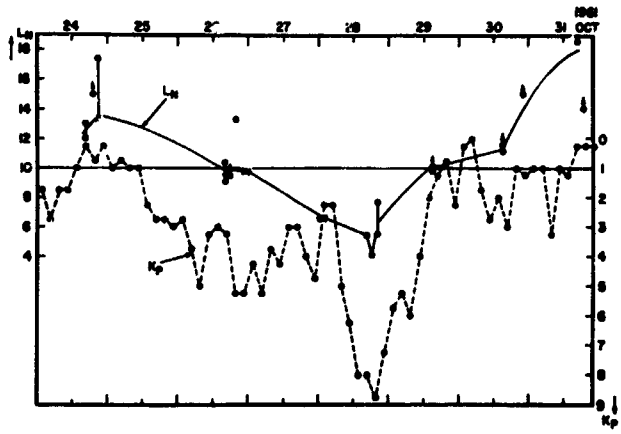

FIGURE 7.—Variation of the northern boundary of trapping with K_p during a geomagnetic storm, as observed by Injun I at a height of about 1000 km. (After Maehlum and O'Brien, 1963.)

reached its maximum value of 9, L_n had its minimum value of 4. Maehlum and O'Brien (1963) also found that the poleward boundary of strong radio wave absorption followed the L_n quite closely during the storm.

The effect of K_p on L_n is similar to the equatorward movement of the region of visual aurora during strong magnetic storms, which has been studied in the last few years in detail for some storms by Akasofu (1962, 1963a, b) and others.

(e) The Spectrum of Precipitated Electrons

Up to now only very rough measurements of the energy spectrum of the precipitated electrons have been reported. In most cases the proposed spectra have been obtained from two instruments with different energy characteristics. They are to be considered as rough equivalent spectra for

measurements made in a defined way. In addition, it has been found that the equivalent spectrum is highly variable both in space and time (cf. O'Brien et al., 1962). Nonetheless the available spectral data are of great interest at the present stage of knowledge in the field, and they even make it possible to draw some interesting conclusions about ionospheric effects of the precipitated electrons. These will be discussed in the following sections.

Most spectra that have been reported hitherto can be divided in two categories if they are expressed in an exponential form. On one hand, the e-folding value, b, in the spectrum of precipitated electrons, written in the form $\alpha \exp(-E/b)$, has been found often to be in the range 2–8 kev (McIlwain, 1960; Stilwell, 1963; Sharp et al., 1964a, b, c). This is a very steep spectrum but even steeper ones have been observed. McIlwain interpreted his rocket measurements in a strong aurora as indicating a monoenergetic flux of electrons with an energy of about 6 kev. Krasovskii et al. (1962) has observed steep spectra for precipitated electrons with a most common equivalent energy value of 14 kev.

The majority of the existing measurements have been made with Geiger tubes, for which the minimum detectable electron energy is about 40 kev. These measurements have mostly given e-folding values much higher than those mentioned above, namely, between 20 and 45 kev. (Davis et al., 1960; McDiarmid et al., 1960; O'Brien et al., 1962; Mann et al., 1963; O'Brien and Taylor, 1964). Mann et al (1963) found from measurements during only some 20 orbits that the values within this range were grouped in two classes, 25 ± 5 kev and 42 ± 3 kev.

The balloon measurements of X-rays at 30–35 km altitude also, in general, give inferred spectra of incident electrons of a fairly flat type, corresponding to e-folding energies in the range 20–45 kev (cf. e.g., Anderson and Enemark, 1960), although power law spectra often are found to fit the observations somewhat better than exponential spectra.

Recently the first direct measurements of precipitated electrons below 1 kev energy have been reported (Sharp et al., 1963; Evans et al., 1964). They showed that there is generally not very much energy flux below 1 kev. In some passages through the auroral zone Sharp et al. (1964c) found the integral fluxes above 0.18 and 10 kev to correspond to equivalent exponential spectra with e-folding values between 2 and 5 kev. On other occasions they did not find any energy flux at all below 1.5 kev. That there is not very much energy flux below 1 kev is also evident from observations of the luminosity distribution with height of aurorae. O'Brien and Taylor (1964) give an example of measurement results obtained on board Injun 3, according to which less than 0.1 percent of the auroral light originated above the satellite, that was at 250 km altitude. From this they conclude that the number of 10 ev electrons in the precipitated flux was no larger than the number of 10 kev electrons. It therefore seems probable that the spectrum, in general, does not increase very fast below 1 kev, which means that it is not of the power law type at these low energies.

Sharp et al. (1964c) found a significantly harder spectrum on the dayside than on the nightside. This observation agrees with multifrequency riometer measurements of auroral absorption by Lerfald et al. (1964), according to which the absorbing ionization is located lower down in the atmosphere in the day than in the night.

Of special interest are the statistical data on electron precipitation published recently. As mentioned earlier the precipitation is most intense near the auroral zone. O'Brien (1964) found an average flux of about 4.10^5 electrons/cm^2 sec in the precipitation cone at an invariant latitude of 65°. Injun 1 had a CdS detector, measuring electrons of energy above about 1 kev (O'Brien, 1962b). O'Brien and Taylor (1964) state that the flux of 4.10^5 electrons/cm^2 sec of energy greater than 40 kev was associated with an energy flux of 4 ergs/cm^2 sec for electrons of $E \gtrsim 1$ kev. These data should be considered as accurate to a factor of about three. Using these two values an equivalent electron spectrum in the range 1–40 kev can be deduced. It is found to be

$$n(E) = 7.8 \cdot 10^7 e^{-E/5.7} \text{ electrons/cm}^2 \text{ sec kev.}$$

For the energy values 40 and 250 kev similar average fluxes have been obtained from the Alouette measurements reported by McDiarmid et al. (1963). While the flux above 40 kev had its maximum at an invariant latitude of 65°, the

flux above 250 kev was maximal at about 60 degrees. McDiarmid et al. (1963) did not present any details for the latitudinal variation of this latter in integral flux. By applying a rough correction factor of 0.1 for the latitude variation of the average flux above 250 kev from 60 to 65 degrees invariant latitude, the following approximate equivalent spectra for the energy range 40–250 kev can be derived for two ranges of magnetic activity in the auroral zone ($\Lambda = 65°$), if isotropy is assumed for the upper hemisphere

$K_p < 4$: $n(E) = 1.2 \cdot 10^4 e^{-E/41}$ electrons/cm^2 sec kev

$K_p > 4$: $n(E) = 2.4 \cdot 10^5 e^{-E/30}$ electrons/cm^2 sec kev

(cf. Hultqvist, 1964b). The applied latitude correction is probably too large as judged from a comparison of the latitude distribution of passes in which the intensity of precipitated electrons with energies greater than 250 kev was greater than $3.2 \cdot 10^3$/cm^2 sec ster (Figure 8 of McDiarmid et al., 1963) and the corresponding diagram for

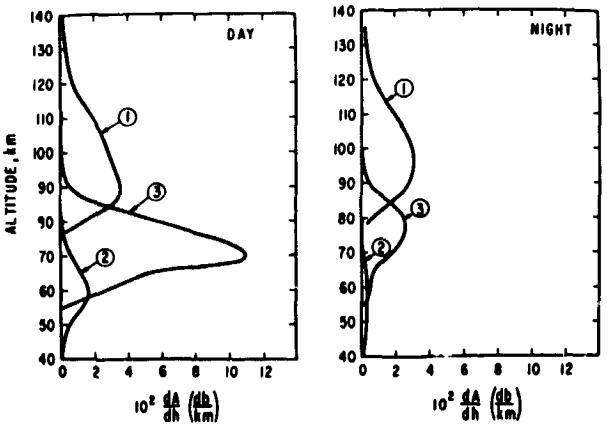

FIGURE 8.—(a) is for daytime and (b) for night. Curves in (a) and (b) show the height distribution of the absorption produced by the differential energy spectrum $N(E) = 5.10^8 e^{-E/5}$ kev electrons cm^{-2} sec^{-1} ster^{-1} kev^{-1}. The total absorption values corresponding to curves 1 amount to 1.04 db in the day and to 0.89 db at night. Curves 2 give the absorption due to the bremsstrahlung of the same electron spectrum. Total absorption in the day is 0.27 db and in the night 0.061 db. Curves 3, finally, represent the absorption distribution produced by the differential energy spectrum $N(E) = 7.10^4 e^{-E/41}$ kev electrons cm^{-2} sec^{-1} kev^{-1}, coming in along the field lines. Total daytime absorption under curves 3 is 1.9 db. The nighttime one is 0.52 db, if the height profiles of the ratio of negative ion to electron density used by Nicolet and Aikin (1960) and others are employed. 40 kev. The resulting spectra are thus too steep rather than too flat, and the absorption caused by electrons in the energy range 40–250 kev is probably larger than the values presented below.

As mentioned, the spectra of precipitated electrons are very variable. There is also an important latitude variation in the steepness, which increases with latitude (O'Brien et al. 1962; McDiarmid et al., 1963; O'Brien, 1964). On the other hand there seems to be no significant dependence of the spectrum on pitch angle or on the intensity of precipitation (O'Brien, 1964).

To obtain the equivalent spectra the averaging has been made over a large number of measured integral fluxes. With a variation of a factor of 10^5 the use of averages may be questioned. It is also questionable whether average integral fluxes are the best values to use when the interest is in the average electron density produced by the particle influx. The average electron density is then defined by the averaging process employed and this method of averaging is not identical with the averaging made in measuring the ionospheric absorption, for instance. It can, however, be shown that the average electron density produced by the precipitated electrons can be expressed in the average integral fluxes measured on the satellites. Since only two experimental integral flux values are available, one has to fit a two-parameter energy relation for the average flux to these experimental data (Hultqvist, 1964b), as has been done above.

QUANTITATIVE RELATIONS BETWEEN ELECTRON PRECIPITATION AND PHOTON EMISSION IN AURORA

Two direct measurements of the quantitative relation between precipitation and photon emission will be discussed here, namely those of McIlwain (1960) and O'Brien and Taylor (1964). It is of interest to compare their results with what is expected on theoretical grounds.

McIlwain did not use any filter, but measured the photon flux integrated over the transmission curve of the photomultiplier. If we assume that $\frac{1}{5}$ of the light was λ 3914Å, the measured photon flux corresponds to an emission rate of about 3 kilorayleigh at this wavelength. The fraction, $\frac{1}{5}$, is fairly arbitrary, but it seems reasonable (cf. e.g., Dalgarno, 1964) and is probably in error by

less than a factor of 2 and ½, respectively, for an ordinary auroral zone aurora. McIlwain's (1960) measured electron flux corresponds to an energy flux of 20 erg/cm² sec, if the spectrum obtained was extrapolated to $E=0$. Thus, the resulting electron energy flux required per unit of λ 3914Å emission rate is 7 ergs/cm² sec per *kR*.

O'Brien and Taylor (1964) reported an average λ 3914Å intensity of $2(+4/-1.5)$ *kR* at the maximum of the latitude distribution, i.e., in the auroral zone. As mentioned above, the electron measurements gave a corresponding average of the flux above 40 kev of $4\cdot10^5$ electrons/cm² sec and an energy flux for $E>1$ kev of about 4 ergs/cm² sec, which values they consider as accurate to a factor of about three. In order to get a value directly comparable with that of McIlwain one would have to extrapolate the energy spectrum from 1 kev down to $E=0$ and evaluate the total energy flux. Using the equivalent exponential spectrum, we find 5 ergs/cm² sec for $E>0$. Thus the Injun 3 results give 2.5 ergs/cm² sec per *kR*. Considering the uncertainties in measurements and the method of evaluation, this is a good agreement.

What energy flux per *kR* does one expect on the basis of existing knowledge about the emission processes? Omholt (1957, 1959), Chamberlain (1961), Rees (1963), and Dalgarno (1964), among others, have discussed this. It has been shown by Stewart (1956) that the ratio between the excitation cross section for the 3914Å band of N^+_2 and the total ionization cross section is constant, at least up to 200 ev energy, and has the value 0.02. Assuming that this value is true over the whole energy range of interest, one finds that 50 electron-ion pairs are produced for each 3914Å photon. Since the mean energy expended by fast electrons in nitrogen per electron-ion pair is 35 ev (at least for energies down to a few hundred ev; it is assumed that the figure is correct down to zero energy), we find that $50\times35=1750$ ev is dissipated per 3914Å photon. Since each photon has an energy of 3.2 ev the efficiency with which energy is converted into 3914Å radiation is $1.8\cdot10^{-3}$. When the initial energies of the fast electrons fall below perhaps 100 ev, these efficiencies must decrease sharply (Dalgarno and Griffing, 1958; Dalgarno, 1964). One *kR* of 3914Å photons corresponds to an energy influx of 2.8 ergs/cm² sec, if the efficiency figure $1.8\cdot10^{-3}$ is employed. Dalgarno (1964) has used the value $1\cdot10^{-3}$. With this conversion efficiency we find the energy flux requirement to be 5.1 ergs/cm^{-2} sec^{-1} per *kR*. The agreement between these values and the experimental ones of McIlwain (1960) and O'Brien and Taylor (1964) is better than expected, when the uncertainties in the analyses are taken into account.

The total efficiency of converting particle energy into photons of any energy is expected to be about 1 percent on theoretical basis (cf. Chamberlain, 1961). McIlwain found from his rocket measurements a value of only 0.2 percent while preliminary Injun 3 results point towards 1 percent (O'Brien and Taylor, 1964).

AURORAL ABSORPTION

Auroral absorption is in general defined on riometer records as all the absorption, generally irregularly varying, which is usually observed during magnetically disturbed conditions and which is not associated with either polar cap absorption (PCA), produced by high energy solar protons, or sudden cosmic noise absorption (SCNA), which is caused by solar ultraviolet radiation. The auroral absorption is thus defined as the remainder when one has excluded two well defined types of absorption. It is therefore not surprising that it recently has been found to contain a number of phenomena differing, for example, in the energy characteristics of the ionizing agent (Ansari, 1963). The name may, however, be motivated by the fact that there is a fairly good correlation between auroral absorption and the general level of magnetic disturbance (cf. e.g., the review by Hultqvist, 1963c).

It has long been known that some of the auroral absorption is located below the *E*-layer, i.e. in or below the *D*-layer. Such evidence arises, for instance, from ionosondes, which frequently are blacked out during magnetic storms. This shows that all the radio energy is absorbed between the earth's surface and the *E*-layer. It has not been clear, however, whether all the absorption, for sufficiency high frequency cosmic noise, takes place below the *E*-layer or whether there may be as much or even more absorption at *E*-layer heights. In fact, there are reasons to believe that the absorption produced by those electrons which

are the cause of the visible aurora should be located mainly up in the altitude range where the aurora occurs. Evidence has recently been presented against the hypothesis of Chapman and Little (1957) that the main part of the radiowave absorption is produced below 90 km by X-rays from the primary auroral electrons. The absorption due to primary electrons of an energy spectrum as measured in visual aurora by McIlwain (1960), is probably at least an order of magnitude greater than that due to the bremsstrahlung X-rays the electrons give rise to (Ansari, 1963; Hultqvist, 1963, 1964; Brown, 1964).

The height of the main part of the auroral absorption became an important parameter for the understanding of the electron reactions in the lower ionosphere when it was found that there is a much smaller influence of the sunlight on the absorption value than was expected on the basis of existing models (cf. e.g., the review by Hultqvist, 1963c). A very small sunlight effect would be expected if all auroral absorption took place up in the height interval of the ordinary visible aurora. But such a height distribution would be in conflict with a large body of other experimental observations (cf. e.g., Hultqvist, 1963a, b, c). It would appear that the satellite measurements reported by Mann et al. (1963), McDiarmid et al. (1963), O'Brien (1964) and O'Brien and Taylor (1964) give a solution of this problem.

An important satellite observation in this respect is that of Mann et al. (1963) that there occurs frequently beside the soft type of spectrum of the precipitated electrons, observed in visible aurora by McIlwain (1960), a harder type with the e-folding energy between 25 and 45 kev. The averages of the extensive statistical satellite data of McDiarmid et al. (1963) and O'Brien (1962b, 1964) correspond to equivalent spectra given on page 11. Thus the e-folding energy is about McIlwain's value for the low energy range and is appreciably higher in the higher range.

Having these average spectra it is possible to calculate how much absorption is produced by the electrons below and above 40 kev energy. This has been done by Hultqvist (1964a, b). Figure 8 shows the height distribution of absorption per km due to the following spectra (Hultqvist, 1964a)

Curves No. 1: $5 \cdot 10^8 e^{-E/5}$ electrons/cm² sec ster kev corresponding to a very strong visual aurora of international brightness coefficient between III and IV;

Curves No. 2: Due to the bremsstrahlung X-rays produced by the electrons giving rise to curve No. 1;

Curves No. 3: $7 \cdot 10^4 e^{-E/41}$ electrons/cm² sec ster kev which was observed over the auroral zone by Mann et al. (1963).

It can be seen from Figure 8 that although curve No. 1 corresponds to a very strong aurora, the riometer absorption due to the hard electron spectrum (curve 3), which has its peak as low as 70 km altitude, is larger. The total absorption for daytime was found to be 0.9 db for the soft electron spectrum and 1.9 db for the hard one. Even if the uncertainty in the computed absolute absorption values is fairly high (cf. Hultqvist, 1964a) it is probably less than a factor of three for the relative values due to the various spectra.

The profiles shown in Figure 8 can, with proper absorption scale, be used for estimating the absorption caused by the average precipitation spectra observed by the Injun and Alouette satellites. The e-folding value in the range 1–40 kev was found to be 5.7 kev (see page 11). This is very close to McIlwain's (1960) value 5.0 kev. In fact, the spectrum $2.4 \cdot 10^8 e^{-E/5}$ electrons/cm² sec kev contains the same number of electrons above 40 kev as the average observed by Injun 3 ($4 \cdot 10^5$ electrons/cm² sec; O'Brien and Taylor, 1964). It corresponds to a total energy flux above 1 kev about twice as high as the average value (4 ergs/cm² sec) given by O'Brien and Taylor (1964). However, the corresponding energy flux per kilorayleigh is about 5 ergs/cm² sec which is equal to the average of the values found by McIlwain (1960) and O'Brien and Taylor (1964).

Using the equivalent spectrum $2.4 \cdot 10^8 e^{-E/5}$ electrons/cm² sec kev for the 1–40 key range and the $1.2 \cdot 10^4 e^{-E/41}$ electrons/cm² sec kev for 40–250 kev during low magnetic activity ($K_p < 4$), the electron density profiles 3 and 1 in Figure 9 are found. The total absorption produced by these two spectra are 0.09 db and 0.32 db, respectively.

For $K_p > 4$ the average fluxes of McDiarmid et al. (1963) above 40 and 250 kev correspond to the exponential spectrum $2.5 \cdot 10^6 e^{-E/30}$ electrons/cm² sec kev. For this spectrum only an upper limit of the electron density and absorption can be obtained with the use of Figure 8. Curve 2 in

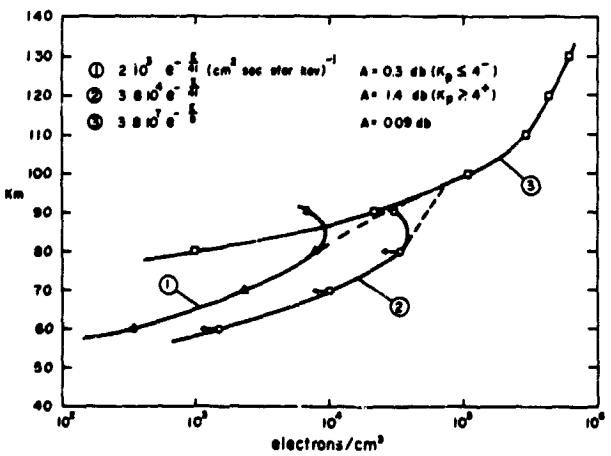

FIGURE 9.—Electron density profiles due to three different energy spectra of pecipitated electrons. The spectra as well as the total absorption, A, at 27.6 are given in the figure. Curve No. 2 gives an upper limit for the equilibrium electron density distribution produced by the spectrum $3.8 \cdot 10^4 \epsilon^{-E/30}$ (cm³ sec ster kev)$^{-1}$. A lower limit for this spectrum is curve No. 1.

Figure 9 shows this upper limit for the electron density. The corresponding upper limit of the total absorption is 1.4 db. Lower limits for the average electron density distribution and absorption are the values given for $K_p < 4$, i.e., curve 1 in Figure 9 and the corresponding absorption value of 0.32 db. The total riometer absorption due to the average electron spectrum in the energy range 40–250 kev is thus found to be about 1 db during the moderately disturbed conditions for which the observations are representative.

Two assumptions were made in the computations described above, which both tend to increase the relative importance of the absorption caused by precipitated electrons in the range 1–40 kev. One is that the equivalent average spectrum for the energy range 40-250 kev is probably less steep than the spectra used in the calculations. The other is that the equilibrium relation between electron density and the ionization rate was used. The computed absorption is therefore certainly overestimated. Since the effective recombination coefficient decreases from 60 km upwards the overestimation will be most important at greater heights. It does not seem probable that the error in the average absorption per unit height in the lowermost part due to unequilibrium would exceed a factor of two, since the rate of variation of the electron content, as seen on riometer records, mostly is slow compared with the recombination time in that part of the ionosphere. It is thus probable that the relative contribution of the absorption caused by the low energy electrons (corresponding to curve no. 3 in Figure 9) is smaller than shown by the figures given above.

Since the average absorption values produced by "soft" and "hard" electrons differ by an order of magnitude at least in the day, it seems possible to draw some conclusions on their basis.

Most of what is called auroral absorption seems to take place below 90 km. Hence the reason for the observed very small influence of sunlight on the intensity of the absorption is *not* that the absorption is located mostly above 90 km altitude, (where, according to virtually all models that have been proposed in the last few years, the density of negative ions is negligible in both day and night). One apparent interpretation of this observation is that the negative ions in fact are negligible, even in the night, down to about 60 km (as proposed by Hultqvist, 1962, 1963a, b). In any case it seems that the electron chemistry in the lowest ionosphere is quite different from what has hitherto been believed.

The virtual absence of sunlight influence on auroral absorption taking place mainly in the range 60–90 km thus leads to the conclusion that photo detachment is not important in that height interval. If this is true, the problem cannot be solved by assuming that the detachment of electrons from negative ions, in the height range mentioned, requires ultraviolet radiation, as proposed and discussed by Eriksen et al. (1960) and Reid and Leinbach (1962), and Reid (1961).

The result that the auroral absorption is produced mainly by electrons of energy above 40 kev, while the visible aurora is caused by lower energy electrons (cf. e.g., McIlwain, 1960) makes the fairly poor observed correlation between visible aurora and absorption understandable. By combining low-energy and high-energy electron spectra in various proportions, one may expect to see visible aurora practically without absorption, strong absorption without visible aurora, and all combinations in between. This is what has been found in the detailed study by Ansari (1963). There is a different local time dependence of the occurrence frequency of the low and high energy parts of the precipitated electron spectra. The auroral absorption has a pronounced maximum

in the auroral zone in the morning hours, whereas the visual aurora has its maximum in the middle of the night. So there seems to be some mechanism that accelerates the electrons on the average to higher energies over the morning side of the auroral zone.

The quantitative estimations of average absorption values presented above refer to the auroral zone. As has been pointed out earlier there is a tendency for the electron spectrum to grow steeper with increasing latitude and the conclusions drawn may not be true far inside the auroral zone. On the other hand the conclusion that auroral absorption is located mainly below 90 km is probably valid at subauroral latitudes. This is indicated also by the observed good correlation between bremsstrahlung X-rays and visual aurora at these latitudes (cf. e.g., the review by Winckler, 1962).

The deductions in this section are based on average fluxes and average spectra derived from widely varying, measured electron fluxes at two energies each, only. Conclusions should certainly be drawn from them with great care (cf. also page 12), but it seems that the order of magnitude results presented above should be fairly significant.

The height distribution of auroral absorption is quite similar to what has recently been found by means of multifrequency riometer measurements by Lerfald et al. (1964). The multifrequency absorption measurements can, however, provide height information only in the interval 35–75 km. A possible contribution from ionization up in the visible aurora in the presence of absorption also at lower altitudes cannot be measured by that technique, whereas the satellite measurements, reviewed above, clearly indicate that, on the average, most absorption is produced 90 km altitude.

The total absorption values obtained from the Injun and Alouette measurements are in quite reasonable accordance with the average absorption during the five most disturbed and five most quiet days per month, as observed over several years at College (geomagnetic latitude 64.5°) by Basler (1963). For the disturbed days he found a daily average of about 1 db in the summer and between 1 and 2 db in winter and at equinoxes—as compared to about 1 db given above for $K_p>4$. For the quiet days the daily average at College was about 0.3 db (to be compared to the value 0.3 db for $K_p<4$ above).

Figure 3 shows the fraction of passages for which the absorption would be estimated to be greater than about 0.2 db for high and low magnetic activity.

THE LOWER IONOSPHERE AT NIGHT

A number of hypothesis of corpuscular ionization of the ionosphere have been advanced to explain the existence of appreciable electron densities in the night and especially during the polar night (see Antonova and Ivanov-Kholodny, 1961). Mariani (1964) has invoked a corpuscular flux with a peak value of about 0.1 erg/cm² sec of electrons with energies of the order of 1 kev at geomagnetic latitudes between 55 and 65° to explain the correlation of maximum electron density in the *F*-region at noon with solar activity. Willmore (1964) has found evidence for a particle energy influx of the order of 20 percent of the UV photon flux from Ariel I measurements of temperatures in the *F*-region. He also found good agreement between the geographical distribution of the temperature and of particle fluxes observed by Sputnik II. Harris and Priester (1962) assume a corpuscular heat source comparable in influence to the ultraviolet solar radiation, i.e. of the order of a few ergs/cm² sec, in their model for the solar cycle variation of the upper atmosphere.

The electron density in the *F*-layer should decrease by a factor of 100 or more in 5–10 hours after sunset, at that altitude, if no ionization took place. As the observed decrease in general is only a factor of 10–20 in the altitude interval 120–200 km and 3–10 in the *F*-region, the obvious conclusion is that some nighttime ionization process exists. The need for such a process is still stronger in order to explain the fairly high electron densities observed over the central polar caps during the long polar nights. For instance, at the Pole Station (latitude 90°*S*) at midnight in the midwinter the *foF* was about 5 Mc/s in the high-solar activity year 1958 and a little above 3 Mc/s three years later. The nighttime *foF* was not very much less than the noon value in the summer. It is true that *foF* is not a good measure of the electron production rate in the upper ionosphere, especially not in the polar night, as dynamical effects within the ionosphere are very important, but

even so it can definitely be said that an ionization source must exist.

Does the observed flux of precipitated electrons contain enough energy to produce the lower ionosphere at night? It is not possible to give any accurate answer to that question now, since no extensive measurements of energy fluxes below 1 erg/cm² sec have been made in the lowest part of the electron energy spectrum of interest. Another piece of missing information is the energy flux associated with low energy protons. Krasovskii et al. (1963) have observed appreciable fluxes of positive ions with energy above 200 ev at low and medium latitudes ($\leq 49°$). The ion flux was usually about 10^8/cm² sec ster and the energy flux associated with it was probably ≤ 0.1 erg/cm² sec. It is not known whether the ions were trapped or precipitated. Above 100 km altitude not only precipitated electrons, as defined in the introduction, but also trapped ones contribute to the production of free electrons, and their contribution may even exceed that of the precipitated electrons. No observational results are yet available from which the energy dissipation into the atmosphere by protons can be evaluated.

It is obvious from Figure 9 that the average electron flux produces quite sufficient electron densities down in the *E*-layer in the auroral zone. A numerical calculation using the same spectrum as for curve 3 in Figure 9, for 200 km altitude gives an electron production rate of 1400 electrons/cm³ sec, corresponding to an equilibrium electron density of from $4 \cdot 10^5$ to $2 \cdot 10^6$/cm³, depending on the recombination coefficient used (Mitra, 1959, Van Zandt et al., 1960, or Schmerling and Grant, 1961). Therefore the corpuscular energy source is probably sufficient for production of the nighttime *F*-layer too in the auroral zone.

The electron densities shown in Figure 9 are astonishingly high. They correspond to critical frequencies higher than are normally observed in the auroral zones. They were derived, however, without taking dynamic effects into account and there may very well be uncertainties of a factor of four or so due to the inaccuracy in the experimental average particle fluxes, as well as in the atmospheric parameters used in the derivation. To this comes that the equilibrium relation has been used in computing the electron density from the ionization rate. Too large values of electron density and absorption is probably obtained in that way. On the other hand the ionization produced by electrons mirroring above 100 km has not been taken into account which counteracts the effect of the use of the equilibrium relation between electron density and ionization rate.

It is not known to this author whether the observed enormous variability of the precipitation fits into the time behaviour of the nighttime ionosphere.

What can be said about the ionosphere over the central polar cap in respect of observed particle energy dissipation? The average flux of precipitated electrons above 40 kev energy was found to be 10–100 times smaller than in the auroral zone at 76° invariant latitude by Injun 3 (O'Brien, 1964) and 100–1000 times smaller by Alouette (McDiarmid et al., 1963). Precipitation did not take place continuously well inside the auroral zones, but it varied in intensity from cosmic ray background to 10^5 electrons/cm² sec ster. Spectral information for the central polar caps is not available at the time or writing. The best that can be done to obtain an idea about the electron production rate over the polar caps from earlier presented results, seems to be to assume that the spectrum is about the same as used above for the auroral zone and to reduce the ionization rate in proportion to the difference between the two regions in counting rate found by Injun 3 and/or Alouette.

The corresponding energy flux for electrons of energy above 1 kev will thus be in the range 10^{-2} to 1 erg/cm² sec and the steady state electron densities 1/30 to 1/3 of those for curve no. 3 in Figure 9. For a 200 km electron density of 10^6 cm^{-3} in the auroral zone a corresponding electron density range of $3 \cdot 10^4 - 3 \cdot 10^5$ electrons/cm³ is obtained for the polar caps, neglecting all dynamical effects. The corresponding plasma frequency is between 1.6 and 4.9 Mc/s. These values should be compared with the *foF* value of about 3 Mc/s observed at the Pole Station during somewhat higher solar activities. At 100 km altitude the plasma frequency would be between half an Mc/s and one and a half Mc/s. Despite the roughness of this estimate it seems possible to state that the observed precipitation of electrons of energies above 1 kev must contribute significantly to the nighttime ionosphere over the polar caps and that one

cannot rule out the possibility that it is the main source.

At subauroral latitudes the average values found from the Injun 3 data (O'Brien, 1964) by making the same assumptions as for the polar caps are the following:

energy flux: $10^{-2}-10^{-1}$ erg/cm² sec,

equilibrium electron density at 200 km: $3\cdot10^{4}-10^{5}$ electrons/cm³

at 120 km: $1.5\cdot10^{4}-4.5\cdot10^{4}$ electrons/cm³

corresponding plasma frequency at 200 km: 1.6−2.8 Mc/s

at 120 km: 1.1−1.9 Mc/s.

Also in this case it seems possible to draw the same conclusion as for the polar caps: the observed precipitation of electrons of energy above 1 kev is certainly of major importance for the nighttime lower ionosphere in subauroral latitudes and it does not seem possible at the present time to exclude the possibility that it is the main source.

A problem with the precipitated-electron source of ionization is that it it is highly discontinuous in space and time. It is not known to this author if the time constants of the ionospheric processes can explain that much slower variations are observed in *foF*, for instance.

If the electron precipitation observed by the Injun and Alouette satellites is the main source of nighttime ionization, one expects a maximum for the average nighttime electron density in the auroral zone. It seems not to be clear if such a maximum exists or not. The situation is complicated by the frequent strong disturbances there, which tend to hide an average effect.

The average absorption at riometer frequencies corresponding to the given electron densities for polar cap and subauroral latitudes is below the lower measurable limit.

The electron density produced in and below the *D*-layer by the average precipitation fluxes described above is orders of magnitude greater than that due to the ordinary cosmic radiation (see e.g. Mohler, 1960) in the auroral zone and is probably of the same order of magnitude or is even larger than that due to cosmic rays in subauroral latitudes, if the height profile of the ratio of negative ion to electron densities of Nicolet and Aikin (1960) and others is valid.

The average energy flux of precipitated electrons observed by Injun 3 and Alouette meets the requirements of Mariani (1964) but is somewhat smaller than that deduced by Willmore and orders of magnitude smaller than that hypothesized by Antonova and Ivanov-Kholodny (1961) and Harris and Priester (1962).

AIRGLOW

The following questions about airglow in connection with particle precipitation are of great interest.

(1) What limits can be put on the particle energy flux in low and medium latitudes on the basis of airglow intensities?

(2) Is it possible that the observed precipitated electrons of energy above 1 kev are responsible for part of, or all airglow?

The second question has been answered with no by O'Brien (1962b) on the basis of energy considerations. The average zenith intensity of 5577Å at midlatitudes is about 250 rayleighs (Hunten et al., 1956) which requires a precipitation rate of the order of 1 erg/cm² sec. The precipitation rate observed at midlatitudes is equivalent to orders of magnitude smaller than this.

The first question has been discussed by e.g. Ivanov-Kholodny (1962), Galperin (1962), and Galgarno (1964). The N^{+}_{2} bands are produced by impact excitation. According to Roach (see Dalgarno, 1964) 60R of 3914Å emission would not occur undetected. This puts an upper limit of about 0.3 erg/cm² sec on the possible electron precipitation rate. Galperin (1962) has claimed that the observable limit can sometimes be put much lower and the corresponding limit of the energy flux has been given as $2\cdot10^{-2}$ erg/cm² sec by Dalgarno (1964).

The energy fluxes derived above from the satellite measurements reported by McDiarmid et al. (1963) and O'Brien (1964) amount to $10^{-2}-10^{-1}$ erg/cm² sec in subauroral latitudes. From this it seems that the limit given by Roach is a safe one, whereas the observed energy flux sometimes may exceed the limit given by Galperin (1962).

RELATION OF PRECIPITATED ELECTRONS TO THE OUTER RADIATION BELT

The idea about the relations between the electrons that are precipitated into the atmosphere and the trapped electrons in the radiation belts, which was prevailing one or two years ago, was roughly that the precipitated particles were dumped from the large storage of energetic trapped particles in the magnetosphere through the influence of disturbing effects caused by the solar plasma, as, for example, the magnetic disturbances. The number of trapped particles was thought to be sufficiently large to allow the precipitation rates observed to occur with only weak and perhaps independent processes of injection and acceleration required to replenish the particles in the radiation belt, the occurrence of which is necessary to be assumed in any case for understanding the existence of the trapped radiation.

This picture has been completely changed recently through the investigations by O'Brien (1962b, 1964) of the measuring results of Injun 1 and Injun 3 and also through a number of balloon studies of X-ray fluxes in the lower atmosphere (Winckler et al., 1962, Anderson, 1964).

O'Brien (1962b) estimated the lifetime of the trapped electrons in the outer radiation belt, assuming that the source was stopped but the loss mechanisms operated at the same rate as observed by Injun 1. He found that the outer zone beyond $L \sim 2$ would drain empty of electrons in a few hours. Similar average lifetimes have also been evaluated from X-ray measurements (see e.g., Winckler et al., 1962 and Anderson, 1964). Sometimes precipitation rates several orders of magnitude above the average (more than 1000 ergs/cm^2 sec) have been observed (Krasovskii et al., 1961, O'Brien and Laughlin, 1962, and Winckler et al., 1962). Thus Winckler et al. (1962) recorded an electron burst reaching 10^{11} electrons/cm^2 sec, a flux which would have used up the total energy of trapped particles in the field tube in half a second, but yet it persisted for about 100 seconds. Some efficient acceleration mechanism, which can reach full efficiency in a fraction of a second, seems required.

O'Brien (1964) has also shown that the flux of trapped radiation increases when precipitation takes place instead of diminishing, which would be expected if the trapped particles were simply dumped into the atmosphere. An acceleration mechanism seems to influence precipitated and trapped particles simultaneously.

Finally, O'Brien (1964) has demonstrated that the precipitation is highly energy dependent. There was no significant precipitation or change in the flux of trapped electrons of energy greater than 1.5 Mev observed in the middle of a strong burst of electrons of energy above 40 kev. This demonstrates that the precipitation could not be due simply to a lowering of the mirror point through a decrease in the geomagnetic field, since such a mechanism would be active over the whole spectrum.

Taken together, this new evidence clearly demonstrates that the precipitated electrons which produce aurora and ionospheric ionization are not produced by dumping trapped electrons into the atmosphere. An acceleration mechanism must be involved. This mechanism must be one that can act with full strength very quickly (in a fraction of a second) and it should not change the flux of Mev electrons more than 10 percent, when the simultaneous changes for trapped electrons of energy above 40 kev is a hundred-fold and for the precipitated electrons above 40 kev is more than three orders of magnitude. O'Brien (1964) mentioned acceleration in an electrostatic field directed along the magnetic field lines and involving a voltage drop of the order of 10 kilovolts as one possible mechanism from the precipitation-observation point of view.

The development in the last one or two years has thus in some respects brought the model of the auroral mechanism back into the situation that existed before the discovery of the Van Allen belts. These belts have been demonstrated to be probably an effect of the same acceleration mechanism that precipitates particles into the atmosphere and produces aurora, but not the source of these particles. The "leaky bucket" model has been replaced by the "splash catcher" model, in the vocabulary of O'Brien.

ACKNOWLEDGEMENT

I am grateful to L. R. Davis, D. S. Evans, and R. A. Hoffman for reading the manuscript and proposing improvements.

REFERENCES

S. I. AKASOFU (1962) J. Atm. Terr. Phys. 24, 723.

S. I. AKASOFU (1963a) J. Geophys. Res. 68, 1667.

S. I. AKASOFU (1963b) J. Atm. Terr. Phys. 25, 163.

S. I. AKASOFU and S. CHAPMAN (1962) J. Atm. Terr. Phys. 24, 785.

K. A. ANDERSON (1964) Paper presented at Lockheed Symposium on Aurora in Palo Alto, Jan. 1964.

K. A. ANDERSON and D. C. ENEMARK (1960) J. Geophys. Res. 65, 3521.

Z. A. ANSARI (1963) Univ. of Alaska, Sci. Rep. No. 4, NSF Grant No. G 14133.

L. A. ANTONOVA and G. S. IVANOV-KHOLODNY (1961) Geomagn. and Aeronomy 1, No. 2 (English translation 1, 149).

R. L. ARNOLDY, R. A. HOFFMAN and J. R. WINCKLER (1960) J. Geoph. Res. 65, 1361.

R. P. BASLER (1963) J. Geoph. Res. 68, 4665.

R. R. BROWN (1964) Arkiv för Geofysik (in print).

R. R. BROWN, K. A. ANDERSON, C. D. ANGER and D. S. EVANS (1963) J. Geophys. Res. 68, 2677.

J. W. CHAMBERLAIN (1961) Physics of the Aurora and Airglow, Academic Press, N. Y.

S. CHAPMAN and C. G. LITTLE (1957) J. Atm. Terr. Phys. 10, 20.

A. DALGARNO (1964) Ann. de Géophys., 20, 65.

A. DALGARNO and W. G. GRIFFING (1958) Proc. Roy. Soc. A248, 415.

L. R. DAVIS, O. E. BERG and L. H. MEREDITH (1960) Space Research, p. 721 (Ed. Kalmann-Bijl) North Holland Publishing Co., Amsterdam.

R. N. DEWITT (1962) J. Geophys. Res. 67, 1347.

K. W. ERICKSEN, O. HOLT, and B. LANDMARK (1960) J. Atm. Terr. Phys. 18, 78.

J. E. EVANS, R. A. JOHNSON, R. D. SHARP and J. B. REGAN (1964). Paper presented at the American Geophys. Union Meeting in Washington, D.C, April 1964.

L. A. FRANK, J. D. CRAVEN, and J. A. VAN ALLEN (1964). Paper presented at the URSI-AGU-AAS Symposium on Solar-Terrestrial Relationships, April 20–21, Wash., D.C.

J. W. FREEMAN (1963) State Univ. Iowa Publ. SUI–63–20.

YU. I. GALPERIN (1962) Bulletin (Izvestiya) Acad. Sci. USSR, Geophys. Series No. 2, 174.

T. HARRIS and W. PRIESTER (1962) J. Geophys. Res. 67, 4585.

R. A. HOFFMAN, R. L. ARNOLDY, and J. R. WINCKLER (1962) J. Geophys. Res. 67, 4543.

B. HULTQVIST (1962) Kiruna Geophysical Observatory, Sci. Rep. No. 2, Contract No. AF 61(052)–601.

B. HULTQVIST (1963a) Planet. Space Sci. 11, 371.

B. HULTQVIST (1963b) J. Atm. Terr. Phys. 25, 225.

B. HULTQVIST (1963c) Radio Astronomical and Satellite Studies of the Atmosphere, p. 163 (Ed. Aarons) North-Holland Pub. Co., Amsterdam.

B. HULTQVIST (1964a) Planet. Space Sci. (in print).

B. HULTQVIST (1964b) Planet. Space Sci. (in print).

G. S. IVANOV-KHOLDNY (1962) Geomagnetism and Aeronomy (English translation) 2, 315.

R. G. JOHNSON, J. E. Evans, R. D. SHARP and J. B. REAGAN (1964). Paper presented at the American Geophysical Union Meeting in Washington, D.C., April 1964.

V. I. KRASOVSKII, I. S. SHKLOVSKI, YU. I. GALPERIN, E. M. SVETLITSKII, YU. M. KUSHNIR, and G. A. BORDOVSKII (1962) Planet. Space. Sci. 9, 27.

V. I. KRASOVSKII, YU. I. GALPERIN, N. V. GALPERIN, N. V. JORJIO, T. M. MULARCHIK, and A. D. BOLUNOVA (1963). Paper presented at symposium in Paris.

G. M. LERFALD, C. G. LITTLE, and R. PARTHASARATHY (1964) J. Geophys. Res. (in print).

C. G. LITTLE, G. M. LERFALD and R. PARTHASARATHY (1963). Personal communication.

B. MAEHLUM and B. J. O'BRIEN (1963) J. Geophys. Res. 68, 997.

L. G. MANN, S. D. BLOOM, and H. I. WEST, JR., (1963) Space Research III, p. 447. (Ed. Priester) North Holland Publishing Co., Amsterdam.

F. MARIANI (1964) J. Atm. Sci. 20, 479.

I. B. MCDIARMID, D. C. ROSE, and E. BUDZINSKI (1961) Can. J. Phys. 39, 1888.

I. B. MCDIARMID, J. R. BURROWS, E. E. BUDZINSKI, and M. D. WILSON (1963) Can. J. Phys. 41, 2064.

C. E. MCILWAIN (1960) J. Geophys. Res. 65, 2727.

A. P. MITRA (1959) J. Geophys. Res. 64, 733.

W. F. MOLER (1960) J. Geophys. Res. 65, 1459.

M. NICOLET and A. C. AIKIN (1960) J. Geophys. Res. 65, 1469.

B. J. O'BRIEN (1962a) J. Geophys. Res. 67, 1227.

B. J. O'BRIEN (1962b) J. Geophys. Res. 67, 3687.

B. J. O'BRIEN (1963) J. Geophys. Res. 68, 989.

B. J. O'BRIEN (1964) J. Geophys. Res. 69, 13.

B. J. O'BRIEN and C. D. LAUGHLIN (1962) J. Geophys. Res. 67, 2667.

B. J. O'BRIEN, C. D. LAUGHLIN, J. A. VAN ALLEN, and L. A. FRANK (1962) J. Geophys. Res. 67, 1209.

B. J. O'BRIEN and H. TAYLOR (1964) J. Geophys. Res. 69,45.

A. OMHOLT (1957) Astrophys. J. 126, 461.

A. OMHOLT (1959) Geophys. Publikasjoner 20 (11), 1.

M. H. REES (1963) Planet. Space Sci. 11, 1209.

G. C. REID (1961) J. Geophys. Res. 66, 4071.

G. C REID and H. LEINBACH (1962) J. Atm. Terr. Phys. 13, 216.

E. R. SCHMERLING and D. GRANT (1961) Penn. State. Univ., Sci. Rep. No. 147.

R. D. SHARP, J. E. EVANS, R. G. JOHNSON and J. B. REAGAN (1963). Paper presented at American Geophys. Union Third Western Nat. Meeting. Boulder, Dec. 1963.

R. D. SHARP, J. E. EVANS, R. G. JOHNSON, and J. B. REAGAN (1963). Paper presented at American Geophys. Union Third Western Nat. Meeting. Boulder, Dec. 1963.

R. D. SHARP, J. E. EVANS, R. G. JOHNSON, and J. B. REAGAN (1964a). Paper presented at COSPAR Fifth Space Sci. Symp., Florence, May 1964.

R. D. SHARP, J. E. EVANS, W. L. IMHOP, R. G. JOHNSON, J. B. REAGAN and R. V. SMITH (1964b). Paper submitted for publication to J. Geophys. Res.

R. D. SHARP et al. (1964c). Personal communication.

D. T. STEWART (1956) Proc. Phys. Soc. A69, 437.

D. E. STILWELL (1963) State Univ. Iowa Publ., SUI 63-28.

T. E. VAN ZANDT, R. B. NORTON, and G. H. STONEBOCKER (1960). Some Ionospheric Results Obtained During the International Geophysical Year, p. 43 (Ed. Beynon), Elsevier Pub. Co., Amsterdam.

A. P. WILLMORE (1964). Personal communication.

J. R. WINCKLER (1962) J. Res. Nat. Bur. Standards, 66D, 127.

J. R. WINCKLER, P. D. BHAVSAR and K. A. ANDERSON (1962) J. Geophys. Res. 67, 3717.

ON THE HEIGHT OF AURORAL ABSORPTION, II

BENGT HULTQVIST†

Statistical data from Alouette and Injun 3 giving the average precipitation rate of electrons in the auroral zone as a function of energy, are analyzed with regard to the average radio wave absorption produced by ionization by electrons in the energy ranges 1—40 kev and 40—250 kev. From the satellite data, it is found that the higher energy range for the primary electrons is the dominating one in producing absoprtion at riometer frequencies. From this it follows that the majority of auroral absorption takes place below 90 km altitude in the auroral zone.

INTRODUCTION

The observation of a very small difference between ionospheric absorption of cosmic radio noise associated with aurora and magnetic disturbances, so called auroral absorption, before and after sunrise and sunset as compared to what was expected from existing models has made the height of auroral absorption a parameter of great importance for the understanding of the electron reactions in the lowest ionosphere (cf. e.g. Hultqvist 1963 a, b, 1964). There would be fewer difficulties in obtaining consistency between different types of experimental results if the auroral absorption could be shown to take place mainly in the height interval where the light emissions are mostly produced, i.e. in the *E*-layer. Proposals have been offered that, in fact, this is what in general occurs (Brown and Barcus, 1963). Several kinds of observational data indicate, however, that most of the auroral absorption is caused by ionization well below the *E*-layer (cf. Hultqvist, 1962, 1963 b, 1964).

Recently more observations relevant to the height of auroral absorption have been obtained. Ansari (1963) has analysed more carefully than before the correlation between auroral type of absorption and visual aurora and has found that "auroral absorption" is not one well defined type of phenomenon but contains at least two absorption phenomena different with regard to the energy characteristics of the ionizing corpuscular radiation. While some radio wave absorption is well correlated with the intensity of visual aurora, especially in the early part of the night, he found that there is one type, occurring after local midnight, that is not correlated with the light intensity. This is the type of auroral absorption which is causing the morning peak of the diurnal variation of the absorption in the auroral zone. The low light emission per absorption unit indicates that the energy of the primary electrons is much higher than for the electrons that cause the visible aurora. The increased penetrability of the higher energy electrons produces the enhancements in ionization much deeper in the atmosphere.

New extensive multiple-frequency riometer measurements of auroral absorption (Little et al., 1963, Lerfald et al., 1964) have shown that some 60 percent of 112 studied cases had the maximum in the absorption-per-km of altitude for 20 Mc/s cosmic radio noise at an altitude higher than 72 km, while for some 10 percent of the cases the maximum absorption-per-km was located at or below 60 km altitude. The multi-frequency absorption technique provides height information in the altitude range 35–75 km. It cannot tell whether there is some significant amount of absorption taking place up in the *E*-layer in the presence of absorption also in the 35–75 km interval, for instance. But even so the fact that in some 40 percent of 112 auroral absorption cases studied the peak absorption-per-km was at or below 72 km taken together with the fact that bremsstrahlung x-rays are probably negligible in producing riometer absorption (Ansari 1963, Hultqvist 1963

*Goddard Space Flight Center Document X-611-64-155, June 1964.

†Goddard Space Flight Center, NASA—National Academy of Sciences—National Research Council Senior Post—Doctoral Resident Research Associate on leave of absence from Kiruna Geophysical Observatory, Kiruna C, Sweden.

c, 1964, Brown, 1964) is enough for demonstrating the importance of higher energy electrons penetrating well below the visible aurora. The above-mentioned new results were obtained from ground observations of cosmic noise absorption.

Measurements on satellites (Mann et al., 1963) of the primary particles which cause the absorption have shown that there sometimes exists an influx of electrons with a spectrum so flat that the absorption-per-km height-profile caused by them has its maximum at about 70 km (Hultqvist, 1964). The total absorption produced by these observed flat-spectrum-electrons is higher than that caused by the steep electron spectra of McIlwain (1960) type, observed in visible aurora, even for very strong aurorae. These direct observations of the primary particles thus showed that at least sometimes most of the auroral absorption is located below 90 km altitude. However, due to the short life time of the satellites from which the measurements were made (only a few days) no good statistical information about the occurrence frequency of the various types of primary electron spectra was obtained. It is the purpose of this note to point out that the measurements by means of Alouette (McDiarmid et al., 1963) and Injun 3 (O'Brien, 1964) of precipitation of electrons into the atmosphere make it possible to attain a rough idea about how important the electrons in the energy ranges 1–40 kev and 40–250 kev, respectively, are for producing the auroral absorption, and, therefore, to provide another piece of experimental information independent of the ground observation of cosmic noise absorption about the height distribution of the auroral absorption. This information, in principle, covers the whole height interval of interest, contrary to the multi-frequency riometer measurements.

SATELLITE OBSERVATIONS OF ELECTRON PRECIPITATION IN THE AURORAL ZONE

McDiarmid et al., (1963) have reported results of electron flux measurements on board the Alouette satellite during several hundred passes through the auroral zone at an altitude of about 1025 km in the period October 1962 through January 1963. The measurements of special interest here were made by means of two Geiger-Müller tubes having electron energy thresholds of 40 and 250 kev. McDiarmid et al., found that the electron spectrum becomes progressively softer and very variable above about 59° invariant latitude. The flux of electrons with energy greater than 40 kev precipitated into the atmosphere had its maximum at an invariant latitude of 65 to 67°. The data were analyzed for two different ranges of K_p, namely <4 and >4. The average flux of precipitated electrons at the maximum in the auroral zone was found to be 3.10^5 electrons/cm^{2}sec ster for the high K_p range and 10 times less for the low K_p range. The half value width of the latitude distribution was some 8 degrees for $K_p > 4$ and about 12 degrees for $K_p < 4$.

On the average, the peak intensity of precipitated electrons with energies greater than 250 kev occurred at an invariant latitude of 60° and was approximately $1.9 \cdot 10^3$ electrons/cm^{2}sec ster and $2.6 \cdot 10^3$ electrons/cm^2 sec ster for the low and high ranges of K_p, respectively. The latitude spread was found to be smaller than for 40 kev electrons.

Because no detailed latitude distribution of the flux of 250 kev electrons is given by McDiarmid et al., we will assume that the average fluxes at an invariant latitude of 65° is down by a factor of ten from the peak values mentioned above. This latitude correction is probably too large (i.e. the correction factor 0.1 is too small) as judged from a comparison of the latitude distribution of passes in which the intensity of precipitated electrons with energies greater than 250 kev was greater than $3.2 \cdot 10^3$/cm^{2}sec ster (Fig. 8 of McDiarmid et al., 1963) and the corresponding diagram for 40 kev. The resulting spectra are thus too steep rather than too flat. The absorption caused by electrons in the energy range 40–250 kev is therefore probably larger, rather than smaller, than the values presented below.

From the two integral flux values given above for each range of magnetic activity we can derive equivalent two-parameter spectra. For $K_p < 4$ an exponential equivalent differential spectrum is found to be $n(E) = 2.10^3 e^{-E/41}$ electrons/cm sec ster kev and for $K_p > 4$: $n(E) = 3.8 \cdot 10^4 e^{-E/30}$ electrons/cm^{2}sec ster kev.

An equivalent two-parameter average differential spectrum for the primary electrons in the energy range 1–40 kev can be obtained from the results of the Injun 3 measurements presented by (O'Brien, 1964).

The data were taken in early 1963 at altitudes between 237 and 2785 km. The inclination of the orbit of Injun 3 was 70.4° and the satellite thus passed over the central polar cap over northern Canada. O'Brien gives the average integral flux for precipitated electrons with $E \geq 40$ kev as 4.10^5 electrons/cm²sec in the auroral zone. This was obtained by means of a Geiger-Müller tube. A Cds-detector on Injun 1 gave the energy flux associated with electrons of energy greater than about one kev. The integral flux of 4.10^5 electrons/cm²sec corresponded to an energy flux of about 4 ergs/cm² sec. O'Brien and Taylor (1964) state that these data can be considered as accurate to a factor of about 3. Corresponding to these two average flux values is the average equivalent exponential spectrum $n(E) = 7.8 \cdot 10^7 e^{-E/5.7}$ electrons/cm²sec kev. This spectrum is fairly close to the spectrum ($\propto e^{-E/5}$) considered in some numerical detail by Hultqvist (1964). In fact $n(E) = 2.4 \cdot 10^8 e^{-E/5}$ electrons/cm²sec kev gives the same integral electron flux for $E \geq 40$ kev as $7.8 \cdot 10^7 e^{-E/5.7}$ electrons/cm²sec kev, but the corresponding energy flux for $E \geq 1$ kev is 9 ergs/cm² sec instead of 4. In fact the energy input rate per unit of light emission rate obtained with the value 9 ergs/cm²sec is 5 ergs/cm²sec per kR, which is midway between the corresponding values of McIlwain (1960) and O'Brien (1964) (cf. Hultqvist, 1964b).

RELATIONS BETWEEN AVERAGE INTEGRAL FLUXES MEASURED IN SATELLITES AND AVERAGE ABSORPTION VALUES

The radio-wave absorption for the riometer frequency 27.6 Mc/s in the auroral zone is given for the ordinary ray by the Appleton-Hartree expression as

$$A = 0.46 \int_0^\infty \frac{N_e \nu}{3.34 \cdot 10^{16} + \nu^2} dh \quad db,$$

where N_e is the electron density and ν the electron collision frequency. The temporal structure of the electron precipitation measured by Alouette and Injun 3 is unknown. However, if the equilibrium relation between N_e and the ionization rate, $q(h)$, is used for evaluation of electron density and absorption, overly large values will certainly be obtained. Since the effective recombination coefficient decreases from 60 to 100 km altitude the overestimation will be most important in the upper part of this height interval. The relative contribution to the absorption from the lowest part of the height interval mentioned will therefore be higher than what is found below in this note. It does not seem probable that the error in the average electron density in the lowermost part of the height range 60 to 100 km due to unequilibrium would exceed a factor of two, since the rate of variation of the electron density, as seen on riometer records, generally is slow compared with the recombination time in that part of the ionosphere. As such an inaccuracy does not invalidate the conclusions drawn in this note we thus write

$$N_e(h) = \{q(h)/\alpha_{eff}\}^{1/2} \quad \text{and}$$

$$\bar{A} = 0.46 \int_0^\infty \frac{\nu}{3.34 \cdot 10^{16} + \nu^2} \overline{\left\{\frac{q(h)}{\alpha_{eff}}\right\}^{1/2}} dh,$$

where the bars indicate average values for the time function in question.

The data obtained from the above-mentioned satellite measurements above the atmosphere are the following time-average values:

$$\int_{40}^\infty \overline{n(E)} dE = \overline{N(>40)}$$

electrons/cm²sec,

$$\int_{250}^\infty \overline{n(E)} dE = \overline{N(>250)}$$

electrons/cm²sec,

and

$$\int_1^\infty \overline{En(E)} dE = \overline{\phi(>1)} \quad \text{ergs/cm²sec.}$$

Here $\overline{N(>40)} = \frac{1}{m} \sum_{i=1}^{m} N_i(>40)$,

$$\overline{n(E)} = \frac{1}{m} \sum_{i=1}^{m} n_i(E) \quad \text{and}$$

$$\overline{En(E)} = \frac{E}{m} \sum_{i=1}^{m} n_i(E) = E\overline{n(E)}.$$

$N_i(>40)$ represents a single satellite measurement of the integral flux above 40 kev energy.

The average ionization rate at height h is given by

$$\overline{q(h)} = \frac{1}{Q}\frac{d}{dh}\int_0^\infty E\overline{n(E,h)}dE \qquad \text{electrons/cm}^3\text{sec},$$

even if the electron precipitation is not homogenous over a large area, due to the effect of the geomagnetic field. Q is the average amount of energy used in producing one electron-ion pair (35 ev in molecular nitrogen) and $n(E,h)$ is the omnidirectional differential flux of electrons of energy E at altitude h. For a given particle energy, E, and angular distribution outside the atmosphere, $n(E,h)$ can be written

$$n(E,h) = n(E)\cdot F(E,h)$$

where $n(E)$ is the omnidirectional differential flux outside the atmosphere and $F(E,h)$, which contains the information about the angular distribution outside the atmosphere, gives the attenuation in the atmosphere. Thus

$$\overline{q(h)} = \frac{1}{Q}\int_0^\infty En(E)\frac{dF(E,h)}{dh}dE$$

$$= \frac{1}{Q}\int_0^\infty E\overline{n(E)}\frac{dF(E,h)}{dh}dE,$$

where the last equality is true if $\frac{dF}{dh}$ is the same for all fluxes used in the averaging i.e. if the directional distribution of the electrons outside the atmosphere does not vary from one passage to another. This is, of course, not necessarily so, but there is some experimental support for angular distribution being identical, namely isotropic, at least in the cases of intense precipitation (O'Brien, 1964), i.e. in those measuring values that contribute most to the average. It was also pointed out by Hultqvist (1964 a) that the radio wave absorption produced by an $e^{-E/b}$ differential spectrum of electrons enetering the atmosphere vertically is smaller by less than 50 percent of its value than the absorption produced by an isotropic flux of identical energy distribution but of 2 π times greater omnidirectional flux value. The variation of the directional distribution of the precipitated electrons from one precipitation event to another does therefore probably not affect the average significantly, and it is neglected in the considerations below.

When the two energy ranges about which information was obtained from Injun 3 (1–40 kev) and Alouette (40–250 kev) are considered, it can be found by numerical computations that the contribution to $\bar{q}$ from particles outside the energy ranges is negligible.

Thus we can write, with the use of the mean value theorem for integrals, for the low energy range

$$\overline{q(h)}_{1-40} = \frac{1}{Q}\int_1^\infty E\overline{n(E)}\frac{aF(E,h)}{dh}dE$$

$$= \frac{1}{Q}\left\{\frac{dF(E,h)}{dh}\right\}_{E_1}\int_1^\infty E\overline{n(E)}dE$$

$$= \frac{1}{Q}\left\{\frac{dF(E,h)}{dh}\right\}_{E_1}\overline{\phi(>1)},$$

where E_1 is a value between 1 and ∞, and for the high energy range

$$\overline{q(h)}_{40-250} = \frac{1}{Q}\int_{40}^\infty E\overline{n(E)}\frac{dF(E,h)}{dh}dE$$

$$= \frac{1}{Q}\left\{E\frac{dF(E,h)}{dh}\right\}_{E_2}\cdot\overline{N(>40)}.$$

If we, for instance, adopt the approximate formula for $F(E,h)$ of Maeda (1963) and derive a two parameter average energy distribution from $\overline{N(>40)}$ and $\phi\ (>1)$ for the energy interval 1–40 kev and from $\overline{N(>40)}$ and $\overline{N(>250)}$ for the interval 40–250 kev, simple closed expressions can be derived for $\left\{\frac{dF(E,h)}{dh}\right\}_{E_1}$ and $\left\{E\frac{dF(E,h)}{dh}\right\}_{E_2}$.

If the differential energy distribution corresponding to the experimental average integral flux values are assumed to be exponential in both energy intervals the expressions are as follows:

$$\left\{\frac{dF(E,h)}{dh}\right\}_{E_1} = -2\pi\zeta(h)\frac{e^{1/b_1}}{b_1(1+b_1)}\int_1^\infty Ee^{-E/b_1}\frac{1}{\sigma(E)}Ei\left(-\frac{x}{\sigma(E)}\right)dE \qquad (4)$$

and

$$\left\{E\frac{dF(E,h)}{dh}\right\}_{E_1} = -2\pi\zeta(h)\frac{e^{40/b_2}}{b_2}\int_{40}^{\infty} Ee^{-E/b_2}\frac{1}{\sigma(E)}Ei\left(-\frac{x}{\sigma(E)}\right)dE \tag{5}$$

b_1 is the e-folding value in the energy interval 1–40 kev and b_2 in the range 40–250 kev. $1/\sigma\ (E) = 3.18\cdot10^6E^{-2.2}$ (Maeda, 1963) and $E_i\ (-x/\sigma)$ is the exponential integral defined by $-E_i(-y) = \int_y^\infty e^{-z}z^{-1}dz$. x is the atmospheric depth in g/cm², $\zeta(h)$ is the atmospheric density, and E is everywhere measured in kev.

We thus see that $\overline{q(h)}$ can be expressed in terms of the satellite-measured averages $\overline{\phi(>1)}$ and $\overline{N(>40)}$. But the average cosmic noise absorption is given in terms of $\overline{q^{\frac{1}{2}}}$ in (1) and not in terms of $\bar{q}$.

However,

$$(\overline{q^{\frac{1}{2}}})^2 = \left\{\frac{1}{n}\sum_{i=1}^{n}q_i^{1/2}\right\}^2 = \frac{1}{n^2}\left\{\sum_{i=1}^{n}q_i + \sum_i q_i^{1/2}\sum_{j\neq i}q_j^{1/2}\right\} = \frac{1}{n^{\frac{1}{2}}}\left\{n\bar{q} + (n-1)n\bar{q}^{\frac{1}{2}}\cdot\bar{q}^{\frac{1}{2}}\right\} = \frac{1}{n}\bar{q} + \left(1-\frac{1}{n}\right)(\bar{q}^{\frac{1}{2}})^2.$$

Thus

$$\overline{q^{1/2}} = (\bar{q})^{1/2}$$

if

$$\sum_{i\neq j} q_j^{1/2} = (n-1)\overline{q^{1/2}}.$$

Numerical calculations show that $\overline{q^{\frac{1}{2}}}$ and $(\bar{q})^{\frac{1}{2}}$ do not differ by as much as 50 percent even for a small number of terms and for ratios between the various q_i as high as 10^6.

We can therefore write with sufficient accuracy for the considerations below:

$$\overline{A_{1-40}} = \frac{0.46}{\overline{Q_{1/2}}}\left\{\overline{\phi(>1)}\right\}^{1/2}\int_0^\infty \frac{\nu\alpha_{\text{eff}}^{-1/2}}{3.34\cdot10^{16}+\nu^2}\left[\left\{\frac{dF(E,h)}{dh}\right\}_{E_1}\right]^{1/2}dh \tag{6}$$

$$\overline{A_{40-250}} = \frac{0.46}{\overline{Q^{1/2}}}\left\{N(>40)\right\}^{1/2}\int_0^\infty \frac{\nu\alpha_{\text{eff}}^{-1/2}}{3.34\cdot10^{16}+\nu^2}\left[\left\{E\frac{dF(E,h)}{dh}\right\}_{E_2}\right]^{1/2}dh \tag{7}$$

where

$$\left\{\frac{dF}{dh}\right\}_{E_1}$$

and

$$\left\{E\frac{dF}{dh}\right\}_{E_2}$$

may be obtained from (4) and (5), respectively. The average absorption is thus expressed in terms of the average integral fluxes measured by the satellites.

The integrands in (6) and (7) depend only on atmospheric properties and the average flux as function of energy and can therefore be evaluated from satellite-measured average spectra. If the average spectrum is defined only in two points, as is the case with the Injun 3 and Alouette results, an assumption has to be made about the shape of the spectrum between those points. Exponential spectra are used below. The main uncertainty in the results obtained is certainly due to the limited amount of available statistical data and the enormous variation that there is in it, while the uncertainty in the detailed shape of the spectrum between the measuring points probably introduces only minor uncertainties.

ELECTRON DENSITY PROFILES AND ABSORPTION DUE TO THE EQUIVALENT AVERAGE SPECTRA

The exponential electron energy spectrum for $K_p<4$ is exactly the same as the spectrum for which Hultqvist (1964) calculated the height profile. The equilibrium electron density curve No. 1 in Fig. 1 has been obtained from Hultqvist's

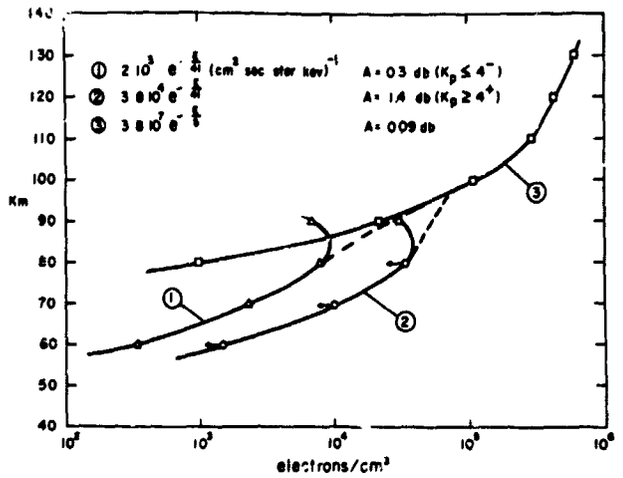

FIGURE 1.—Equilibrium electron density profiles due to three energy spectra of precipitated electrons. The spectra as well as the total absorption, A, at 27.6 Mc/s are given in the figure. Curve No. 2 gives an upper limit for the equilibrium electron density distribution produced by the spectrum $3.8 \cdot 10^4\ e^{-E/30}$ (cm² sec ster kev)$^{-1}$. A lower limit for this spectrum is curve No. 1.

(1964) results by multiplying by $\sqrt{2/70}$. Hultqvist's computations were made for vertically incident electrons of energy spectrum proportional to $\exp(-E/41)$. However, the absorption produced by $ce^{-E/41}$ electrons/cm²sec kev, entering the atmosphere vertically, is probably less than that caused by $ce^{-E/41}$ electrons/cm²sec ster kev, having isotropic directional distribution outside the atmosphere, by less than 50 percent of this higher value. The total absorption for a frequency of 27.6 Mc/s expected from the electron density curve No. 1 in Fig. 1 is 03.2 db.

An upper limit to the electron density profile and total absorption produced by an electron energy spectrum of $3.8 \cdot 10^4 e^{-E/30}$ is obtained from $3.8 \cdot 10^4 e^{E/41}$, which in turn can easily be found from the values computed by Hultqvist (1964). In this way curve No. 2 in Fig. 1 has been derived. The corresponding limiting total absorption for radio waves of frequency 27.6 Mc/s is 1.4 db. Probably the correct value for the spectrum with an e-fold value of 30 kev is close to 1 db. A lower limit for it is, of course, the value given above for $K_p < 4$ (0.32 db).

For the equivalent average spectrum for the range 1–40 kev, $2.4 \cdot 10^8 e^{-E/5}$ electrons/cm²sec kev, the numerical calculations of Hultqvist (1964) can be employed. The electron density profile No. 3 in Fig. 1 has been derived by means of them. The total absorption at 27.6 Mc/s due to this electron density profile is 0.09 db.

DISCUSSION

The increase of the pitch angle of an electron due to the magnetic forces when it passes along the field line down into the atmosphere has not been taken into account. As all measurements were made close to the earth's surface this neglection does certainly not introduce any large error. Its effect, if any, would be to increase the height of the ionization produced by the particle precipitation.

There are several simplifying assumptions and approximations made, which tend to make the deduced effect on the electrons in the energy range 40–250 kev too small relative to that of the 1–40 kev electrons. One is that Hultqvist's (1964a) numerical values for vertically penetrating electrons have been employed. As mentioned earlier, this may make the absorption too small by not more than 50 percent of the value for the case of isotropic electron angular distribution outside the atmosphere, and by still less of the value for the electrons in the loss cone. A second fact contributing to the computed absorption value for 40–250 kev electrons being too small is that the equivalent average spectrum in this energy interval is probably less steep than the spectra used in the numerical estimations. A third approximation working in the same direction is that the equilibrium relation between electron density and the ionization rate was used. This makes the computed absorption overestimated. Since the effective recombination coefficient decreases from 60 km upwards the overestimation will be most important at greater heights. It does not seem probable that the error in the average absorption per unit height in the lowermost part due to unequilibrium would exceed a factor of two, since the rate of variation of the electron content, as seen on riometer records, mostly is slow compared with the recombination time in that part of the ionosphere.

On the other hand there was an assumption made which tends to make the contribution by electrons in the 1–40 kev range too small compared to that of the 40–250 kev electrons. The average precipitated electron flux above 40 kev

energy was given by O'Brien as 4.10^5 electrons/cm²sec. It was assumed above that this omnidirectional flux was isotropic over the upper hemisphere just outisde that level where the energy loss of the electrons starts to be significant, i.e. at 200 km, say. This is probably not far from the truth, but the flux may have been limited to a somewhat smaller solid angle than 2π. Had this real angular distribution been known and taken into account the calculated absorption would have been somewhat greater.

Although only the order of magnitude of the absolute values of absorption seems to be significant, the ratio of contributions of the two energy intervals of precipitated electrons, discussed in this note, is probably uncertain by no more than a factor of three. A more accurate analysis than the one given above seems not worthwhile or possible on the basis of existing experimental data.

The electron density profiles in Fig. 1 as well as the total absorption values derived from them are those for the daytime. On the night side of the earth the electron densities may possibly be somewhat lower than those in Fig. 1 for altitudes less than 90 km due to negative ion production.

The values used as basis for the model spectra are average fluxes. The range of variation is, as mentioned, very large. O'Brien (1964) found that there was always some precipitation in the aurotal zone. The lowest value observed by him there was about $2 \cdot 10^{-4}$ of his average value quoted above. The maximum values shown in his paper were about 15 times greater than the average. To these minimum and maximum values of the ionization rate correspond extreme values of equilibrium electron densities 70 times smaller and 4 times greater than the average respectively. McDiarmid et al. (1963) showed similar variation ranges.

The use of exponential model spectra was motivated simply by the fact that numerical values were already available from Hultqvist (1964). It should be remembered that each of these spectra were obtained from only two pieces of experimental information and they are only very rough descriptions of spectra which are not known in detail. If an equivalent spectrum is to be used, as in this case, there seems to be at least as good reasons to use exponential ones as power law spectra. The observational indications of a fairly flat spectrum without any "infrared catastrophy" below a few kev (O'Brien, 1964, O'Brien and Taylor, 1964) support the use of exponential spectra in the low energy range.

The observations of both McDiarmid et al. (1963) and of O'Brien (1964) indicate a fairly strong latitude dependence of the spectral slope and the equivalent spectra used above should therefore be considered as representative only in the auroral zone.

The average total absorption values for 27.6 Mc/s given above for the various electron spectra:

(a) $n(E) = 3.8 \cdot 10^7 e^{-E/5}$ electrons/cm²sec ster kev $A = 0.090$ db

(b) $n(E) = 3.8 \cdot 10^4 e^{-E/30}$ electrons/cm²sec ster kev $(K_p > 4)$ $A < 1.4$ db

(c) $n(E) = 1.9 \cdot 10^3 e^{-E/41}$ electrons/cm²sec ster kev $(K_p < 4)$ $A = 0.32$ db,

indicate that the flat type of electron spectrum with e-fold values generally between 25–45 kev are the dominating one in producing auroral absorption in the average. The absorption due to these spectra takes place mainly between 60 and 90 km and not in the height interval where most visible auroae are located.

The range of variation of the 27.6 Mc/s absorption corresponding to the wide variations of electron fluxes reported by McDiarmid et al.(1963) and O'Brien (1964) is from the order of 0.01 db to 4 db, if smoothing due to time constants in the ionosphere is neglected, and is caused by the variation of the flux of the hard spectrum electrons. It should be remembered that there were no strong geomagnetic storms included in the material presented by McDiarmid et al. (1963).

The absorption values computed from the satellite measured electron fluxes for the two ranges of magnetic activity are in quite good accordance with the multifrequency riometer measurements mentioned in the introduction, as well as with the average absorption during the five most disturbed days and five most quiet days in each month, as observed over several years at College (geomagnetic latitude 64.5°) by Basler (1963). For the disturbed days he found a daily average of about 1 db in the summer and between 1 and 2 db in winter and at equinoxes. For the quiet days the daily average obtained from his figure 7 is about 0.3 db.

ACKNOWLEDGEMENT

I am grateful to A. C. Aikin, L. R. Davis, D. S. Evans, and R. A. Hoffman for reading the manuscript and offering criticism.

REFERENCES

Z. A. Ansari (1963) The spatial and temporal variations in high latitude cosmic noise absorption and their relation to luminous aurora. University of Alaska, Scientific Report No. 4, NSF Grant No. 14133.

R. P. Basler (1963) Radio wave absorption in the auroral ionosphere. J. Geophys. Res., 68, 4665–4681.

R. R. Brown (1964) Features of the auroral electron energy spectrum inferred from observations of ionospheric absorption. Arkiv for Geofysik (in print).

R. R. Brown and J. R. Barcus (1963) Day-night ratio for auroral absorption events associated with negative magnetic bays. J. Geophys. Res., 68, 4175–4180.

B. Hultqvist (1962) Kiruna Geophysical Observatory. Scientific Report No. 2, Contract No. AF 61(052)–601.

B. Hultqvist (1963a) Sunrise and sunset effects on cosmic noise absorption associated with aurora and magnetic storms. Planet. Space Sci. 11, 371-383.

B. Hultqvist (1963b) On the height distribution of the ratio of negative ion and electron densities in the lowest ionosphere. J. Atm. Terr. Phys. 25, 225–240.

B. Hultqvist (1963c) On the height of auroral absorption. Goddard Energetic Particles Preprint Series X-611-63-257.

B. Hultqvist (1964) On the height of auroral absorption, I. Planet Space Sci. (in print).

B. Hultqvist (1964b) Aurora and the lower ionosphere in relation to satellite observations of particle precipitation. Paper presented at the COSPAR Fifth International Space Science Symposium in Florence, May, 1964.

G. M. Lerfald, C. G. Little, and R. Parthasarathy (1964) D-region electron density profiles during auroras. J. Geophys. Res. (in print).

C. G. Little, G. M. Lerfald and R. Parthasarathy (1963). Personal communication.

L. G. Mann, S. D. Bloom and H. I. West, Jr. (1963) The electron spectrum from 90 to 1200 kev as observed on Discoverer satellites 29 and 31. Space Research III, pp. 1194–1205. North-Holland Publishing Co., Amsterdam.

J. B. McDiarmid, J. R. Burrows, E. E. Budzinski and M. D. Wilson (1963) Some average properties of the outer radiation zone at 1000 km. Can. J. Phys. 41, 2064–2079.

C. E. McIlwain (1960) Direct measurements of particles producing visible auroras. J. Geophys. Res. 65, 2727–2747.

C. E. McIlwain (1960) Direct measurements of particles producing visible auroras. J. Geophys. Res. 65, 2727–2747.

B. J. O'Brien (1964) High-latitude geophysical studies with satellite Injun 3.3. Precipitation of electrons into the atmosphere. J. Geophys. Res. 69, 13–143.

B. J. O'Brien (1964b) Paper presented at the Lockheed symposium on aurora in Palo Alto, Calif., January 1964.

B. J. O'Brein and H. Taylor (1964) High-latitude geophysical studies with satellite Injun 3. 4. Auroras and their excitation. J. Geophys. Res. 69, 45–63.

R. D. Sharp, J. E. Evans, R. G. Johnson and J. B. Regan (1963) Satellite measurements of low energy electrons in the northern auroral zone. Paper presented at the American Geophysical Union, Third Western National Meeting in Boulder, December 1963.

ON THE STRUCTURE OF A COLLISION FREE WAVE IN A PLASMA TRANSVERSE TO A MAGNETIC FIELD*

R. K. JAGGI AND A. P. STOKES

In this paper we have considered the problem of the structure of a strong collision free wave in a plasma perpendicular to its magnetic field. It is shown that conditions on the two sides of the wave are the same and are separated by a solitary pulse provided the kinetic energy of the motion at one end of the wave ($x=-\infty$, say) is less than the sum of magnetic and thermal energy of the plasma. If the kinetic energy is more than the sum of magnetic and thermal energy, no wave exists and the constant solution at $x=-\infty$ is the only solution of the equations describing the wave form.

1. INTRODUCTION

The subject of the structure of a strong collision free wave, in a plasma perpendicular to the magnetic field has been treated by Adlam and Alan[1], Burgers[2] and Hain, Lüst and Schlüter[3]. Hain, Lüst and Schlüter in particular have obtained solutions of the wave structure by solving the non-linear equations on a computer.

In this paper we have investigated mathematical properties of the equations which help us to guess the correct solution out of the many solutions obtained on a computer. As an illustrative example we shall consider a plasma with isotropic pressure. The generalization to the anisotropic case is quite straight forward. Burgers has made an extensive study of the wave structure when the plasma pressure is anisotropic and he arrives at the same general result that there is no change of state on the two sides of the wave, i.e., that no shock wave exists in a collisionless plasma perpendicular to the magnetic field.

The result of our paper is that a solitary wave only exists if the kinetic energy of motion, which produces the wave, is less than the sum of magnetic and thermal energy of the plasma; that no stationary wave exists if the kinetic energy of motion is more than the sum of magnetic and thermal energy of the plasma. In the latter case the constant solution at one end of the wave is the only solution of the differential equation (section 4).

*Goddard Space Flight Center Document X-640-64-34, February 1964.

2. EQUATIONS DESCRIBING THE WAVE FORM

Consider a stream of plasma at $x=-\infty$ with a constant velocity u along x-axis and a constant magnetic field B_1 along z-axis. The electrons and ions of the plasma will drift in the y-direction because of the magnetic field.

Our object is to obtain conditions at $x=+\infty$ and the form of the wave or waves which start from the given solution at $x=-\infty$. As a simplification we assume that the electrons and ions satisfy Maxwellian distribution function with variable number density, velocity components and the temperature. Therefore, if f_e, f_i denote the electron and ion distribution functions

$$f_e(x, v)=n_e(x)\left(\frac{m}{2\pi kT_e(x)}\right)^{3/2}\cdot$$

$$\exp\left\{-\frac{m}{2kT_e(x)}[(u-u_e(x))^2+(v-v_e(x))^2+w^2]\right\} \quad (1)$$

$$f_i(x, v)=n_i(x)\left(\frac{M}{2\pi kT_i(x)}\right)^{3/2}\cdot$$

$$\cdot\exp\left\{-\frac{M}{2kT_i(x)}[(u-u_i(x))^2+(v-v_i(x))^2+w^2]\right\} \quad (2)$$

In cartesian coordinates, assuming steady state, the Boltzmann equation can be written as

$$mu_e\frac{\partial f_i}{\partial x}-eE_x\frac{\partial f_e}{\partial u}-eE_y\frac{\partial f_e}{\partial v}-$$

$$-\frac{eB}{c}\left(v\frac{\partial f_e}{\partial u}-u\frac{\partial f_e}{\partial v}\right)=0 \quad (3)$$

for electrons, and

$$Mu\frac{\partial fi}{\partial x}+eE_x\frac{\partial fi}{\partial u}+eE_y\frac{\partial fi}{\partial v}+ +\frac{eB}{c}\left(v\frac{\partial fi}{\partial u}-u\frac{\partial fi}{\partial v}\right)=0 \quad (4)$$

for the ions. Multiplying by 1, u_e, v_e, u_e^2 and $u_e^2+v_e^2+w_e^2$ and generating moments of equation (3) we obtain

$$\frac{\partial}{\partial x}[n_e(x)u_e(x)]=0 \quad (5)$$

$$mn_eu_e\frac{du_e}{dx}+\frac{d}{dx}(n_ekT_e)+n_eeE_x+\frac{1}{c}n_eev_eB=0 \quad (6)$$

$$mn_eu_e\frac{dv_e}{dx}-n_eeE_y-\frac{1}{c}n_eeBu_e=0 \quad (7)$$

$$\frac{d}{dx}\left(u_e^2+\frac{3kT_e}{m}\right)+\frac{2eE_x}{m}+\frac{2eB}{mc}v_e=0 \quad (8)$$

$$\frac{d}{dx}u_e[mn_eu_e^2+mn_ev_e^2+5n_ekT_e]+ 2en_eu_eE_x-2en_ev_eE_y=0 \quad (9)$$

and similar equations for the ions. Let us call the similar ion equations as (5)′—(9)′. Maxwell's equations yield

$$E_y=\text{constant} \quad (10)$$

$$\frac{dE_x}{dx}=4\pi e(n_i-n_e) \quad (11)$$

$$\frac{dB}{dx}=-\frac{4\pi e}{c}(n_iv_i-n_ev_e) \quad (12)$$

To further simplify the problem, we will make the assumption that the space charge can be neglected. The characteristic length of space charge oscillations is of the order of the Debye length[4] $R_D=\left(\frac{kT}{4\pi ne^2}\right)^{1/2}$ while, as we shall see in this paper, that of magnetohydrodynamic oscillations is of the order of $c/w_p=c\sqrt{\frac{m}{4\pi Ne^2}}$. Thus assuming that the electron thermal velocity is well below the velocity of light, the space charge oscillations are of much lower scale than the oscillations we are interested in. With the assumption $E_x\simeq 0$ and $n_e=n_i=n$ (to a good approximation we then have $u_e=u_i=u$, say) equation (6), (6)′ and (8), (8)′ yield, respectively

$$\frac{d}{dx}[Mnu_i^2-n_ikT_i+nkTe]=-\frac{1}{8\pi}\frac{dB^2}{dx} \quad (13)$$

$$\frac{d}{dn}[Mu_i^2+3kTi+3kTe]=-\frac{1}{2\pi}\frac{B}{n}\frac{dB}{dn} \quad (14)$$

Equation (5) now gives

$$nu=n_1v_1 \quad (15)$$

where $\underset{x\to-\infty}{\text{Limit}}\, n(x)=n_1$ and $\underset{x\to-\infty}{\text{Limit}}\, u(x)=u_1$.

Equation (13) can be integrated and yields

$$Mnu^2+nkTi+nkTe+\frac{B^2}{8\pi}= Mn_1u_1^2+2nkT_1+\frac{B_1^2}{8\pi} \quad (16)$$

where $\underset{x\to-\infty}{\text{Limit}}\, B(x)=B_1$. Eliminating T_i+T_e from equations (16) and (14) we obtain

$$u\frac{d}{dx}\left[u\frac{dB}{dx}\right]+\frac{4\pi n_1e^2}{mc^2}u_1uB-\frac{4\pi n_1e^2}{mc^2}u_1^2B_1=0 \quad (17)$$

Dividing by $\sqrt{8\pi Mn_1u_1^2}$ and using the transformations

$$\frac{u}{u_1}=U,\ \frac{B}{\sqrt{8\pi n_1M}u_1^2}=H,$$

$$\frac{kT_{i,e}}{Mu_1^2}=\theta_{i,e},\ \beta_1^2=\frac{B_1^2}{8\pi n_1Mu_1^2} \quad (18)$$

we finally obtain the equations

$$H^2=\alpha-U-\frac{2\theta_1}{U^3} \quad (19)$$

and

$$U\frac{d}{dy}\left(U\frac{dH}{dy}\right)+UH-\beta_1=0 \quad (20)$$

where

$$\alpha=1+2\theta_1+\beta_1^2 \quad (21)$$

Equations (19), (20) satisfy the boundary conditions $H=\beta_1$, $U=1$ at $y=-\infty$.

3. A MATHEMATICAL DISCUSSION OF EQUATIONS (19), (20)

The pair $(U, H)=(1, \beta_1)$ is a constant solution of these equations. We shall study other constant solutions represented by (19), (20), but we first examine the stability of the solutions of (19), (20) in the neighborhood of $(1, \beta_1)$ and determine the nature of this critical point.

Let $U=1+U_1$, $H=\beta_1+H_1$. We then obtain from (19)

$$H_1=U_1\,F\,(H_1, U_1) \quad (22)$$

where

$$F(H_1, U_1)=\frac{2\theta_1(3+3U_1+U_1^2)-(1+U_1^3)}{(2\beta_1+H_1)(1+U_1)^3} \tag{23}$$

From (22) and (23) we obtain

$$H_1=b_1U_1+b_2U^2_1-b_3U_1^3+\cdots \tag{24}$$

where

$$b_1=F(0, 0)=\frac{6\theta_1-1}{2\beta_1} \tag{25}$$

$$b_2=F(0, 0)\frac{\partial F}{\partial H_1}(0, 0)+\frac{\partial F}{\partial U_1}(0, 0)$$

$$=-\frac{(6\theta_1-1)^2}{8\beta_1^3}-\frac{6\theta_1}{\beta_1} \tag{26}$$

etc.

Equations (20), (24) yield,

$$\frac{d^2U_1}{dy^2}+\gamma_1(U_1)\left(\frac{dU_1}{dy}\right)^2+KU_1+\gamma_2(U_1)=0 \tag{27}$$

where γ_1, γ_2 are analytic in U_1 near $U_1=0$, $\gamma_2(U_1)=0(U_1^2)$ and

$$K=1+\frac{\beta}{b_1}=\frac{1-2\beta_1^2-6\theta_1}{1-6\theta_1} \tag{28}$$

To determine the nature of the point $U=1$, we linearize equations (23), (27). The linearized form of equation (27) is

$$\frac{d^2U_1}{dy^2}+KU_1=0 \tag{29}$$

In all the discussion that follows we shall assume the flow velocity to be much higher than the thermal velocity of particles constituting the plasma, so that $6\theta_1<1$ or $1-6\theta_1>0$. The sign of k^1 is therefore determined by the expression $1-2\beta_1^2-6\theta_1$. In case I when $1-2\beta_1^2-6\theta_1>0$, k^1 is positive and therefore $U=1$ is a center in both (27) and (29) according to a known result of Lyapounov, see Malkin[5], pp 123–4, (as no odd powers of dU_1/dy occur). In case II when $1-2\beta_1^2-6\theta_1<0$, k^1 is negative; the point $U=1$ is a saddle point in both equations (27) and (29).

Let us now consider all the constant solutions represented by the equations (19), (20). According to equation (20) constant solutions satisfy the equation $HU=\beta_1$. This condition, together with equation (19) then gives the equation

$$f(U)\equiv U^4-U^3(1+2\theta_1+\beta_1^2)+\beta_1^2U+2\theta_1=0 \tag{30}$$

$f(U)$ may also be written as

$$f(U)=(U-1)[U^3-(\beta+2\theta_1)(U^2+U)-2\theta_1]$$
$$=(U-1)\,h(U) \tag{31}$$

From Descarte's rule of signs $h(U)$ cannot have more than one positive root. Also it is easy to see that it has a positive root. Let this positive root be denoted by U_o. Since $f(0)<0$, U_o will be less than or greater than 1 when $f'(1)>0$, $f'(1)<0$ respectively. We therefore again have two cases:

(I) $f'(1)=1-2\beta_1^2-6\theta_1>0$

and

(II) $1-2\beta_1^2-6\theta_1<0$.

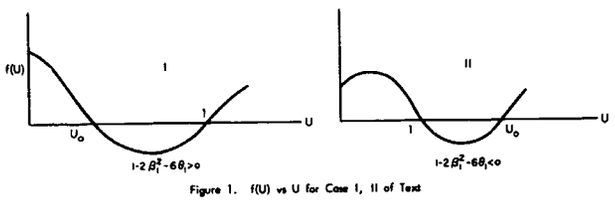

Figure 1. f(U) vs U for Case I, II of Text

FIGURE 1.—$f(U)$ vs U for Cases I, II of text.

As we require that $6\theta_1<1$, Case I may occur. Figure 1 shows a rough sketch of $f(U)$ versus U for cases I and II above.

To find the nature of the other critical point $U=U_o$, we write equation (20) as

$$\frac{d^2U}{dy^2}+\left(\frac{dU}{dy}\right)^2\left[\frac{Ug''(U)+g'(U)}{Ug'(U)}\right]+\frac{Ug(U)-\beta_1}{U^2g'(U)}=0 \tag{32}$$

where

$$H\equiv g(U)\left[a-U-\frac{2\theta_1}{U^3}\right]^{1/2} \tag{33}$$

$g'(U)$ has a zero at $U^*=(6\theta_1)^{1/4}$. It is interesting to note that this singularity of the differential equation can be quite close to 1. For example, for $\theta_1=.1$, $(6\theta_1)^{1/4}\simeq.880117$. Higher values of θ_1 can bring this singularity still closer to $U=1$.

When equation (32) is linearized about the zero U_o of $f(U)$, we obtain the equation

$$\dot{U}_1+L(U_o)U_1=0 \tag{34}$$

where $U=U_o+U_1$ and $UL(U)=1+\dfrac{2\beta_1^2}{U^2(6\theta_1-U^4)}$.

The nature of the point $U_o=1$ has already been discussed. Now let us assume in addition to

$6\theta_1<1$, that $U_o^4>6\theta_1$. We wish to establish for equation (32) that in case I when the point $U=1$ is a center the other equilibrium point $U_o<1$ is a saddle point and conversely, in case II when $U=1$ is a saddle point, the other equilibrium point $U_o>1$ is a center. By arguments similar to those given above for equation (27) and (29), this is equivalent to showing that if $h(U_o)=0$, h gvien in (31), then $U_o<1$ implies $L(U_o)<0$ and $U_o\cdot 1$ implies $L(U_o)>0$.

It can be shown that

$$Ug(U)-\beta_1=\frac{-f(U)}{U[\beta_1+Ug(U)]} \tag{35}$$

Now, consider case I. $f(U)$ has a zero at $U=U_o$ (<1) and $U=1$. In the $U,\dot{U}$ plane construct a closed loop C enclosing U_o and 1 and lying so close to the U-axis that the sign of $\dot{U}$ is determined by the last term on the left in (32).

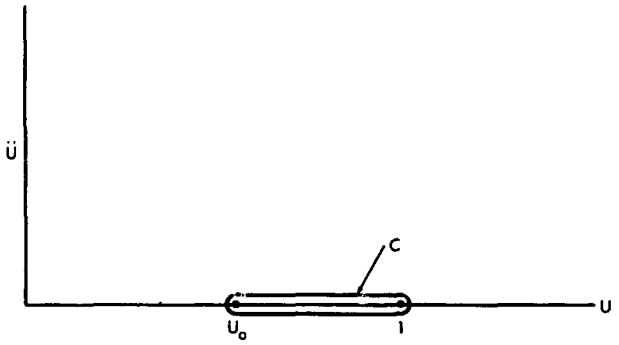

FIGURE 2.—The closed curve C enclosing the points $U=U_0$ and $U=1$ and lying close to the U axis.

(see Figure 2). Then using (35) and upon considering the changes in the sign of $f(U)$, it follows that the index of C with respect to (32) is 0[6]. As the index of a center $(U=1)$ is 1, this implies that the index of U_o is -1. If $L(U_o)\neq 0$, i.e., if U_o is an elementary critical point, then U_o of necessity must be a saddle point and $L(U_o)<0$ will hold. A similar arrangement for $U_o>1$ in case II shows that the index of U_o is 1 and therefore $L(U_o)>0$ holds (provided of course $L(U_o)\neq 0$).

Thus the problem is reduced to showing that the two polynomials $h(U)=U^3-bU^2-h_2-2\theta$, and $M(U)=U_6-6\theta_1U^2+4\theta_1-2b$ have no common positive zeros in either case I or case II. Here we have used the definition $b=2\theta_1+\beta_1^2$ in deriving the form of $M(U)$ which is the numerator of $UL(U)$.

This has not been shown in general, although for particular choices of β_1, θ_1, it is relatively straightforward. The critical case, however, is when $b+\theta_1=\frac{1}{2}$ or $2\beta_1^2+6\theta_1=1$, for then the two roots U_o and 1 become equal and, of course, in this case $M(1)=0$.

Let us suppose that $b+\theta_1$ is close to $\frac{1}{2}$, i.e., U_o is close to 1 so that $(U_o-1)^2$, $(U_o-1)^3$ are negligible in comparison with U_o-1. Now let $R=U^2$ and expand h and M about $U=1$ and $R=1$. This gives

$$h(U)=1-2(b+\theta_1)+3(1-b)(U-1)+(3-b)(U-1)^2+(U-1)^3 \tag{36}$$

and

$$M(R)=1-2(b+\theta_1)+3(1-2\theta_1)(R-1)+3(R-1)^2+(R-1)^3 \tag{37}$$

The zeros U_o, R_o $(=U^2-1)$ of h and M may be approximated by

$$U_0=1+\frac{2(b+\theta_1)-1}{3(1-b)}$$

$$R_0=1+\frac{2(b+\theta_1)-1}{3(1-2\theta_1)} \tag{38}$$

Now suppose we are in case I, that is $b+\theta_2<\frac{1}{2}$. Then as $b>2\theta_1$, we have $U_o-1<R_o-1=\bar{U}^2-1<0$; where $M(\bar{U})=0$, $\bar{U}>0$. This implies

$$1-U_o>(1-U)(1+U)>(1-U)$$

Therefore

$$U_o<\bar{U}<1$$

In case II, $b+\theta_2>\frac{1}{2}$, it follows similarly from $U_o-1>\bar{U}^2-1$, that $1<\bar{U}<U_o$. Thus the positive roots of M and R, which coincide for $b+\theta_1=\frac{1}{2}$, do separate as required, for $b+\theta_1$ near $\frac{1}{2}$. Although a proof for the general case is lacking, the following calculations may be of some interest.

Taking $\theta_1=.1$, $b=.3$, we find $(6\theta_1)^{1/4}=.880117$, $U_o\simeq.88978$ and $M(U_o)=-.1788<0$. With $\theta_1=.1$, $b=.5$, we find $U_o\simeq1.1116$ and $M(U_o)\cong.54567>0$. Thus we observe that at $b=.3$, U_o is very close to $U^*=(6\theta_1)^{1/4}$ and so b could not be decreased further and still have $U_o^4>6\theta_1$.

Thus we have seen that in case II, that is $U_o>1$, if $M(U_o)>0$, then U_o is a center. In this

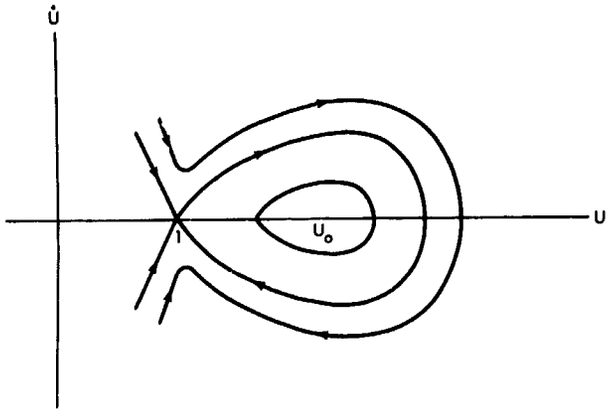

FIGURE 3.—Approximate phase plane picture of the solution for the case II when $U=1$ is a saddle point and $U=U_0$ is a center.

case the phase plane portrait of the solution is shown in figure 3. In the other case, in which U_0 is a saddle point and 1 a center, the phase plane picture is the same as figure 3 with the role of 1, U_0 reversed. As is clear from our analysis we have tried to determine the structure of the solutions of equations (19), (20) from the properties of the differential equations (27) or (32). In the next section, we shall verify our predictions by obtaining some solutions on a computer.

4. COMPUTER CALCULATIONS

Some of the results given in the previous section were verified by computing the solution of equations (19), (20) on an IBM 7094. The way to do this is to choose values of U, H (different from 1, β_1) lying on the eigen solution by using the linear equation (29). All calculations were started close to $U=1$, $H=\beta_1$. Since the solution depends critically on the position of the point of start in the phase plane we ran several cases using values slightly different from those obtained from the linear equation (29). For example, for $\beta_1=.81$, $\theta_1=.05$, we obtained the solution using (a) $U=1.0001$, $\frac{dU}{dy}=.00001$ and (b) $U=1.0001$,

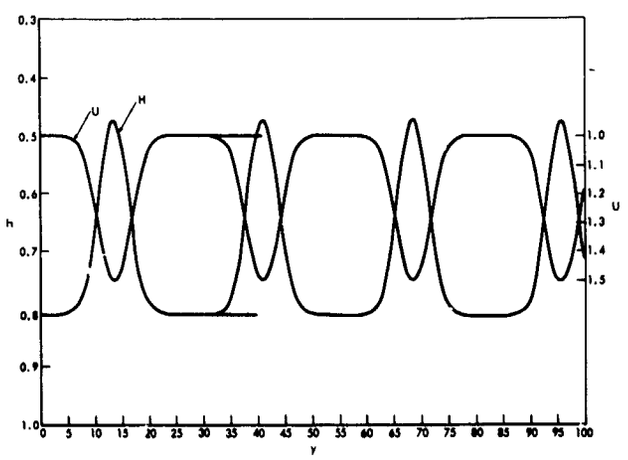

FIGURE 4a.—Computed solution of equations (19), (20) for $\beta_1=.81, \theta_1=.05$, using perturbed values $U=1.0001$, $\frac{dU}{dy}=100$.

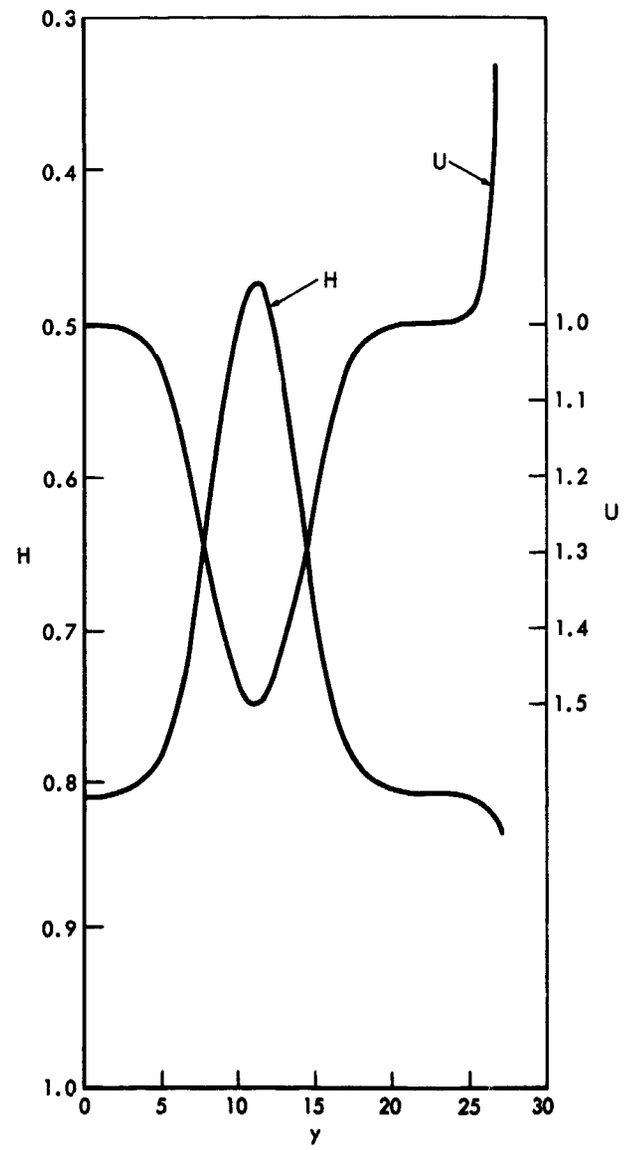

FIGURE 4b.—Computed solution of equations (19), (20) for $\beta_1=.81, \theta_1=.05$, using perturbed values $U=1.0001$, $\frac{dU}{dy}=.001$.

$\frac{dU}{dy}=.001$ while from the linear equation we obtain a value of $\frac{dU}{dy}$ which lies between .00001, .001. Figures 4a and 4b give the solution for the cases (a), (b) above. In the case (b) the solution becomes unstable because we happen to use a value of $\frac{dU}{dy}$ which lies outside the oval of figure 3. In the case (a), we obtain a solution which almost returns back to its initial value and repeats itself. (The repetitions are evidently the cause of the computational error, which if decreased will show that the solution is a solitary pulse. Since only two branches of the curve approach $U=1$, $U=0$ the solitary pulse is the required solution of the wave form.)

We now turn to a calculation of case I considered in section 3. We used $\beta_1=.1$, $\theta_1=.1$. Taking a point away from $U=1$, $\frac{dU}{dy}=0$, we obtained a solution consisting of oscillations having $U=1$ $\frac{dU}{yd}=0$ for its center in accord with the fact that $U=1$, $\frac{dU}{dy}=0$ is a center. We see therefore that in case (I) even the solitary wave does not exist.

We have not made any computations about the point $U=U_0$ as this point is of no interest to us. This corresponds to a solution lying just within the oval pictured in figure 3. A more accurate choice of initial conditions would show that the boundary of this oval corresponds to a solitary pulse, that is, the solution forming the boundary of the oval leaves $U=1$, $U=0$ at $y=-\infty$, and returns to this point at $y=+\infty$.

ACKNOWLEDGEMENTS

One of us (R.K.J.) is grateful to the National Academy of Sciences, National Research Council for the award of the fellowship during which this work was done. Part of this work (R.K.J.) has been supported by AEC under a subcontract 2220 with Oak Ridge National Laboratory.

REFERENCES

1. J. H. Adlam and J. E. Allen, Phil. Mag. 3, 448 (1958)
2. J. M. Burgers, Rev. Mod. Phys. 32, 868 (1960)
3. K. Hain, R. Lust and A. Schluter, Rev. Mod. Phys. 32 967 (1960)
4. O. W. Greenberg and Y. M. Treve, Phys. Fluids 5, 769 (1960)
5. I. G. Malkin, "Theory of Stability of Motion." AEC-tr-3352 (Russian Edition 1952)
6. V. V. Nemytskii and V. V. Stepanov, "Quantitative Theory of Differential Equations," Princeton University Press, 1960 (pp 125–130)